


The Effects of Cigarette Smoke on Airway Smooth Muscle Function

JinHeng Lin

Thesis submitted for the degree of Doctor of Philosophy

Newcastle University Biosciences Institute (NUBI), Faculty of Medical Sciences, Newcastle University

December 2020

Abstract

Cigarette smoking is the largest risk factor for developing chronic obstructive pulmonary disease (COPD), which is associated with hyperresponsiveness of airway smooth muscle. While it is well established that chronic exposure to cigarette smoke (CS) leads to dysregulated calcium signalling, airway inflammation and remodelling of the airway smooth muscle, there is limited information about the acute effects of CS or CS extract (CSE) on human airway smooth muscle cell (hASMC) function, particularly Ca^{2+} homeostasis. Dysfunction of the cystic fibrosis transmembrane conductance regulator (CFTR) anion channel is also linked to disrupted Ca^{2+} homeostasis in ASMC, but its role in ASMC function remains poorly understood.

This study investigated the following: (1) The role of CFTR in regulating Ca^{2+} homeostasis in ASMC; (2) The acute effects of aqueous CSE on hASMC Ca^{2+} homeostasis; and (3) The acute effects of gaseous CS on hASMC Ca^{2+} homeostasis. The results demonstrate that (1) CFTR inhibition in rat ASMC had minor effects on store-operated Ca^{2+} entry and the extent of Ca^{2+} reuptake; (2) Acute exposure to CSE or CS rapidly elevated cytosolic Ca^{2+} in hASMC through stimulation of plasmalemmal Ca^{2+} influx, but not through the release of calcium from intracellular sarcoplasmic reticulum stores; (3) Both CSE and CS specifically stimulated Ca^{2+} influx through the neurogenic pain receptor channel, transient receptor potential ankyrin 1 (TRPA1), but not through L-type or store-operated Ca^{2+} channels; (4) The CSE/CS-induced calcium influx through TRPA1 led to myosin light-chain phosphorylation, a key process regulating ASMC contractility.

Overall, results suggest that CFTR plays a minor role in regulating calcium homeostasis in ASM. However, this study provides the first experimental evidence that TRPA1 is an important target of both CSE and CS in hASMC. The CSE/CS-induced activation of TRPA1 may lead to exacerbated ASMC contraction thus contributing to airway hyperresponsiveness in COPD.

Acknowledgements

Firstly, I would like to acknowledge my supervisory team, Dr Mike Gray, Prof Mike Taggart, Dr Malcolm Brodlie, and Prof Robert Tarran for their continued support over the project. Mike G and Mike T were highly dedicated mentors involved in helping me drive the project, who rigorously assessed experimental data, provoked deep analysis, and provided countless valuable feedback and suggestions for both my experimental and written work – ultimately training me to mature as a young scientist. I would also like to specially thank Dr Vinciane Saint-Criq, who was very patient and helpful in getting me accustomed to the lab environment and housekeeping, and trained me on tissue culture. I also thank Livia Delpiano, Dr Iram Haq, and Dr Sara Cuevas Ocaña for general advice and moral support, both scientifically and in career development.

This PhD was funded by Newcastle University's JJ Bequest PhD Studentship, and I am extremely grateful for the university for providing me with this fantastic opportunity of personal and career development.

A significant portion of the data presented in this thesis was generated in a collaborating lab – Prof Robert Tarran's lab in University of North Carolina at Chapel Hill, USA. Rob has very kindly integrated me into his lab over two separate extended outside study periods in Chapel Hill, arranged trainings on laboratory techniques, and provided valuable insights to drive the progression of my project. I would also like to thank current and former lab members of the Tarran lab, specifically, Dr Tongde Wu for training me on dissection of rodent airway and isolation of airway smooth muscle cells; Dr Waseema Patel for training me on Ca^{2+} imaging and transfection; Dr Arunava Ghosh for training me on the automated smoke machine; Dr Michael Chua for training me on confocal microscopy; and Dr's Flori Sassano, Saira Ahmad, Megan Webster, Patrick Moore, and Joe Wrennall for general advice and lab housekeeping. Other than the Tarran lab, I would like to acknowledge Dr Scott Randell and his team, running the tissue culture core of the CF research centre in UNC, for procuring excess donor lung tissue for my use.

In Newcastle, I would like to acknowledge Dr Lee Borthwick and his lab members for procuring excess donor lung and explanted lung tissue for my use, from Freeman Hospital, Newcastle upon Tyne. The ethical approval holder for the collection of these tissues was Prof Andrew Fisher, to whom I'm grateful for allowing me to make experimental use of these tissue. Moreover, I would like to thank Dr Mark Levasseur for generously allowing me to use his epifluorescence microscope for Ca^{2+} imaging experiments, as well as Dr Timothy Cheek, Prof David Thwaites, Prof Jeff Pearson, and Prof Neil Perkins for lending lab space and equipment

for my use. Tim and Lee were also on my annual progression panel, and both of them have given me useful suggestions to improve the rigour of my work.

I have also received numerous technical supports over the course of the project. I'm grateful to superintendents of the tissue culture suite, Maxine Geggie and Helen Glenwright, who provided me with cell culture space, equipment, and various reagents. I would also like to thank Julie Taggart for training me on Western blot, and Barbara Innes for training me on immunohistochemistry. Furthermore, I would like to acknowledge the experimental assistance of Helena Gowing and Sophie Davies, undergraduate project students co-supervised by Dr Mike Gray and myself, for performing a few Ca^{2+} imaging experiments (data presented in Figures 4.1 and 6.1).

Last but not least, I would like to dedicate my greatest gratitude towards my close friends and family for their unwavering support over the past 4 years, and especially to my parents – for raising me with love, shaping my morals and principles, granting me the trust and freedom to explore the world, and supporting my career ambitions.

Table of Contents

List of Figures

List of Tables

List of Abbreviations

α-SMA	Alpha-smooth muscle actin
ABC	ATP-binding cassette
ACh	Acetylcholine
AChR	Acetylcholine receptor
AHR	Airway hyperresponsiveness
Ano1	Anoctamin 1
APS	Ammonium persulfate
AQP	Aquaporin
ASL	Airway surface liquid
ASM	Airway smooth muscle
ATP	Adenosine triphosphate
BSA	Bovine serum albumin
C/EBP	CCAAT/enhancer-binding protein
$[Ca^{2+}]_i$	Cytosolic calcium concentration
CaCC	Calcium-activated Cl^- channels
cADP ribose	Cyclic adenosine diphosphate ribose
CaM	Calmodulin
cAMP	Cyclic adenosine monophosphate
cDNA	Complementary DNA
CF	Cystic fibrosis
CFTR	Cystic fibrosis transmembrane conductance regulator
cGMP	Cyclic guanosine monophosphate
CICR	Calcium-induced calcium release
COPD	Chronic obstructive pulmonary diseases
CPA	Cyclopiazonic acid

CS	Cigarette smoke
CSC	Cigarette smoke condensate
CSE	Cigarette smoke extract
CT	Cycle threshold
CTGF	Connective tissue growth factor
CXCL1	Chemokine (C-X-C motif) ligand
DAB	3'-Diaminobenzidine
DAG	Diacylglycerol
DAPI	4',6-Diamidino-2-Phenylindole
DIDS	4,4'-Diisothiocyanatostilbene-2,2'-disulfonate
DMEM/F-12	Dulbecco's modified eagle's medium/Ham's nutrient mixture F-12
DMSO	Dimethyl sulfoxide
DPC	Diphenylamine-2-carboxylate
ECL	Enhanced chemiluminescence
ECM	Extracellular matrix
EDTA	Ethylenediaminetetraacetic acid
EGFR	Epidermal growth factor receptor
EGTA	Ethylene glycol-bis(2-aminoethylether)-N,N,N′,N′-tetraacetic acid
EMEM	Eagle's minimum essential medium
ENaC	Epithelial Na^+ channel
EP_2	Prostaglandin E_2 receptor 2
ER	Endoplasmic reticulum
EV	Empty control vector
FBS	Fetal bovine serum
FEV1	Forced expiratory volume in the first second
Fura-2-AM	Fura-2-acetoxymethylester

FVC	Forced vital capacity
GABA	Gamma-Aminobutyric acid
GAPDH	Glyceraldehyde 3-phosphate dehydrogenase
Gd^{3+}	Gadolinium
GPCR	G-protein coupled receptor
GTP	Guanosine triphosphate
H_1R	Histamine 1 receptor
hASMC	Human airway smooth muscle cell(s)
HCl	Hydrochloric acid
HEK	Human embryonic kidney
HRP	Horseradish peroxidase
IBMX	3-isobutyl-1-methylxanthine
IF	Immunofluorescence
IgG	Immunoglobulin G
IHC	Immunohistochemistry
IL	Interleukin
IP_3R	Inositol triphosphate receptor
ISC	Short-circuit current
JNK	c-Jun N-terminal kinase
KCl	Potassium chloride
LABA	Long-acting β_2-agonist
LAMA	Long-acting muscarinic antagonist
LB	Lysogeny broth
LTCC	L-type calcium channel
M-MLV	Moloney-Murine Leukemia Virus
M_3R	Muscarinic 3 receptor

MCP-1	Monocyte chemoattractant protein 1
MCU	Mitochondrial calcium uniporter
MLC	Myosin light-chain
MLCK	Myosin light-chain kinase
MLCP	Myosin light-chain phosphatase
MMP	Matrix metalloproteinase
NAC	N-acetylcysteine
NaHEPES	4-(2-Hydroxyethyl)piperazine-1-ethanesulfonic acid sodium salt
NBC	Na^+/bicarbonate cotransporter
NBD	Nucleotide-binding domain
NCX	Na^+-Ca^{2+} exchanger
NEAA	Non-essential amino-acid
NF-kB	Nuclear factor kappa-light-chain-enhancer of activated B cells
NGS	Normal goat serum
NHS	National Health Service
NKCC1	Na^+-K^+-Cl^- cotransporter 1
NNK	4-(methylnitrosamino)-1-(3-pyridyl)-1-butanone
NO	Nitric oxide
NPPB	5-nitro-2-(3-phenylpropyl-amino) benzoic acid
p-MLC	Phospho-myosin light-chain
PAS	Protein A-Sepharose
PBS	Phosphate-buffered saline
PD	Potential difference
PDE	Phosphodiesterase
PGE_2	Prostaglandin E_2
PKA	Protein kinase A

PLC	Phospholipase C
PM	Plasma membrane
PMCA	Plasma membrane calcium ATPase
PVDF	Polyvinylidene difluoride
qPCR	Quantitative polymerase chain reaction
rASMC	Rat airway smooth muscle cell(s)
RD	Regulatory domain
RhoA	Ras homolog gene family, member A
RIPA buffer	Radioimmunoprecipitation assay buffer
ROCC	Receptor-operated calcium channel
ROCK	Rho-associated coiled-coil protein kinase
ROS	Reactive oxygen species
RyR	Ryanodine receptor
SDS-PAGE	Sodium dodecyl sulfate-polyacrylamide gel electrophoresis
SEM	Standard error of mean
SERCA	Sarco-/endoplasmic reticulum calcium ATPase
shRNA	Short hairpin RNA
siRNA	Small interfering RNA
SLC26A9	Solute Carrier Family 26 Member 9
SOCC	Store-operated calcium channel
SOCE	Store-operated calcium entry
SR	Sarcoplasmic reticulum
STIM	Stromal interaction molecule
TBS-T	Tris-buffered saline-Tween20
TEMED	Tetramethylethylenediamine
TER	Transepithelial resistance

TGF	Transforming growth factor
TIMP	Tissue inhibitors of matrix metalloproteinase
TMD	Transmembrane spanning domain
TMEM16A	Transmembrane member 16A
TNF	Tumour necrosis factor
TRPA1	Transient receptor potential ankyrin 1
TRPC	Transient receptor potential canonical
TRPM	Transient receptor potential melastatin
TRPML	Transient receptor potential mucolipin
TRPV	Transient receptor potential vanilloid
TV	Vector encoding shRNA targeted against TRPA1
UTP	Uridine triphosphate
VEGF	Vascular endothelial growth factor
VIP	Vasoactive intestinal peptide
VOCC	Voltage-operated calcium channel
VSM	Vascular smooth muscle
WB	Western blot
WHO	World Health Organisation
WT	Wild-type

Chapter 1: Introduction

1.1 Physiology of the human airway

1.1.1 Anatomical and cellular structure of the human airway

The human airway is formed of a continuous tract that transports air between the outside environment and the lungs, where gas exchange takes place. CO_2 from the body, predominantly a waste product of cellular metabolism, is exchanged with O_2 from the outside air to provide the human body with a constant supply of oxygen, required for cellular respiration to provide energy for a myriad of cellular functions. In addition to gas exchange, the airway is also the first line of defence against inhaled allergens, pathogens and environmental irritants, acting to protect against, and remove, the infiltration of these insults.

Anatomically, the human respiratory tract can be separated into two regions, namely, the upper and the lower airway. The upper airway is composed of the nasal cavities, pharynx, and larynx, acting as the entry system of outside air into the respiratory tract. The upper airway importantly warms and humidifies air, and filters out large particulates and foreign bodies, before air reaches the lower airway. The lower airway is further divided into the conducting zone (beginning with the trachea, which branches into the bronchi, bronchioles, and terminal bronchioles), and the respiratory zone (with subsequent branches of respiratory bronchioles, alveolar ducts, and finally alveolar sacs), as illustrated in Figure 1.1A (Barrett *et al.*, 2015). The conducting zone is also termed the anatomical dead space of the lungs, as it is not involved in gas exchange. The cross-sectional area of the lumen exposed to air increases with each subsequent generation of branches, and gas exchange takes place in the respiratory zone, primarily at the alveolar ducts and sacs, where the surface area of exposure is the highest (Figure 1.1B). Gas exchange is a passive process through diffusion of various gases, importantly O_2, CO_2, H_2O (water vapour), and N_2, depending on the partial pressure and concentration gradient. At the alveoli, O_2 constantly diffuses into the bloodstream through the alveolocapillary membrane, connecting the alveoli to pulmonary capillaries, whereas CO_2 is constantly lost, from the blood into the alveoli, down a CO_2 gradient.

* Image removed from e-thesis due to copyright.*

Figure 1.1: Structure and branching of the human lower airway. (A) The levels of branching of the lower respiratory tract. (B) The cross-sectional surface area of airway lumen increases exponentially as the airway branches out. Adapted from Barrett *et al.* (2015). Image removed from e-thesis due to copyright.

Anatomically, the structures of the tracheal, bronchial, and bronchiolar walls differ as the airway branches. The trachea is surrounded anteriorly and laterally by rings of C-shaped hyaline cartilage, and a smooth muscle layer that completes the ring, located at the posterior end. In contrast, the bronchi walls contain less cartilaginous support as the airway branches out, and the smooth muscle layer is continuous, encircling the wall. The contractile tone of the smooth muscle regulates the calibre of the airway. In the walls of the larger airways, i.e. the trachea and bronchi, mucus-secreting glands are also present (Figure 1.2). The bronchioles, on the other hand, lack supporting cartilages as well as mucus-secreting glands, unlike the larger airways (Figure 1.2).

At a microscopic level, the surface of the lower airway is lined with a layer of heterogenous, pseudostratified epithelium, attached to a basement membrane, that acts as a protective physical barrier against inhaled insults (Figure 1.2A). The different types of epithelial cells in this layer are illustrated in Figure 1.2B. Other than mucus, the secretory airway epithelial cells, including goblet cells and Clara cells, also release antimicrobials, polysaccharides, and immunoglobulins, as well as various chemokines and cytokines to recruit immune cells, further strengthening the defence mechanism of the airway epithelium. Another main physiological function of the epithelial cells is the maintenance of fluid balance of the airway surface liquid (ASL), by tightly regulating the transport of ions and fluid.

* Image removed from e-thesis due to copyright.*

Figure 1.2: The cellular architecture of the lower airway. (A) Cross-sectional view of the wall of different lower airway sections, highlighting the differences in structure, cellular composition, and wall thickness. Taken from Barrett *et al.* (2015). (B) The major epithelial cell types in the large and small airways. The small airways are typically bronchi/bronchioles after 6 generations of branches from the trachea. The secretory goblet cells shift to a Clara cell type in the smaller airways. Taken from Crystal *et al.* (2008).

1.1.2 Regulation of the airway surface liquid

The ASL is formed of a periciliary fluid layer, in which the cilia are bathed, and a mucus layer, acting to bind and trap inhaled foreign particles (Figure 1.3). Importantly, the ciliated cells and mucus-secreting cells are essential for mucociliary clearance, acting to remove inhaled foreign particles. Small foreign particles and pathogens, not filtered out by the nasal hair and nasal mucosa in the upper airway, can enter the lower airway and deposit onto the walls, and trapped by the mucus layer of the ASL (Figure 1.3). These agents are transported out of the airway by the constantly beating cilia, which move the mucus layer upwards, and expelled through spitting, coughing, or swallowed into the antimicrobial, acidic environment in the stomach. Defects in

the mucociliary clearance mechanism, for instance dysregulation in the ASL fluid secretion that affects ciliary motility, lead to the inability of the airway to remove external insults, and hence predisposes the host to pathogen infections. This is evident in obstructive diseases such as chronic obstructive pulmonary disease (COPD), whereby impaired mucociliary clearance, partially due to attenuated ciliogenesis and ciliary beat (Tamashiro *et al.*, 2009; Yaghi *et al.*, 2012), leads to recurrent bacterial infections (Jansen *et al.*, 1995; Sethi, 2000).

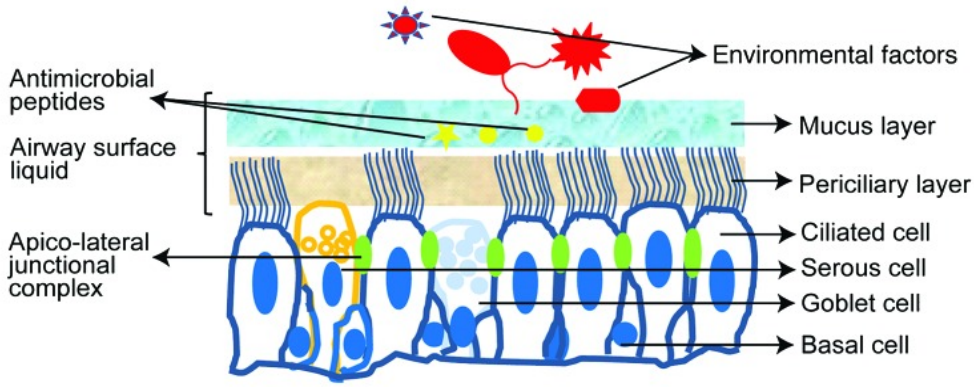

Figure 1.3: The airway surface liquid (ASL) of human airway epithelia. The ASL is propelled by cilia to remove inhaled agents from the environment. Taken from Ganesan *et al.* (2013). Permission to redistribute granted under a CC BY-NC 3.0 license (https://creativecommons.org/licenses/by-nc/3.0/).

The height of the ASL is determined by tightly balanced water absorption and secretion, which is regulated by the osmotic driving force created by transepithelial ion transport across the airway epithelia. In particular, absorption of Na^+ and secretion of Cl^- across the airway epithelia drive water movement through transcellular and/or paracellular pathways (Figure 1.4; reviewed in Saint-Criq and Gray (2017)). The main absorptive Na^+ channel in airway epithelia is the epithelial Na^+ channel (ENaC), whereas Cl^- secretion is primarily mediated by the cystic fibrosis transmembrane conductance regulator (CFTR) and Ca^{2+}-activated Cl^- channels (CaCC) such as Anoctamin 1 (Ano1; also named TMEM16A) (Figure 1.4). Defective Cl^- secretion or over-active Na^+ absorption dehydrate, and hence increase the viscosity of, the ASL, reducing ciliary beat frequency and mucus clearance (Collawn *et al.*, 2012).

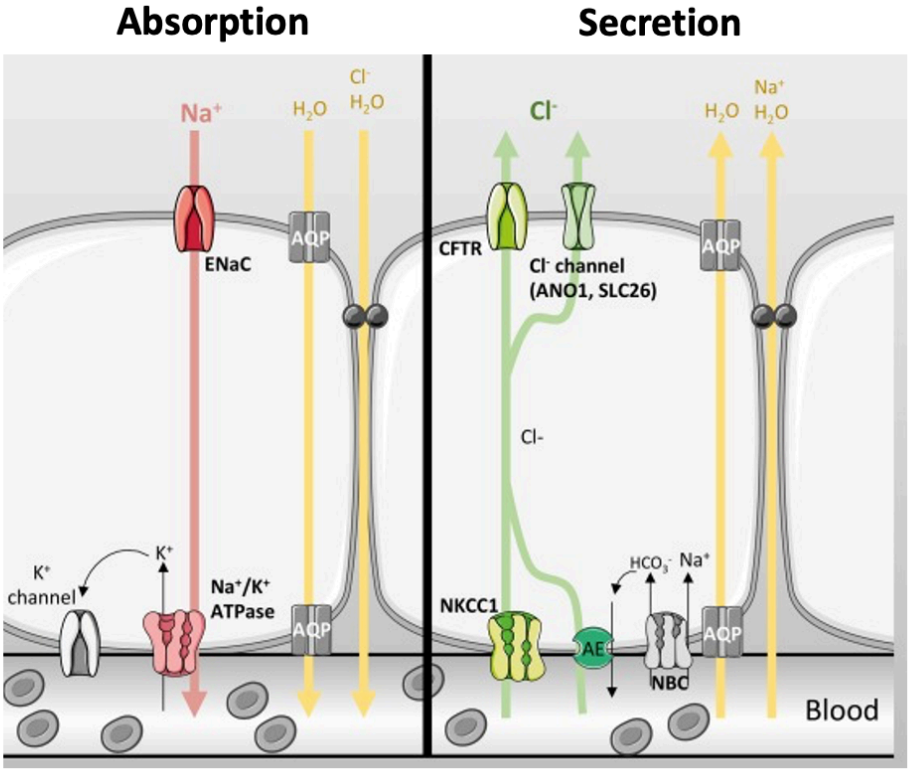

Figure 1.4: Regulation of ASL hydration by transepithelial ion and water movement. Water movement via the transcellular aquaporins (AQP) or paracellular pathways follow the osmotic driving force created by transepithelial Na^+ and Cl^- movement. Transcellularly, Na^+ is absorbed through ENaC, while Cl^- is secreted through various Cl^- channels including CFTR, on the apical membrane. The basolateral transporters, e.g. K^+ channels, Na^+/K^+ ATPase, Na^+-K^+-Cl^- cotransporter 1 (NKCC1), anion exchangers (AE), and Na^+/bicarbonate cotransporter (NBC), maintain the electrochemical gradient for transcellular Na^+ absorption and Cl^- secretion, as well as paracellular passive Cl^- and Na^+ movement. Taken from Saint-Criq and Gray (2017). Permission to redistribute granted under a CC BY 4.0 license (https://creativecommons.org/licenses/by/4.0/).

1.2 Obstructive airway diseases

A number of defects in the normal function of airway cells, including the epithelial cells and smooth muscle cells, can lead to pathogenesis of airway diseases. There are two broad classes of airway diseases, namely, restrictive and obstructive lung disease. In restrictive diseases, the lungs are restricted from fully expanding, due for example to stiffening of lung tissue or muscle weakness; a prime example of this is pulmonary fibrosis. On the other hand, obstructive lung diseases are characterised by obstruction of the airway, for example due to airway narrowing or excessive inflammation, the most common being cystic fibrosis (CF), COPD, and asthma.

Lung function can be measured through the non-invasive spirometry technique, an instrument that collects airflow from a human subject performing different ventilation manoeuvres depending on the test. Modern spirometers directly digitise the collected airflow, both inspiration and expiration, allowing for quantitative analysis of airflow data. In obstructive

airway diseases, the ratio of forced expiratory volume in the first second (FEV_1) over the forced vital capacity (FVC; measured by forced inhalation followed by forced expiration) is significantly lower, typically <70%, compared to the FEV_1/FVC of a healthy subject.

1.2.1 Cystic fibrosis and CFTR

CF is a life-threatening, autosomal recessive hereditary disease, with an incidence rate of 1 in 2500 newborns in the UK. The airway of a CF patient exhibits defects that lead to an obstructive phenotype, including airway hyperresponsiveness (AHR), impaired mucociliary clearance, mucus plugging, frequent infections, chronic inflammation, thickening of airway walls, and ASL dehydration. Many of these disease characteristics are similar to those seen in COPD, most notably AHR, the augmented sensitivity and/or maximal contractile response of the airway to inhaled stimuli.

Despite being a multiorgan disease, CF is most commonly characterised by progressively reduced respiratory function, due to defective fluid secretion from airway epithelial cells that leads to accumulation of viscous mucus in the airway, predisposing patients to infection and inflammation. This is attributed to loss-of-function mutations in the CFTR gene, which codes for a Cl^- channel that is expressed most notably in the apical surface of secretory epithelial cells and ionocytes (Montoro *et al.*, 2018; Plasschaert *et al.*, 2018), but also in other cell types such as airway smooth muscle cells (ASMC). CFTR is a cyclic adenosine monophosphate (cAMP)-dependent, protein kinase A (PKA)-activated, ATP-gated anion (primarily Cl^-) channel, and as explained in section 1.1.2, attenuated CFTR-mediated Cl^- secretion can lead to ASL dehydration.

CFTR was first identified and cloned in 1989 (Riordan *et al.*, 1989). It is a member of the ATP-binding cassette (ABC) transporter family, and has two cytoplasmic nucleotide-binding domains (NBD) that bind and hydrolyse ATP. The binding of ATP at NBD1 causes conformational change that allows its dimerisation with NBD2; the binding of a second ATP to this dimer at NBD2 then causes further conformational changes to the transmembrane spanning domains (TMD1 and TMD2), opening the channel (Hwang and Sheppard, 2009). The channel closes following the hydrolysis of the second ATP. The opening of the CFTR channel is also dependent on phosphorylation of its regulatory domain (RD), most prominently by cAMP-activated PKA.

In the initial molecular cloning analysis, it was found that ~ 70% of CF patients had a specific mutation: the deletion of phenylalanine at amino acid position 508 (termed F508del) of the CFTR protein (Kerem *et al.*, 1989). Subsequently, CFTR mutations have been divided into 6 classes according to the functional defect caused by the mutation. These range from defective

production of CFTR mRNA in the nucleus to defects in CFTR conductance and gating at the plasma membrane (MacDonald *et al.*, 2007). F508del-CFTR is a class II CFTR mutation, featuring defective processing or trafficking of the protein to the plasma membrane, and is by far the most common mutation in the UK (*UK Cystic Fibrosis Registry: Annual Data Report 2019*, 2020). F508del-CFTR is unable to transport ions at the plasma membrane of epithelial cells, as it is retained in the ER due to a processing defect (Cheng *et al.*, 1990). However, in epithelial cells, ER-localised F508del-CFTR retains moderately functional ion transport capabilities across the ER membrane (Dalemans *et al.*, 1991; Pasyk and Foskett, 1995).

1.2.2 COPD

On the other hand, COPD is a persistent respiratory disease characterised by non-reversible airflow limitation, and exhibits a wide range of traits including emphysema (destruction of the alveoli in the lung parenchyma, leading to reduced gas exchange and lung capacity), chronic bronchitis (long-term inflammation and enhanced mucus production), frequent and recurrent infections, and AHR. In their latest estimate in 2016, the World Health Organisation (WHO) listed COPD as the 3rd leading cause of death worldwide. In the UK, COPD represents a £1.9 billion burden for the NHS annually. The pathogenesis of COPD is complex and involves a variety of cellular processes, including enhanced secretion of inflammatory mediators, increased number and infiltration of inflammatory cells, protease/anti-protease imbalance, remodelling and hyperplasia of epithelial and smooth muscle cells, increased basal tone of ASMC, defective mucociliary clearance, and augmented sensitivity to contractile stimuli. There are genetic risk factors for the development and progression of COPD (reviewed in Mayer and Newman (2001); Eisner *et al.* (2010); Ragland *et al.* (2019)), but the majority of risk factors identified are environmental. These include exposure to cigarette smoke, household air pollution (Fullerton *et al.*, 2008; Gordon *et al.*, 2014), biomass smoke, mineral dust, and various gases, fumes, metals, and particulates identified from occupational exposure studies (reviewed in Eisner *et al.* (2010)). In particular, cigarette smoking has been identified as by far the most important causal factor (Eisner *et al.*, 2010; Hooper *et al.*, 2012), which is linked to various cellular processes responsible for pathogenesis of COPD mentioned above (explored below in section 1.4).

Interestingly, many of these processes that contribute to an obstructive airway phenotype, including cell proliferation, migration, secretion of inflammatory mediators, hyperresponsiveness and ciliary motility are regulated, at least partially, by intracellular calcium (Ca^{2+}) signalling (Evans and Sanderson, 1999; Bergner *et al.*, 2006; Gerthoffer, 2008; Mahn *et al.*, 2010; Zou *et al.*, 2011). Most importantly, intracellular Ca^{2+} is a central signalling

molecule for regulating smooth muscle contraction, which modulates the tone, and hence calibre, of the airway.

1.3 Regulation of Ca^{2+} signalling and ASMC contraction

1.3.1 Regulation of Ca^{2+} homeostasis in non-excitable mammalian cells

Calcium is a crucial messenger in mammalian cells, and is required for a wide range of physiological functions such as muscle contraction, proliferation, gene expression, activation of ion channels, and inflammation (Berridge *et al.*, 2003; Ribeiro *et al.*, 2005b; Lee and Foskett, 2010; Capiod, 2013). To accommodate such variety of functions, Ca^{2+} signalling needs to be very tightly regulated, both spatially and temporally, to deliver specific signals. The diffusion of Ca^{2+} across the cytoplasm is slow, and therefore Ca^{2+} mobilisation is often spatially organised into cellular microdomains, composed of select channels, organelles, and signalling proteins, to facilitate efficient and rapid, as well as highly specific, signalling events (Berridge, 2006; Petersen *et al.*, 2017). The dynamic regulation of Ca^{2+} microdomains, oscillations, or global Ca^{2+} transients in response to different stimuli, is complex (reviewed in detail by Berridge *et al.* (2003); Berridge (2006); Petersen *et al.* (2017); Samanta and Parekh (2017)). Dysregulated calcium homeostasis could lead to a range of diseases, for example airway hypercontractility brought about by elevated intracellular Ca^{2+} levels in ASMC (Mahn *et al.*, 2010; Wylam *et al.*, 2015).

Figure 1.5 presents a general model of Ca^{2+} homeostasis in non-electrically excitable mammalian cells, highlighting prominent Ca^{2+} transporters, signalling pathways, and other Ca^{2+}-binding proteins of interest. Generally, there are two main sources for elevating intracellular Ca^{2+} concentration ($[Ca^{2+}]_i$): Ca^{2+} influx, via receptor-, voltage-, or store-operated calcium channels situated on the plasma membrane (ROCC, VOCC, and SOCC, respectively), and Ca^{2+} release from intracellular stores, via IP_3R or RyR activation. The endoplasmic reticulum (ER), or sarcoplasmic reticulum (SR) in muscle cells, is generally the largest Ca^{2+} storage organelle, although the mitochondria, Golgi bodies, and lysosomes also act as Ca^{2+} stores. After release of Ca^{2+}, ER stores are replenished via the sarco/endoplasmic reticulum calcium ATPase (SERCA), an active Ca^{2+} pump. The concentration gradient of extracellular vs. intracellular Ca^{2+} is approximately 1mM to 100nM, providing a 10,000-fold gradient favouring rapid Ca^{2+} influx when Ca^{2+}-permeable channels open. This gradient is maintained primarily by the main extrusion (NCX and PMCA) and reuptake (SERCA) pathways, which are also responsible for bringing intracellular calcium concentration back to basal levels after a signalling event. The mitochondrial Ca^{2+} uniporter also plays a small role in calcium reuptake (Babcock *et al.*, 1997). On the other hand, the lysosome is a notable calcium store, with a high

resting [Ca^{2+}] of ~0.5mM generated by an active Ca^{2+} transport pathway, secondary to a proton gradient generated by the H^+-ATPase; a known channel for lysosomal Ca^{2+} release is TRPML, or mucolipin (Christensen *et al.*, 2002; Xu and Ren, 2015).

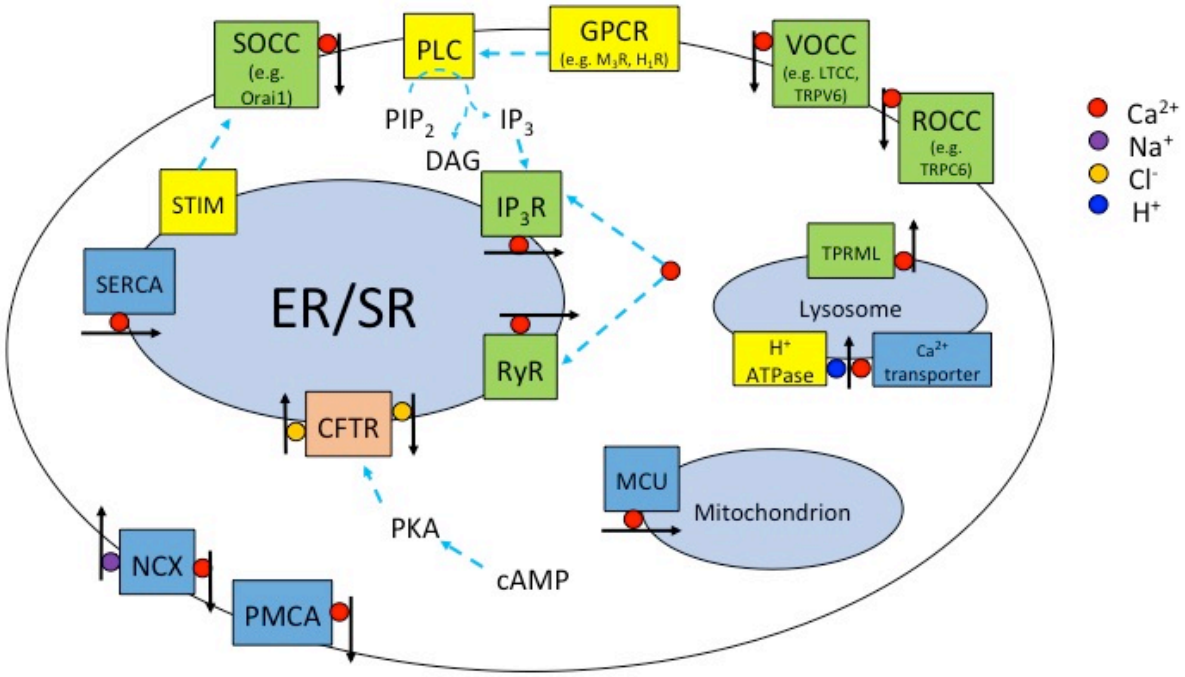

Figure 1.5: Model of mammalian cell Ca^{2+} homeostasis. Ca^{2+} influx or release pathways are in green, Ca^{2+} extrusion or reuptake pathways are in blue, while other proteins associated in Ca^{2+} homeostasis are in yellow. Black arrowheads indicate direction of ion movement. Blue dotted arrowheads indicate activation. Abbreviations: ER = endoplasmic reticulum; SR = sarcoplasmic reticulum; CFTR = cystic fibrosis transmembrane conductance regulator; PKA = protein kinase A; cAMP = cyclic adenosine monophosphate; SOCC = store-operated calcium channel; STIM = stromal interaction molecule; SERCA = sarco/endoplasmic reticulum calcium ATPase; RyR = ryanodine receptor; IP_3R = inositol triphosphate receptor; PLC = phospholipase C; GPCR = G-protein coupled receptor; M_3R = Muscarinic 3 receptor; H_1R = Histamine 1 receptor; VOCC = voltage-operated calcium channel; LTCC = L-type calcium channel; TRPV6 = transient receptor potential vanilloid channel 6; ROCC = receptor-operated calcium channel; TRPC6 = transient receptor potential canonical channel 6; PMCA = plasma membrane calcium ATPase; NCX = sodium-calcium exchanger; MCU = mitochondrial calcium uniporter; TRPML = transient receptor potential cation channel, mucolipin family.

Receptor-mediated Ca^{2+} release is initiated by binding of agonists, such as acetylcholine (ACh) and histamine, to their respective receptors, activating PLC, which catalyses the production of second messengers IP_3 and DAG (Berridge *et al.*, 2003). Binding of IP_3 to its receptor(s) (IP_3R1-3) on the ER then triggers Ca^{2+} release from the ER store, hence elevating $[Ca^{2+}]_i$. Another prominent Ca^{2+} release channel on the ER, mainly expressed in excitable cells, is the RyR (RyR1-3). RyR can also be directly activated, and IP_3R-mediated Ca^{2+} release can be augmented, by intracellular Ca^{2+} in close proximity to the ER, a process termed Ca^{2+}-induced Ca^{2+} release (CICR).

On the other hand, SOCC, such as Orai1, is activated upon ER/SR store depletion, leading to store-operated calcium entry (SOCE). A drop in ER Ca^{2+} levels is detected by the ER-localised STIM1 proteins, which undergo conformational changes and form oligomers. These STIM1 oligomers migrate to the ER-plasma membrane (PM) junctions, where they physically interact with Orai1 subunits in the PM, and cause Orai1 to also oligomerise, forming functional Ca^{2+} influx channels (Parekh, 2010). Other main Ca^{2+} influx channels include the VOCC (e.g. L-type Ca^{2+} channel, which is crucial in cardiac action potential and elevation of $[Ca^{2+}]_i$ in SMC) and the ROCC (e.g. TRPC6, which can be activated by the second messenger DAG).

1.3.2 Regulation of Ca^{2+} homeostasis in ASMC

Calcium homeostasis in ASMC is regulated in a similar manner as described in Figure 1.5, with similar influx, extrusion, release, and reuptake pathways (Figure 1.6). Within the ASMC, the sarcolemma membrane, the SR, and the mitochondria are localised in close proximity to allow for cross-talks between different regulatory aspects of Ca^{2+} homeostasis (Figure 1.6). IP_3R can exist as clusters on the SR membrane, and activation of IP_3R clusters leads to a high local release of Ca^{2+}, often termed "calcium puffs", that subsequently activate nearby RyR via CICR (Mahn *et al.*, 2010). RyR can be directly activated by Ca^{2+} from the cytosolic side, and sensitised by Ca^{2+} from within the SR lumen; RyR-mediated rapid release of local Ca^{2+} is termed "calcium sparks" (Berridge *et al.*, 2003). RyR can also be activated by cADP ribose, synthesised by the ADP-ribosyl cyclase CD38. In addition, although it is primarily an extrusion pathway, the NCX can also work in reverse mode to facilitate Ca^{2+} influx when there is an outward Na^+ gradient, and may contribute to store refilling in ASMC (Algara-Suarez *et al.*, 2007; Hirota *et al.*, 2007b).

The tightly regulated release, influx, and removal of calcium lead to Ca^{2+} oscillations, which modulate downstream effects such as contraction and proliferation. Indeed, the capacity of ASMC contraction is dependent on the frequency of Ca^{2+} oscillations, which requires refilling of intracellular stores primarily via SOCE (Perez and Sanderson, 2005; Chen and Sanderson, 2017).

* Image removed from e-thesis due to copyright.*

Figure 1.6: Model of ASMC Ca^{2+} homeostasis. Regulated Ca^{2+} influx, release, reuptake, and removal lead to Ca^{2+} oscillations. Influx is mediated via ROC, VOC (not shown), and SOC, removal via NCX and PMCA, reuptake of excess Ca^{2+} into the SR and mitochondrial stores, and SR Ca^{2+} release via IP3R and RyR. Ca^{2+} oscillations modulate ASMC function such as contraction and proliferation. In asthma, a disease featuring prominent airway hyperresponsiveness, various components of Ca^{2+} homeostasis are disrupted, such as TRPC (an influx channel), SERCA, and mitochondria. Abbreviations are as in Figure 1.5. Adapted from Mahn et al. (2010).

1.3.3 Intracellular Ca^{2+} regulates ASMC contractility

The airway smooth muscle is innervated by the autonomic nervous system, and serves to regulate the tone, and hence the calibre, of the airway lumen. In ASMC, intracellular Ca^{2+} acts as a secondary messenger to activate the contractile machinery, termed excitation-contraction coupling (Figure 1.7). An elevated $[Ca^{2+}]_i$ in response to stimulus activates the Ca^{2+}-binding protein calmodulin, which in turn binds to and activates myosin light-chain (MLC) kinase (MLCK). MLCK phosphorylates MLC, leading to the formation and cycling of actin-myosin cross-bridges that physically generate contractile force. Contraction is terminated by MLC phosphatase (MLCP), which de-phosphorylates myosin.

However, the elevation of $[Ca^{2+}]_i$ by GPCR-coupled Ca^{2+} release or voltage-gated Ca^{2+} influx is usually transient. The sustained contractile response of ASMC is mediated by the Ca^{2+}-sensitisation pathway, mainly through the RhoA pathway. RhoA is a GTPase activated by $G_{\alpha q}$, stimulated by GPCR activation, and the GTP loading of RhoA can also be enhanced by intracellular Ca^{2+} (Figure 1.7). RhoA then activates Rho-associated coiled-coil protein kinase (ROCK), which inhibits MLCP, leading to sustained MLC phosphorylation and cross-bridge formation. Alteration of MLC phosphorylation, at a constant $[Ca^{2+}]_i$, increases Ca^{2+} sensitivity of contraction.

* Image removed from e-thesis due to copyright.*

Figure 1.7: Calcium signalling leads to downstream activation of excitation-contraction coupling in smooth muscle cells. Ca^{2+} influx (through e.g. voltage-gated Ca^{2+} channels) or Ca^{2+} release from the sarcoplasmic reticulum through IP_3R activation initiate the contractile machinery by MLCK-mediated phosphorylation of MLC. On the other hand, the RhoA-mediated inhibition of MLCP sensitises the ASMC contractile machinery. CaM = calmodulin; MLCK = myosin light chain kinase; MLCP = myosin light chain phosphatase; RhoA = Ras homolog gene family, member A; ROCK = Rho-associated coiled-coil protein kinase. Adapted from Erle and Sheppard (2014).

On the other hand, relaxation of ASMC is initiated by a decline in $[Ca^{2+}]_i$ through inactivation of Ca^{2+} influx channels, removal of Ca^{2+}-agonists, or activation of Ca^{2+} extrusion or reuptake mechanisms, depicted in Figure 1.5 and 1.6. Lowering $[Ca^{2+}]_i$ reduces the activity of the MLCK- and RhoA-mediated pro-contractile pathways. Additionally, the relaxation of ASMC is largely dependent on MLCP to de-phosphorylate MLC. Physiologically, nitric oxide (NO), produced by airway epithelia and innervation, diffuses through to SMC and activates guanylyl cyclase which catalyses the conversion of cyclic guanosine monophosphate (cGMP) from guanosine triphosphate (GTP); cGMP-dependent protein kinase then activates MLCP to promote relaxation.

Furthermore, ASMC relaxation is also regulated by elevation of cAMP levels. For instance, agonist binding to the β_2-adrenoceptor, a G_S-coupled receptor, activates adenylyl cyclase, catalysing the production of cAMP by breaking down ATP. cAMP in turn activates PKA, which is then able to phosphorylate key targets to mediate relaxation. The downstream effects of cAMP, which may be PKA-mediated, include reduced Ca^{2+} influx (Prakash *et al.*, 1997; Ay *et al.*, 2006), inhibition of IP_3 formation and IP_3R (Ding *et al.*, 1997; Bai and Sanderson, 2006), increased Ca^{2+} reuptake and extrusion (Yamanaka *et al.*, 2003; Janssen *et al.*, 2004), activation of K^+ channels to induce hyperpolarisation (Tanaka *et al.*, 2003), reduced affinity of MLCK to bind to Ca^{2+} and activated calmodulin (Conti and Adelstein, 1981), and activation of MLCP (Janssen *et al.*, 2004).

1.4 Cigarette smoke and the pathogenesis of COPD

As mentioned previously, cigarette smoking is known to be by far the largest etiological factor for the development of COPD. The history and frequency of smoking correlated to rapid decline in FEV_1 in COPD patients, whereas smoking cessation significantly slowed down the decline in lung function (Anthonisen *et al.*, 1994; Tashkin *et al.*, 1996; Anthonisen *et al.*, 2005). Moreover, the mortality rate of COPD patients with a smoking history was higher compared to non-smoking COPD patients (Anthonisen *et al.*, 2005; Tamimi *et al.*, 2012). However, many of the pathological changes initiated by smoking may not be reversible. For instance, in a cessation study, the inflammatory profile in COPD lungs was not reversed by 12 months of smoking cessation, and the levels of inflammatory cells and markers, including number of neutrophils, leukocytes, and concentration of interleukin (IL)-8 increased after the cessation period (Willemse *et al.*, 2005). There is now an extensive amount of evidence in the literature supporting the link between smoking and various aspects of COPD pathogenesis.

1.4.1 Properties and experimental models of cigarette smoke

Cigarette smoke (CS) is a concentrated aerosol produced by combustion of tobacco-based cigarettes and comprises a complex mix of over 4000 chemicals (Burns, 1991), many of which are toxic, irritants, or carcinogens. The most prominent of these are nicotine, acrolein, N-nitrosamines, aromatic hydrocarbons, various volatile compounds and heavy metals (reviewed comprehensively in Centers for Disease Control and Prevention (2010)). Nicotine is highly associated with addiction, a large driving force for returning to, and chronic smoking (Benowitz, 2010). On the other hand, combustion of cigarettes produces a large number of free radicals, reactive oxygen and nitrogen species, which can disturb cellular redox balance to initiate deleterious downstream effects (Pryor, 1992; Valavanidis *et al.*, 2009). Commercial blends of cigarettes contain different relative concentrations of various constituents, and therefore

research-grade cigarettes with standardised constituents, such as the 3R4F and 1R6F reference cigarettes from the University of Kentucky, are typically used for more recent CS research (Eldridge *et al.*, 2015).

The smoke produced from lighting up a cigarette can be separated into the mainstream (smoke drawn through the tobacco and inhaled by the user) and sidestream smoke, which is released from the burning end of the cigarette into the environment (second-hand smoke). Experimental investigation into the effects of mainstream CS to study the effect of active smoking utilises one, or both, of its two distinct phases: the gaseous phase and the particulate phase. The gaseous phase entails the smoke that passes through a glass fibre filter with 0.3 μm pores, while the particulate phase, also known as the tar phase, consists of the relatively larger aerosol particles trapped in these pores (Pillsbury *et al.*, 1969). To study the particulate phase of CS, CS condensate (CSC) can be produced by dissolving weighed particulate matter, trapped on a glass fibre filter, into DMSO or other solvents. On the other hand, there are two main experimental delivery methods for the gaseous phase of CS, one of which is direct aerosolisation of mainstream smoke from a lit cigarette into a closed chamber. This system is commonly used for animal smoking studies, but has also been employed for *in vitro* experiments to expose cell cultures to CS (Rasmussen *et al.*, 2014; Ghorani *et al.*, 2017). Another delivery model is known as CS extract (CSE), which is produced by bubbling CS into media or a physiological buffer solution. This can then be diluted and applied to *in vitro* or *ex vivo* samples, or collected for chemical analysis. Direct exposure to gaseous CS, or to diluted CSE, are often reported in the literature as though to be synonymous, but certain volatile constituents potentially lost through vigorous bubbling during the production of CSE are retained in the closed chamber in the CS model. Therefore, one of the aims of the PhD project was to investigate potential differences in the effect of gaseous CS and CSE exposure on ASMC function.

Another CS-related product of interest is the e-cigarette liquid (e-liquid), a trending substitute for traditional cigarettes that has been proposed to be a less toxic alternative. However, recent studies have shown that e-liquid or vaping causes a wide range of adverse pulmonary effects on various cell cultures and animal models, including toxicity, augmented inflammation and oxidative stress, disruption of gas exchange, emphysema, perpetuation of nicotine addiction, and suppression of pulmonary host defence (reviewed in Rowell and Tarran (2015); Hiemstra and Bals (2016); Herman and Tarran (2020); Miyashita and Foley (2020); Tsai *et al.* (2020)).

1.4.2 CS exposure leads to inflammation and oxidative stress in the airway

Excessive inflammation of the airways is a hallmark of COPD progression, typically observed in the smaller airways and the lung parenchyma. An increased number of various inflammatory

cells, such as neutrophils, macrophages, eosinophils, mast cells, $CD4^+$ T-lymphocytes, $CD8^+$ T-lymphocytes, and natural killer lymphocytes, were found in the glands, epithelium (Saetta *et al.*, 1997; de Boer *et al.*, 1998; Retamales *et al.*, 2001; Hogg *et al.*, 2004), and subepithelium (Di Stefano *et al.*, 1996; Di Stefano *et al.*, 1998) layers of the smaller airways and lung parenchyma, as well as sputum (Keatings *et al.*, 1996), of COPD patients with a smoking history. These inflammatory cells can be recruited by cytokines such as IL-8 and TGF-β1 (de Boer *et al.*, 1998), released upon lung injury induced by CS insult, to infiltrate different layers of the airway walls and promote inflammation of the airway.

Chronic inflammation of the lower airways could lead to deleterious effects on lung function, including initiation of airway remodelling that leads to emphysema and chronic bronchitis phenotypes seen in COPD. Inflammatory cells are capable of releasing cytokines to further recruit other inflammatory cells and guide tissue remodelling, extracellular matrix (ECM) proteins, and various proteases that could damage the airway walls. Indeed, the number of macrophages, neutrophils, and various lymphocytes were directly correlated to the degree of alveolar wall destruction (Retamales *et al.*, 2001), and inversely correlated to FEV_1 of smokers with COPD (Di Stefano *et al.*, 1996; Di Stefano *et al.*, 1998). The mRNA expression or protein concentration of several pro-inflammatory cytokines, e.g. IL-6, IL-8, TNF-α, monocyte chemoattractant protein 1 (MCP-1), were elevated in the bronchial epithelium (de Boer *et al.*, 2000), exhaled breath condensate (Gessner *et al.*, 2005), and the sputum or bronchoalveolar lavage (Keatings *et al.*, 1996; Mio *et al.*, 1997) of chronic smokers. This augmentation of inflammatory markers was replicated in a CS-exposed guinea pig model (Kubo *et al.*, 2005). These cytokines further recruit immune cells and initiate pro-inflammatory processes. *In vitro*, treatment with CSE or its constituents also enhanced the secretion of IL-8 in cultured human bronchial epithelial cells and fibroblasts (Mio *et al.*, 1997; Facchinetti *et al.*, 2007; Miglino *et al.*, 2012).

Other than initiating chronic inflammation, tobacco smoking has also been shown to elevate the oxidative stress levels in lung tissue. For instance, elevated levels of H_2O_2 was found in exhaled breath condensate of COPD smokers (Dekhuijzen *et al.*, 1996). Also, Zeng *et al.* (2013) observed both systemic (plasma) and local (induced sputum) progressive elevation in cellular antioxidants, including glutathione, superoxide dismutase and GSH peroxidase, in three subject groups: COPD patients, healthy smokers, and non-smokers. Oxidative stress was sufficient to induce airway hyperresponsiveness and inflammation in mice, and contributed to mitochondrial dysfunction in ASMC from COPD smokers (Wiegman *et al.*, 2015). A major source of this oxidative stress is cigarette smoke, combustion of which releases many reactive oxygen and

nitrogen species. However, neutrophils and macrophages, as well as airway epithelial cells, can also release cellular oxidants upon stimulation (Rahman *et al.*, 1996; Noguera *et al.*, 2001; McGuinness and Sapey, 2017). One of the downstream effects of oxidative stress is the activation of the transcription factor NF-κB, which can upregulate pro-inflammatory genes (Adcock *et al.*, 1994). Oxidative stress can also induce production and secretion of pro-inflammatory cytokines (reviewed in McGuinness and Sapey (2017)), further promoting a positive feedback loop with airway inflammation. Oxidative stress and inflammation of the airway are upstream of many processes that govern airway remodelling, which contributes to emphysema and airway obstruction in COPD.

1.4.3 CS exposure is linked to airway remodelling

Airway remodelling is directly, and at least partially, responsible for the development of emphysema and airway obstruction. Remodelling of the airway is associated with pathological changes in various cell types, including the inflammatory cells mentioned above, as well as secretory epithelial cells, fibroblasts, and ASMC. In COPD, airway remodelling is usually found in the smaller airways and lung parenchyma, but there is also evidence of remodelling in larger airways, whereby thicker layers of the epithelium, basement membrane, larger area of smooth muscle, and increased deposition of ECM proteins were observed (Tiddens *et al.*, 1995; Kranenburg *et al.*, 2006; Liesker *et al.*, 2009; Pini *et al.*, 2014). The most notable features of COPD smaller airways that lead to an obstructive phenotype are increased overall volume of lung tissue, thickening of airway walls, and mucus plugging (Hogg *et al.*, 2004), whereas destruction of alveolar wall attachments (Saetta *et al.*, 1985), connective tissue, and other structural cells contribute to emphysema.

The destruction of healthy lung tissue is a result of several inter-connected processes, including oxidative stress, inflammatory signals, protease/anti-protease imbalance, inhibition of the repair pathways, and excess cell death. In lung tissue sections of COPD patients with a smoking history, increased apoptosis was observed in endothelial, alveolar epithelial, and inflammatory cells (reviewed in Demedts *et al.* (2006a)). This was consistent with *in vitro* experiments showing that exposure to CSE can initiate apoptosis of fibroblasts (Carnevali *et al.*, 2003), alveolar epithelial cells (Hoshino *et al.*, 2001; Chen *et al.*, 2015), and ASMC (Yoon *et al.*, 2011). In the inflamed airway, cytotoxic, $CD8^+$ T-lymphocytes release perforins and TNF-α, signals that may initiate apoptosis of epithelial cells (Liu *et al.*, 1999). In addition, the growth factor VEGF is an important regulator of emphysemal apoptosis, as lung-targeted knockdown of VEGF in mouse led to increased apoptosis of alveolar and bronchial epithelial cell (Tang *et al.*, 2004). Accordingly, an elevated level of oxidative stress markers, and reduction in VEGF levels,

in sputum of COPD patients correlated with the severity of the disease (Kanazawa and Yoshikawa, 2005). Other than initiating apoptosis, exposure to CS condensate also led to necrosis of alveolar epithelial cells *in vitro* (Wickenden *et al.*, 2003), whereas *in vivo* exposure of rats to CS resulted in excess bronchiolar epithelial cell necrosis, accompanied by DNA strand breaks (Jung *et al.*, 2000). The epithelial barrier integrity and cell-cell contact was also disrupted by CSE treatment, further enhancing the destruction of alveolar tissue (Heijink *et al.*, 2012).

In addition to excessive cell death, defective alveolar regeneration further contributes to emphysemal insults. One of the main tissue regeneration mechanisms is through migration and secretion of various growth factors and ECM proteins by fibroblasts, including secretion of fibronectin and chemotaxis towards fibronectin, and CS exposure induces a number of fibroblast dysfunctions. For instance, CSE inhibited fibroblast proliferation, and induced oxidative stress and apoptosis in fibroblasts (Nakamura *et al.*, 1995; Nobukuni *et al.*, 2002; Miglino *et al.*, 2012). Moreover, fibronectin production, chemotaxis of fibroblasts towards fibronectin, and fibroblast contraction were inhibited by CSE treatment, specifically by acrolein and acetaldehyde contained in CS (Nakamura *et al.*, 1995; Carnevali *et al.*, 1998; Togo *et al.*, 2008). CSE treatment also led to oxidative stress, DNA damage, and apoptosis of lung fibroblasts, further amplifying defective tissue repair mechanisms (Carnevali *et al.*, 2003; Kim *et al.*, 2004; Lee *et al.*, 2016). Similar inhibitory effects of CS on the tissue repair functions of endothelial and epithelial cells have also been reported (reviewed in Rennard *et al.* (2006)).

Other than direct disruption of cell death/regeneration, the destruction of connective tissue and ECM, and hence loss of structural integrity, also contribute to airspace enlargement, and hinges largely on protease/anti-protease imbalance. A number of proteases can directly break down ECM proteins such as elastin and collagen, leading to loss of airway tissue and elastic recoil of the lungs. One of the initial indications for the role of proteases in emphysema was a genetic risk factor for COPD, whereby patients with a deficiency in α_1-antitrypsin were pre-disposed to a higher probability of developing COPD, with worse disease severity (reviewed in Hatipoglu and Stoller (2016)). A number of proteases, such as neutrophil elastase, proteinase-3, and matrix metalloproteinases (MMP)- 1, 8, 9, and 12, were elevated in the sputum or lavage of COPD patients, which correlated with airflow limitation (Imai *et al.*, 2001; Vernooy *et al.*, 2004; Molet *et al.*, 2005; Demedts *et al.*, 2006b; Paone *et al.*, 2011). These are mainly secreted by macrophages and neutrophils, cells that are also elevated in COPD (Finlay *et al.*, 1997; Russell *et al.*, 2002; Gupta *et al.*, 2016). Indeed, alveolar macrophages are localised to sites of alveolar wall destruction (Barnes, 2004), and macrophages and neutrophils from COPD

patients exhibit enhanced elastolytic activity and chemotaxis (Burnett *et al.*, 1987). CS exposure also induced the expression of MMP-1 and 2 in lung fibroblasts (Ning *et al.*, 2007), as well as MMP-12 from macrophages (Owen, 2008). Additionally, the ratio of MMP-9 to the tissue inhibitors of MMP (TIMP) correlated with the amount of smoking in subjects studied, emphasising the disruption of protease/anti-protease balance by CS (Kang *et al.*, 2003). Furthermore, oxidative stress from smoking also activates proteases (Owen, 2005) and deactivates α_1-antitrypsin (Taggart *et al.*, 2000). The breakdown of basement membrane and ECM by MMPs can also lead to anoikis – apoptosis initiated by inadequate or lack of interaction between cells and ECM, further causing tissue damage (Frisch and Screaton, 2001). Other than directly breaking down lung tissue, these proteases can also cleave signalling peptides to generate pro-inflammatory and secretory signals, further contributing to airway remodelling (reviewed in (Barnes *et al.*, 2003; Barnes, 2014)).

Aside from emphysema, airway remodelling may also lead to an obstructive phenotype in COPD. For instance, excessive mucus secretion directly blocks the airway lumen, and alters the balance and surface tension of ASL. This excessive secretion can be attributed to hyperplasia of the secretory goblet cells seen in the small airways of COPD smokers and rats exposed to CS (Saetta *et al.*, 2000; Takeyama *et al.*, 2001). The increased mucus plugging is, at least partially, secondary to airway inflammation, as chemokines e.g. IL-13 and TNF-α, and neutrophil elastase can stimulate mucin secretion (Takeyama *et al.*, 1998; Smirnova *et al.*, 2000; Shim *et al.*, 2001). However, CS exposure can also directly activate mucin synthesis and secretion (Basbaum *et al.*, 1999). At a cellular level, the expression of the mucin protein MUC5AC was found to be upregulated in epithelial cells by chronic CS exposure, which activates both the EGFR and the JNK pathways via ROS production (Takeyama *et al.*, 2001; Gensch *et al.*, 2004; Shao *et al.*, 2004).

In addition to mucus blocking the airway lumen, the airway walls are also thickened in COPD patients. One of the contributing factors to this is ECM deposition within the airway walls. As such, it was observed that expression of collagen I, III, and IV and laminin-β2 were significantly higher in various layers of the bronchial walls in COPD smokers, which correlated with FEV_1 measurements (Kranenburg *et al.*, 2006). The growth factor TGF-β, secreted by immune cells and ASMC, plays an important role in ECM deposition, as it signals for expression of connective tissue growth factor (CTGF), as well as induces collagen deposition and expression of anti-proteases to reduce ECM breakdown in the airway walls (reviewed in (Ihn, 2002; de Boer *et al.*, 2007)).

Furthermore, airway smooth muscle cells have also been implicated in airway remodelling, mainly as effector cells responsible for thickening of airway walls. Indeed, the mass of the smooth muscle layer is increased in COPD small airways, especially in more severe diseased states (Bosken *et al.*, 1990; Kuwano *et al.*, 1993; Kranenburg *et al.*, 2006), which can be attributed to ASMC hypertrophy (Ebina *et al.*, 1990) or hyperplasia, as well as thickened ECM surrounding the smooth muscle cells. ASMC hyperplasia, i.e. augmented proliferation of ASMC, is one of the main contributors of this thickened layer. Chronic treatment with CSE promoted ASMC proliferation, through several mechanisms such as upregulating cyclin D1, E, M2, M3, activating the ERK1/2 signalling pathway (Pera *et al.*, 2010; Xu *et al.*, 2010; Zhang *et al.*, 2010; Xu *et al.*, 2012; Wylam *et al.*, 2015), upregulating TRPM7 (Lin *et al.*, 2016), upregulating TRPC6 and α7 nicotinic AChR (Hong *et al.*, 2017; Jiang *et al.*, 2019) and suppressing CCAAT/enhancer-binding protein (C/EBP)-α expression (Guan *et al.*, 2017). Other than growth and proliferation, ASMC can also release various cytokines, e.g. IL-8 (Oltmanns *et al.*, 2005), CXCL1 (Chen *et al.*, 2014), and TNF-α (Wylam *et al.*, 2015), MMPs and collagen (Chen *et al.*, 2014) in response to CSE treatment. Furthermore, signals from the inflamed airway, e.g. TNF-α and interferon-γ, can also cause upregulation of CXCL10, a potent chemokine for various immune cells, in ASMC, further enhancing the inflammatory profile of the airway (Hardaker *et al.*, 2004). Indeed, the phenotypic shift of ASMC from a contractile to a synthetic/proliferative state may underlie airway remodelling in response to CS exposure (Pera *et al.*, 2010), accompanied by ASMC metabolic reprogramming that supports the biosynthetic pathways (Michaeloudes *et al.*, 2017). The synthetic ASMC can also directly produce and secrete ECM proteins such as collagen, fibronectin, elastin, laminin, as well as regulating the protease/anti-protease balance in ECM of the smooth muscle layer (reviewed in Parameswaran *et al.* (2006)). In particular, ASMC secreted MMP-1, -3, and -10, as well as collagen VIII-α1 in response to CSE treatment (Chen *et al.*, 2014), consolidating a direct link between CS exposure and airway remodelling and obstruction.

1.4.4 CS exposure disrupts contractility and Ca^{2+} homeostasis in ASMC

As outlined above, exposure to CS leads to a cascade of downstream signalling events that contribute to various aspects of COPD pathogenesis. However, in comparison to research on airway inflammation and remodelling, few studies have investigated the direct effects of CS on the contractile function of ASMC, even though airway hyperresponsiveness is a major hallmark of COPD (Tashkin *et al.*, 1992; Tashkin *et al.*, 1996), and is correlated with smoking history as well as amount of current smoking (Tashkin *et al.*, 1993). AHR is the enhanced sensitivity of ASMC to contractile stimuli, and may be attributed to alterations in the intrinsic contractility

of ASMC, or linked to upregulation of pro-contractile signals by other airway cell types and the outside environment (reviewed by Prakash (2016)). However, the intrinsic contractility of ASMC in the diseased state is difficult to isolate, since airway inflammation is prominent in COPD lungs. Indeed, pro-inflammatory cytokines such as IL-1β, IL-13, and TNF-α can directly alter contractility and Ca^{2+} homeostasis in ASMC (Rizzo *et al.*, 2002; Deshpande *et al.*, 2003; Deshpande *et al.*, 2004; Sathish *et al.*, 2009; Sieck *et al.*, 2019).

AHR in response to cholinergic stimulation can be reproduced in CS-exposed models of rat (Xu *et al.*, 1993) and guinea pig (Wu and Lee, 1999). In addition to *in vivo* measurements of AHR, a number of myography studies demonstrated that chronic exposure to CS *in vivo* (Chiba *et al.*, 2005), or CSE incubation of the intact airway rings *ex vivo* (Xu *et al.*, 2010; Xu *et al.*, 2012; Sathish *et al.*, 2015) sensitised the airway, leading to augmented contractility of human or rat bronchial or tracheal rings to cholinergic or bradykinin stimulation. Incubation with acrolein, an irritant present in CS, also led to hypercontractility of rat and human airway rings (Ben-Jebria *et al.*, 1993; Ben-Jebria *et al.*, 1994; Roux *et al.*, 1998). However, Pera *et al.* (2010) observed the opposite effect, with CSE-treated bovine tracheal strips exhibiting lower maximal contraction in response to metacholine and KCl. However, these contractile studies did not investigate the intrinsic contractility of ASMC, as the intact airway rings are surrounded by the epithelium, connective tissue, and immune cells that may release contractile or relaxation signals. As such, at a cellular level, Yoon *et al.* (2011) discovered that human bronchial ASMC treated with CSE were also hypocontractile in a collagen gel contraction assay, and this was abolished by addition of the antioxidant N-acetylcysteine (NAC).

Although hyperresponsiveness of the ASMC *in vivo* is dependent on the chronic inflammatory state of the airway and resulting changes in gene expression, acute exposure to CS may also directly affect ASMC contractility. A few early studies from the 60s-80s have detected increased airway resistance and decreased flow, indicative of bronchoconstriction, in both smoking and non-smoking subjects in response to acute cigarette smoking, but whether ASMC contractility was directly involved is not known (Zamel *et al.*, 1963; McDermott and Collins, 1965; Sterling, 1967; Higenbottam *et al.*, 1980). Moreover, Andre *et al.* (2008) found that acute treatment with CSE led to constriction of the *ex vivo* guinea pig isolated bronchi. In contrast, Streck *et al.* (2010) found that acute CSE administration led to relaxation of mouse lung slices, and this was partially blocked by a nicotinic receptor antagonist. Similarly, administration of acrolein caused rapid release of PGE_2 from lung epithelia, leading to acute relaxation of mouse tracheal rings through EP_2 receptor activation (Cheah *et al.*, 2014). This acute relaxation due to PGE_2 production may be attributed to activation of TRPA1, a target of acrolein and several

irritants present in CS; as such, Marsh *et al.* (2020) demonstrated that TRPA1 agonists prevented vagally-stimulated bronchoconstriction *in vivo* of guinea pigs, as well as relaxed pre-constricted guinea pig, mouse, and human *ex vivo* airway.

The contractility of ASMC is governed largely by spatial and temporal regulation of intracellular Ca^{2+} levels, and CS exposure brings about long-term changes to ASMC Ca^{2+} homeostasis. Chronic treatment with CSE augmented GPCR-coupled Ca^{2+} release and SOCE in human ASMC (hASMC), which was attributed to increased expression and function of various Ca^{2+}-homeostatic regulators, namely TRPC3, CD38 (which catalyses synthesis of cADP ribose, the endogenous activator of RyR), STIM1, and Orai1 (Sathish *et al.*, 2015; Wylam *et al.*, 2015). Wylam *et al.* (2015) also observed upregulation of CD38 and TRPC in the bronchial tissue of chronic smokers, compared to non-smokers. In addition, pre-treatment with nicotine alone was sufficient to augment both ROCE and SOCE in hASMC (Hong *et al.*, 2017). Outside of ASMC, CS treatment also disrupted Ca^{2+} signalling in cardiac and skeletal myocytes, most notably blunting contractility, and delaying Ca^{2+} reuptake (Pei *et al.*, 2014; Robison *et al.*, 2017; Nogueira *et al.*, 2018).

Clearly, the above studies have considered the impact of chronic exposure to cigarette smoke. However, not many studies have investigated the acute effect of CS exposure on airway smooth muscle constriction *per se* and intracellular Ca^{2+} levels in hASMC. Yoon *et al.* (2011) previously observed that CSE administration led to a rise in $[Ca^{2+}]_i$ in 64% of hASMC sampled, whereas Nassini *et al.* (2012) reported a global $[Ca^{2+}]_i$ elevation. The mechanism and response profiles behind these transient Ca^{2+} responses were not thoroughly characterised, and therefore is one of the aims of this project.

1.5 CS exposure disrupts CFTR function and dehydrates the ASL

1.5.1 CS-induced airway dehydration and defective mucociliary clearance in COPD

As described in section 1.2, CF and COPD share similar characteristics in regard to airway obstruction, including severe mucus plugging, inflammation, airway remodelling, and ASL dehydration. Importantly, ASL dehydration leads to impaired mucociliary clearance, which can initiate chronic inflammation and recurrent infections (Collawn *et al.*, 2012; Haq *et al.*, 2016).

The importance of maintaining airway hydration is exemplified in a βENaC-overexpressing mouse model, where CS-induced characteristics of COPD, such as ASL dehydration, excessive mucus secretion, inflammation, and emphysema, along with decline in lung function, was aggravated compared to in wild-type (WT) mice (Seys *et al.*, 2015). Exposure to CS can also bring about depletion of ASL volume in primary cultures of human airway epithelial cells,

which correlated to slower ciliary beat frequency and mucociliary transport (Clunes *et al.*, 2012; Sloane *et al.*, 2012; Raju *et al.*, 2017a). In human patients, the mucus sampled from both the trachea and smaller airways of chronic smokers was significantly more dehydrated compared to those from healthy non-smokers (Clunes *et al.*, 2012). On the other hand, rehydration of the airway, through inhaled hypertonic saline to drive fluid secretion, restored mucociliary transport in patients with chronic bronchitis (Clunes *et al.*, 2012; Bennett *et al.*, 2016).

This defect in mucociliary clearance, due to impaired ASL hydration, is also a hallmark of CF airways, suggesting a common aetiology, i.e. CFTR-mediated Cl^- secretion. In fact, even before the CFTR gene was cloned, Welsh (1983) already showed that anion transport was inhibited by CS exposure. Indeed, measuring the transepithelial nasal and lower airway potential difference (PD) *in vivo* of smokers, with or without COPD, revealed that cAMP-activated, Cl^--dependent change in PD was abolished compared to non-smoking subjects, indicating defective Cl^- secretion, a similar trait seen in CF patients (Cantin *et al.*, 2006b; Clunes *et al.*, 2012; Sloane *et al.*, 2012; Dransfield *et al.*, 2013). CFTR-mediated sweat Cl^- secretion was also impaired in COPD patients, suggesting a systemic downregulation of CFTR function (Raju *et al.*, 2013; Courville *et al.*, 2014).

1.5.2 Cigarette smoke disrupts CFTR function and Ca^{2+} homeostasis in airway epithelial cells

Over the past decade, evidence has emerged regarding the cellular and molecular mechanisms of acquired CFTR defects in response to cigarette smoking. In cell cultures, overnight exposure to CSE inhibited cAMP-activated, CFTR-mediated Cl^- secretion in various epithelial cell lines (Cantin *et al.*, 2006b), primary human bronchial epithelial cells (Kreindler *et al.*, 2005; Sloane *et al.*, 2012; Raju *et al.*, 2017a), and intact human bronchial tissue (Raju *et al.*, 2017a). This was replicated by incubating the cells with plasma acquired from smoker, suggesting that CFTR inhibition was caused by water-soluble, circulating components of CS (Raju *et al.*, 2013). On the other hand, potentiating CFTR with ivacaftor, or activating cAMP-dependent activation of CFTR with roflumilast, restored CS-induced downregulation of CFTR activity, as well as ASL hydration and mucociliary transport (Sloane *et al.*, 2012; Raju *et al.*, 2017a; Raju *et al.*, 2017b). It has also been shown that exposure to CS condensate inhibited Ca^{2+}-activated Cl^- and voltage-dependent K^+ channels in human and mouse airway epithelial cells, potentially further amplifying the ASL dehydration in COPD smokers (Virgin *et al.*, 2010; Sailland *et al.*, 2017).

The reduction in CFTR activity was associated with diminished CFTR mRNA and protein following CS or CSE exposure in human bronchial epithelial cells, with significant downregulation observed within 10 min of exposure (Cantin *et al.*, 2006b; Clunes *et al.*, 2012;

Sloane *et al.*, 2012). This is consistent with the finding that CFTR protein expression was reduced in the lower airway tissues of COPD smokers (Dransfield *et al.*, 2013). The downregulation of CFTR protein can be attributed to CS-induced internalisation of CFTR into an aggresome-like perinuclear compartment, with surface expression of CFTR significantly reduced within 10 min of CS exposure (Clunes *et al.*, 2012; Rasmussen *et al.*, 2014). The internalisation of CFTR was dependent on the rise in intracellular Ca^{2+} released from lysosomes, observed in several epithelial cell lines as well as primary bronchial epithelial cells (Rasmussen *et al.*, 2014). More recent studies discovered that the internalised CFTR underwent retrograde trafficking to the ER, mediated by clathrin- and dynamin-dependent endocytosis (Marklew *et al.*, 2019; Patel *et al.*, 2019). This trafficking mechanism relied on dephosphorylation of CFTR by calcineurin, a Ca^{2+}-dependent phosphatase, highlighting the importance of Ca^{2+} signalling in mediating CS-induced ASL dehydration (Marklew *et al.*, 2019; Patel *et al.*, 2019). This is especially pertinent as Ca^{2+} homeostasis is dysregulated in CF airway epithelial cells (see below in section 1.6.1).

Other than causing internalisation, CS may also directly affect CFTR channel activity. For instance, acrolein, a component of CS that was found to be higher in the serum of smokers with COPD, directly inhibited CFTR gating (Raju *et al.*, 2013; Raju *et al.*, 2017a). The inhibitory effect of acrolein was blunted by the antioxidant NAC, suggesting an involvement of oxidative stress in inhibiting CFTR function (Raju *et al.*, 2013). Indeed, it has been shown that ROS/RNS can downregulate CFTR expression and consequently airway epithelial Cl^- secretion (Bebok *et al.*, 2002; Cantin *et al.*, 2006a). Interestingly, however, Wong *et al.* (2017) reported that acute exposure to low concentrations of CSE enhanced CFTR-mediate Cl^- secretion through ROS-mediated cAMP signalling, whereas prolonged exposure led to downregulation of CFTR functional expression as previously described, indicating time- and concentration-dependency of the action of CS on CFTR activity.

Altogether, current evidence suggests that CS-induced downregulation of CFTR activity and function in airway epithelia is, at least partially, responsible for chronic ASL dehydration and impaired mucociliary clearance in smokers.

1.6 CFTR regulates Ca^{2+} homeostasis in both airway epithelial cells and ASMC

1.6.1 Dysfunction of Ca^{2+} homeostasis in CF epithelial cells

Ca^{2+} homeostasis in CF epithelial cells is disrupted at several levels of Ca^{2+} signalling. Note that CF cells in this section refer to epithelial cells expressing homozygous F508del-CFTR, unless otherwise specified.

Agonist-mediated calcium mobilisation is dysregulated in CF epithelial cells. Two studies in the 90's reported that calcium responses to histamine and PGE_2 were attenuated in CF epithelial cells (Reinlib *et al.*, 1992; Jacquot *et al.*, 1996). However, more recent studies have found enhanced Ca^{2+} mobilisation in CF epithelial cells in response to agonists such as ATP, UTP, bradykinin, and histamine (Paradiso *et al.*, 2001; Ribeiro *et al.*, 2005a; Antigny *et al.*, 2008a; Antigny *et al.*, 2008b; Antigny *et al.*, 2009; Martins *et al.*, 2011). CFTR-associated Ca^{2+} signalling may be compartmentalised, as apical, but not basolateral, administration of UTP and ATP led to a significantly greater Ca^{2+} response in polarised CF cells (Paradiso *et al.*, 2001; Ribeiro *et al.*, 2005a).

The source of the enhanced Ca^{2+} response to these agonists in CF epithelial cells was attributed to enhanced IP_3R activity at the ER (Figure 1.8), as this was inhibited by IP_3R inhibitors and was not dependent on extracellular Ca^{2+} (Antigny *et al.*, 2008b; Antigny *et al.*, 2009; Philippe *et al.*, 2015). This augmented IP_3R activity was due to ER retention of F508del-CFTR, which was normalised following correction of F508del-CFTR trafficking to the PM (Norez *et al.*, 2006; Hybiske *et al.*, 2007; Antigny *et al.*, 2008a; Antigny *et al.*, 2008b). Other than IP_3R activity, ER calcium stores were expanded, and the ER was condensed around the nucleus, in CF cells (Ribeiro *et al.*, 2005a; Antigny *et al.*, 2008b). Moreover, in a CF bronchial epithelial (CFBE) cell line, refilling of ER Ca^{2+} store was faster and of greater amplitude, due to a physical interaction of CFTR with SERCA2b (Philippe *et al.*, 2015). Interestingly, in contrast, mitochondrial Ca^{2+} reuptake was faulty in CF cells due to a depolarised mitochondrial membrane potential compared to non-CF cells, since mitochondrial Ca^{2+} uniporter activity is dependent on membrane potential to drive electrogenic Ca^{2+} uptake into the mitochondrion (Gunter and Pfeiffer, 1990; Antigny *et al.*, 2009). This suggests that CFTR may modulate Ca^{2+} movement across the membrane of intracellular organelles via regulating membrane potential. Together, these findings provide a mechanistic basis for the modulation of ER/SR Ca^{2+} stores by CFTR, possibly by modulating membrane potential or through direct protein-protein interactions, which is highly relevant for ASMC where CFTR is localised primarily to the SR (see section 1.6.3 below).

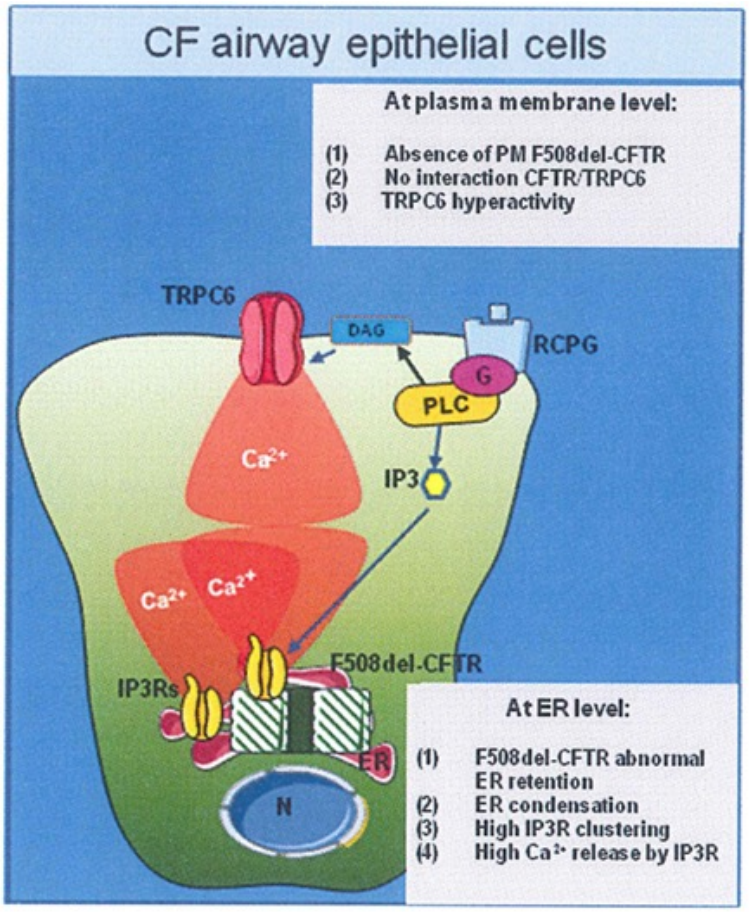

Figure 1.8: Multiple components of Ca^{2+} homeostasis is dysregulated in F508del-CFTR CF airway epithelial cells. The mutant F508del-CFTR is retained in the ER, and is linked to clustering of IP_3R and IP_3R-mediated Ca^{2+} release, as well as expansion and condensation of the ER. The absence of functional CFTR at the plasma membrane, which regulates with TRPC6, leads to enhanced TRPC6-mediated Ca^{2+} influx. Taken from Antigny *et al.* (2011a). Permission to redistribute granted under open access license from Frontiers Media SA.

Other than ER Ca^{2+} release, TRPC6-mediated receptor-activated Ca^{2+} influx was also upregulated in CF cells, due to a loss of physical interaction between CFTR and TRPC6 at the PM (Figure 1.8; (Antigny *et al.*, 2011b)). Similarly, in CF cells, constitutive Ca^{2+} influx via TRPV6 was also upregulated (Vachel *et al.*, 2015). On the other hand, as a consequence of a larger ER Ca^{2+} store, SOCE was also enhanced in CFBE cells (Philippe *et al.*, 2015). Interestingly, the increased ER Ca^{2+} concentration, refilling, and SOCE were normalised following correction of F508del-CFTR trafficking, suggesting that PM-localisation of CFTR is important in regulating these processes (Philippe *et al.*, 2015). However, Balghi *et al.* (2011) found that cyclopiazonic acid (CPA)-induced store depletion was similar in CF and non-CF epithelial cells, but SOCE was still greatly elevated in CF cells. This was attributed to increased exocytotic insertion of Orai1, hence a higher density of Orai1/STIM1 complexes at the PM, during store depletion in CF cells, which was normalised by correcting the trafficking of F508del-CFTR (Balghi *et al.*, 2011). They proposed that CFTR may be recruited to the same

protein microdomain as the Orai1/STIM1 complex following store depletion, where it modulates insertion of Orai1 and hence SOCE. Therefore, in CF epithelial cells, ER retention of F508del-CFTR increases IP_3R-mediated Ca^{2+} release, while its absence from the PM increases TRPC6- and TRPV6-mediated Ca^{2+} influx as well as Orai1-mediated SOCE.

1.6.2 CFTR in cardiac and skeletal muscle

Although the physiology and function of CFTR has been extensively studied in epithelial cells, it is also expressed in muscle cells, and this was first discovered in 1992 in the guinea pig cardiac myocytes (Nagel *et al.*, 1992). CFTR has since been found to be functionally expressed in both atrial and ventricular myocytes of several mammalian species, including human, rabbit, and rat (Warth *et al.*, 1996; Yajima *et al.*, 1997; Lader *et al.*, 2000), and is thought to be localised in clusters on the sarcolemmal membrane (James *et al.*, 2010). CFTR plays an important role in modulating the cardiac action potential as well as contractility of cardiac myocytes, and is implicated in various cardiac diseases including heart failure, right ventricular dysfunction, arrhythmia, and sudden death (Gadsby *et al.*, 1995; Vizza *et al.*, 1998; Wong *et al.*, 2000; Kuzumoto *et al.*, 2008; Solbach *et al.*, 2008; Duan, 2009; Sellers *et al.*, 2010; Ye *et al.*, 2011; Jiang *et al.*, 2016).

The skeletal muscle system is also affected in CF; most notably, CF patients showed reduced muscle strength and mass, and exercise intolerance (Hussey *et al.*, 2002; Lamhonwah *et al.*, 2010). In human skeletal muscle, CFTR is localised intracellularly and co-localises with IP_3R and RyR, suggesting localisation to the SR (Divangahi *et al.*, 2009; Lamhonwah *et al.*, 2010). Divangahi *et al.* (2009) found that genetic deletion and pharmacological inhibition of CFTR in mouse diaphragm myotubes led to an enhanced Ca^{2+} increase in response to KCl-induced depolarisation. This larger response was primarily attributed to greater IP_3R-mediated SR Ca^{2+} release, reminiscent of the enhanced Ca^{2+} release in F508del-CF epithelial cells (Antigny *et al.*, 2008b; Divangahi *et al.*, 2009).

1.6.3 CFTR regulates smooth muscle cell Ca^{2+} homeostasis

In addition, recent evidence has also pointed to the expression of CFTR mRNA and/or protein in mammalian airway and vascular smooth muscle cells (Robert *et al.*, 2004; Vandebrouck *et al.*, 2006; Robert *et al.*, 2007; Michoud *et al.*, 2009; Norez *et al.*, 2014; Cook *et al.*, 2016). On a western blot, CFTR from WT porcine ASMC appeared as a 180kDa protein band known as band C, representing the fully-glycosylated form of CFTR (Cheng *et al.*, 1990; Cook *et al.*, 2016). Immunofluorescence studies revealed a diffuse pattern of CFTR expression in both the PM and intracellularly, with intracellular CFTR localising to the SR (Vandebrouck *et al.*, 2006; Norez *et al.*, 2014; Cook *et al.*, 2016). In rat tracheal smooth muscle cells, Vandebrouck *et al.*

(2006) noted highly similar pharmacological profiles of various CFTR activators and inhibitors on CFTR-induced ion flux to those in epithelial CFTR in iodide-efflux studies.

CFTR modulates the vascular SM (VSM) tone and contractility, as putative CFTR activators produced relaxation of rat aortic and intrapulmonary arterial rings, which was severely impaired in aortic rings from $CFTR^{-/-}$ mice (Robert *et al.*, 2004; Robert *et al.*, 2005; Robert *et al.*, 2007). Interestingly, Guo *et al.* (2014) reported reduced aortic vascular tone as well as constriction response to KCl in homozygous F508del-CFTR piglets, which was recapitulated with the combined inhibition of RyR and IP_3R in WT aorta, suggesting that F508del-CFTR may negatively regulate the SR Ca^{2+} release pathways. In terms of Ca^{2+} homeostasis, F508del-CFTR VSM cells had diminished Ca^{2+} response to the agonist angiotensin II, whereas $CFTR^{-/-}$ VSM had a lower resting Ca^{2+} baseline (Guo *et al.*, 2014).

On the other hand, CFTR in ASMC also regulates Ca^{2+} homeostasis, and hence muscular tone and contractility. In early clinical studies, airway hyperresponsiveness to histamine and methacholine was found in 40-56% of CF patients studied, suggesting a potential link between CF and other respiratory diseases involving airway hyperresponsiveness (Mitchell *et al.*, 1978; Van Asperen *et al.*, 1981; van Haren *et al.*, 1992). More recently, Cook *et al.* (2016) found that CFTR inhibition with GlyH-101 significantly increased basal tone of WT airway smooth muscle strips. Furthermore, isoproterenol treatment led to a ~10% bronchodilation in lung slices of $CFTR^{-/-}$ pigs, but not WT pigs, at resting state, indicating a basally constricted tone in airway lacking CFTR function. The increased basal tone may be attributed to elevated baseline levels of MLC phosphorylation in both the trachealis muscle and cultured primary ASMC from these CF pigs (Cook *et al.*, 2016).

Other than regulating basal tone, CFTR activators relaxed rat and human epithelium-denuded tracheal rings pre-constricted by carbachol in a dose-dependent manner (Vandebrouck *et al.*, 2006; Norez *et al.*, 2014). In both studies, this bronchodilation was inhibited by $CFTR_{inh}$-172 (Vandebrouck *et al.*, 2006; Norez *et al.*, 2014). Building on this, Cook *et al.* (2016) reported that cholinergic-induced bronchoconstriction was inhibited by ~50% when porcine lung slices were pre-treated with the CFTR potentiator ivacaftor, and this inhibition was not present in $CFTR^{-/-}$ pigs, indicating specific CFTR-dependent inhibition of bronchoconstriction. Ivacaftor may be able to stimulate CFTR function even if the protein is localised to the SR, as it is cell-permeable. To explore the impact of these findings on CF patients, Adam *et al.* (2016) targeted G551D-CFTR patients, featuring CFTR gating defects, with ivacaftor administration. Within 48 hours of treatment, they found marked improvements in airway function, including reduced airway obstruction and air trapping, and increased distensibility of small airways.

However, the cellular mechanisms of CFTR's regulation of Ca^{2+} homeostasis and AHR are less well-characterised. Despite hypercontractility of the CF airway, the trachea of $CFTR^{-/-}$ mice had reduced sensitivity and contractility in response to carbachol, which was not found using other agonists, suggesting a specific dysregulation of the cholinergic, IP_3-mediated Ca^{2+} release from the SR (Bonvin *et al.*, 2008; Wallace *et al.*, 2013). Accordingly, the peak Ca^{2+} response to IL-8 and histamine were diminished in F508del-CFTR ASMC (Govindaraju *et al.*, 2008; Michoud *et al.*, 2009). Interestingly, in contrast, Cook *et al.* (2016) did not observe a significantly different peak Ca^{2+} response to ACh in $CFTR^{-/-}$ ASMC (Figure 1.9A-C). While Cook *et al.* (2016) used ASMC from $CFTR^{-/-}$ pigs, the ASMC studied by Michoud *et al.* (2009) were isolated from human CF patients, all with the F508del mutation. This suggests that the regulation of Ca^{2+} mobilisation by CFTR may well be genotype-dependent. However, a delayed recovery of $[Ca^{2+}]_i$ after the ACh response was noted (Figure 1.9D-E), suggesting that pathways involved in Ca^{2+} reuptake or extrusion were impaired in CF ASM. In essence, compared to WT ASMC, F508del-CFTR ASMC exhibited diminished agonist-mediated Ca^{2+} response and faster recovery, while $CFTR^{-/-}$ ASMC had the same peak Ca^{2+} response but a delayed recovery (Michoud *et al.*, 2009; Cook *et al.*, 2016). These results suggest that CFTR plays a complex role in regulating Ca^{2+} homeostasis, including aspects of Ca^{2+} influx, SR store release, and recovery pathways, in ASMC. However, the mechanisms behind this interaction remain unclear, and so another aim of the thesis was to investigate this in more detail.

* Image removed from e-thesis due to copyright.*

Figure 1.9: Abnormal recovery following ACh-induced Ca^{2+} response in porcine $CFTR^{-/-}$ ASMC. (A) Representative traces of ACh-induced (arrowhead) Ca^{2+} response in ASMC. (B, C) Resting Ca^{2+} levels (B) and peak Ca^{2+} response to ACh (C). (D) Normalised recovery of intracellular Ca^{2+} following ACh stimulation (arrowhead) over time. (E) Percent peak recovery of intracellular Ca^{2+} following ACh stimulation. * = $p<0.05$. Adapted from Cook *et al.* (2016).

1.7 Aims and objectives

In summary, chronic smoking is closely related to the development of chronic bronchitis and emphysema, two main characteristics of COPD, and CS exposure is directly associated with various cellular mechanisms contributing to airway inflammation, remodelling, and hyperresponsiveness. Additionally, CS also disrupts mucociliary clearance through inhibition of CFTR activity and expression, dehydrating epithelial ASL and aggravating COPD symptoms, through elevation of $[Ca^{2+}]_i$ in airway epithelial cells. CFTR itself also modulates Ca^{2+} signalling in epithelial cells and ASMC.

However, whether acute exposure to CS/CSE directly affects Ca^{2+} homeostasis and contractility in hASMC remains poorly characterised. Also, the role of CFTR in regulating ASMC Ca^{2+} homeostasis remains an under-explored area. This PhD project aimed to investigate the role of CFTR, as well as direct effects of cigarette smoke, on ASMC function. The main objectives are:

- Investigate the effects of pharmacological modulators of CFTR on Ca^{2+} homeostasis in ASMC and airway epithelial cells.
- Determine the expression and localisation of CFTR in cultured hASMC.
- Characterise the effects of gaseous CS and diluted CSE on Ca^{2+} homeostasis and contractile signalling mechanisms in hASMC isolated from multiple donors.
- Identify cellular mechanisms responsible for CS-induced disruption in Ca^{2+} homeostasis and contractile signalling in hASMC.
- Compare and contrast the effects of gaseous CS and aqueous CSE in disrupting hASMC function.

Chapter 2: Materials and Methods

2.1 Reagents

Reagents used in this project were purchased from Sigma-Aldrich (Gillingham, UK) unless otherwise specified.

2.1.1 Cell culture media

Calu-3 cells were cultured in Eagle's minimum essential medium (EMEM; Sigma-Aldrich M2279); HEK293 cells were cultured in Dulbecco's modified Eagle's medium (DMEM; Sigma-Aldrich D5671); rat and human ASMC were cultured in DMEM/Ham's nutrient mixture F-12 (DMEM/F-12; Sigma-Aldrich D6421).

All culture media were supplemented with 100 U/ml penicillin, 100µg/ml streptomycin, 2mM L-glutamine, 1% non-essential amino-acid (NEAA), and 10% fetal bovine serum (FBS). Smooth muscle cells were serum-starved (same supplements above but without FBS) before Ca^{2+} imaging experiments (see section 2.3.3 and 2.3.4).

2.1.2 Antibodies

Details of the antibodies used in this project for Western blotting (WB), immunoprecipitation (IP), immunofluorescence (IF), and immunohistochemistry (IHC), are listed in Table 2.1.

Primary antibodies				
Target	**Species**	**Product code**	**Source**	**Dilution (WB/IF)**
CFTR	Mouse	CFFT-596	CF Foundation's Antibody Distribution Program (http://cftrantibodies.web.unc.edu/; Chapel Hill, USA)	1:1000 (WB) 1:200-300 (IF) 1:1000 (IP)
CFTR	Rabbit	ACL-006	Alomone Labs (Jerusalem, Israel)	1:500-1000 (WB) 1:200 (IF)
Phospho-myosin light chain (p-MLC)	Mouse	3675S	Cell Signaling Technology (London, UK)	1:500 (WB)
Myosin light chain (MLC)	Mouse	M4401	Sigma-Aldrich	1:1000 (WB)

β-actin	Mouse	A5441	Sigma-Aldrich	1:30,000 (WB)
α-smooth muscle actin	Mouse	A5228	Sigma-Aldrich	1:200-1000 (IF)
h-caldesmon	Mouse	C4562	Sigma-Aldrich	1:20-50 (IHC)
Secondary antibodies				
Mouse IgG, HRP linked	Goat	7076S	Cell Signaling Technology	1:2000-3000 (WB)
Rabbit IgG, HRP linked	Goat	7074S	Cell Signaling Technology	1:2000-3000 (WB)
Protein ladder for western blot; HRP linked	N/A	1610381	Bio-Rad (Watford, UK)	1:5000 (WB)
Mouse IgG, Alexa Fluor 594	Goat	A-11032	Thermo Fisher Scientific (Cramlington, UK)	1:1000 (IF)
Rabbit IgG, Alexa Fluor 488	Goat	A-11034	Thermo Fisher Scientific	1:1000 (IF)

Table 2.1: Details of the primary and secondary antibodies used in this study.

For immunofluorescence, 4',6-Diamidino-2-Phenylindole (DAPI; 1:1000 dilution, Sigma Aldrich D-9542) was also used to counterstain the cell nuclei.

2.1.3 Solutions

The composition of the solution used for Ca^{2+} fluorimetry and Ca^{2+} imaging experiments was a HEPES-buffered solution containing (in mM): 130 NaCl, 5 KCl, 1 $CaCl_2$, 1 $MgCl_2$, 10 4-(2-Hydroxyethyl)piperazine-1-ethanesulfonic acid sodium salt (NaHEPES), 10 D-glucose, with pH adjusted to 7.4 using HCl with constant stirring. For the nominally Ca^{2+}-free solution, $CaCl_2$ was omitted and replaced with 1mM ethylene glycol-bis(2-aminoethylether)-N,N,N′,N′-tetraacetic acid (EGTA; a Ca^{2+} chelator). Solutions were stored at 4°C. D-glucose was added on the day of experiment.

The lysis buffer used for the preparation of Western blot samples was the radioimmunoprecipitation assay (RIPA) buffer (50mM Tris, 150mM NaCl, 1mM ethylenediaminetetraacetic acid (EDTA), 1% Triton-X 100, 0.25% sodium deoxycholate, 0.1%

sodium dodecyl sulfate (SDS)), supplemented with 20µl/ml protease inhibitor (Sigma-Aldrich P8340) and 5µl/ml phosphatase inhibitor (Sigma-Aldrich P5726) cocktails. RIPA buffer was stored at -20°C. Protease and phosphatase inhibitors were added on the day of lysate preparation.

The polyacrylamide gel used for Western blotting consisted of the stacking gel (top) and resolving gel (bottom), made on the day of experiment. The stacking gel composition (for 4x 1.0mm gels; 6.6ml dH_2O, 1.66ml 30% acrylamide (Sigma-Aldrich), 2.5ml 1.0M Tris pH 6.8, 100µl 10% SDS, 50µl 10% ammonium persulfate (APS), 18µl tetramethylethylenediamine (TEMED)) was the same regardless of the acrylamide content in the resolving gel. TEMED was added immediately before gels was poured, under a fume cupboard. For resolving high molecular mass proteins (e.g. CFTR), 8% acrylamide gel (9.3ml dH_2O, 5.3ml 30% acrylamide, 5.0ml 1.5M Tris pH 8.8, 200µl 10% SDS, 200µl 10% APS, 18µl TEMED) was used. For lower molecular mass proteins (e.g. phospho-myosin light-chain (p-MLC)), 12% gel was used (6.6ml dH_2O, 8.0ml 30% acrylamide, 5.0ml 1.5M Tris pH 8.8, 200µl 10% SDS, 200µl 10% APS, 18µl TEMED).

The running buffer (for 1L: 100ml 10x Tris Glycine buffer, 900ml dH_2O, 10ml 10% SDS, pH 8.3) for SDS-polyacrylamide gel electrophoresis (SDS-PAGE), as well as the transfer buffer (for 1L: 100ml 10x Tris Glycine buffer, 200ml methanol, 700ml dH_2O, 10ml 10% SDS, pH 8.3) for Western blot transfer, were diluted from a concentrated Tris Glycine buffer (10x Tris Glycine buffer; 250mM Tris, 1.9M Glycine).

The Tris-buffered saline, Tween 20 (TBS-T; 150mM NaCl, 20mM Tris, 0.1% Tween 20, pH 7.6) was used for Western blot membrane washes and antibody incubation. The phosphate-buffered saline (PBS; in mM: 137 NaCl, 2.7 KCl, 10 phosphate buffer, pH 7.4, Sigma-Aldrich) was used to wash cell cultures before trypsinisation, as well as washes and antibody incubation in IF staining.

2.1.4 Primers

PCR primers were designed using the NCBI Primer-BLAST tool, and purchased from Integrated DNA Technologies (Leuven, Belgium). The primer sequences are listed in Table 2.2.

Primer	Sequence (5' to 3')	Product length	Position on mRNA/rRNA template
CFTR 1 (forward)	AGG AGG CAG TCT GTC CTG AA	237	2363-2382
CFTR 1 (reverse)	CAC TGC TGG TAT GCT CTC CA		2580-2599
CFTR 2 (forward)	AAT GTA ACA GCC TTC TGG GAG	391	1256-1276
CFTR 2 (reverse)	GTT GGC ATG CTT TGA TGA CGC TTC		1623-1646
TRPA1 (forward)	GTG GAA CTT CAT ACC AGC TTA GA	99	3113-3135
TRPA1 (reverse)	AGA TCT GGG TTT GTT GGG ATA C		3190-3211
GAPDH (forward)	TGC ACC ACC AAC TGC TTA GC	87	476-495
GAPDH (reverse)	GGC ATG GAC TGT GGT CAT GAG		542-562
18S (forward)	CTC TAG ATA ACC TCG GGC CG	209	293-312
18S (reverse)	GTC GGG AGT GGG TAA TTT GC		482-501

Table 2.2: Sequences of primers used in qPCR analysis. Primer pairs were designed using the NCBI Primer-BLAST tool.

2.1.5 Pharmacological agents

Thapsigargin, forskolin, $CFTR_{inh}$-172, GlyH-101, HC-030031, felodipine, and cyclopiazonic acid (CPA) were purchased from Tocris (Abington, UK). These drugs were dissolved in dimethyl sulfoxide (DMSO) at the following stock concentrations: 2mM thapsigargin; 100mM forskolin; 50mM $CFTR_{inh}$-172; 100mM GlyH-101; 50mM HC-030031; 100mM felodipine; 100mM CPA, and stored at -20°C.

Tannic acid and adenosine 5′-triphosphate disodium salt (ATP) were from Sigma-Aldrich, and were dissolved in distilled water on the day of experiment at a concentration of 100mM for both agents.

2.1.6 Cigarettes

3R4F reference cigarettes were procured from the Kentucky Tobacco Research & Development Centre, University of Kentucky, USA. This cigarette is a mixture of several tobacco blends (Flue Cured 35.41%, Burley 21.62%, Oriental 12.07%, Maryland 1.35%, Reconstituted (Schweitzer Process) 29.55%, Glycerine (dry-weight basis at 11.6% oven volatiles) 2.67%, Isosweet (sugar) 6.41%). Cigarettes were stored at 4°C, and warmed up to room temperature on the day of experiment.

2.2 Ethical approval

Human tracheal rings were procured from non-smoker excess donor lungs or explanted lungs from Freeman Hospital, Newcastle upon Tyne and the Cystic Fibrosis Centre, UNC Chapel Hill. Ethical approval was obtained for tissue collection from non-smoking unused donor lungs (16/NE/0230), or explanted lungs (11/NE/0291), from Newcastle and North Tyneside Local Regional Ethics Committee, and the University of North Carolina Institutional Review Board (tissue procurement was done in accordance to protocol 03-139 as described previously (Randell *et al.*, 2011)). Informed consent was obtained for procurement of these tissues.

Adult male Sprague-Dawley rats (325-375g) were ordered from Charles River (Margate, UK), and animals were housed in the Comparative Biology Centre, Newcastle University for at least 7 days before culling and tissue collection. Ethical approval for collection of rat tissue was obtained from the Animal Welfare and Ethical Review Board (AWERB; Project ID 628), Newcastle University. Rats were euthanised via CO_2 overdose in accordance to Schedule 1 of Animals (Scientific Procedures) Act 1986, performed by CBC technicians.

2.3 Cell culture

All cell lines and cultured primary cells used in this study were grown in a humidified incubator at 37°C with 5% CO_2. Culture media was replaced every 48-72 hours, performed in aseptic conditions under a class II laminar flow hood.

Cells were typically passaged at 70-90% confluence under aseptic conditions. After removing culture media, cells were washed twice using PBS, and incubated at 37°C for 5 min with 5ml (for T75 culture flask) or 2ml (for T25 culture flask) trypsin solution (0.05% trypsin, 0.02% EDTA) to detach the cells. For Calu-3 cells, 2-3 trypsinisation cycles (15 min each instead of 5 min) were required. Then, the trypsin was inactivated by adding an equal volume of the

complete cell culture media, and cells were centrifuged (1,500g for 5 min). The pellet was resuspended in complete culture media and seeded into cell culture flasks or plates as required. The seeding density for various cell culture vessels is listed in Table 2.3.

Cell type	Culture vessel	Media volume (ml)	Seeding density (# of cells)
Calu-3	T75 culture flask	15	3×10^6
	25mm glass coverslips, in 6-well culture plate (per well)	2	1 to 5×10^5
	6.5mm Transwells (per well)	0.5 apical, 1.5 basolateral	1×10^5
HEK293	T75 culture flask	15	1×10^5
	25mm glass coverslips, in 6-well culture plate (per well)	2	0.5×10^5
rASMC/ hASMC	T25 culture flask	8	1×10^5
	T75 culture flask	15	1 to 3×10^5
	25mm glass coverslips, in 6-well culture plate (per well)	2	0.3 to 1×10^5
	8-well glass chamber slide (per well)	0.8	6×10^3

Table 2.3: Seeding density for Calu-3 cells, HEK293 cells, and cultured rat and human ASMC grown in different cell culture vessels. Variation in seeding density was dependent on when cells would be needed for experiments.

2.3.1 Calu-3

The human lung adenocarcinoma cell line, Calu-3, was cultured in T75 cell culture flasks as described above, and used for experiments up to passage 48.

For Ca^{2+} fluorimetry and imaging, as well as IF experiments, cells were grown on 25mm glass coverslips in 6-well plates. Cells were used for experiments when they have formed a confluent monolayer (Figure 2.1). For Ussing chamber experiments, cells were grown on 6.5mm semi-permeable inserts (Corning Costar® Transwells®, Sigma-Aldrich) until a confluent polarised

monolayer was formed, and cells were used for experiments 10-14 days after seeding. Care was taken to not physically rupture the monolayer when replacing apical media.

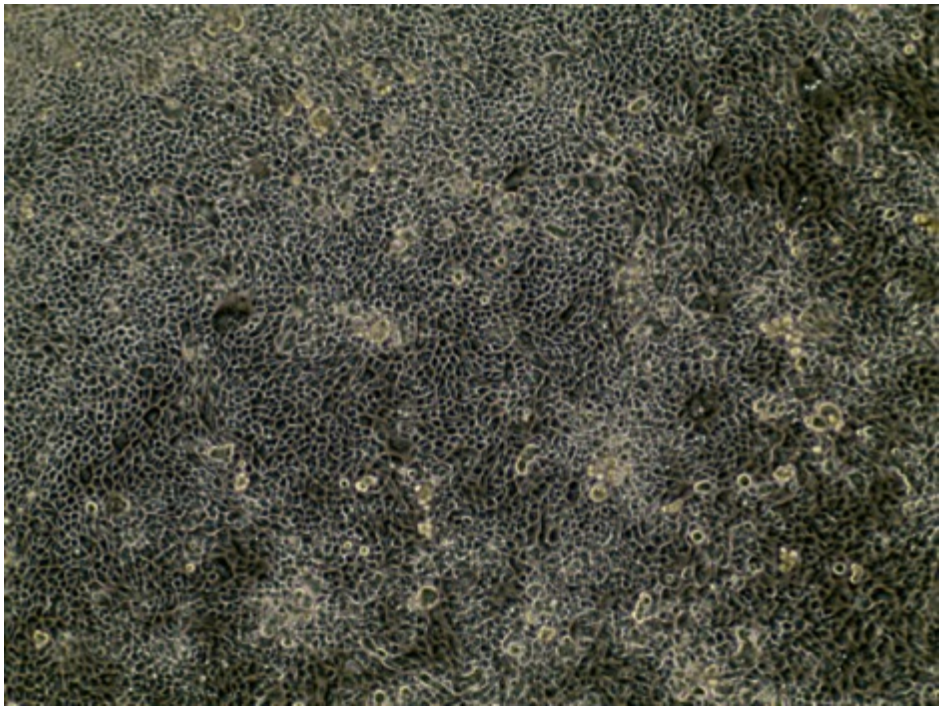

Figure 2.1: Phase contrast image of a confluent Calu-3 monolayer grown on glass coverslip. Photo was acquired at 10x magnification.

2.3.2 HEK293 cells

The human embryonic kidney (HEK) 293 cell line was cultured in T75 cell culture flasks as described above. For Ca^{2+} fluorimetry experiments, cells were grown on 25mm glass coverslips, and used for experiments when a confluent monolayer was formed.

2.3.3 rASMC

The intact trachea was surgically removed from adult male Sprague-Dawley rats following Schedule 1 culling, and placed in sterile PBS on ice. Connective tissue around the trachea was carefully removed, and the tracheal tube was cut open on the anterior side into a sheet. The cartilage portions were trimmed as much as possible, leaving the sheet of smooth muscle, located posteriorly.

The isolation protocol of ASMC was modified from Panettieri (2001). Briefly, dissected smooth muscle tissue was digested using an enzyme mix (2 mg/ml collagenase IV (Thermo Fisher Scientific 17104019), 3 mg/ml elastase (LS002292 Worthington Biochemical, Reading, UK), 1 mg/ml trypsin inhibitor (Sigma-Aldrich T6522), 1mM EGTA dissolved in M199 media) at 37°C for at least 60 min with constant shaking, until the released cells and tissue debris were visible in the media. The mixture was then filtered through a 100 μm cell strainer to exclude

large tissue pieces, and an excess volume (at least 5x enzyme mixture volume) of the complete DMEM/F-12 culture media was added to deactivate the enzymes. The mixture was centrifuged (1,500g for 5 min), the pellet resuspended in DMEM/F-12 media, and cells were seeded into a T25 culture flask.

Cells typically attached within 48 hours, and the typical elongated morphology of ASMC was observed 3-5 days post-isolation (Figure 2.2). Excess rASMC in passage 1 were frozen down (2.5 x 10^5 cells per 1ml vial) using freezing media (50% complete DMEM/F-12 media, 40% FBS, 10% DMSO). The vials of cells were placed in a Nalgene Mr. Frosty^{TM} Freezing Container, filled with isopropanol, and kept in -80°C overnight, before being transferred to liquid nitrogen for long-term storage.

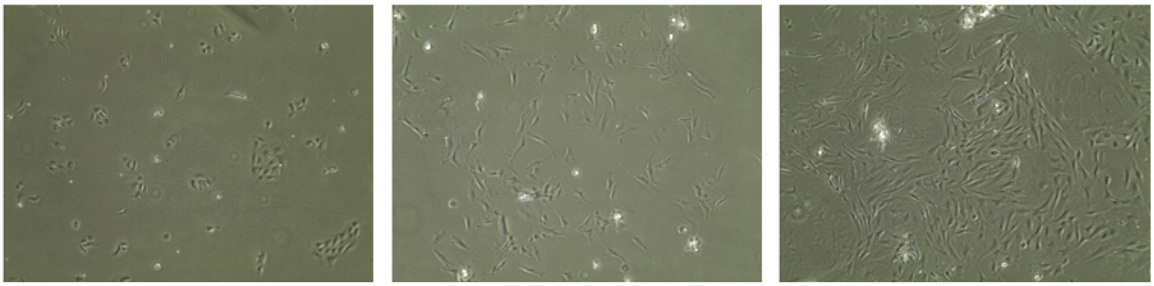

Figure 2.2: Phase contrast images of isolated rat ASMC grown in a T25 cell culture flask, at different stages after isolation. The elongated morphology was observed typically 3-5 days post-isolation. Photos were acquired at 10x magnification.

Cultured primary rASMC were stained for α-smooth muscle actin (α-SMA) and imaged by IF (Figure 2.3A), and h-caldesmon by IHC (Figure 2.3B), to ascertain smooth muscle identity of the isolated cells (see section 2.11 and 2.12 for IF/IHC methods). Cultured rASMC up to passage 8 were used for experiments. For IHC staining, cells were grown on glass chamber slides (Falcon 8 well culture slide, Scientific Laboratory Supplies, Nottingham, UK) until 30-50% confluence. For Ca^{2+} imaging and IF experiments, cells were grown on 25mm glass coverslips until ~60-90% confluence (Ca^{2+} imaging) or ~40-60% confluent (IF). Culture media was replaced with serum-free DMEM/F-12 (DMEM/F-12^{-FCS}) for 48-72 hours before Ca^{2+} imaging experiment, in order to promote a contractile instead of proliferative smooth muscle phenotype (Ma *et al.*, 1998).

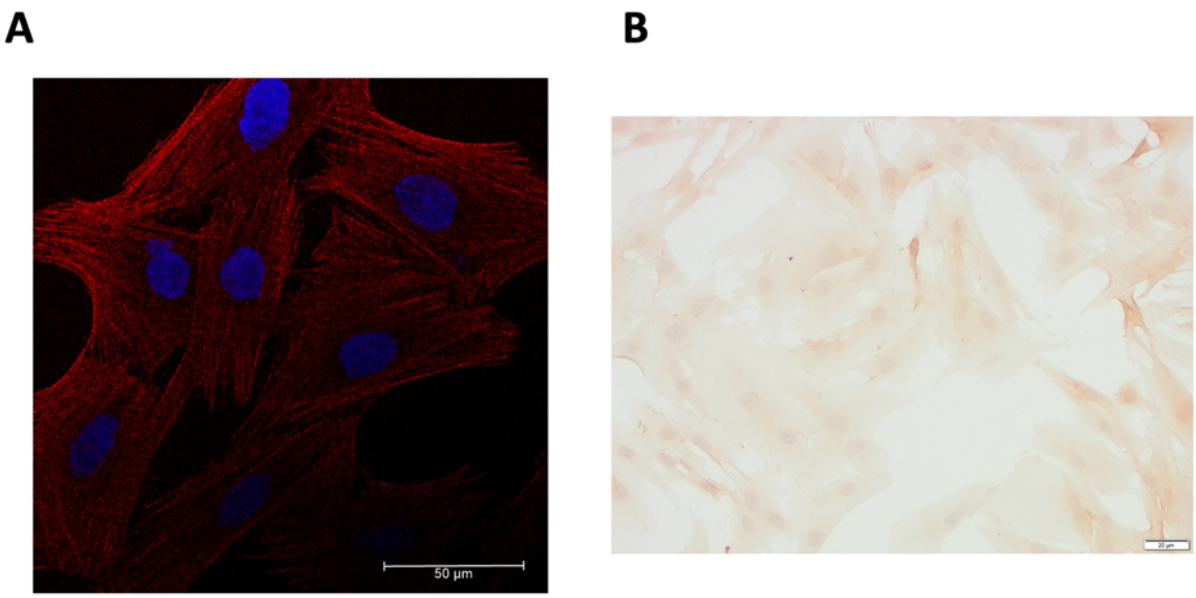

Figure 2.3: Smooth muscle markers in cultured primary rASMC. (A) Representative immunofluorescence image of methanol-fixed rASMC at passage 5, stained for α-smooth muscle actin (red; 1:1000 dilution). Cell nuclei were stained with DAPI (blue). Photo was acquired at 63x magnification and scale bar represents 50µm. (B) Representative immunohistochemistry image of methanol-fixed rASMC at passage 6, stained for h-caldesmon (brown; 1:20 dilution). Photo was acquired at 20x magnification and scale bar represents 20µm.

2.3.4 hASMC

Primary hASMC were isolated from tracheal rings procured from non-smoking adult donor lungs. The tracheal ring was immersed in ice cold PBS, and a piece of smooth muscle tissue, located posteriorly, was cut from the tracheal ring. The cartilage of the ring was discarded. The piece of smooth muscle was carefully trimmed free of connective tissue, and cut into small (~1mm cubes) pieces. The pieces of smooth muscle tissue were enzymatically digested, and released cells filtered and seeded into a T25 culture flask, as described in the rASMC section.

Isolated hASMC typically attached within 24 hours, exhibiting the typical elongated ASMC morphology 1-3 days post-isolation (Figure 2.4). Excess cells were frozen down as described above. Isolated hASMC from a total of 7 non-smoking donors were used for experiments presented in this thesis, with the distribution of usage indicated in Table 2.4; most of the major results were replicated in cells from at least 3 independent donors (indicated in figure legends in results).

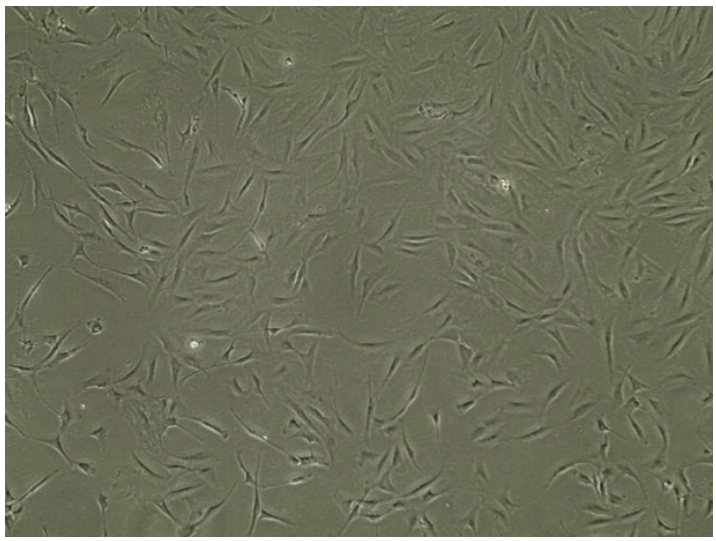

Figure 2.4: Phase contrast image of isolated human ASMC grown in a T25 cell culture flask, 14 days after isolation. The elongated morphology was observed typically 1-3 days post-isolation. Photo was acquired at 10x magnification.

Donor	Used for experiments presented in:
NCL 1	Figure 10, 11 in Chapter 3.
NCL 2	All Figures except 4, 16, 19 in Chapter 4.
NCL 3	Figure 7, 12 in Chapter 4.
UNC 1	All Figures in Chapter 5.
UNC 2	Figure 2, 3, 4, 5, 6, 7, 8, 10, 11, 16, 18, 19, 20, 21, 22, 23, 24, 25 in Chapter 4. All Figures except 3, 6, 7A-B, 12 in Chapter 5.
UNC 3	Figure 2, 3, 4, 5, 6, 7, 8, 10, 13, 16, 18, 19, 20, 21, 22, 23, 25. All Figures except 3, 4, 5, 6, 7A-B, 12 in Chapter 5.
UNC 4	All Figures except 3, 7A-B, 12 in Chapter 5.

Table 2.4: Distribution of hASMC from 7 non-smoking donors in experiments presented in this thesis. NCL = tissue acquired in Newcastle; UNC = tissue acquired in Chapel Hill, USA.

Cultured primary hASMC were also stained with α-SMA (Figure 2.5A) and h-caldesmon (Figure 2.5B) for validation of smooth muscle lineage. α-SMA staining was detected in IF for all donors used for experiments, up to passage 8 of subculture in the same donor (NCL 2; Figure 2.5A). hASMC up to passage 8 were used for experiments. For IHC staining, cells were grown on glass chamber slides until 30-50% confluence. For Ca^{2+} imaging experiments, shRNA transfection, and IF, hASMC were seeded onto 25mm glass coverslips, and grown in 6-well

plates until ~60-90% confluent (Ca^{2+} imaging) or ~40-60% confluent (transfection, IF). For the MLC phosphorylation assay, hASMC were seeded directly onto 6-well plates until fully confluent. Cells were serum-starved for 48-72 hours before Ca^{2+} imaging experiments or MLC phosphorylation assay.

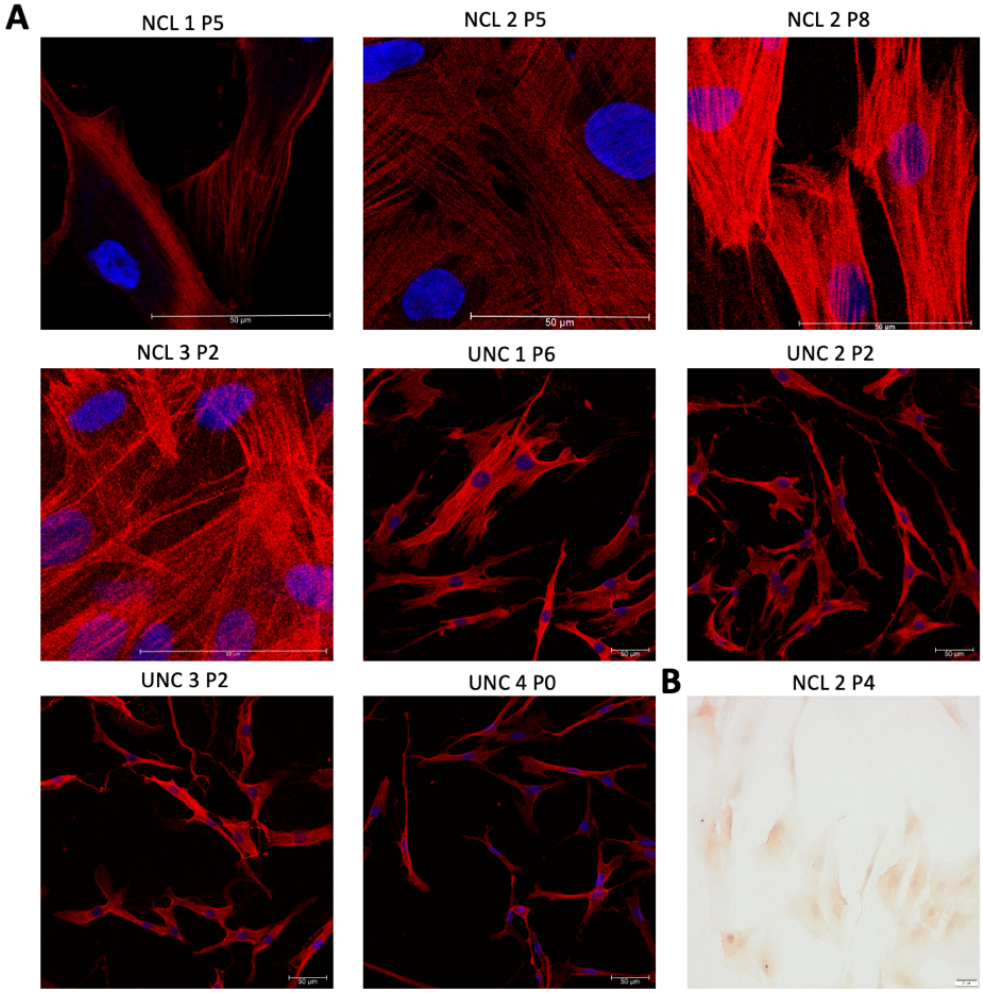

Figure 2.5: Smooth muscle markers in cultured primary hASMC. (A) Representative immunofluorescence image of methanol-fixed hASMC, from 7 different donors and various passage numbers (indicated by "P"), stained for α-smooth muscle actin (red; 1:500 dilution). Cell nuclei were stained with DAPI (blue). Photos were acquired at 63x magnification for NCL donors and 40x magnification for UNC donors. Scale bars represent 50µm. (B) Representative immunohistochemistry image of methanol-fixed hASMC, stained for h-caldesmon (brown; 1:20 dilution). Photo was acquired at 20x magnification and scale bar represents 20µm.

2.4 Measurement of intracellular Ca^{2+}

2.4.1 Ca^{2+} fluorimetry

Intracellular Ca^{2+} ($[Ca^{2+}]_i$) was measured using the ratiometric Ca^{2+}-sensitive fluorescent indicator fura-2-acetoxymethylester (fura-2-AM; Thermo Fisher Scientific) (Grynkiewicz *et al.*, 1985). Cells grown on 25mm glass coverslips were washed twice with HEPES-buffered solution, incubated with 5µM fura-2-AM for 60 mins at room temperature (Calu-3 and HEK293

cells) or 37°C (rat and human ASMC). Cells were then washed twice with HEPES-buffered solution, and left for 15 mins to de-esterify. The coverslip was then placed into a plastic chamber, and mounted onto a Nikon epifluorescence microscope with a 40x oil-immersion lens, equipped with filter wheels for appropriate wavelengths and a photomultiplier to collect emitted fluorescence. Fura-2 was excited alternately, for 250ms each, at 340nm (excites the Ca^{2+}-bound form of fura-2) and 380nm (excites the Ca^{2+}-unbound fura-2) of light, and emission was captured at 510nm; the 340/380 emission ratio (F340/380) of fura-2 fluorescence reflects intracellular Ca^{2+} levels. Ca^{2+} measurements were recorded continuously, at room temperature in a dark room, controlled using the InCyt Pm2™ software (Intracellular Imaging Inc., Ohio, USA). Background fluorescence reading was performed at the start of each experiment day, using cells that were not loaded with fura-2, and this reading was subtracted from the total fluorescence measurements. A perfusion system utilising peristaltic pumps was set up at an exchange rate of 3ml/min, with a total bath volume of 1ml, to allow for changes in perfusion solutions during an experiment.

The raw data was exported to Excel, and parameters of Ca^{2+} responses were analysed by manually selecting appropriate data points (illustrated in Figure 2.6). The rate of Ca^{2+} responses was estimated by linear regression, fitted onto the steepest portion of the $[Ca^{2+}]_i$ increase. Degree of fit was validated through R^2 values, typically >0.9.

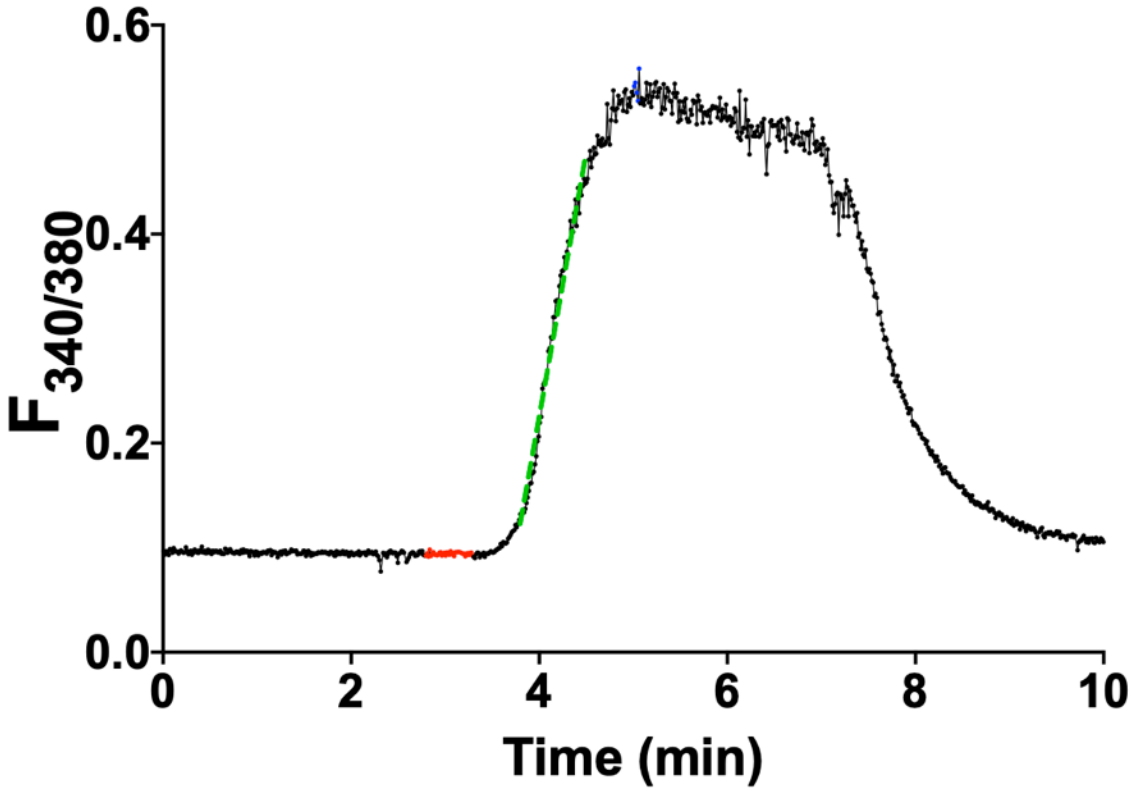

Figure 2.6: Quantification of Ca^{2+} response parameters. Analysis of different parameters is illustrated through a typical store-operated Ca^{2+} entry response in Calu-3 cells. Baseline value was taken as average of red points (typically 30 s before a calcium response was initiated through switching perfusion solution). Peak value was taken as average of blue points (at least 5 points at the peak). The amplitude of a Ca^{2+} response was calculated as peak – baseline. Rate of influx was acquired by performing linear regression (green line, fitted to the steepest increase).

2.4.2 Ca^{2+} imaging

Cells grown on glass coverslips were loaded with fura-2-AM as described above. Coverslips were placed into a plastic chamber, and mounted onto a Nikon epifluorescence microscope equipped with a 20x lens and appropriate filters for excitation and collection of fura-2 fluorescence. Real-time images of the cells were visualised and acquired through a Princeton Instruments (for experiments performed in Newcastle) or Hamamatsu (experiments performed in Chapel Hill) CCD camera, and controlled through the Molecular Devices MetaFluor® or the Hamamatsu HCImage software, respectively. From the images, single cells were circled as regions of interest (ROI; typically 10-20 cells were randomly selected, and were as evenly spaced as possible to include cells from each quadrant), as illustrated in Figure 2.7. Image acquisition was not continuous in order to minimise photobleaching. Images were acquired every 15 s; this interval was changed to 5 s for the influx phase of rapid Ca^{2+} responses (e.g. ATP-induced Ca^{2+} response, CSE-activated Ca^{2+} influx). The $F_{340/380}$ ratios of single cells in the same experiment were averaged for each time point, and data was analysed on the averaged trace. The analysis of Ca^{2+} response parameters was performed similarly as illustrated in Figure

2.6, but fewer points (typically 5 points for baseline, and 1 point for peak) were used for measurement of baseline and peak values, due to longer interval between image acquisitions.

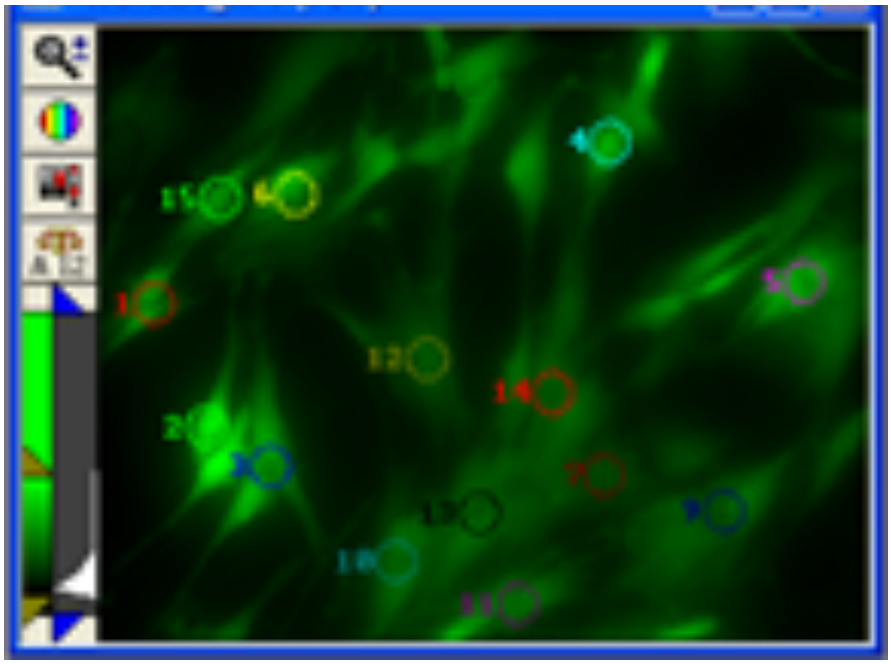

Figure 2.7: Representative illustration of ROI selection in Ca^{2+} imaging experiments. Cells grown on glass coverslips were imaged under 20x magnification. Single cells were circled, with equal number of cells circled in each quadrant wherever possible.

For experiments involving exposure to CS, cells were left in a static bath (1 ml HEPES-buffered solution) and were covered with a customised chamber with tubing connected to the smoke machine for CS delivery (see section 2.5.2). For other experiments, a perfusion system was set up as described in the Ca^{2+} fluorimetry section, with an exchange rate of 2ml/min. All experiments were performed at room temperature.

2.5 Exposure to CS and CSE

2.5.1 Preparation of CSE

The stock solution of 100% CSE was produced by bubbling one 3R4F reference cigarette into 25ml of the HEPES-buffered solution. This was performed manually using a 50ml syringe, with tubing connected to the bud of the cigarette, to aspirate smoke from a lit cigarette, and then the smoke was bubbled into the HEPES-buffered solution (Figure 2.8A). The stock CSE solution was made fresh at the beginning of each day of experiments and kept on ice throughout the day. CSE was diluted into HEPES-buffered solution (with 1mM Ca^{2+} or $0Ca^{2+}$ depending on experiment) for use immediately prior to each experiment.

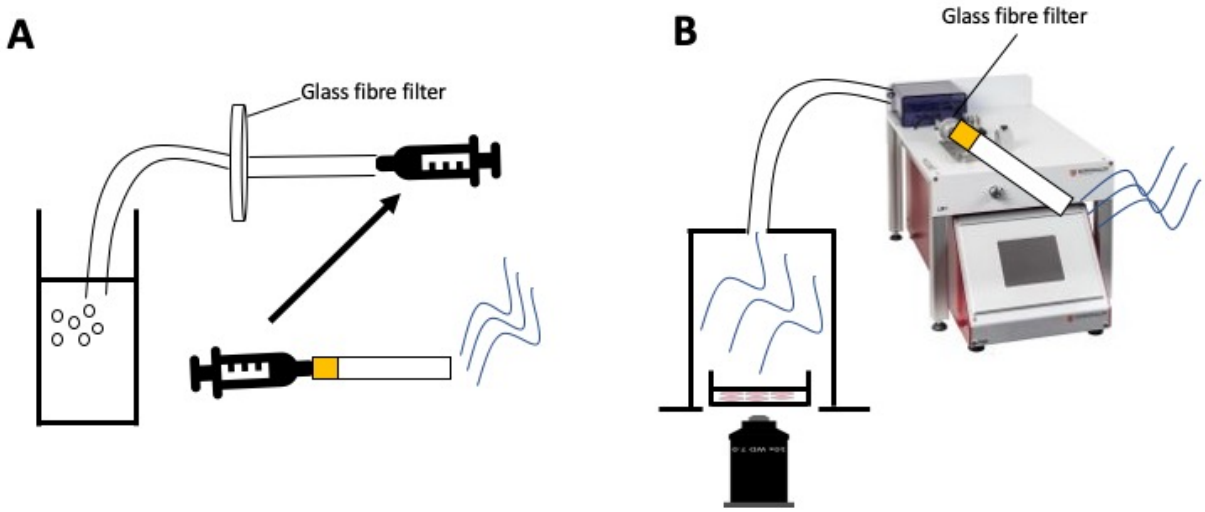

Figure 2.8: Schematic representation of CSE preparation (A) and exposure to gaseous CS (B). The particulate phase of the mainstream smoke was filtered before bubbling into a buffer solution (A) or direct exposure through a smoke chamber (B).

A glass fibre Cambridge filter pad (0.3µm pore size) was placed in the tubing to filter out the particulate tar phase, since the particulate phase was autofluorescent at wavelengths exciting fura-2, even when diluted to working concentrations as low as 5% on a blank coverslip in the absence of any cells or dye (Figure 2.9A). After filtering the smoke before bubbling into solution, the autofluorescence deflection induced by 100% CSE was minimal, in contrast with that induced by 100% unfiltered CSE (Figure 2.9B). At 10%, filtered CSE had no effect on the baseline of fura-2 fluorescence ratio (Figure 2.9C).

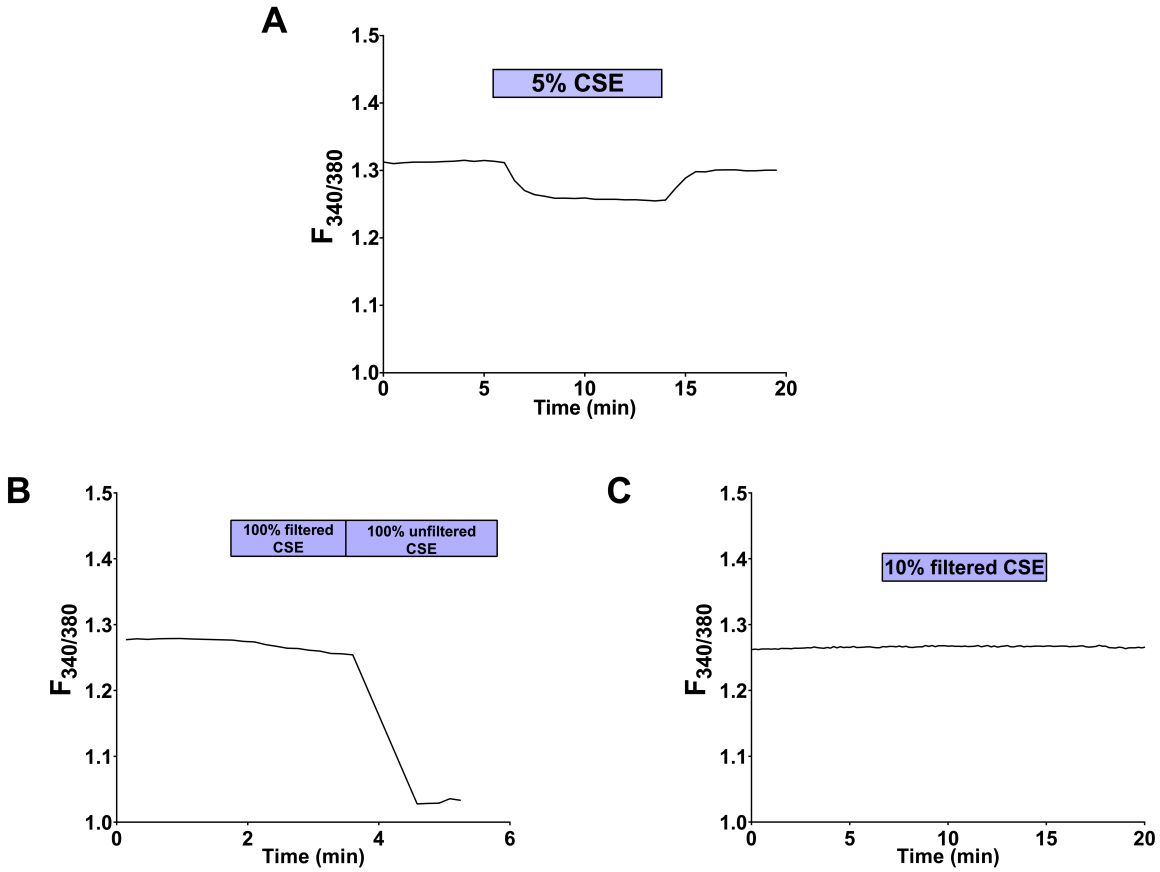

Figure 2.9: CSE containing the particulate phase is autofluorescent at wavelengths exciting fura-2. All four traces are Ca^{2+} imaging traces with empty, cell-free coverslips, perfused with diluted CSE of various concentrations and filtering procedures. (A) Unfiltered CSE. (B) CSE produced with the particulate phase filtered out using the Cambridge filter pad, in contrast with unfiltered CSE. (C) Working concentration of particulate-filtered CSE is not autofluorescent.

2.5.2 Exposure to gaseous CS

CS generated from one Kentucky 3R4F reference cigarette was delivered through a Borgwaldt LM1 smoke engine (Hamburg, Germany), into a closed chamber in which hASMC were situated (Figure 2.8B), with the particulate phase filtered out as described above. Exposure of hASMC to CS was carried out in 13 puffs with a 30 s interval in between; each puff was 35ml, delivered over a duration of 2 s, in accordance to the standard agreed upon by the International Standardization Organization (International Organization for Standardization, 2012). CS persists in the closed chamber after delivery for the full duration of each experiment. Exposure to room air, with identical puff delivery conditions, but with a different set of tubing and chamber not previously exposed to CS, was used as a control.

2.6 Ussing chamber

Media was removed from both apical and basolateral sides of polarised Calu-3 cells, grown on 6.5mm semi-permeable inserts, and these were washed twice with HEPES-buffered solution.

The washed inserts were mounted onto the EasyMount Ussing Chamber Systems (EM-CSYS-6; Physiologic Instruments, San Diego, USA); up to 6 inserts were mounted to perform experiments in parallel, according to manufacturer's instructions. Cells were bathed in HEPES-buffered solution on both the apical and basolateral side, bubbled with 100% O_2, and maintained at 37°C using a circulating water bath. Cells were left to equilibrate for at least 30 minutes before the start of experiment. Addition of pharmacological agents was performed according to experimental protocols, directly into either the apical or basolateral side of the bath.

Voltage (Ag-AgCl pellet electrode) and current (Ag wire electrode) electrodes were immersed in 3M KCl solution, topped with an agar salt bridge (4% agar in 3M KCl). One of each electrode was attached to each side of the Ussing chamber, and connected to a VCC MC6 multichannel clamp (Physiologic Instruments) to monitor transepithelial resistance (TER) and short-circuit current (I_{SC}) across the epithelial membrane. The membranes were voltage-clamped to 0 mV, and real-time measurements of TER and I_{SC} were recorded by injecting current pulses across the membrane every 10 s, through the Acquire and Analyze software (Physiologic Instrument). The I_{SC}, representing the summation of ion currents across the membrane, was normalised to the membrane area of 0.33cm^2.

2.7 shRNA-driven knockdown

2.7.1 Isolation of plasmid DNA from bacterial stocks

Glycerol stocks of bacteria carrying the plasmid vector encoding shRNA targeted against TRPA1 (TV) or the empty control vector (EV) were procured from Lenti-shRNA Core Facility, UNC Chapel Hill, and stored at -80°C until use. The target sequence and oligo sequences of each shRNA construct are presented in Table 2.5.

Clone ID	Target Sequence (5' to 3')	Oligo sequence (5' to 3')
TRCN0000044799 "A12"	CGA GAC TAT TAT ATC GAG TAT	Forward: CCG GCG AGA CTA TTA TAT CGA GTA TCT CGA GAT ACT CGA TAT AAT AGT CTC GTT TTT G
		Reverse: AAT TCA AAA ACG AGA CTA TTA TAT CGA GTA TCT CGA GAT ACT CGA TAT AAT AGT CTC G
TRCN0000044800 "B1"	GCA ATG TTC TTG AAT GGA TTA	Forward: CCG GGC AAT GTT CTT GAA TGG ATT ACT CGA GTA ATC CAT TCA AGA ACA TTG CTT TTT G
		Reverse: AAT TCA AAA AGC AAT GTT CTT GAA TGG ATT ACT CGA GTA ATC CAT TCA AGA ACA TTG C
TRCN0000044801 "B2"	CCA CAA ATA ATA GCG AAG CAT	Forward: CCG GCC ACA AAT AAT AGC GAA GCA TCT CGA GAT GCT TCG CTA TTA TTT GTG GTT TTT G
		Reverse: AAT TCA AAA ACC ACA AAT AAT AGC GAA GCA TCT CGA GAT GCT TCG CTA TTA TTT GTG G
TRCN0000044802 "B3"	CCT CCG AAA CTT CAA CAT GAT	Forward: CCG GCC TCC GAA ACT TCA ACA TGA TCT CGA GAT CAT GTT GAA GTT TCG GAG GTT TTT G
		Reverse: AAT TCA AAA ACC TCC GAA ACT TCA ACA TGA TCT CGA GAT CAT GTT GAA GTT TCG GAG G

Table 2.5: Target sequence and oligo sequence of shRNA constructs targeting TRPA1 (transcript ID NM_007332.2).

Glycerol stocks of bacteria were expanded in lysogeny broth (LB) medium (3µl glycerol stock in 500ml LB) overnight on an orbital shaker at 37°C, supplemented with ampicillin (100µl/ml) as the selection agent. Plasmid DNA was isolated from the harvested bacterial cultures using Plasmid Maxi Kit (Qiagen, Germantown, USA) following manufacturer's instructions. Precipitated DNA was dissolved in nuclease-free water and stored at -20°C until use.

2.7.2 shRNA transfection

Cultured hASMC were transfected with plasmids encoding TRPA1-targeted shRNA or the empty vector using the Lipofectamine 3000 transfection reagent kit (Thermo Fisher Scientific) according to manufacturer's instructions. Plasmid DNA (1.5µg/well) and P3000 reagent (3µl/well) were diluted in 125µl Opti-MEM (125µl/well; Thermo Fisher Scientific), and the Lipofectamine 3000 reagent was also diluted in Opti-MEM (3.75µl/well). The two diluted reagents were mixed together, and incubated at room temperature for 20 min. The complete

culture media DMEM/F-12 on hASMC was replaced with 1ml DMEM/F-12 without penicillin/streptomycin (DMEM/F-12$^{-P/S}$) per well prior to transfection. The transfection mix was added drop-wise onto each well, swirled, and cells were left overnight in the incubator. DMEM/F-12$^{-P/S}$ was replaced with complete DMEM/F-12 after the transfection period. Cells were studied in Ca^{2+} imaging experiments 72 hours post-transfection.

2.8 Real-time quantitative PCR (qPCR) analysis

2.8.1 RNA extraction

Cell lysis and RNA extraction was performed using the RNeasy Mini Kit (Qiagen) according to manufacturer's instructions. Isolated RNA was eluted in nuclease-free water, and the concentration of RNA was quantified using a NanoDrop Spectrophotometer. Isolated RNA was stored at -80°C.

2.8.2 cDNA synthesis

300ng RNA from each sample was subjected to DNAse (0.5 U/µl; Roche, Welwyn Garden City, UK) treatment (10 min at 37°C) to remove DNA contamination. Reverse transcription was performed by incubating 300ng of the DNase-treated RNA with a mix of random primers (6.25µg/µl; Promega, Southampton, UK), RNasin ribonuclease inhibitor (0.5 U/µl; Promega), Deoxynucleotide Triphosphates (300µM; New England Biolabs, Hitchin, UK) and Moloney-Murine Leukemia Virus Reverse Transcriptase (M-MLV, 5 U/µl; Promega) for 60 min at 37°C to obtain complementary DNA (cDNA). cDNA was stored at -20°C.

2.8.3 Real-time qPCR

Real-time qPCR was performed by mixing the cDNA (1.5µl), forward and reverse primers (2 µM each), and 2X LightCycler® 480 SYBR Green I Master mix (7.5µl; Roche), to a total volume of 15µl in each well of a 96-well plate. The housekeeping genes 18S and GAPDH were used as internal controls. Sequences for the primer pairs are listed in Table 2.2. The PCR was ran using a standard protocol consisting of the activation stage (95°C for 10 min), followed by 45 cycles of amplification (95°C for 10 s, 60°C for 20 s, 72°C for 1 s) before cooling down. The cycle threshold (CT) values for the detection of each sample was calculated using the built-in Second Derivative Maximum Method in the LightCycler® 480 programme (Roche).

Relative quantification of TRPA1 in shRNA-transfected samples was performed using the $2^{-\Delta\Delta CT}$ method (Livak and Schmittgen, 2001), normalising to the two different housekeeping genes (ΔCT), and then normalised to the average TRPA1 ΔCT of samples transfected with the EV in the same plate, day/donor-matched.

2.9 Western blotting

2.9.1 Lysate preparation

Cells were lysed using ice-cold RIPA buffer, supplemented with protease and phosphatase inhibitors; volume of RIPA buffer added depended on the size of cell culture vessel (Table 2.6).

Cell culture vessel	Area (cm^2)	RIPA buffer added (µl)
T25 culture flask	25	500
T75 culture flask	75	1000
6-well culture plate	9.6	200

Table 2.6: Volume of RIPA lysis buffer added for each type of culture vessel.

Cell lysis was performed on ice to minimise protein degradation. After addition of RIPA buffer, cells were scraped using plastic cell scrapers (Corning CLS3010), and lysates transferred to 1.5ml Eppendorf tubes, vortexed, and incubated at 4ºC for 1 h. Lysates were centrifuged at 12,000g for 15 min at 4ºC, and pellets were discarded. Protein concentration was quantified through the BCA assay (Pierce BCA Protein Assay Kit, Thermo Fisher Scientific) according to manufacturer's instructions. 1/3 volume of 4X Laemmli buffer (Bio-Rad), supplemented with 10% β-mercaptoethanol as a reducing agent (Sigma-Aldrich), was added to the cell lysates. Samples were vortexed and stored at -20ºC until use.

Cell lysates were either incubated in a water bath (37ºC, 30 min; for samples to be probed for CFTR) or boiled (95ºC, 5 min; for samples to be probed for p-MLC and MLC). Then, lysates were diluted, using RIPA buffer with Laemmli buffer (LB) added, to desired concentrations for gel loading (total volume 40µl each well; 1.0mm gel, Mini-PROTEAN Tetra electrophoresis system, Bio-Rad).

2.9.2 SDS-PAGE, transfer, and membrane staining

The Mini-PROTEAN Tetra electrophoresis chamber (Bio-Rad) was assembled and filled with running buffer according to manufacturer's instructions. A protein ladder (5µl protein ladder + 35µl RIPA+LB; Precision Plus Protein WesternC Blotting Standards, Bio-Rad 1610376), or cell lysates, were loaded into each well on an SDS-PAGE gel (8% gel for CFTR, 12% gel for p-MLC and MLC). Gel electrophoresis was ran at 70V for 30 min followed by 150V for 60 min (CFTR), or 150V for 60 min (p-MLC and MLC). Gels and PVDF membranes (GE

Healthcare Life Sciences, UK; activated using 100% methanol) were equilibrated in cold transfer buffer for 10 min, and protein was transferred to PVDF membranes under semi-dry conditions using the Bio-Rad Trans-Blot Turbo Transfer System (0.1A constant, 60 min for CFTR; 25V constant, 10 min for p-MLC and MLC).

Following transfer, membranes were blocked with 5% milk (for CFTR and MLC) or 5% BSA (for p-MLC) in TBS-T for 1 hour at room temperature (CFTR and p-MLC) or overnight (MLC). Membranes were then incubated with primary antibody diluted in 1% milk (for CFTR and MLC) or 1% BSA (for p-MLC) TBS-T (dilutions indicated in Table 2.1) at 4ºC overnight (CFTR and p-MLC) or 1 hour at room temperature (MLC). After 3 washes in TBS-T, secondary antibodies (Table 2.1) were incubated for 1 hour at room temperature. Membranes were washed 3x, and incubated with enhanced chemiluminescence (ECL; Bio-Rad) for 2 min at room temperature. Excess ECL was removed, and membranes were developed on a Fujifilm LAS-3000 imager.

2.9.3 Myosin light-chain phosphorylation assay

After 1 h equilibration in HEPES-buffered solution, confluent hASMC grown in 6-well plates were subjected to treatment with a positive control cocktail (100µM ATP, 10µM CPA, and 10mM Ca^{2+}) or CSE for various durations to stimulate myosin light-chain phosphorylation. For the negative control samples, cells were treated with the HEPES-buffered solution only. Lysates were then processed as described above and Western blot probing for p-MLC was performed. For parallel processing of phospho- and total MLC, membranes were cut vertically to perform staining with two different antibodies (p-MLC and MLC) on the same protein sample run on the same gel. Protein bands were quantified using ImageJ software. Band density of p-MLC was normalised to band density of total MLC of the same protein sample.

2.10 Immunoprecipitation

Immunoprecipitation of CFTR was performed on Calu-3 and hASMC lysates. Cell lysates were extracted as indicated in the Western blotting section. CFFT-596 primary antibody was added to cell lysates (1:1000 dilution), vortexed, and incubated at 4°C overnight with constant shaking.

Protein A-Sepharose (PAS) beads (P9424 Sigma-Aldrich) were washed before use, by adding 100µl of RIPA buffer to 100µl PAS beads, then centrifuging at 2,000g for 2 mins. The supernatant was discarded, and pellet resuspended in 100µl RIPA buffer. 100µl washed PAS beads were added to 1ml primary antibody-bound cell lysate, vortexed, and incubated at 4°C for 1 h with constant shaking. Then, lysates were centrifuged (2,000g for 2 mins), and washed 3x with 1ml ice cold RIPA buffer, with supernatant discarded after each wash. The supernatant was aspirated using a 2ml syringe with 21G needle to avoid loss of beads.

50µl 1X Laemmli buffer was added to the washed PAS beads bound with the protein of interest, vortexed, and incubated at room temperature for 15 minutes. The samples were then centrifuged at 13,000g for 2 mins to release the immunoprecipitated proteins from the beads. The supernatant was collected and stored at -20°C until use.

2.11 Immunofluorescence

Immunofluorescence staining was performed on cells grown on 25mm glass coverslips, to 40-60% confluence before fixing. Cells were washed 3x with ice-cold PBS (5 mins each on a benchtop shaker at 60 rpm), supplemented with 1mM $CaCl_2$ and 1mM $MgCl_2$ (PBS^{++}), then fixed in 100% ice-cold methanol in –20°C for 10 minutes. After washing 3x with PBS^{++}, cells were incubated with the blocking solution (5% normal goat serum (NGS) and 1% bovine serum albumin (BSA) in PBS^{++}) for 1 hour at room temperature. Cells were then incubated with the primary antibody at 4°C overnight in a moisturised chamber to minimise evaporation. After 3x washing with PBS^{++}, cells were incubated with the secondary antibody for 1 hour at room temperature. Primary and secondary antibodies were diluted in 0.5% BSA PBS^{++}; dilutions of antibodies are presented in Table 2.1. Finally, cells were washed 3x in PBS^{++}, with 1:1000 DAPI included in the second wash.

Imaging was performed on the Leica SP8 confocal microscope, operated through the Leica Application Suite (LAS) X software (Leica Microsystems, Milton Keynes, UK). Glass coverslips containing stained cells, immersed in PBS, were mounted onto an oil-immersion lens with 63x magnification. Images were acquired sequentially to avoid spectral overlap. Images were exported, and scalebars added, using the LAS X software.

2.12 Immunohistochemistry

Immunohistochemical staining was performed on cells grow on glass chamber slides, using the ImmPRESS™ Universal Antibody Detection Kit (MP-7500 Vector Laboratories, Burlingame, USA) according to manufacturer's instructions. Cells were washed 2x with PBS, fixed with 100% ice-cold methanol at -20°C for 10 min, and washed 2x with PBS. After removing PBS, slides were incubated with the ImmPRESS ready-to-use 2.5% normal horse serum solution for 10 min at room temperature. Blocking solution was removed, and slides were incubated with primary antibody, diluted in TBS, for 60 min at room temperature. Slides were washed 2x with TBS, then incubated for 30 min at room temperature with the ImmPRESS™ Universal anti-mouse IgG Reagent. After washing 2x in TBS, slides were incubated with 3'-Diaminobenzidine (DAB) for 1 min, washed in running tap water, then counterstained in Mayer's Haematoxylin for 30 s. After washing in running tap water, slides were blued in Scott's Tap Water substitute

for 30 s. Slides were washed one last time in running tap water, then subjected to serial dehydration in graded concentrations of ethanol (30 s each in 70%, 90%, 99% ethanol). Slides were cleared in xylene for 5 min, then one drop of DPX mountant was added to the slide, and a glass coverslip was mounted on top of the samples. Slides were left to dry overnight prior to imaging through light microscopy.

2.13 Statistical analysis

Summary data is presented as mean ± SEM. For experiments involving cultured rat or human ASMC, the number of donors (biological replicates) was included in the respective figure legends. n in figure legends denotes number of repeated independent experiments (technical replicates).

Statistical analysis was performed using GraphPad Prism 8 (GraphPad Software, San Diego, USA), with statistical significance indicated by an alpha value of $p<0.05$. The type of analysis for each dataset, including post-hoc analysis, is indicated in the respective figure legend. The choice between parametric or non-parametric statistical tests was selected by performing the package of normality tests (Anderson-Darling test, D'Agostino & Pearson test, Shapiro-Wilk test, Kolmogorov-Smirnov test) provided by GraphPad Prism to test for Gaussian distribution; if the majority of datasets examined followed a Gaussian distribution, then parametric tests were performed. Dose-response curves and associated EC_{50} values presented were computed through built-in equations in GraphPad Prism 8, with a standard Hill Slope set to 1.0.

Chapter 3: Role of CFTR in regulation of calcium homeostasis in epithelial cell lines and cultured ASMC

3.1 Introduction

To date, there has been extensive literature linking disruption in CFTR function to alterations in Ca^{2+} homeostasis. As explored in the section 1.6.1 of the Introduction chapter, these include changes in Ca^{2+} store release, reuptake, and influx, in both human primary CF airway epithelial cells (mostly with the F508del mutation), and CF airway epithelial cell lines, compared to non-CF airway epithelial cells expressing WT-CFTR (Paradiso *et al.*, 2001; Ribeiro *et al.*, 2005a; Antigny *et al.*, 2008a; Antigny *et al.*, 2008b; Antigny *et al.*, 2009; Antigny *et al.*, 2011b; Balghi *et al.*, 2011; Martins *et al.*, 2011; Philippe *et al.*, 2015; Vachel *et al.*, 2015). More recently, this link has been extended to ASMC. For instance, blunted histamine-coupled Ca^{2+} release in cultured CF hASMC (Michoud *et al.*, 2009), and delayed Ca^{2+} reuptake in freshly isolated CF porcine ASMC (Cook *et al.*, 2016), have been reported. However, the functional role of CFTR in regulating Ca^{2+} homeostasis in ASMC remains poorly understood, partially due to the reported intracellular localisation of CFTR in ASMC (Vandebrouck *et al.*, 2006; Michoud *et al.*, 2009; Cook *et al.*, 2016), in contrast to the plasma membrane-bound CFTR in airway epithelia.

More recently, an important connection between cigarette smoking, Ca^{2+} signalling, and CFTR has emerged, with reports that direct exposure to CS caused a sustained increase in $[Ca^{2+}]_i$ in several epithelial cell types, including airway cells, which led to clathrin/dynamin-mediated internalisation of CFTR from the plasma membrane (Rasmussen *et al.*, 2014; Marklew *et al.*, 2019; Patel *et al.*, 2019). However, whether CS exposure disrupts Ca^{2+} homeostasis and/or CFTR expression, localisation, and function in ASMC has not been reported.

In addition, despite many reports linking CFTR dysfunction with alterations in Ca^{2+} signalling, very few studies have investigated the effects of pharmacological modulation of CFTR on calcium signalling in non-CF epithelial cells such as smooth muscle cells. Furthermore, the characterisation of pharmacological modulation of CFTR activity on cellular Ca^{2+} signalling is an important gap in knowledge to fill, as these agents have been used as primary tools for studying CFTR function in many cell types. Agents that elevate intracellular cAMP, including forskolin, 3-isobutyl-1-methylxanthine (IBMX), vasoactive intestinal peptide (VIP), and salbutamol are able to stimulate CFTR activity. A specific small-molecule potentiator of CFTR, ivacaftor (VX-770), emerged just a decade ago, and it increases the open probability of CFTR (Van Goor *et al.*, 2009). As the current standard treatment for CF, particularly for patients with F508del-CFTR mutation, ivacaftor is administered alongside correctors such as lumacaftor,

tezacaftor, and elexacaftor, which facilitate the folding and transport of F508del-CFTR to the cell membrane (Middleton *et al.*, 2019; Bose *et al.*, 2020). On the other hand, early studies utilised diphenylamine-2-carboxylate (DPC) and glibenclamide to inhibit CFTR, but these drugs often have off-target effects on other ion channels (Alton *et al.*, 1991; Kubo and Okada, 1992; Sheppard and Welsh, 1992; Sakamoto *et al.*, 1996; Yamazaki and Hume, 1997). More recently, two relatively selective inhibitors have emerged: $CFTR_{inh}$-172 and GlyH-101 (Ma *et al.*, 2002; Muanprasat *et al.*, 2004), and these have since become staple inhibitors for studying the role of CFTR in laboratory settings. It is worth noting, however, that these putative CFTR modulators have been primarily tested on CFTR expressed on the plasma membrane, and thus may not be fully functional in modulating intracellular CFTR as observed in ASMC.

Since CFTR has been extensively studied in epithelial cells, Calu-3 cells, a human epithelial cell line with high CFTR expression (Shen *et al.*, 1994), was selected to conduct initial characterisation of the effects of several CFTR modulators on intracellular Ca^{2+} signalling. The initial focus of this chapter investigated store-operated calcium entry (SOCE). This is a core mechanism in maintaining Ca^{2+} homeostasis in mammalian cells, including epithelial-derived cells such as Calu-3 cells (Prakriya and Lewis, 2015; Lewis, 2020). It is also a prominent mechanism regulating Ca^{2+} refilling in SMC (Flores-Soto *et al.*, 2013) and has been reported to be enhanced in ASMC treated with CSE (Wylam *et al.*, 2015).

3.2 Aims and objectives

The main aim of the chapter was to explore the role of CFTR in regulating Ca^{2+} homeostasis in human epithelial as well as rat and human ASMC. The objectives of the chapter were:

- To characterise the effects of pharmacological modulators of CFTR, specifically forskolin and $CFTR_{inh}$-172, on Ca^{2+} homeostasis in Calu-3 cells.
- To establish a robust protocol for applying CFTR modulators to study Ca^{2+} signalling in ASMC, informed by results from Calu-3 cells.
- To validate the global expression of CFTR in rat and human ASMC.
- To visualise the localisation of CFTR protein in rat and human ASMC and investigate the effects of CFTR modulators on ASMC Ca^{2+} homeostasis.

3.3 Results

3.3.1 Pharmacological inhibition of CFTR reduced SOCE in Calu-3 cells in a time-dependent manner

To investigate the effect of CFTR inhibition on SOCE, a repeated Ca^{2+} addback protocol was employed to study the effect of the selective CFTR inhibitor, $CFTR_{inh}$-172 (Ma *et al.*, 2002),

on SOCE in Calu-3 cells. Figure 3.1 illustrates a control experiment, with the vehicle DMSO, using this protocol. To activate SOCE, ER calcium stores were first depleted with 200nM thapsigargin (Tg), a SERCA inhibitor, for 15 mins in the absence of external Ca^{2+} (nominally Ca^{2+}-free solution; white bars). Calcium was then added back (1mM Ca^{2+} solution; black bars) to measure SOCE #1, the reference SOCE before pharmacological intervention. After reaching a peak, extracellular calcium was removed and $[Ca^{2+}]_i$ was allowed to return to baseline levels. SOCE #2 was initiated and monitored following 10-min treatment of DMSO. Then, external Ca^{2+} and DMSO were removed for 15 mins before SOCE #3 was measured, to examine potential reversibility of effects. Using this protocol, Figure 3.1 shows that in cells treated with the vehicle alone, multiple reproducible SOCE in Calu-3 cells could be recorded, in which peak amplitude and rate of Ca^{2+} entry was similar to SOCE #1. This reproducibility allowed for paired analysis of pre- and post-treatment SOCE. In subsequent Ca^{2+} fluorimetry traces shown in this chapter, the Tg portion of the trace was curtailed to focus more on the individual SOCE responses.

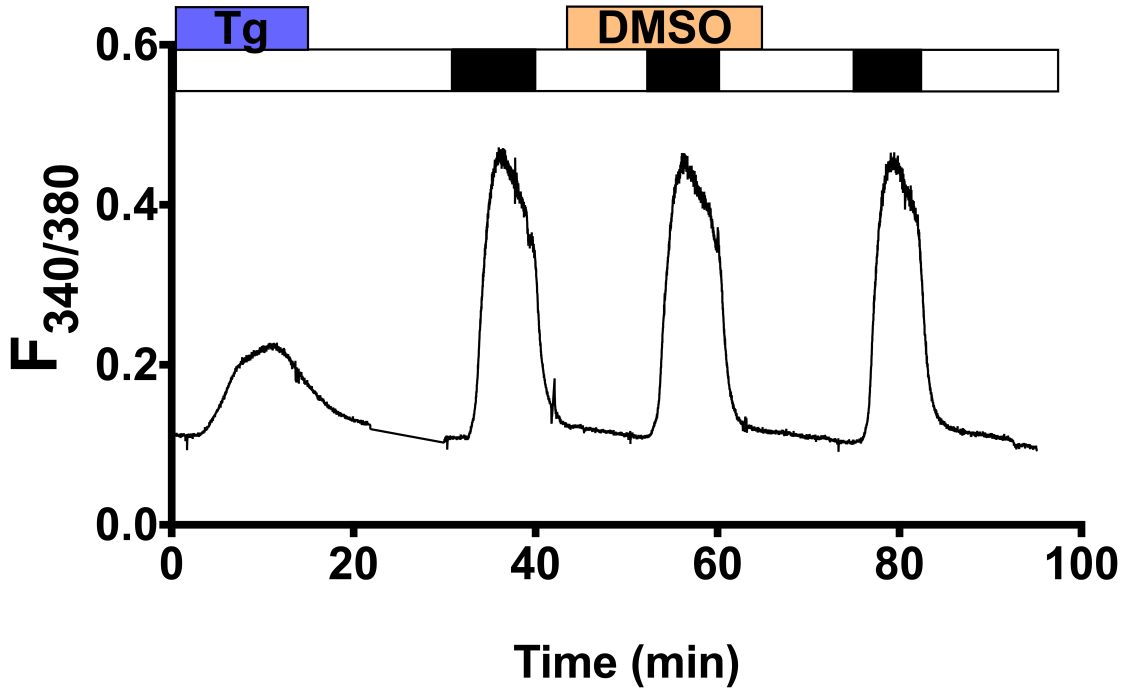

Figure 3.1: Ca^{2+} fluorimetry protocol for measuring multiple SOCE. Representative Ca^{2+} fluorimetry traces tracking changes in $[Ca^{2+}]_i$ following a Tg (200nM)-activated, repeated Ca^{2+} addback protocol, alternating between nominally Ca^{2+} free solution (white bars) and adding back 1mM Ca^{2+} (black bars) to initiate SOCE.

The same protocol was applied to examine the effect of a 10-min treatment with 20μM $CFTR_{inh}$-172, a reportedly selective CFTR inhibitor, on SOCE (Figure 3.2). In 3/6 experiments, no visible inhibition of SOCE #2 was observed (e.g. Figure 3.2A), whereas in the other half, this treatment attenuated the second SOCE (e.g. Figure 3.2B). Interestingly, in all 6 experiments,

SOCE #3 (following a 15-min washout of inhibitor) had a lower peak compared to SOCE #1, indicating that the inhibitory effect of $CFTR_{inh}$-172 on SOCE was not reversible in the short-term. Moreover, in the 3 experiments where SOCE #2 was not affected, SOCE #3 was reduced, suggesting that the inhibition by $CFTR_{inh}$-172 may be time-dependent.

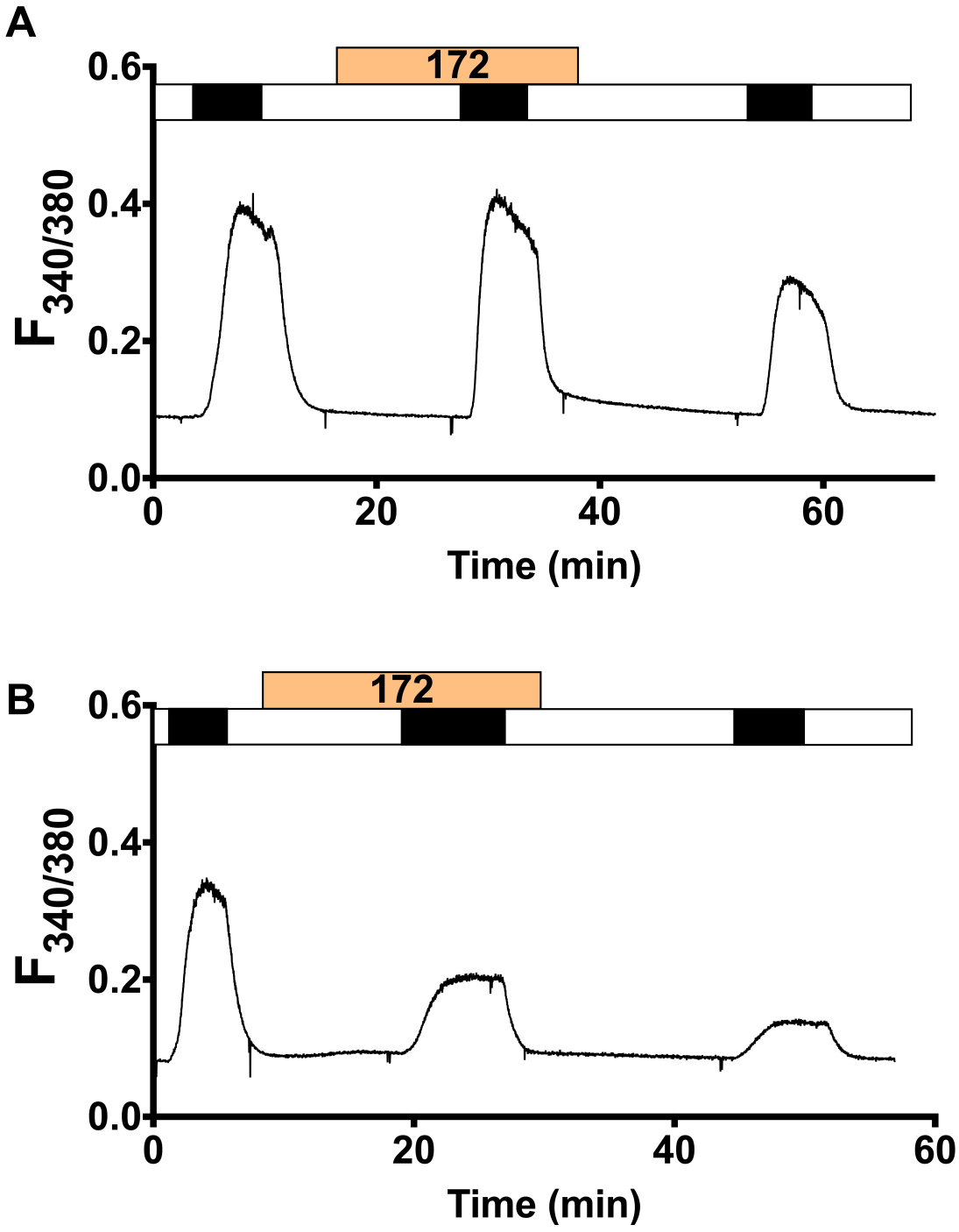

Figure 3.2: The effects of $CFTR_{inh}$-172 treatment on SOCE in Calu-3 cells. Representative Ca^{2+} fluorimetry traces tracking changes in $[Ca^{2+}]_i$ following a Tg-activated, repeated Ca^{2+} addback protocol. Cells were exposed to the vehicle 20μM $CFTR_{inh}$-172 in a nominally Ca^{2+} free solution (white bars) for 10 mins before the second SOCE was induced by adding back 1mM Ca^{2+} (black bars). The agents were removed from the perfusing solution for 15 mins before the third SOCE was activated. (A) shows an experiment where $CFTR_{inh}$-172 treatment did not affect SOCE #2, whereas it was reduced in (B).

To investigate the time-dependency of SOCE inhibition by $CFTR_{inh}$-172, a shorter (3-min; Figure 3.3A) and a longer (30-min; Figure 3.3B) exposure to $CFTR_{inh}$-172 was applied. The frequency of a visible inhibition of SOCE #2 was notably higher in cells treated for 30-min with $CFTR_{inh}$-172. Repeated-measure ANOVA with multiple comparisons was performed to examine the effect of $CFTR_{inh}$-172 on SOCE (SOCE #1 vs. SOCE #2), as well as any potential reversibility (SOCE #1, 2 vs. SOCE #3); the summary data for the peak amplitude and rate of each SOCE is presented in Table 3.1.

In the vehicle control experiments, with data from various treatment durations pooled together, the amplitudes of the 3 repeated SOCE were not significantly different ($p>0.05$ for all multiple comparisons), validating the reproducibility of this repeated-addback protocol. However, the rates of SOCE #2 and 3 were significantly higher than that of SOCE #1 ($p<0.05$, SOCE #2 and 3 vs. 1), suggesting that longer exposure to a Ca^{2+}-free external solution may have further depleted Ca^{2+} stores.

In terms of inhibition of SOCE peak amplitude by $CFTR_{inh}$-172, both SOCE #2 and 3 were not significantly lower than SOCE #1 in the cells pre-treated for 3-min with the drug ($p>0.05$ for all multiple comparisons). On the other hand, SOCE #2 was significantly attenuated only in the 30-min exposure group ($p<0.05$, SOCE #2 vs. 1), and this was not reversible following 30-min washout of the compound ($p<0.05$, SOCE #3 vs. 1). In contrast, in the 10-min treatment group, SOCE #3 was significantly lower than both SOCE #1 and 2 ($p<0.05$ for SOCE #3 vs. 1 and 2), again suggesting that $CFTR_{inh}$-172 requires >10 minutes to consistently exert an irreversible inhibitory effect on SOCE. Although none of the multiple comparisons between SOCE rates returned statistical significance, similar trends were observed – the rate of SOCE #2 was visibly lower than SOCE #1 in the 30-min treatment group, while only SOCE #3 appeared to be lower than SOCE #1 in the 3- and 10-min exposure experiments.

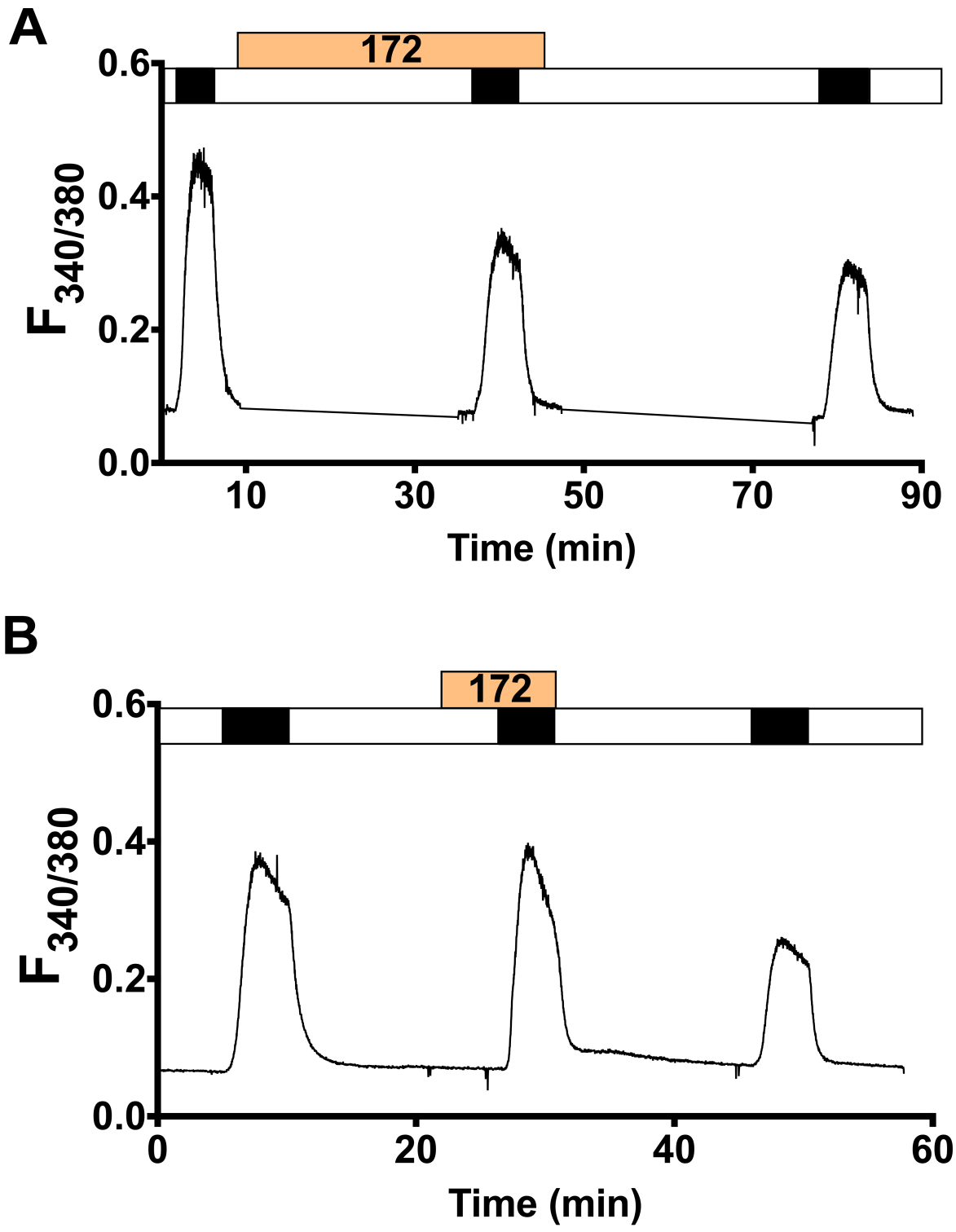

Figure 3.3: CFTR$_{inh}$-172 inhibits SOCE in Calu-3 cells in a time-dependent manner in Calu-3 cells. Representative Ca^{2+} fluorimetry traces tracking changes in $[Ca^{2+}]_i$ following a Tg-activated, repeated Ca^{2+} addback protocol, with 3-min (A) or 30-min (B) CFTR$_{inh}$-172 pre-treatment before the second SOCE was activated.

Treatment	Amplitude			Rate		
	SOCE #1	SOCE #2	SOCE #3	SOCE #1	SOCE #2	SOCE #3
DMSO	0.33±0.03	0.35±0.03	0.35±0.03	0.24±0.03$^{*\$}$	0.31±0.04	0.31±0.04
3 mins $CFTR_{inh}$-172	0.21±0.04	0.24±0.03	0.13±0.03	0.15±0.04	0.18±0.04	0.09±0.03
10 mins $CFTR_{inh}$-172	0.34±0.04$^{\$}$	0.25±0.04$^{\$}$	0.14±0.03	0.28±0.08	0.21±0.06	0.08±0.02
30 mins $CFTR_{inh}$-172	0.42±0.07$^{*\$}$	0.23±0.05	0.26±0.06	0.27±0.05	0.11±0.03	0.18±0.06

Table 3.1: Summary data of SOCE peak amplitude and rate in cells pre-treated for different durations with the vehicle DMSO or $CFTR_{inh}$-172. Data from different durations of DMSO treatment were pooled together. n=4-14. Repeated-measure one-way ANOVA with Holm-Sidak multiple comparisons tests was performed across the three SOCE, within each of the four datasets. Data presented as mean ± SEM. * = $p<0.05$ vs. SOCE #2; $ = $p<0.05$ vs. SOCE #3.

Examining the percentage inhibition, from SOCE #1 to SOCE #2, revealed a significantly greater inhibition of SOCE amplitude by 10-min and 30-min exposure to $CFTR_{inh}$-172, compared to 3-min exposure and the vehicle control experiments (Figure 3.4A; $p<0.05$, Holm-Sidak multiple comparisons). Similarly, the inhibition of SOCE rate was significantly greater in cells treated with $CFTR_{inh}$-172 for 30-min, compared to those cells treated for 3-min with $CFTR_{inh}$-172 or with DMSO (Figure 3.4B; $p<0.05$, Holm-Sidak multiple comparisons). To investigate whether treatment duration correlated with an increased inhibition, a chi-square test was performed. A -10% change was used as the threshold for significant inhibition, as it was observed that in all experiments, the vehicle control and the 3-min treatment with $CFTR_{inh}$-172 caused less than 10% inhibition (Figure 3.4A, B). For both peak amplitude (Figure 3.4C) and rate (Figure 3.4D), the frequency of >10% inhibition increased as duration of exposure increased. The chi-square test was statistically significant for the frequency distribution of both parameters, suggesting a time-dependency of SOCE inhibition by $CFTR_{inh}$-172 in Calu-3 cells.

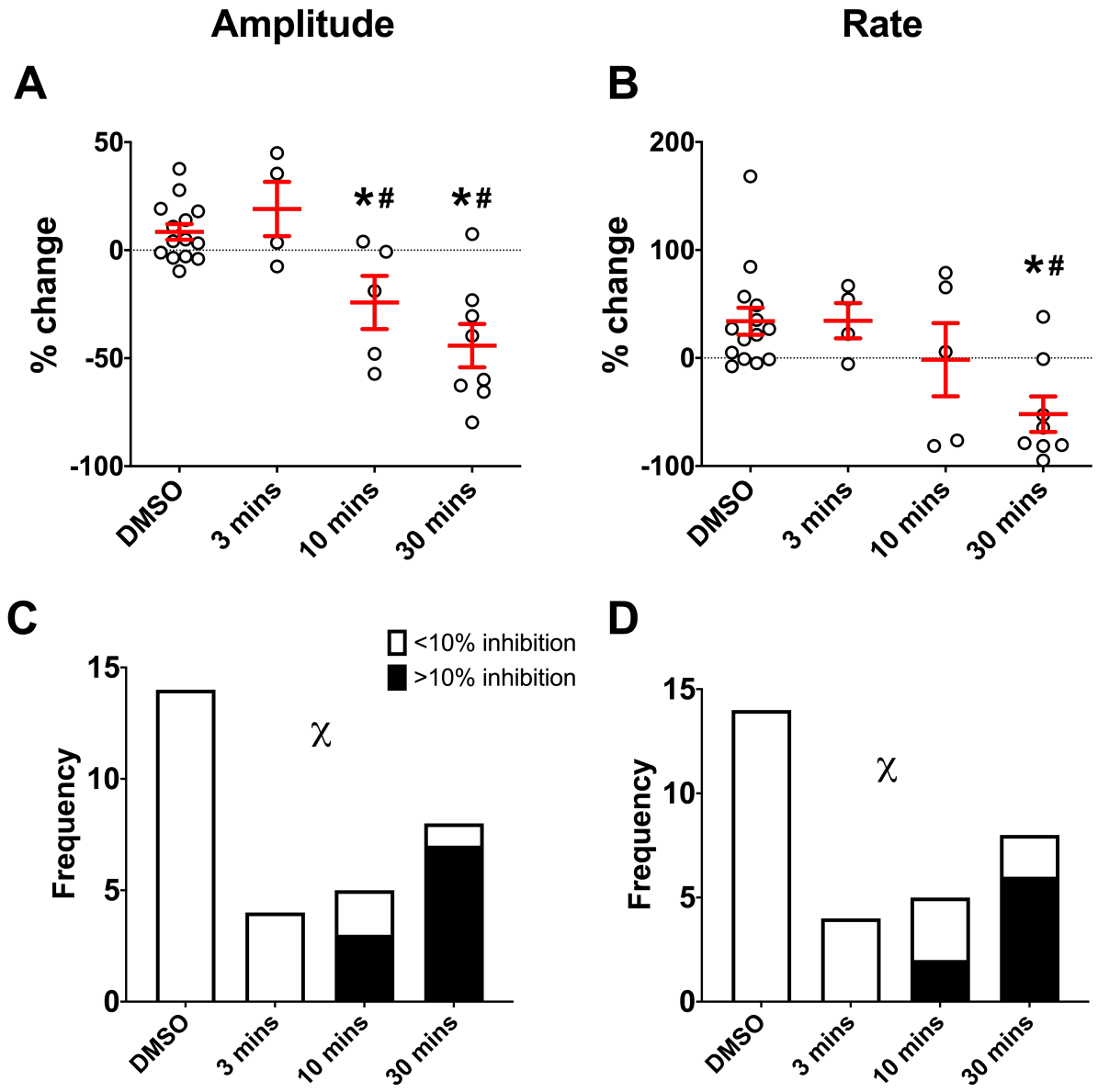

Figure 3.4: Duration of CFTR$_{inh}$-172 exposure determines the extent and frequency of SOCE inhibition in Calu-3 cells. (A-B): Summary of percentage change in SOCE peak amplitude (A) and rate (B), from SOCE #1 to SOCE #2, following DMSO or CFTR$_{inh}$-172 treatment of different durations. One-way ANOVA with Holm-Sidak multiple comparisons tests was performed across the four groups. Data presented as mean ± SEM. * = $p<0.05$ vs. DMSO; # = $p<0.05$ vs. 3 mins. (C-D) Frequency of >10% inhibition of SOCE amplitude (C) and rate (D) by DMSO or CFTR$_{inh}$-172 treatment of different durations. n = 4-14. A chi-square test was performed across the four groups. χ = $p<0.05$ for chi-square test.

3.3.2 Forskolin and CFTR$_{inh}$-172 additively inhibit SOCE in Calu-3 cells

As the CFTR inhibitor significantly reduced SOCE in Calu-3 cells, the dependency of this response on CFTR activity was further investigated. The repeated addback protocol was applied to study the effects of pre-treating the cells with forskolin (Figure 3.5B), an indirect activator of CFTR. This enabled the examination of whether a purported increased CFTR activity would augment SOCE given that the CFTR inhibitor CFTR$_{inh}$-172 reduced SOCE. Moreover, the specificity of any potential effects of forskolin was studied by blocking CFTR with CFTR$_{inh}$-

172 before forskolin exposure (Figure 3.5D). Experiments where cells were exposed to $CFTR_{inh}$-172 only for 10- or 30-min, shown above in Table 3.1, were also included (Figure 3.5C), as a reference to identify any additional effects of forskolin following $CFTR_{inh}$-172 treatment. The summary of peak amplitude and rate of individual SOCE in each treatment group is presented in Table 3.2.

The vehicle control for this set of experiments also exhibited reproducible SOCE, where all 3 SOCE response reached a similar amplitude (Figure 3.5A). However, the influx rate was significantly higher in SOCE #2 and 3 ($p<0.05$, SOCE #2 and 3 vs. 1), consistent with the trend observed in Table 3.1. On average, a 10-min pre-treatment with 5μM forskolin did not significantly alter the peak SOCE response ($p>0.05$ for all multiple comparisons), but did attenuate the influx rate ($p<0.05$, SOCE #2 vs. SOCE #1), indicating that forskolin alone slowed down Ca^{2+} influx.

On the other hand, pooling together data from 10- or 30-min treatment with $CFTR_{inh}$-172, the amplitude, but not rate, of SOCE #2 was significantly reduced ($p<0.05$ for amplitude, SOCE #2 vs. SOCE #1). However, the inhibition of the peak amplitude and rate were significant after an extended period, following washout ($p<0.05$, SOCE #1 vs. 3). Surprisingly, a 10-min exposure to the combination of forskolin and $CFTR_{inh}$-172, after 20-min treatment with $CFTR_{inh}$-172 (30-min total for $CFTR_{inh}$-172), induced a significant, irreversible inhibition of both the amplitude and rate of SOCE ($p<0.05$ for both amplitude and rate, SOCE #2 and 3 vs. 1).

Comparing the percentage change in amplitude (Figure 3.5E) and rate (Figure 3.5F) from SOCE #1 to SOCE #2, all three treatment groups induced significantly greater inhibition on both the amplitude and rate of SOCE compared to the vehicle control group ($p<0.05$ for both amplitude and rate, for all treatment groups vs. DMSO). Treatment with $CFTR_{inh}$-172 inhibited the peak SOCE amplitude to a greater extent than forskolin, but the % change in rate was similar between the two groups, consistent with the significant inhibition of SOCE rate, but not amplitude, by forskolin shown in Table 3.1. More interestingly, the percentage reduction in SOCE amplitude exerted by the combination of 172+fsk was significantly higher than by either forskolin or $CFTR_{inh}$-172 individually; the same was observed for the rate of 172+fsk against $CFTR_{inh}$-172-treated SOCE. These results were surprising as forskolin treatment was hypothesised to augment SOCE, as $CFTR_{inh}$-172 alone inhibited SOCE; instead, the significant differences in the efficacy of SOCE inhibition when cells were exposed to both agents suggest that forskolin acts additively with $CFTR_{inh}$-172 to inhibit SOCE in Calu-3 cells.

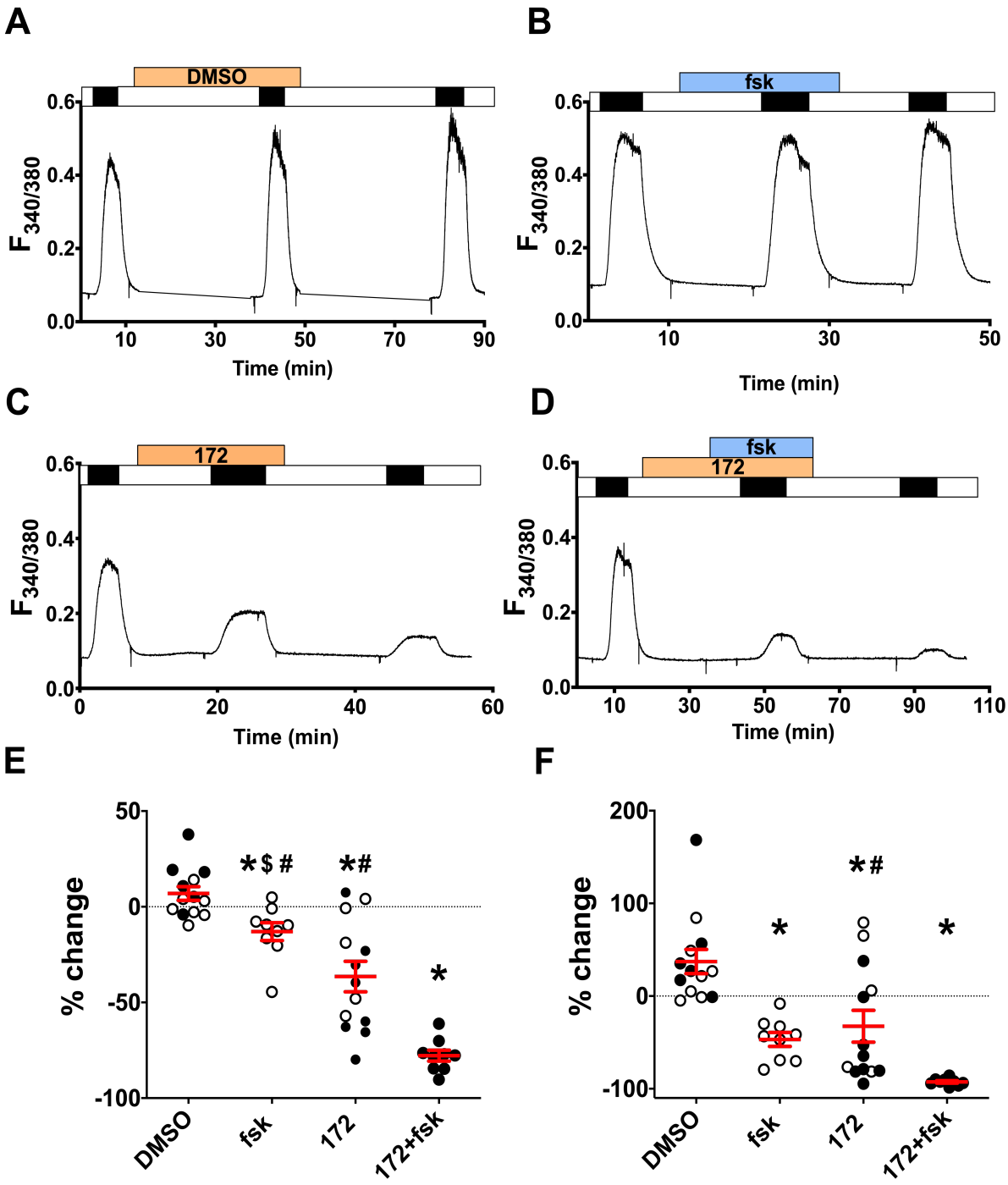

Figure 3.5: Forskolin and CFTR$_{inh}$-172 additively inhibit SOCE in Calu-3 cells. (A-D) Representative Ca^{2+} fluorimetry traces tracking changes in $[Ca^{2+}]_i$ following a Tg-activated, repeated Ca^{2+} addback protocol, with a pre-treatment with DMSO for 10 or 30 mins (A); 5μM forskolin for 10 mins (B); 20μM CFTR$_{inh}$-172 for 10 or 30 mins (C); or CFTR$_{inh}$-172 for 20 mins followed by addition of forskolin for 10 mins (D) before the second SOCE was induced. (E-F) Summary of percentage change in SOCE peak amplitude (E) and rate (F), from SOCE #1 to SOCE #2, following treatment of DMSO or CFTR modulators as described above. One-way ANOVA with Holm-Sidak multiple comparisons tests was performed across the four groups. * = $p<0.05$ vs. DMSO; $ = $p<0.05$ vs. 172; # = $p<0.05$ vs. 172+fsk. n = 9-14. Data presented as mean ± SEM.

Treatment	Amplitude			Rate		
	SOCE #1	SOCE #2	SOCE #3	SOCE #1	SOCE #2	SOCE #3
DMSO	0.33±0.03	0.35±0.03	0.35±0.03	0.24±0.03*$	0.31±0.04*$	0.32±0.04
Forskolin	0.38±0.05	0.33±0.04	0.33±0.05	0.37±0.07*	0.17±0.03	0.21±0.04
$CFTR_{inh}$-172	0.39±0.05*$	0.24±0.03*$	0.21±0.04	0.27±0.04$	0.24±0.03	0.21±0.04
Forskolin + $CFTR_{inh}$-172	0.26±0.02	0.06±0.01	0.05±0.01	0.20±0.02*$	0.01±0.00	0.02±0.00

Table 3.2: Summary data of SOCE peak amplitude and rate in cells pre-treated with the vehicle DMSO or different CFTR modulators, as detailed in Figure 3.5. Data from various durations (10 or 30-min) of DMSO/$CFTR_{inh}$-172 treatment was pooled together, including data from Table 3.1. Repeated-measure one-way ANOVA with Holm-Sidak multiple comparisons tests was performed across the three SOCE, within each of the four datasets. n=9-14. Data presented as mean ± SEM. * = $p<0.05$ vs. SOCE #2; $ = $p<0.05$ vs. SOCE #3.

3.3.3 Inhibition of SOCE in epithelial cells does not require CFTR

The surprising observation that both forskolin and $CFTR_{inh}$-172 had additive inhibitory effects on SOCE suggests that the action of one or both of these agents was independent of CFTR. To investigate whether the inhibitory effects of $CFTR_{inh}$-172 and forskolin required CFTR, the HEK293 cell line was studied as these cells have been reported to not express CFTR (Domingue *et al.*, 2014).

To validate that HEK cells do not express CFTR, qPCR analysis was performed to study mRNA levels. Two different primers were used to detect CFTR, whereas the housekeeping genes GAPDH and 18S were used to ensure even loading. The amplification curves for these genes are displayed in Figure 3.6A. The two CFTR primers detected expression in Calu-3 cell samples with a CT value of 25.8 and 28.3, respectively. In contrast, in HEK cell samples, the CT values were 39.2 and 34.7, respectively, close to the maximum detection CT range (40) for the LightCycler 480 system used.

In addition, the lack of CFTR protein expression in HEK cells was validated by Western blotting, using a widely applied CFTR antibody from the CF Foundation, CFFT-596 (Mall *et al.*, 2004). Calu-3 cells, which have a very high expression of CFTR (Shen *et al.*, 1994), were used as a positive control. With the same amount of loaded protein, a diffuse ~180kDa band was observed in Calu-3 cell lysates, which was absent in lysates of HEK cells (Figure 3.6B).

Therefore, the Western blot and qPCR results provide evidence that HEK cells do not express appreciable levels of CFTR.

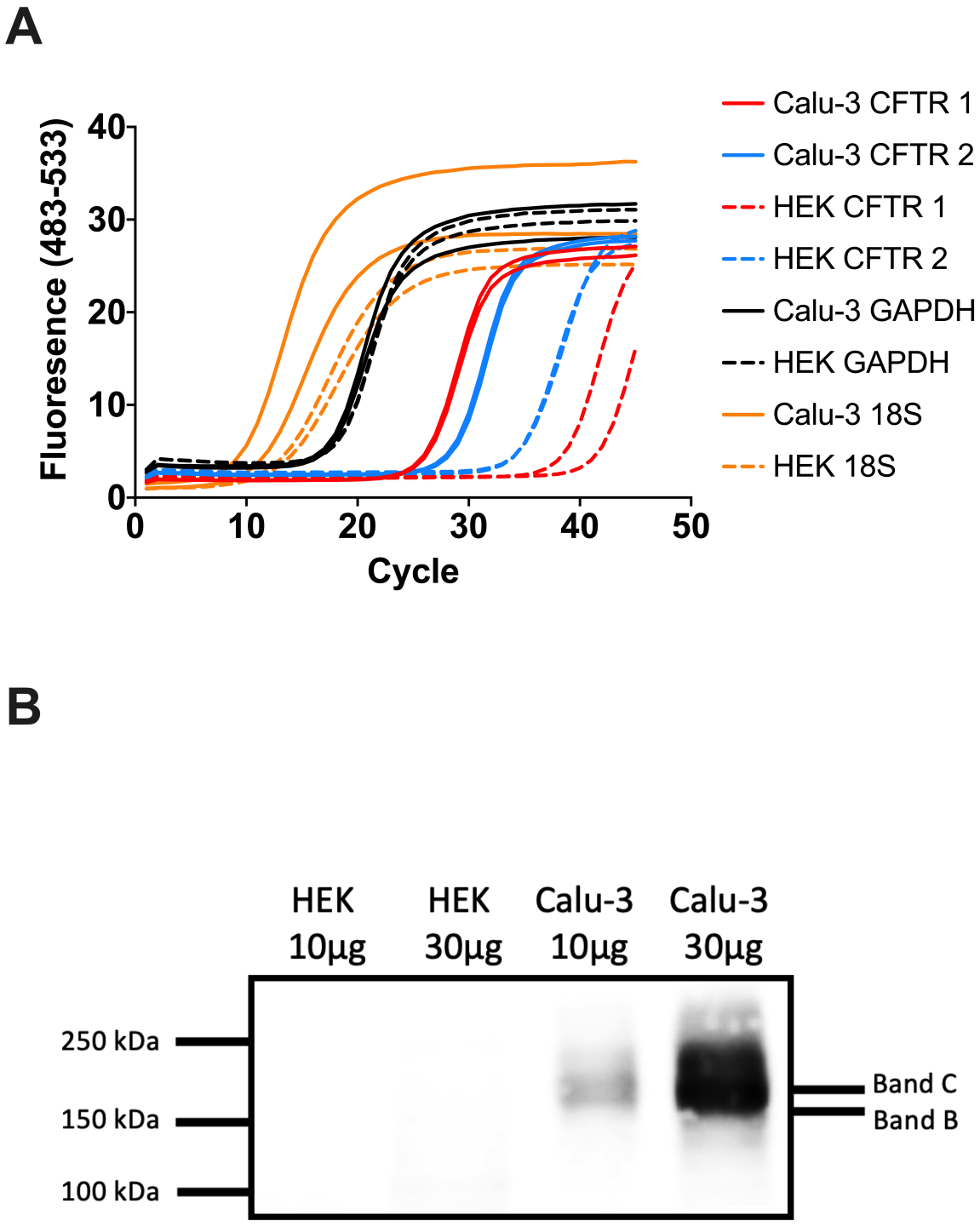

Figure 3.6: HEK cells do not express CFTR. (A) Amplification curves for CFTR, using two different primers, and housekeeping genes GAPDH and 18S, in qPCR analysis. Each sample was ran in duplicates. (B) Western blot image of samples probed for CFTR expression using the CFFT-596 primary antibody (n = 1). The molecular mass of fully glycosylated (Band C) CFTR is ~180kDa.

To ascertain whether the inhibition of SOCE by $CFTR_{inh}$-172 was dependent on CFTR, HEK cells were exposed to $CFTR_{inh}$-172 for 30 mins in the repeated SOCE protocol shown above (Figure 3.7B). The vehicle DMSO was used as a negative control (Figure 3.7A). The peak amplitude and rate of individual SOCE is summarised in Table 3.3.

Similar to in Calu-3 cells, the vehicle control experiments in HEK cells also had reproducible SOCE amplitude and rate ($p>0.05$ for all multiple comparisons). However, the higher influx rate in SOCE #2 and 3, compared to SOCE #1, was still observed, although this did not reach statistical significance.

Despite HEK cells not expressing CFTR, 30-min treatment with $CFTR_{inh}$-172 caused a significant inhibition of SOCE ($p<0.05$ for amplitude and rate, SOCE #2 vs. 1). This inhibition was not reversible following 30-min washout of the compound ($p<0.05$ for amplitude and rate, SOCE #3 vs. 1), suggesting that $CFTR_{inh}$-172 exerted an off-target effect, i.e. not involving CFTR, to inhibit SOCE.

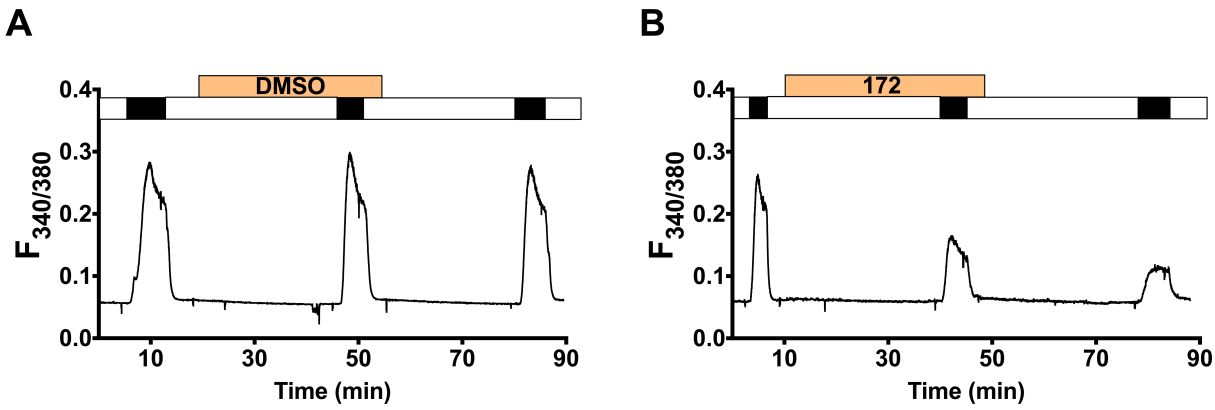

Figure 3.7: $CFTR_{inh}$-172 also inhibited SOCE in HEK293 cells. Representative Ca^{2+} fluorimetry traces tracking changes in $[Ca^{2+}]_i$ following a Tg-activated, repeated Ca^{2+} addback protocol, with pre-treatment of DMSO (A) or 20μM CFTRinh-172 (B) for 30 mins.

Treatment	Amplitude			Rate		
	SOCE #1	SOCE #2	SOCE #3	SOCE #1	SOCE #2	SOCE #3
DMSO	0.14±0.03	0.15±0.04	0.14±0.03	0.11±0.02	0.16±0.04	0.15±0.03
$CFTR_{inh}$-172	0.19±0.02$^{*\$}$	0.08±0.01$^{\$}$	0.05±0.00	0.21±0.03$^{*\$}$	0.06±0.01	0.03±0.00
GlyH-101	0.11±0.01$^{*\$}$	0.06±0.01	0.04±0.01	0.11±0.01$^{*\$}$	0.04±0.01$^{\$}$	0.01±0.00
Tannic acid	0.20±0.01$^{\$}$	0.09±0.02	0.03±0.00	0.19±0.01	0.01±0.00$^{*\$}$	0.01±0.00

Table 3.3: Summary data of SOCE peak amplitude and rate in HEK293 cells pre-treated with the vehicle DMSO or different chloride channel inhibitors. Data from various durations of DMSO treatment (10 or 30 mins) was pooled together. Repeated-measure one-way ANOVA with Holm-Sidak multiple comparisons tests was performed across the three SOCE, within each of the four datasets. n = 4-6. Data presented as mean ± SEM. * = $p<0.05$ vs. SOCE #2; $ = $p<0.05$ vs. SOCE #3.

To investigate if the off-target effect of $CFTR_{inh}$-172 was unique to this compound or evident in other supposed CFTR-specific agents, the effect of GlyH-101 (Muanprasat *et al.*, 2004), a pore blocker of CFTR, on SOCE was studied (Figure 3.8A). Similar to $CFTR_{inh}$-172, a 10-min pre-treatment with 10μM GlyH-101 significantly inhibited the amplitude and rate of SOCE #2 in HEK cells (Table 3.3; $p<0.05$, SOCE #2 vs. 1), and this inhibition was also irreversible ($p<0.05$, SOCE #3 vs. 1), indicating that SOCE inhibition may be a wider off-target effect of CFTR blockers.

To investigate whether inhibitors of chloride channels other than CFTR exhibit a similar off-target effect, the impact of tannic acid, an inhibitor of calcium-activated chloride channels (CaCC), that does not block CFTR (Namkung *et al.*, 2010), on SOCE was examined (Figure 3.8B). HEK293 cells are not known to conduct CaCC currents, or to express appreciable levels of TMEM16A protein, the putative CaCC in epithelial cells (Tian *et al.*, 2011). It was observed that a 10-min treatment with 100μM tannic acid did not significantly inhibit the amplitude of SOCE #2 (Table 3.3; $p>0.05$, SOCE #2 vs. 1), but SOCE #3 was significantly attenuated ($p<0.05$, SOCE #3 vs. 1) – a similar delayed inhibition as seen in 10-min exposure to $CFTR_{inh}$-172. However, the rate of SOCE was significantly and irreversibly inhibited by tannic acid ($p<0.05$, SOCE #2 and 3 vs. 1).

In terms of the percentage change from SOCE #1 to SOCE #2, all three chloride channel blockers exerted significantly greater inhibition on both the amplitude and rate of SOCE, compared to the vehicle DMSO (Figure 3.8C-D; $p<0.05$ for both amplitude and rate, for all treatment groups vs. DMSO). The percentage change in both parameters was comparable

amongst the three compounds, with no significant difference between any of the three drugs. Together, these data indicate that several chloride channel inhibitors reduce SOCE in HEK293 cells, independent of CFTR.

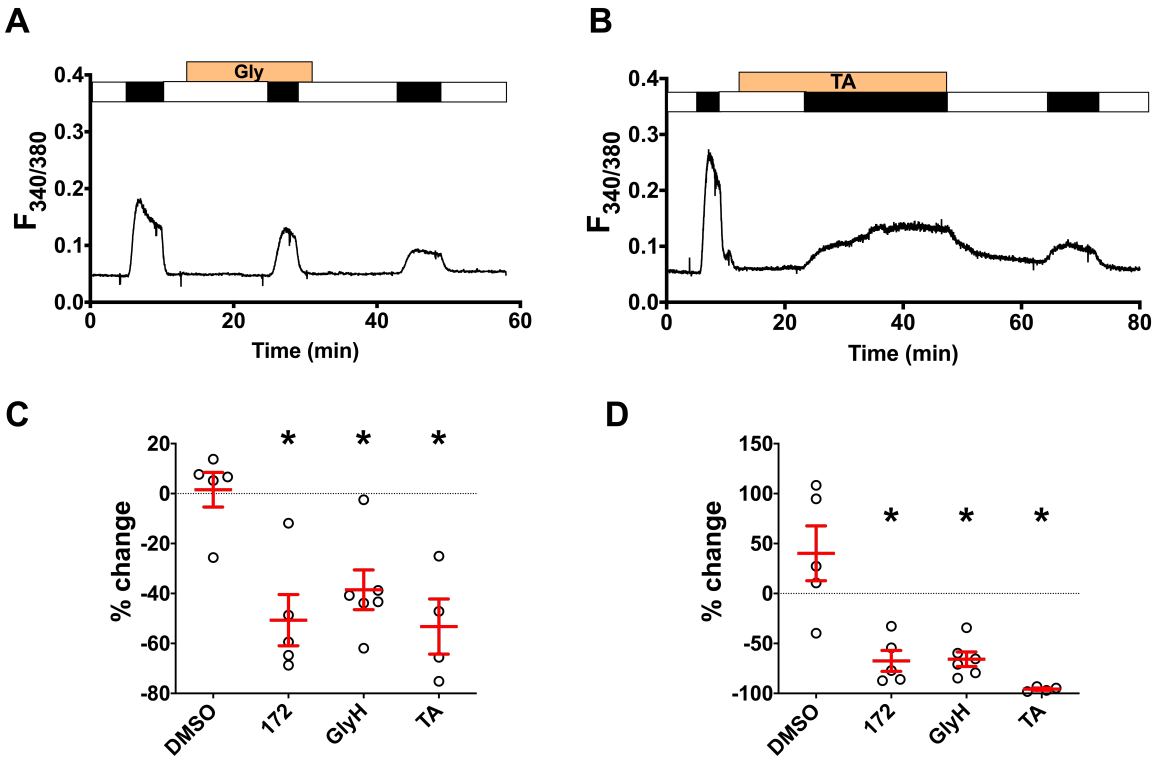

Figure 3.8: Distinct chloride channel blockers inhibit SOCE in HEK293 cells. (A-B) Representative Ca^{2+} fluorimetry traces tracking changes in $[Ca^{2+}]_i$ following a Tg-activated, repeated Ca^{2+} addback protocol, with pre-treatment with 10µM GlyH-101 (A) or 100µM tannic acid (B) for 10 mins before the second SOCE was activated. (C-D) Summary of percentage change in SOCE peak amplitude (C) and rate (D), from SOCE #1 to SOCE #2, following treatment of DMSO or various chloride channel inhibitors as described above. n = 4-6. One-way ANOVA with Holm-Sidak multiple comparisons tests was performed across the four groups. Data presented as mean ± SEM. * = $p<0.05$ vs. DMSO.

The unexpected off-target effect of supposedly selective CFTR inhibitors on SOCE presented an obstacle for using these agents to investigate the effects of CFTR function on Ca^{2+} handling in ASMC. In the original screening study that characterised $CFTR_{inh}$-172, the CFTR current was inhibited within 2 minutes after drug exposure (Ma *et al.*, 2002). However, the time-dependency of $CFTR_{inh}$-172 inhibition of SOCE presented an opportunity to shorten the exposure time to the drug to study CFTR-specific effects, before such off-target effects manifested. Since the results in Figure 3.3 showed that a 3-min exposure did not significantly inhibit SOCE, this treatment duration could be used to examine the effects of specific CFTR inhibition on SOCE or other aspects of Ca^{2+} homeostasis in ASMC.

To ascertain the efficacy of CFTR inhibition by $CFTR_{inh}$-172 within 3 minutes, Ussing chamber experiments were performed using polarised Calu-3 cells, and CFTR-dependent short-circuit current (I_{SC}) was measured. Under a basolateral to apical Cl^- gradient, addition of 5µM forskolin

induced a rapid, biphasic increase in I_{SC}, and the second phase of the response reached a stable plateau after 10 minutes (Figure 3.9A). After the plateau was reached, 20µM $CFTR_{inh}$-172 (or DMSO as the vehicle control) was added to inhibit the portion of the fsk-induced current specific to CFTR. The inhibition of CFTR-specific currents reached a new plateau within 10 minutes (Figure 3.9A), with a maximal change in I_{SC} of 60.6±9.0 µA/cm^2 that was significantly greater than the change induced by DMSO alone (Figure 3.9B; $p<0.05$, DMSO vs. 172). This maximal change was used to normalise the percent inhibition over time, with 100% being the change in I_{SC} after 10 mins of $CFTR_{inh}$-172 exposure for each individual experiment. At 1 min, $CFTR_{inh}$-172 inhibited 13.5±2.6% of CFTR-specific currents, and this reached 60.1±5.7% at 3 mins (Figure 3.9C). Such significant inhibition of CFTR currents within 3 mins lent confidence using this exposure duration for studying the effects of CFTR modulation by $CFTR_{inh}$-172 on Ca^{2+} signalling in cultured ASMC.

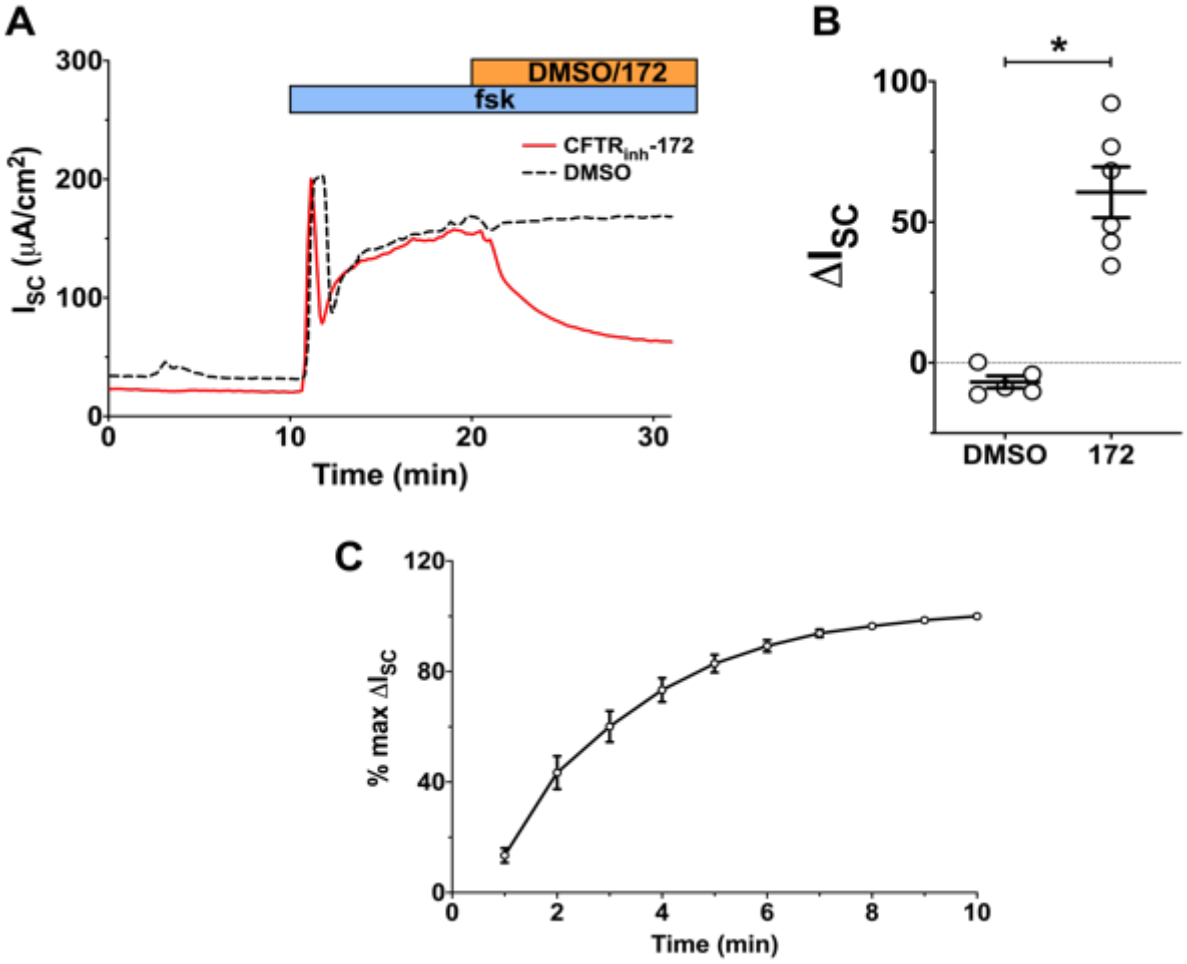

Figure 3.9: Inhibition kinetics of $CFTR_{inh}$-172 on CFTR-mediated short circuit current (I_{SC}) in Calu-3 cells. (A) Representative Ussing chamber traces tracking I_{SC} in polarised Calu-3 cells. Amiloride was added in the beginning of each experiment to block ENaC currents. A Cl^- gradient of 134mM basolateral to 0mM apical was applied to amplify Cl^- secretion. (B) Summary of peak negative change in I_{SC} induced by DMSO or 20µM $CFTR_{inh}$-172. Unpaired t-test was performed between the two treatment groups. (C) The percentage of peak change in I_{SC} induced by $CFTR_{inh}$-172 over time, with 100% being the maximal ΔI_{SC} at 10 mins. n = 5-6. Data presented as mean ± SEM.

3.3.4 CFTR is expressed in rat and human ASMC

As detailed in the Introduction chapter, CFTR has been reported to be expressed in rat and human ASMC, and localised intracellularly. Before studying CFTR in ASMC, the expression of CFTR was validated in isolated rat and human ASMC. The global expression of CFTR was examined by Western blot analysis, and lysates from Calu-3 cells were used as the positive control. The CFFT-596 antibody, which detected mature, fully glycosylated (Band C; ~180 kDa) CFTR in Calu-3 cells (Figure 3.6B), was not able to pick up CFTR in rASMC and hASMC. Using a different, rabbit polyclonal antibody from Alomone Labs, ACL-006, the partially glycosylated form of CFTR (Band B; ~160 kDa) was clearly detected in Calu-3 cells (Figure 3.10A). This CFTR band was not present in the negative control, where blots were probed without the primary antibody (right panels in Figure 3.10). However, under the same exposure conditions, only a faint band was observed in rASMC lysate, and no bands were detected in hASMC. After prolonged exposure, Band B was detected in both rat and human ASMC (Figure 3.10A). Another notable result from Figure 3.10A was the prominent low molecular mass bands (~110 and 90 kDa) in all three samples that were inconsistent with the mass of the two distinct CFTR bands, which may be attributed to non-specific binding of the antibody, or degradation products of CFTR in these samples. These are not likely to be Band A, the non-glycosylated form, of CFTR (~130 kDa). These low molecular mass bands were also faintly present in the negative control under longer exposure.

To circumvent the potential non-specific binding of ACL-006, cell lysates were first immunoprecipitated using CFFT-596 prior to Western blot analysis with ACL-006. This protocol combined the sensitivity of ACL-006 and the specificity of CFFT-596, as Western blotting with CFFT-596 did not produce low molecular mass bands (Figure 3.6B), but was not able to detect CFTR in rASMC and hASMC. Following immunoprecipitation, a prominent Band C, along with a faint Band B, was observed in Calu-3 cell lysates, and low molecular mass bands were mostly undetectable (Figure 3.10B). With a prolonged exposure, Band C was also detected in hASMC lysates (Figure 3.10B). Therefore, CFTR is expressed in rat and human ASMC, but expression levels are low relative to in Calu-3 cells.

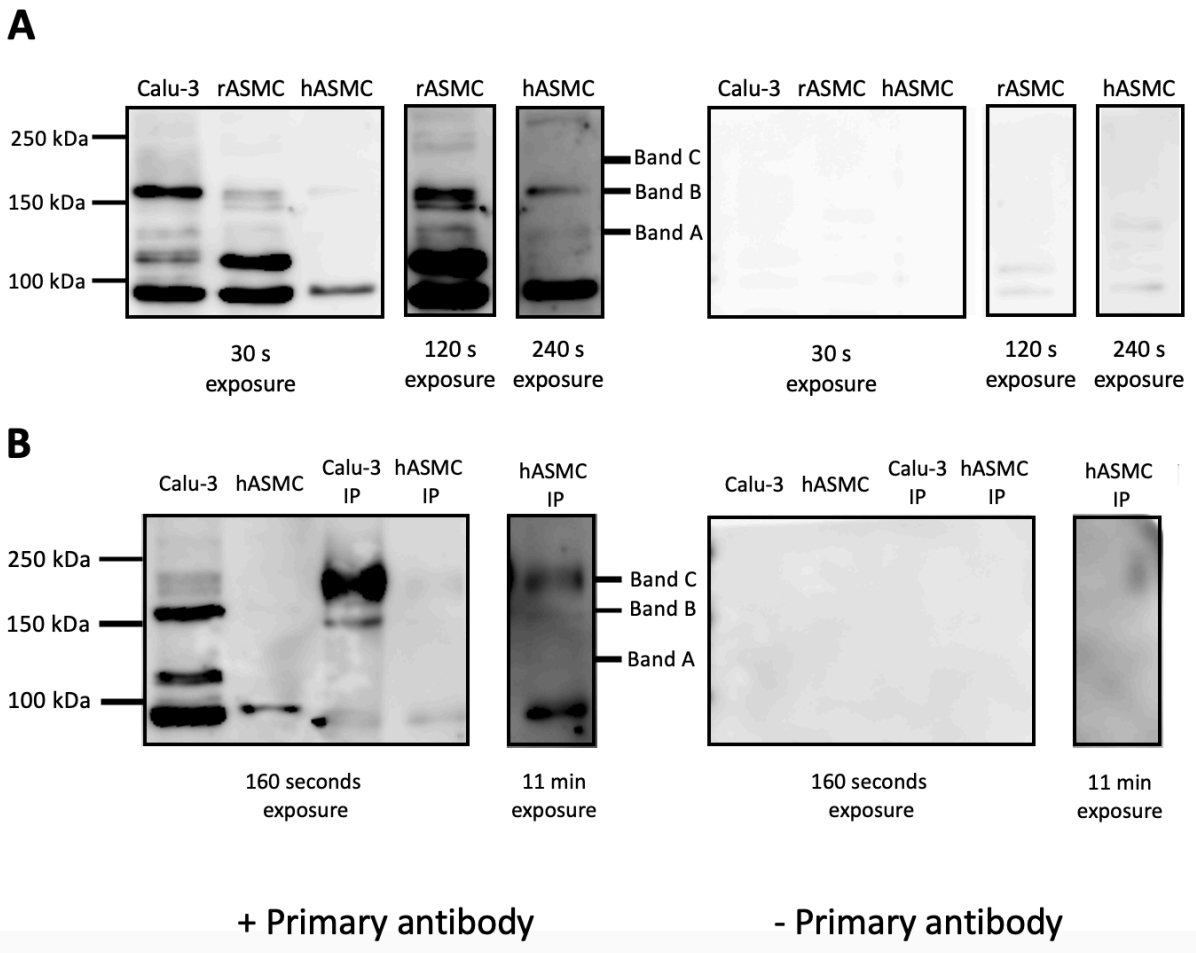

Figure 3.10: CFTR is expressed in cultured rat and human ASMC. (A) Representative Western blot images of samples probed for CFTR using the ACL-006 primary antibody (1:1000 dilution). n = 3 for Calu-3 and rASMC, n = 2 for hASMC. Longer exposure durations were applied to rASMC and hASMC samples to detect CFTR. (B) Representative Western blot images demonstrating detection of mature CFTR through immunoprecipitation (n = 2). Lanes labelled "IP" were samples that were immunoprecipitated using the CFFT-596 primary antibody before Western blotting. Samples were probed for CFTR using the ACL-006 primary antibody (1:1000 dilution). A longer exposure duration was applied to the immunoprecipitated hASMC sample to detect CFTR. The molecular mass for fully glycosylated CFTR is 180 kDa (Band C); the 160 kDa band (Band B) is partially glycosylated CFTR; the non-glycosylated form of immature CFTR appears as Band A (130 kDa). Right panels are negative control blots for the left panels, probed without the primary antibody.

After confirming the expression of CFTR in rat and human ASMC, its cellular localisation was investigated by immunofluorescence. The relatively specific antibody, CFFT-596, was not able to detect CFTR by immunofluorescence labelling in rASMC after multiple attempts. Therefore, ACL-006 was used to stain for CFTR in rASMC, while CFFT-596 was used to probe for hASMC CFTR. In Calu-3 cells, both ACL-006 (Figure 3.11A) and CFFT-596 (Figure 3.11B) produced perinuclear fluorescent staining patterns, with signals detected in both the plasma membrane and intracellular compartments of the cells. In contrast, in rASMC and hASMC, the CFTR staining was mostly intracellular, with no obvious plasma membrane staining. These results indicate that CFTR is predominantly expressed intracellularly in rat and human ASMC.

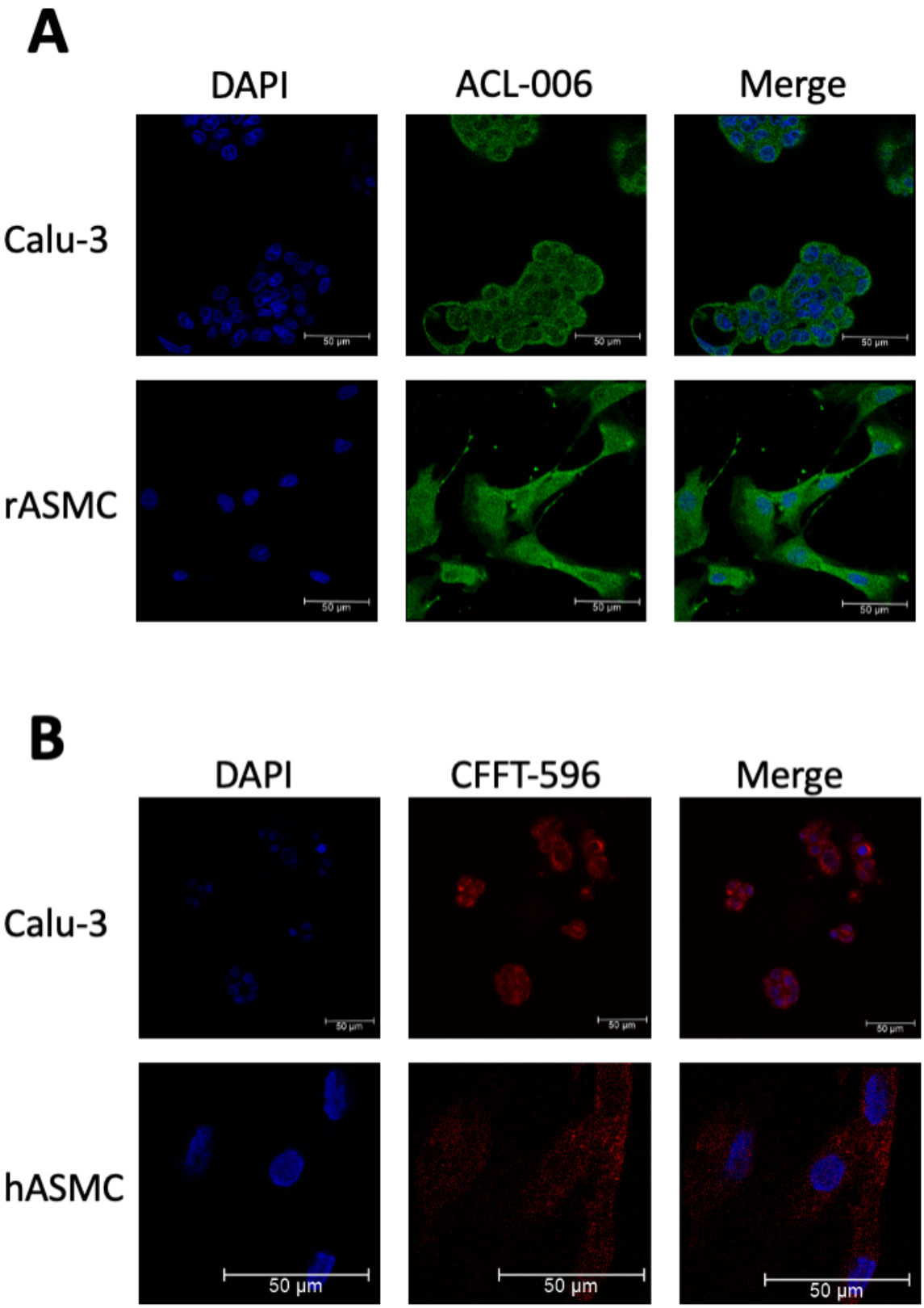

Figure 3.11: Cellular localisation of CFTR in cultured rat and human ASMC. Representative immunofluorescence images of methanol-fixed Calu-3 cells, rASMC (A), and hASMC (B) stained for CFTR using the ACL-006 (A; 1:100 dilution) or the CFFT-596 (B; 1:300 dilution for Calu-3 and 1:200 for hASMC) primary antibody. 2-3 independent experiments were performed for rASMC and hASMC, and images from at least 2 fields of view were gathered. Cell nuclei were stained with DAPI. Scale bars are 50µm.

3.3.5 The effects of pharmacological CFTR inhibitor on SOCE and Ca^{2+} store release in rASMC

After confirming that CFTR was expressed in cultured rat and human ASMC, the role of CFTR in ASMC Ca^{2+} homeostasis was examined. The repeated Ca^{2+} addback protocol used previously on Calu-3 cells was applied to cultured rASMC, with 3-min exposure to $CFTR_{inh}$-172, to investigate the effects on SOCE (Figure 3.12B). The summary data is presented in Table 3.4.

A similar vehicle control protocol (Figure 3.12A) was also applied to demonstrate reproducibility of repeated SOCE responses. In rASMC, this reproducibility was maintained across 3 repeated SOCE, with no significant difference between any of the three response amplitude or rate (Table 3.4; $p>0.05$ for all multiple comparisons).

On the other hand, a 3-min pre-treatment with $CFTR_{inh}$-172 did not significantly reduce the peak amplitude of SOCE #2 (Table 3.4; $p>0.05$, SOCE #2 vs. 1). However, the rate of SOCE was significantly attenuated by $CFTR_{inh}$-172 treatment ($p<0.05$, SOCE #2 vs. 1). This inhibition was not reversible ($p<0.05$, SOCE #3 vs. 1), but the persistent effects of $CFTR_{inh}$-172 on SOCE #3 may be non-specific. The significant inhibition in the rate of SOCE, despite the short treatment duration of 3 mins, suggests that the effect of the inhibitor was potentially CFTR-specific.

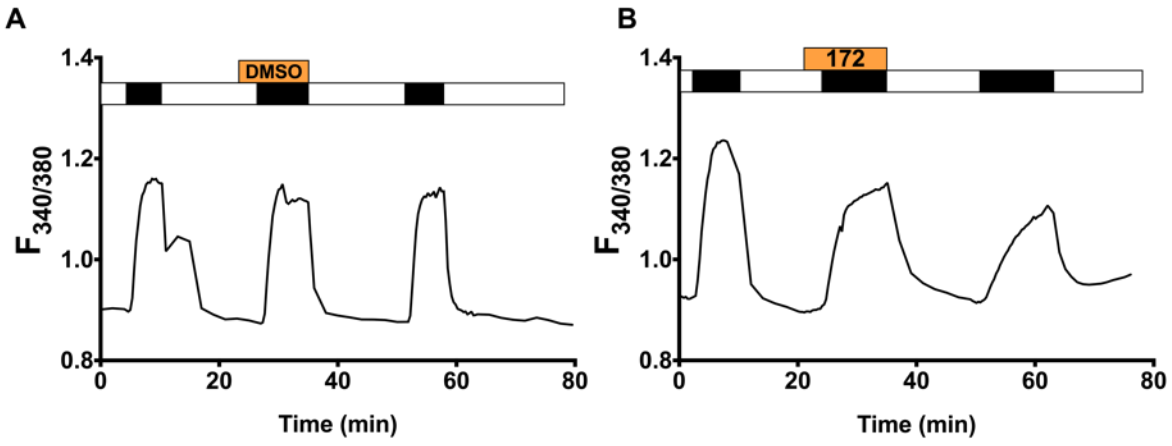

Figure 3.12: $CFTR_{inh}$-172 reduces the rate of SOCE in rASMC. Representative Ca^{2+} imaging traces tracking changes in $[Ca^{2+}]_i$ following a Tg-activated, repeated Ca^{2+} addback protocol, with 3-min pre-treatment of DMSO (A) or 20μM $CFTR_{inh}$-172 (B) before the second SOCE was activated.

Treatment	Amplitude			Rate		
	SOCE #1	SOCE #2	SOCE #3	SOCE #1	SOCE #2	SOCE #3
DMSO	0.19±0.05	0.16±0.04	0.16±0.04	0.09±0.03	0.07±0.02	0.06±0.02
$CFTR_{inh}$-172	0.22±0.07	0.15±0.03	0.13±0.03	0.10±0.02*$	0.04±0.01	0.04±0.01

Table 3.4: Summary data of SOCE peak amplitude and rate in rASMC pre-treated for 3 mins with the vehicle DMSO or $CFTR_{inh}$-172. Repeated-measure one-way ANOVA with Holm-Sidak multiple comparisons tests was performed across the three SOCE. n = 6-7. Data presented as mean ± SEM. * = $p<0.05$ vs. SOCE #2; $ = $p<0.05$ vs. SOCE #3.

In addition to SOCE, Ca^{2+} release from intracellular stores, another core component of Ca^{2+} homeostasis, was investigated. In particular, the effect of CFTR activation and inhibition on GPCR-coupled Ca^{2+} store release, a major mechanism in initiating ASMC contraction, was examined. Here, rASMC were exposed to 100μM ATP to activate Ca^{2+} release following a 3-min pre-treatment with the vehicle DMSO (Figure 3.13A), forskolin (Figure 3.13B), $CFTR_{inh}$-172 (Figure 3.13C), or both (Figure 3.13D). As repeated exposures to ATP was not possible due to receptor desensitisation, an unpaired approach comparing separate individual experiments was used. Day-matched controls were performed to minimise variability for these unpaired comparisons, with the same number of experiments for each treatment group per day, with cells from the same plate. A summary of the peak amplitude, rate, recovery rate, and extent of recovery are presented in Table 3.5.

A 3-min pre-treatment with forskolin, $CFTR_{inh}$-172, or the combination did not produce any significant effects on the amplitude or rate of ATP-induced Ca^{2+} release, compared to the vehicle control (Table 3.5; $p>0.05$ vs. DMSO for all 3 groups). Similarly, the recovery rates following the peak of the ATP response were also similar in all four groups ($p>0.05$ for all multiple comparisons).

However, an elevated plateau following recovery of ATP-induced Ca^{2+} release was observed in ASMC that were treated with 172+fsk (Figure 3.13D). Analysis of the amplitude of this elevated plateau, in relation to the baseline ratio prior to ATP stimulation, revealed a significantly higher plateau in the 172+fsk-treated group, compared to the vehicle-treated, fsk-treated, and the 172-treated group (Table 3.5). Moreover, exposure to forskolin or $CFTR_{inh}$-172 individually also resulted in a higher post-recovery plateau compared to the vehicle control experiments, in which the plateau was slightly lower than baseline before ATP stimulation ($p<0.05$ for DMSO vs. 172 or fsk). These data suggest that $CFTR_{inh}$-172 and forskolin, individually or in combination, inhibited the extent, but not the rate, of calcium reuptake in rASMC.

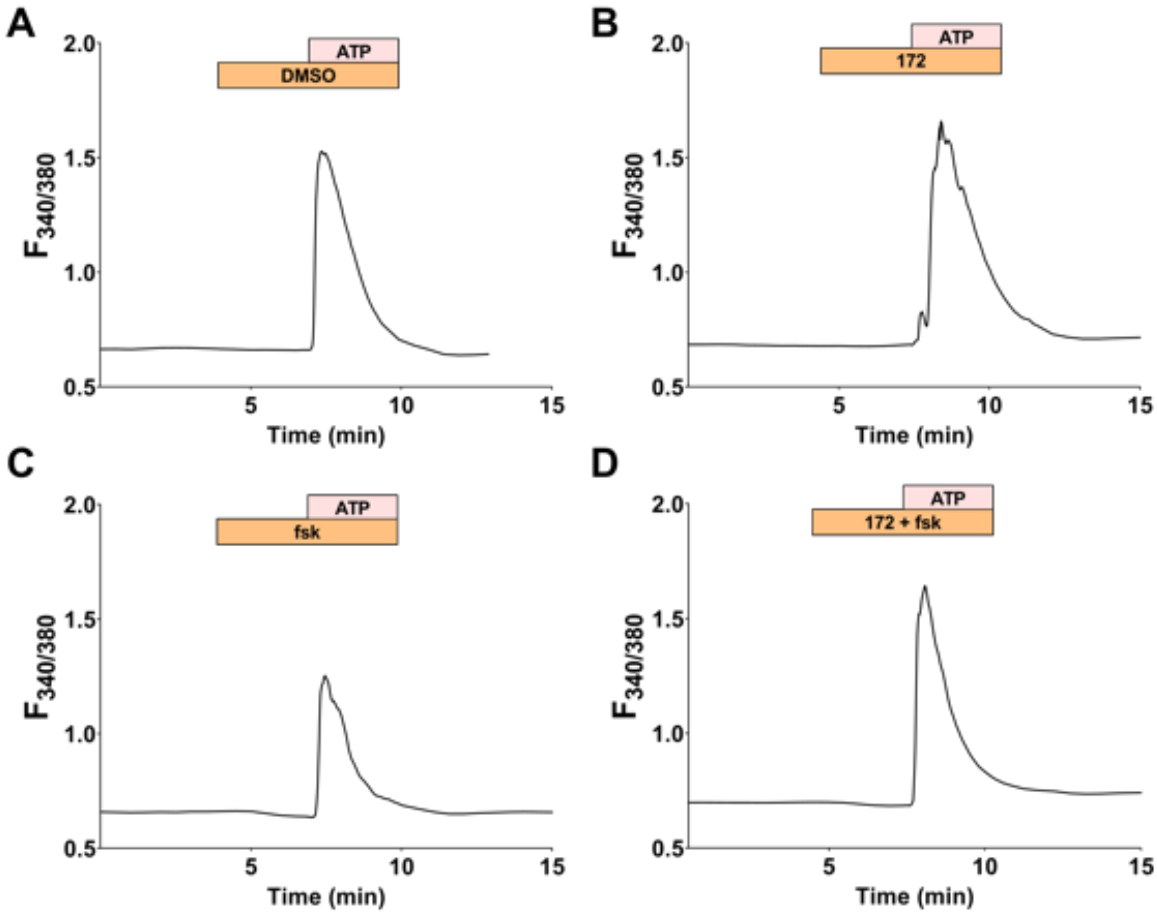

Figure 3.13: CFTR activation and inhibition do not markedly affect ATP-induced Ca^{2+} store release in rASMC. Representative Ca^{2+} imaging traces tracking changes in $[Ca^{2+}]_i$ following stimulation of Ca^{2+} store release with 100µM ATP, with 3-min pre-treatment of DMSO (A); 5µM forskolin (B); 20µM $CFTR_{inh}$-172 (C); or the combination of forskolin and $CFTR_{inh}$-172 (D).

Treatment	Amplitude	Rate	Recovery rate	Recovery extent
DMSO	0.80±0.15	8.90±3.77	-0.48±0.11	-0.03±0.00
Forskolin	0.87±0.15	7.44±1.94	-0.40±0.05	-0.01±0.01*$
$CFTR_{inh}$-172	0.64±0.11	4.93±0.91	-0.30±0.07	-0.01±0.01*$
Forskolin + $CFTR_{inh}$-172	0.73±0.10	7.92±1.61	-0.48±0.09	0.06±0.01*

Table 3.5: Summary of peak amplitude, rate, recovery rate, and extent of recovery of ATP-coupled Ca^{2+} release in rASMC following treatment with different CFTR modulators. Extent of recovery was calculated as level of plateau above the pre-ATP-stimulated baseline. One-way ANOVA with Holm-Sidak multiple comparisons tests were performed across the four treatment groups. n = 6. Data presented as mean ± SEM. * = $p<0.05$ vs. DMSO; $ = $p<0.05$ vs. fsk+172.

3.4 Discussion

The results presented in this chapter indicate that activation of CFTR with forskolin in Calu-3 cells significantly reduced the rate of SOCE, while specific inhibition of CFTR with a short exposure to $CFTR_{inh}$-172 did not affect SOCE. In addition, previously unknown off-target effects of several Cl^- channel inhibitors were identified. Specifically, two inhibitors of CFTR, $CFTR_{inh}$-172 and GlyH-101, exerted CFTR-independent, time-dependent inhibition of SOCE in human epithelial cells, which was also observed with a blocker of another Cl^- channel, tannic acid. After characterising these off-target effects, it was established that a short-exposure to $CFTR_{inh}$-172 was suitable for studying CFTR-specific effects, as a 3-min exposure to $CFTR_{inh}$-172 inhibited cAMP activated I_{SC}, but did not significantly attenuate SOCE in Calu-3 cells. Furthermore, CFTR was found to be expressed, and localised intracellularly, in both rat and human ASMC. Using the short-exposure protocol for $CFTR_{inh}$-172, it was observed that CFTR inhibition in cultured rASMC significantly attenuated the rate, but not the capacity, of SOCE, as well as the extent, but not the rate, of $[Ca^{2+}]_i$ recovery following ATP-induced store release.

A number of previous studies have demonstrated that CF epithelial cells exhibit enhanced Ca^{2+} mobilisation (explored in section 1.6.1). Notably, Balghi *et al.* (2011) showed that F508del-CFTR epithelial cells had upregulated SOCE compared to non-CF cells. However, the effect of CFTR activation on SOCE has not been reported. In this current study, activation of CFTR in Calu-3 cells by forskolin irreversibly inhibited the rate, but not the peak amplitude, of SOCE (Figure 3.5), which could be attributed to CFTR activation, or other downstream signalling pathways as a result of elevated intracellular cAMP levels. From an electrochemical perspective, cAMP-activated Cl^- efflux by CFTR would significantly depolarise the membrane potential to near the equilibrium potential for Cl^- (E_{Cl}; ~35mV assuming 30mM intracellular Cl^-), reducing the electrochemical driving force for Ca^{2+} entry (Devor *et al.*, 1999).

In a study investigating the link between SOCE and CF, Balghi *et al.* (2011) reported an increased exocytic insertion of the SOCC, Orai1, at the plasma membrane in CF human epithelial cells, which contributed to augmented SOCE, which was reversed by the rescue of F508del-CFTR trafficking to the plasma membrane. They proposed that the presence of CFTR protein, but not its activity, at the plasma membrane was responsible for regulation of SOCE, by showing that $CFTR_{inh}$-172, added at the same time as Ca^{2+} was added back following store depletion, did not affect SOCE in CFBE cells transduced with WT-CFTR. However, this protocol did not allow enough time for $CFTR_{inh}$-172 to take effect, since $CFTR_{inh}$-172 is an allosteric inhibitor that needs to cross the plasma membrane and bind to the cytoplasmic NBDs of CFTR (Ma *et al.*, 2002), and therefore its actions are not immediate; for instance, in Calu-3

cells, only <20% inhibition was observed after a 1 min treatment with $CFTR_{inh}$-172 (Figure 3.9). The protocol in this current study thus pre-treated the cells with the inhibitor for a certain duration before SOCE was initiated, and the results were in agreement with Balghi *et al.* (2011), that the intended specific inhibition of CFTR activity at the plasma membrane did not significantly affect SOCE in human epithelial cells expressing functional WT-CFTR.

On the other hand, the off-target inhibition of SOCE by $CFTR_{inh}$-172 was validated in HEK293 cells, a cell line that does not express CFTR. The lack of CFTR expression was confirmed in the current study using qPCR analysis (Figure 3.6A), which demonstrated high CT values for amplification of CFTR, using two different primers, in HEK cell samples. The maximum detection CT range for the LightCycler 480 system used was 40, and signals detected at cycles close to the maximal detection range (last 5 cycles according to the LightCycler 480 software) have high uncertainty as expression levels are either too low to be reliably detected, or may be due to artefacts such as cross-contamination or non-specific amplification (Nolan *et al.*, 2006; Burns and Valdivia, 2008). Thus, the expression of CFTR mRNA in HEK cells was negligible, especially compared to the high CFTR expression levels in Calu-3 cells. Using these HEK cells, it was demonstrated that $CFTR_{inh}$-172 and GlyH-101, two supposedly selective CFTR inhibitors, exerted an off-target effect to reduce SOCE. However, despite the results on HEK cells, it is not certain whether the SOCE-inhibitory effects of $CFTR_{inh}$-172 on Calu-3 cells are completely independent of CFTR.

The specificity of both $CFTR_{inh}$-172 and GlyH-101 has previously been questioned. Melis *et al.* (2014) showed that, in addition to CFTR, these agents also inhibited volume-sensitive Cl^- channels (VSCC), and GlyH-101 inhibited CaCC, in both CFTR-expressing kidney cells and the non-CFTR-expressing PS120 cell line. Moreover, GlyH-101, but not $CFTR_{inh}$-172, was also shown to inhibit SLC26A9, a member of the Solute-Linked Carrier transporter family, which facilitates Cl^- conductance in epithelial cells (Bertrand *et al.*, 2009). Outside of Cl^- channels, both $CFTR_{inh}$-172 and GlyH-101 have also been shown to induce ROS production and mitochondrial membrane depolarisation in cells lacking functional CFTR, including human CF lung epithelial cells and non-CFTR-expressing cell lines (Kelly *et al.*, 2010). However, the results in this chapter are the first report of the off-target inhibitory effects of several chloride channel inhibitors on SOCE in epithelial cells. Interestingly, CFTR itself has shown to be indirectly activated by Ca^{2+} (reviewed in Billet and Hanrahan (2013)). For instance, Ca^{2+} activates several isoforms of adenylyl cyclase (1 and 8), which catalyses cAMP production (reviewed in Halls and Cooper (2011)), as well as Pyk2/Src, tyrosine kinases that directly phosphorylate CFTR, and inhibit dephosphorylation of CFTR (Billet *et al.*, 2013). Therefore,

the inhibitory effects of $CFTR_{inh}$-172 and GlyH-101 on CFTR-mediated anion transport may be partially attributed to the off-target downregulation of $[Ca^{2+}]_i$.

An interesting aspect of this inhibitory effect of $CFTR_{inh}$-172 on SOCE was the time lag. In the original study that identified the compound, Ma *et al.* (2002) found that it reversibly inhibited CFTR current within 2 minutes in airway epithelial cells. However, as shown in Figure 3.2-3, a 3-min and 10-min exposure was not always sufficient to attenuate SOCE, and this inhibition was not reversed following 15-30 minutes of washout. This delayed effect suggests that $CFTR_{inh}$-172 is unlikely to be a pore-blocker of SOCC. The inhibition of SOCE may involve binding to SOCC leading to allosteric changes in channel gating (similar to how $CFTR_{inh}$-172 inhibits CFTR), or changes in the function, expression and/or spatial localisation of SOCE-related proteins, specifically the STIM1/Orai1 complex. Another possible explanation is the involvement of ROS in regulating SOCE, as $CFTR_{inh}$-172 and GlyH-101 treatment led to ROS production (Kelly *et al.*, 2010). Moreover, the time-lag of $CFTR_{inh}$-172 in reducing SOCE in the present study corresponded with the time-course of intracellular ROS elevation reported by Kelly *et al.* (2010), detectable after 5-min and peaking after 30-min following $CFTR_{inh}$-172 or GlyH-101 treatment. However, the literature on the interaction between ROS and SOCE presents conflicting results, which appeared to be cell-type specific. Oxidative stress and ROS were shown to enhance SOCE in rat arterial SMC (Chen *et al.*, 2017), healthy primary human prostate epithelial cells (Holzmann *et al.*, 2015), and DT40 chicken B-cell line (Hawkins *et al.*, 2010), but attenuated SOCE in mouse hippocampal cells (Henke *et al.*, 2013), human T-helper cells (Bogeski *et al.*, 2010), and prostate cancer cell lines (Holzmann *et al.*, 2015). Calu-3 cells and HEK293 cells used in the present study were most similar to human prostate cancer cells in Holzmann *et al.* (2015); the inhibition of SOCE by $CFTR_{inh}$-172 and GlyH-101, which elevate intracellular ROS levels, in the present study was consistent with the inhibition of SOCE by H_2O_2 in prostate cancer cells. To further validate this mechanism, the kinetics of intracellular ROS concentration elevation could be measured following $CFTR_{inh}$-172 or GlyH-101 exposure, and the effect of ROS scavengers (e.g. N-acetylcysteine) on disrupting the $CFTR_{inh}$-172/GlyH-101-induced inhibition of SOCE could be investigated.

As outlined in the Introduction chapter, CFTR has been shown to be expressed in cultured rat ASMC (Vandebrouck *et al.*, 2006), cultured human ASMC (Michoud *et al.*, 2009; Norez *et al.*, 2014), and freshly isolated porcine ASMC (Cook *et al.*, 2016), and all four studies have reported diffuse intracellular localisation of CFTR protein, distinct from the predominantly plasma membrane localisation in epithelial cells. It is worth noting, however, that both Vandebrouck *et al.* (2006) and Michoud *et al.* (2009) used a different CFTR antibody (clone 24-1, R&D

systems) than the two used in the current study. The detectable expression, as well as immunofluorescence signals predominantly within the cytoplasmic space reported here, are consistent with the results from these studies (Figure 3.10). However, there was uncertainty regarding the specificity of the ACL-006 primary antibody, which detected low molecular mass bands that were removed by immunoprecipitation with the CFFT-596 antibody. Therefore, immunofluorescent staining results of rASMC using ACL-006 should be validated using other specific antibodies, or techniques such as in-situ hybridisation to examine localisation of CFTR mRNA. In terms of specific localisation to cell organelles, Cook *et al.* (2016) demonstrated that CFTR co-localised with markers of the SR in porcine ASMC using the CFFT-596 antibody. Similarly, it is likely that rat and human ASMC CFTR localises to the SR, but this requires further investigation. It would also be informative to examine the endogenous processing and trafficking of the CFTR protein in ASMC, for example by transfecting fluorescent-tagged CFTR, to examine the time-lapse expression pattern and localisation of CFTR to intracellular organelles.

Another direction for future experiments, would be to investigate the effect of cigarette smoke on the localisation of CFTR in ASMC, as CFTR was shown to be internalised from the plasma membrane following smoke exposure (Rasmussen *et al.*, 2014). In epithelial cell models, this internalisation of CFTR, which then underwent retrograde trafficking to the ER, was clathrin/dynamin-mediated, and dependent on dephosphorylation of CFTR by calcineurin, a Ca^{2+}-dependent phosphatase (Marklew *et al.*, 2019; Patel *et al.*, 2019). In ASMC, where CFTR is not predominantly expressed on the sarcolemma membrane, CS exposure could potentially induce a different mechanism and direction of CFTR trafficking. Understanding the potential changes in the trafficking of CFTR could further elucidate how functional CFTR regulates Ca^{2+} homeostasis in ASMC, as well as its role in the pathophysiology of CS-related airway diseases.

Using the protocol established following characterisation of the off-target effects of $CFTR_{inh}$-172, it was observed that blocking CFTR activity in rASMC significantly inhibited the rate, but not peak amplitude, of SOCE (Figure 3.12). This finding was surprising, since activation of CFTR by forskolin also attenuated the rate of SOCE in Calu-3 cells (Figure 3.5), and CF epithelial cells were found to have upregulated SOCE (Balghi *et al.*, 2011). A possible explanation for these discrepancies is the difference in cell types, and the reported differences in the localisation of CFTR, as SR-localised CFTR in ASMC may serve a different cellular function than the plasmalemmal CFTR in epithelial cells. For instance, Cl^- channels on the SR membrane of SMC could act to neutralise any build-up of positive charges resulting from SR Ca^{2+} release or plasmalemmal Ca^{2+} influx, through Cl^- efflux from the SR, as detailed in section

1.6.3 of the Introduction chapter. This is coupled with Cl^- efflux through plasmalemmal Cl^- channels, to dissipate the accumulation of negative charges across the SR membrane from SR Cl^- efflux, further enhancing SR Ca^{2+} release (reviewed in (Janssen, 2002; Hirota *et al.*, 2007a; Janssen, 2012)). Indeed, Barro-Soria *et al.* (2010) have proposed that bestrophin-1, a CaCC localised on the ER membrane that enhanced purinergic-induced Ca^{2+} release in airway epithelial cells, facilitates counterion flux to balance changes in ER membrane potential caused by Ca^{2+} release and reuptake. Therefore, the counterion flux facilitated by SR-bound Cl^- channels could participate in enhancing the driving force for plasmalemmal Ca^{2+} influx, and hence could explain the inhibitory effect of $CFTR_{inh}$-172 on SOCE in rASMC observed in the current study. Indeed, the role of Cl^- channels, primarily CaCC, in regulating Ca^{2+} homeostasis and ASMC contraction has long been documented (reviewed in Kitamura and Yamazaki (2001); Janssen (2002)). Specifically, Cl^- channel blockers, including tannic acid, niflumic acid, DIDS, and NPPB, are known to attenuate agonist-induced contraction, and potentiate relaxation, in various smooth muscle cell types, including human and rat airway smooth muscle (Criddle *et al.*, 1996; Nelson *et al.*, 1997; Wang *et al.*, 1997; Yuan, 1997; Lamb and Barna, 1998; Yim *et al.*, 2013; Bernstein *et al.*, 2014; Danielsson *et al.*, 2014). Classically, the activation of CaCC in SMC has been shown to depolarise cells, thereby activating voltage-gated Ca^{2+} channels, allowing influx of Ca^{2+} to facilitate SMC contraction (reviewed in Leblanc *et al.* (2005)).

More recently, TMEM16A has been identified as the protein responsible for prevalent Ca^{2+}-activated Cl^- currents in a variety of cell types (reviewed in Jin *et al.* (2016)). However, despite predominantly plasma membrane expression in epithelial cells (Schroeder *et al.*, 2008), TMEM16A was shown to localise intracellularly in mouse VSMC (Davis *et al.*, 2010) and hASMC (Gallos *et al.*, 2013), and functionally regulate ASMC Ca^{2+} homeostasis and airway contraction. In particular, it was reported that antagonism of TMEM16A by potent blockers, e.g. niclosamide and benzbromarone, or TMEM16A knockdown, inhibited airway smooth muscle depolarisation and contraction, reduced Ca^{2+} influx and SR Ca^{2+} release, and induced bronchodilation of maximally contracted airways under inflamed conditions (Huang *et al.*, 2012; Gallos *et al.*, 2013; Zhang *et al.*, 2013; Dam *et al.*, 2014; Danielsson *et al.*, 2015; Miner *et al.*, 2019). In contrast, activation of TMEM16A was reported recently to elevate $[Ca^{2+}]_i$, and led to significant contraction of human airway smooth muscle and guinea pig tracheal rings, further supporting the importance of Cl^- flux in modulating ASMC calcium homeostasis (Danielsson *et al.*, 2020). However, the limited literature on the role of CFTR in regulating ASMC Ca^{2+} homeostasis provided results contradicting data from these recent TMEM16A studies. For instance, potentiators of CFTR were shown to facilitate relaxation of pre-constricted human bronchial rings and inhibition of cholinergic-induced airway narrowing in

porcine lung slices, and improved airway distensibility in CF patients (Norez *et al.*, 2014; Adam *et al.*, 2016; Cook *et al.*, 2016). These results suggest that although both TMEM16A and CFTR were shown to be functional Cl^- channels that are localised predominantly intracellularly in ASMC (Vandebrouck *et al.*, 2006; Michoud *et al.*, 2009; Gallos *et al.*, 2013; Norez *et al.*, 2014; Cook *et al.*, 2016), the physiological role of these two channels at regulating ASMC contractility may employ distinct mechanisms.

On the other hand, experiments studying the effects of CFTR modulation on ATP-induced Ca^{2+} release revealed that $CFTR_{inh}$-172 and forskolin, individually and in combination, significantly inhibited the extent, but not rate, of Ca^{2+} reuptake/extrusion in rASMC (Figure 3.13). Moreover, no significant effects of $CFTR_{inh}$-172 or forskolin on the amplitude and rate of Ca^{2+} release was observed. These findings are in contrast to a number of studies in the literature. For instance, reduced SR Ca^{2+} release was reported by Michoud *et al.* (2009) in CF hASMC, as well as non-CF hASMC treated with the relatively non-selective CFTR blockers glibenclamide and DPC. Similarly, Hirota *et al.* (2006) showed that blocking Cl^- channels with NPPB or depletion of intracellular Cl^- reduced the peak amplitude of caffeine-induced SR Ca^{2+} release in bovine ASM, which was not observed here with ATP-induced Ca^{2+} release. Moreover, Pollock *et al.* (1998) reported that blocking Cl^- channels, albeit using the relatively non-selective Cl^- channel inhibitors NPPB and indanyloxyacetic acid 94, as well as substituting extracellular Cl^- with SO_4^{2-}, reduced the rate of SR Ca^{2+} refilling in saponin-permeabilised rabbit gastric SMC. A slower rate of Ca^{2+} reuptake following a cholinergic-agonist challenge was also observed by Cook *et al.* (2016) in isolated CF porcine ASMC, compared to non-CF ASMC. It is worth noting, however, that in both Pollock *et al.* (1998) and Hirota *et al.* (2006), SR Ca^{2+} release was not inhibited by niflumic acid, suggesting that the functional SR Cl^- channel in SMC modulating SR Ca^{2+} store release is not likely to be TMEM16A.

Moreover, the seemingly paradoxical effect of forskolin, which activates CFTR, in also inhibiting the extent of Ca^{2+} reuptake additively with $CFTR_{inh}$-172, was surprising, especially considering the important role of cAMP in ASMC relaxation. Indeed, one of the primary bronchorelaxation mechanism is through stimulation of β_2-adrenoceptors, which leads to increased production of cAMP. One of the downstream actions of cAMP is the activation of cAMP-dependent PKA, phosphorylating phospholamban; the dephosphorylated form of phospholamban normally inhibit SERCA, and so elevated intracellular cAMP levels would activate SERCA, and thus the reuptake of cytosolic Ca^{2+} (Bers, 2002; MacLennan and Kranias, 2003). Therefore, the inhibition of Ca^{2+} reuptake by forskolin, which increases intracellular cAMP levels, is likely due to cAMP-independent mechanisms. However, it is worth noting that

the expression of phospholamban in rASMC has not been reported, although phospholamban protein was detected in murine and bovine ASMC (Koller *et al.*, 2003; McGraw *et al.*, 2006), but expression levels in hASMC were very low (Sathish *et al.*, 2009).

On the other hand, the relatively low expression of CFTR in ASMC may underlie the lack of effect of CFTR inhibition on the maximal extent of SOCE, ATP-induced Ca^{2+} release, and rate of Ca^{2+} reuptake. It is also possible that, although a 3-min exposure to $CFTR_{inh}$-172 rapidly inhibited over 60% of CFTR-specific currents in Calu-3 cells (Figure 3.9), the same degree of inhibition may not have been reached in ASMC due to the intracellular localisation of CFTR, which may require more time for the compound to cross multiple membranes and bind to CFTR. Moreover, the results obtained using $CFTR_{inh}$-172 cannot be deemed absolutely CFTR-specific, despite limiting exposure to 3-min to circumvent the off-target effects observed. Other alternative techniques to modify CFTR function, such as genetic silencing using shRNA and CRISPR/Cas9 technology, as well as investigating primary ASMC isolated from CF patients/animals, are required to validate these findings. In addition, a limitation of the experiments described in this chapter was that the ATP experiments were unpaired, and this introduced relatively more variability compared to the repeated SOCE protocol; if possible, reproducible Ca^{2+} release manoeuvres should be performed within the same experiment to validate these results, potentially using other GPCR agonists such as histamine, serotonin, bradykinin, and various cholinergic agonists.

Based on the results in this chapter, there remains a number of crucial research questions that need to be investigated, specifically, validating the findings obtained using $CFTR_{inh}$-172 with genetic techniques, further exploring the localisation and function of CFTR in ASMC, and examining the effects of CFTR modulation on any CS/CSE-induced change in calcium homeostasis. However, the low endogenous expression of CFTR in ASMC, coupled with concerns over specificity of $CFTR_{inh}$-172 and the relatively minor effects of CFTR modulators, made continuing future experiments on the role of CFTR in ASMC problematic. Therefore, the majority of this thesis instead focused on studying the effects of CS and CSE on calcium signalling in ASMC, as it directly relates to the pathophysiology of CS-related airway diseases.

Chapter 4: Cigarette smoke extract (CSE) disrupts calcium homeostasis in hASMC

4.1 Introduction

Given the challenges involved in fully characterising the role of CFTR in hASMC Ca^{2+} signalling, the remainder of this thesis will focus on exploring the effects of CS on hASMC Ca^{2+} homeostasis and contractile signalling. As reviewed in the Introduction chapter, ASMC is partially responsible for airway remodelling and is the central effector of airway hyperresponsiveness, which has been extensively linked to tobacco smoking (Hogg *et al.*, 2004; Chiba *et al.*, 2005; Caramori *et al.*, 2015; Jones *et al.*, 2016; Prakash, 2016). Therefore, clarifying the effects of CS on ASMC function is a key objective to this thesis.

The two common experimental models of CS delivery, namely direct aerosolisation of gaseous CS and aqueous CSE, are described in section 1.4.1. CSE is generated by bubbling mainstream smoke into a physiological solution. It can be argued that CSE is a more physiological model for investigating the effects of cigarette smoking on ASMC, since these cells would not be directly exposed to CS during smoking as the airway smooth muscle layer is situated deep within the airway submucosa. Rather, the water-soluble and lipophilic constituents of CS could diffuse through the epithelial barriers of the airway and enter the circulation, and dissolve in the blood similar to CSE. The dissolved constituents could then diffuse through the endothelial walls, and through the submucosa, to exert effects on ASMC. Another advantage of the CSE model is the relative ease and precision with which researchers can tightly control the delivery and removal of diluted CSE via fluid perfusion systems. This is especially useful for studying dose-response relationships, investigating reversibility of action, etc. Therefore, the first approach, described in this chapter, focuses on experiments utilising CSE.

As detailed in the section 1.4, chronic exposure to CSE can lead to a wide range of adverse effects to the ASMC that contribute to inflammation and airway remodelling, and more importantly, the intrinsic contractility and Ca^{2+} homeostasis of ASMC (Oltmanns *et al.*, 2005; Pera *et al.*, 2010; Xu *et al.*, 2010; Yoon *et al.*, 2011; Yoshiyama *et al.*, 2011; Xu *et al.*, 2012; Chen *et al.*, 2014; Sathish *et al.*, 2015; Wylam *et al.*, 2015). However, the acute effects of CSE exposure on hASMC Ca^{2+} homeostasis have not been fully characterised, aside from two studies that reported increased $[Ca^{2+}]_i$ in hASMC following transient exposure to diluted CSE (Yoon *et al.*, 2011; Nassini *et al.*, 2012). In particular, the involvement of various calcium signalling pathways, and the subsequent downstream effects of disrupted Ca^{2+} homeostasis on the contractile signalling mechanisms of hASMC, have not been thoroughly explored.

Additionally, both of these studies have used hASMC procured from commercial sources, and gave no indication of investigating variability between multiple donors.

4.2 Aims and Objectives

The main aim of this chapter was therefore to explore in detail the effects of acute exposure to diluted aqueous CSE on Ca^{2+} homeostasis in primary hASMC isolated from multiple donors. The objectives of this chapter are:

- To examine whether acute CSE exposure, on its own, elicits a change in $[Ca^{2+}]_i$ in primary hASMC.
- To investigate the effect of CSE on various components of hASMC intracellular Ca^{2+} signalling, including Ca^{2+} influx pathways and SR Ca^{2+} store release.
- To investigate the potential impact of acute CSE exposure on downstream contractile signalling mechanisms of hASMC.

It was hypothesised that acute CSE treatment would elicit a significant elevation in $[Ca^{2+}]_i$ in hASMC, leading to downstream exacerbation of ASMC contraction.

4.3 Results

4.3.1 CSE elevates $[Ca^{2+}]_i$ in a concentration-dependent manner, and requires extracellular Ca^{2+}

To investigate the effects of CSE on $[Ca^{2+}]_i$ in isolated primary hASMC, diluted CSE was delivered to hASMC through a perfusion system at a rate of 2 ml/min. CSE was produced as described in section 2.5.1. Briefly, one 3R4F reference cigarette was manually aspirated, and bubbled into 25 ml of HEPES-buffered solution to produce 100% CSE, which was then diluted before perfusing onto hASMC in Ca^{2+} imaging experiments.

As previously discussed, there was little evidence in the literature pointing to a direct, acute, effect of CSE on hASMC $[Ca^{2+}]_i$. Additionally, there was no consensus on the concentration of CSE to use in acute exposure experiments. For instance, Yoon *et al.* (2011) used 10% CSE for acute treatment of hASMC, whilst a range of concentrations (from 1-15%) are common for chronic exposure studies (Pera *et al.*, 2010; Xu *et al.*, 2010; Xu *et al.*, 2012; Sathish *et al.*, 2015; Wylam *et al.*, 2015). To investigate whether diluted CSE elicits a change in $[Ca^{2+}]_i$ on its own, and to determine the optimal CSE concentration to apply in subsequent experiments, cultured hASMC were exposed to incremental doses of CSE for 10 mins each (Figure 4.1A). Across 3 independent experiments, 0.1% CSE did not change $[Ca^{2+}]_i$; at 1% CSE, hASMC $[Ca^{2+}]_i$ began to rise within the 10-min perfusion window (Figure 4.1A). The activation threshold for CSE-

induced Ca^{2+} response therefore appeared to be between 0.1 and 1%. Subsequently, exposure to 10% and 50% CSE induced a further, concentration-dependent rise in $[Ca^{2+}]_i$, with an EC_{50} value of 2.1% (95 CI = 0.9-5.1%) (Figure 4.1A, B).

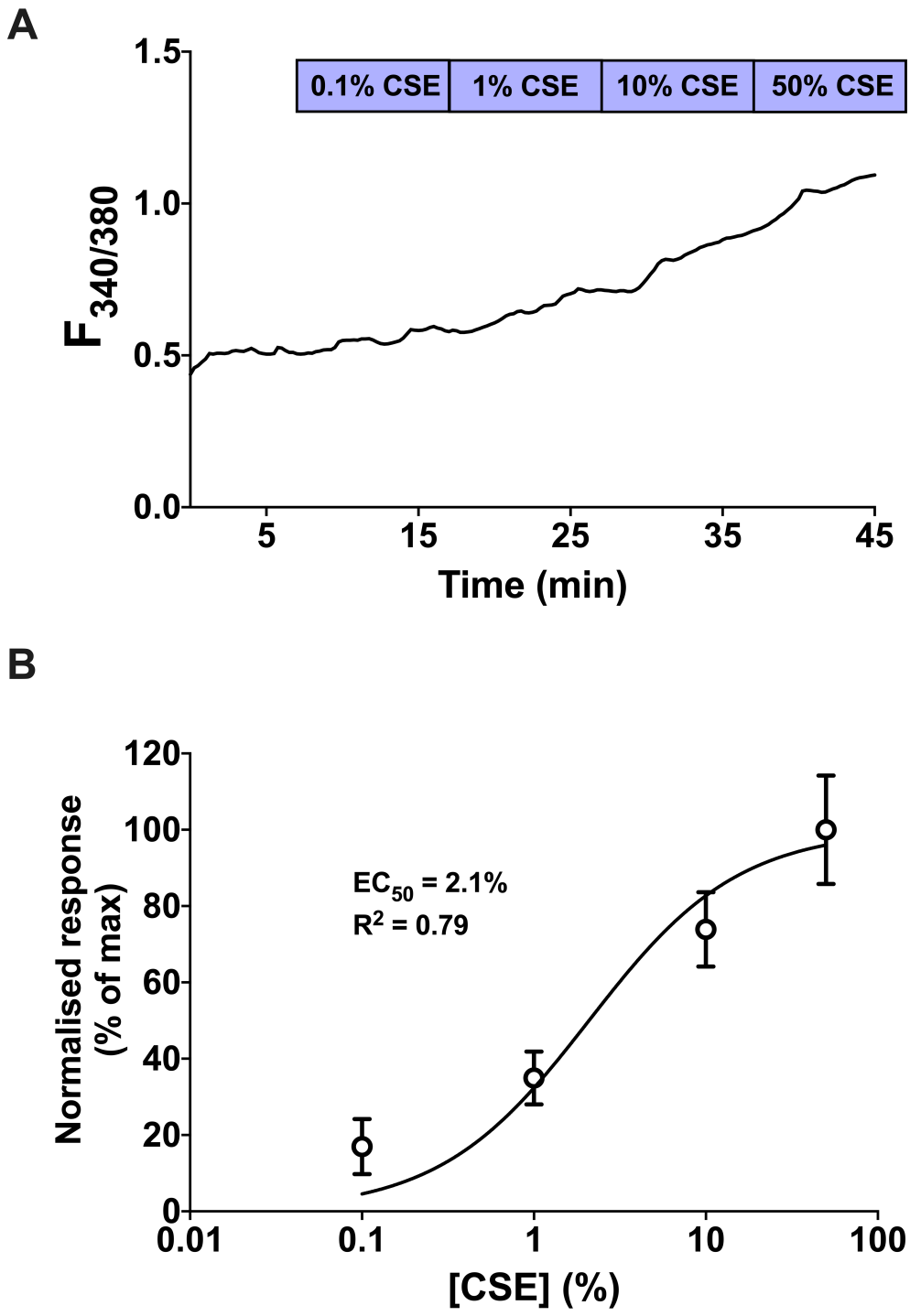

Figure 4.1: Diluted CSE elevates intracellular Ca^{2+} in hASMC in a concentration-dependent manner. (A) Representative trace tracking changes in $[Ca^{2+}]_i$ following perfusion with incremental concentrations of diluted CSE. Each concentration of CSE was perfused onto the cells for 10 minutes. (B) Dose-response curve for the normalised amplitude of Ca^{2+} responses induced by different concentrations of CSE (normalised as % of the response elicited by 50% CSE; final point); n=3, from 1 donor. Data presented as mean ± SEM. Experiments were performed by undergraduate students Helena Gowing and Sophie Davies.

In independent experiments, a rapid response profile was observed when hASMC were acutely exposed immediately to only 10% or 50% CSE in the presence of 1mM extracellular Ca^{2+} (Figure 4.2A). Such a profile allowed calculation of the steady-state magnitude and also the rate of CSE-induced Ca^{2+} elevation. Consistent with the concentration-dependency from Figure 4.1B, the amplitude and rate of the response induced by 50% CSE was significantly greater than that induced by 10% CSE (Figure 4.2A, B; $p<0.05$ for both amplitude (0.44±0.05 vs. 0.28±0.03) and rate (0.32±0.07 vs. 0.10±0.02), 50% vs. 10% CSE in 1mM Ca^{2+}). This response typically reached a peak within 3.4±1.2 mins of exposure to 50% CSE, and 6.2±1.3 mins following exposure to 10% CSE. The calcium response induced by 50% CSE typically recovered to a raised plateau within 3.9±1.5 mins, by 14-51% from the peak amplitude.

To investigate the source of this $[Ca^{2+}]_i$ elevation, hASMC were exposed to 10% CSE in a nominally Ca^{2+}-free solution ($0Ca^{2+}$; Figure 4.2A). The 10% CSE-induced change in $[Ca^{2+}]_i$ was abolished by the removal of extracellular Ca^{2+}, when compared to the change induced by the same concentration of CSE in the presence of 1mM Ca^{2+} (Figure 4.2A, B; $p<0.05$ for both amplitude (0.28±0.03 vs. 0.01±0.00) and rate (0.10±0.02 vs. 0.00±0.00), 10% CSE in 1mM Ca^{2+} vs. in $0Ca^{2+}$). This points to calcium influx from the extracellular space as the primary source of the CSE-induced calcium response, and that intracellular Ca^{2+} stores are not likely to contribute to this response.

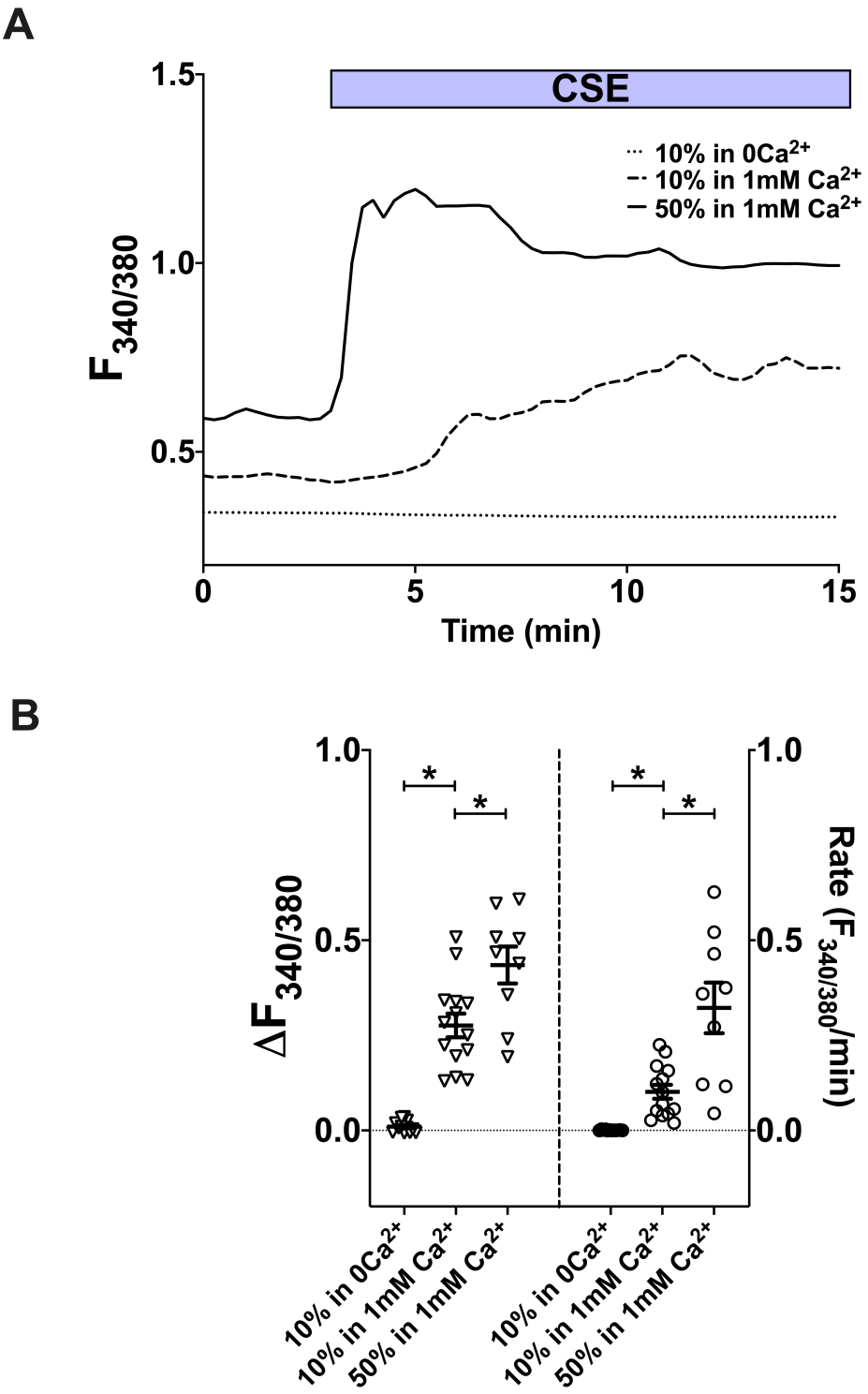

Figure 4.2: CSE-induced elevation of intracellular Ca^{2+} in hASMC requires extracellular Ca^{2+}. (A) Representative traces tracking changes in $[Ca^{2+}]_i$ for individual experiments, following perfusion with diluted CSE with or without extracellular Ca^{2+}. (B) Summary of amplitude and rate of CSE-induced $[Ca^{2+}]_i$ changes. One-way ANOVA with Holm-Sidak's multiple comparisons test was performed amongst the 3 groups (3 independent donors; n=9-14). Data presented as mean ± SEM. * = $p<0.05$.

4.3.2 CSE does not deplete CPA-sensitive Ca^{2+} stores

Since previous work has shown that CS induces intracellular Ca^{2+} release in human airway epithelial cells (Rasmussen *et al.*, 2014), the effect of CSE on intracellular SR Ca^{2+} stores was investigated. To do this, CPA, a SERCA pump inhibitor, was added to cells following a 15-20 min exposure to CSE, using both 1mM extracellular Ca^{2+} or $0Ca^{2+}$ solution (Figure 4.3A, C). In the presence of 1mM extracellular Ca^{2+}, without CSE exposure, CPA induced a prominent, transient rise in $[Ca^{2+}]_i$ (Figure 4.3A, dotted curve). Following exposure to 10% or 50% CSE, CPA treatment was still able to elicit a similar response (Figure 4.3A, dashed and solid curves). However, although CPA-sensitive SR calcium stores were not depleted by CSE (Figure 4.3A), the CPA response following 15-min exposure to 50% CSE was significantly attenuated compared to the CPA response after exposure to 10% CSE (Figure 4.3B; $p<0.05$, 0.15±0.01 vs. 0.26±0.04, 50% vs. 10% CSE in 1mM Ca^{2+}). Similarly, the CPA response in $0Ca^{2+}$ was significantly smaller in cells pre-exposed to 50% CSE than to 10% CSE (Figure 4.3D; $p<0.05$, 0.05±0.00 vs. 0.11±0.01, 50% CSE vs. 10% CSE in $0Ca^{2+}$), suggesting that although there was no evidence of intracellular Ca^{2+} store release in the absence of extracellular Ca^{2+}, SR Ca^{2+} stores were somewhat diminished.

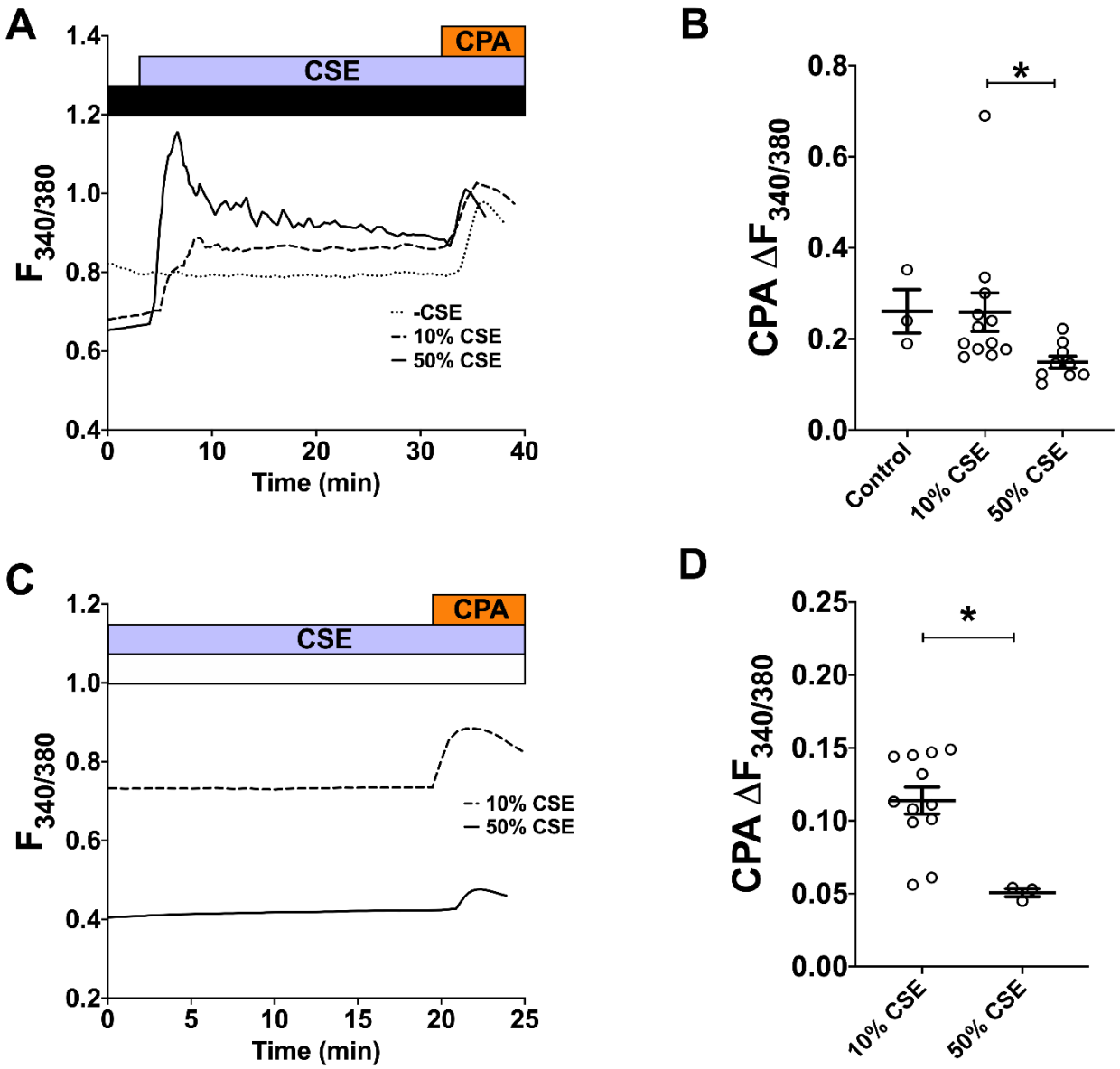

Figure 4.3: CSE does not deplete CPA-sensitive SR Ca^{2+} stores. (A) Representative Ca^{2+} imaging traces tracking changes in $[Ca^{2+}]_i$ following perfusion with diluted CSE, or negative control without CSE (-CSE). 10µM CPA was added at the end of each experiment to examine effects on Ca^{2+} store release. Black bar indicates presence of 1mM extracellular Ca^{2+}. (B) Summary of amplitude of CPA-induced Ca^{2+} release at the end of each experiment from (A). Kruskal-Wallis test with Dunn's multiple comparisons was performed amongst the 3 groups (1-3 independent donors; n=3-14). (C) Representative Ca^{2+} imaging traces tracking changes in $[Ca^{2+}]_i$ following perfusion with diluted CSE in a nominally $0Ca^{2+}$ solution (indicated by the white bar), with 10µM CPA added at the end. (D) Summary of amplitude of CPA-induced Ca^{2+} release at the end of each experiment from (C). Mann-Whitney test was performed between the two groups (1-3 independent donors, n=3-12). Data presented as mean ± SEM. * = $p<0.05$.

4.3.3 Continual presence of CSE is not required for maintained Ca^{2+} influx

It was established that CSE activates Ca^{2+} influx in hASMC, but an accurate estimation of the Ca^{2+} influx amplitude and rate was challenging due to asynchronous activation of the influx pathway in individual cells. Figure 4.4 illustrates raw data tracings from individual cells within one experiment (black traces), as well as the averaged response across all cells (red traces). When cells were exposed to CSE in 1mM extracellular Ca^{2+}, asynchronous activation of $[Ca^{2+}]_i$ elevation was observed (Figure 4.4A), presenting a challenge to accurately estimate the rate of Ca^{2+} influx from the averaged trace. To circumvent this issue, a calcium-addback protocol was developed. Since a 5-min exposure to CSE appeared sufficient to activate Ca^{2+} influx (Figure 4.2A), cells were first exposed to CSE in $0Ca^{2+}$ for 5 mins to synchronise activation of Ca^{2+} influx pathway for the population of cells examined, then 1mM Ca^{2+} was added back (Figure 4.4B), achieving temporal synchronisation of Ca^{2+} influx. Exposure to CSE in $0Ca^{2+}$ before Ca^{2+} addback therefore reduced inter-experiment variability in response profiles and influx rate estimation.

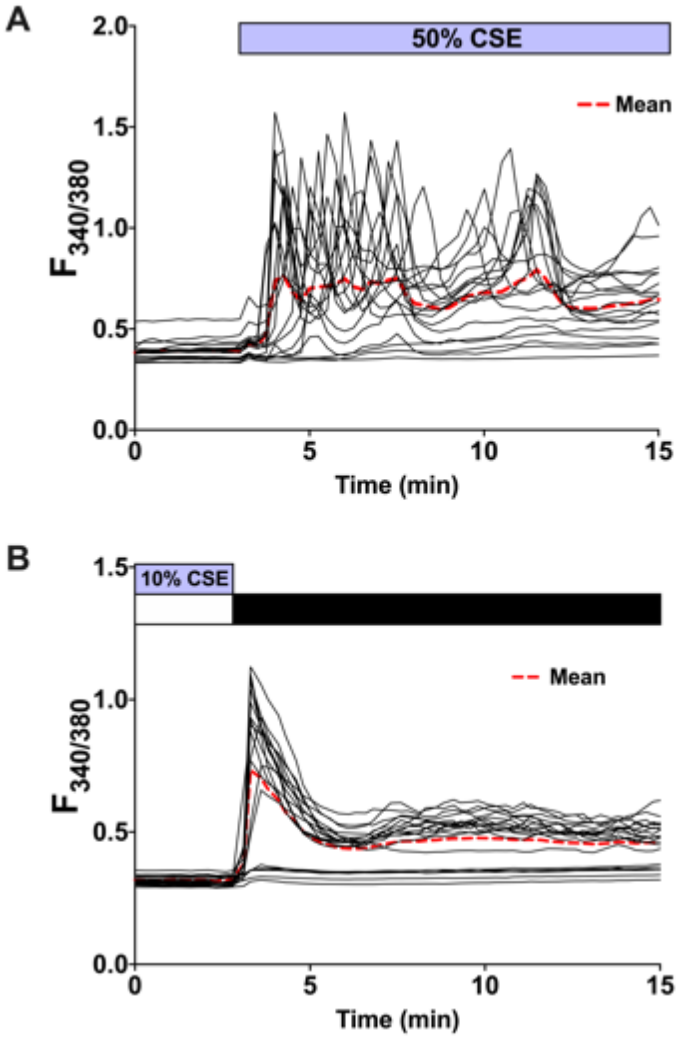

Figure 4.4: Synchronisation of CSE-induced Ca^{2+} influx using the Ca^{2+} addback protocol. Representative single-cell traces tracking changes in $[Ca^{2+}]_i$ following perfusion with diluted CSE in the presence of 1mM extracellular Ca^{2+} (A; n=18) or the Ca^{2+} addback protocol (B; n=20). The red dashed lines are the mean traces of all single-cell traces within one independent experiment. The peak amplitude and rate of CSE-induced Ca^{2+} influx can be more accurately estimated when the influx is synchronised (B).

To examine whether the continual presence of CSE was required to maintain Ca^{2+} influx, the addback protocol was employed, first activating Ca^{2+} influx with 10% CSE in $0Ca^{2+}$, then adding back 1mM Ca^{2+} with (Figure 4.5A) or without (Figure 4.5B) 10% CSE. A rapid influx was observed following calcium addback under both conditions. Moreover, a prompt decrease in $[Ca^{2+}]_i$, likely due to calcium efflux, was observed when external Ca^{2+} was removed, suggesting that the CSE activated Ca^{2+} influx pathways, which remained active for at least 20 mins after the initial 5-min CSE exposure. More interestingly, CSE-activated Ca^{2+} influx, in the immediate short term, did not require the continued presence of CSE in the 1mM Ca^{2+} solution (Figure 4.5C; n.s. for both amplitude (0.50±0.08 vs. 0.46±0.06) and rate (0.64±0.17 vs. 0.46±0.09), with vs. without CSE). However, the recovery profiles for the two groups were

different – in 3/6 experiments with CSE in the 1mM Ca^{2+} solution, the recovery was rather slow and noisy (e.g. Figure 4.5A), rather than that seen in Figure 4.5B, whereby 8/8 experiments without CSE present at the influx phase exhibited this rapid recovery followed by a stable raised plateau. Indeed, the extent of recovery from peak, as a percentage of the peak amplitude, without the continual presence of CSE was significantly higher (Figure 4.5D; $p<0.05$, 59.3±3.4% vs. 35.9±4.7%, without vs. with CSE).

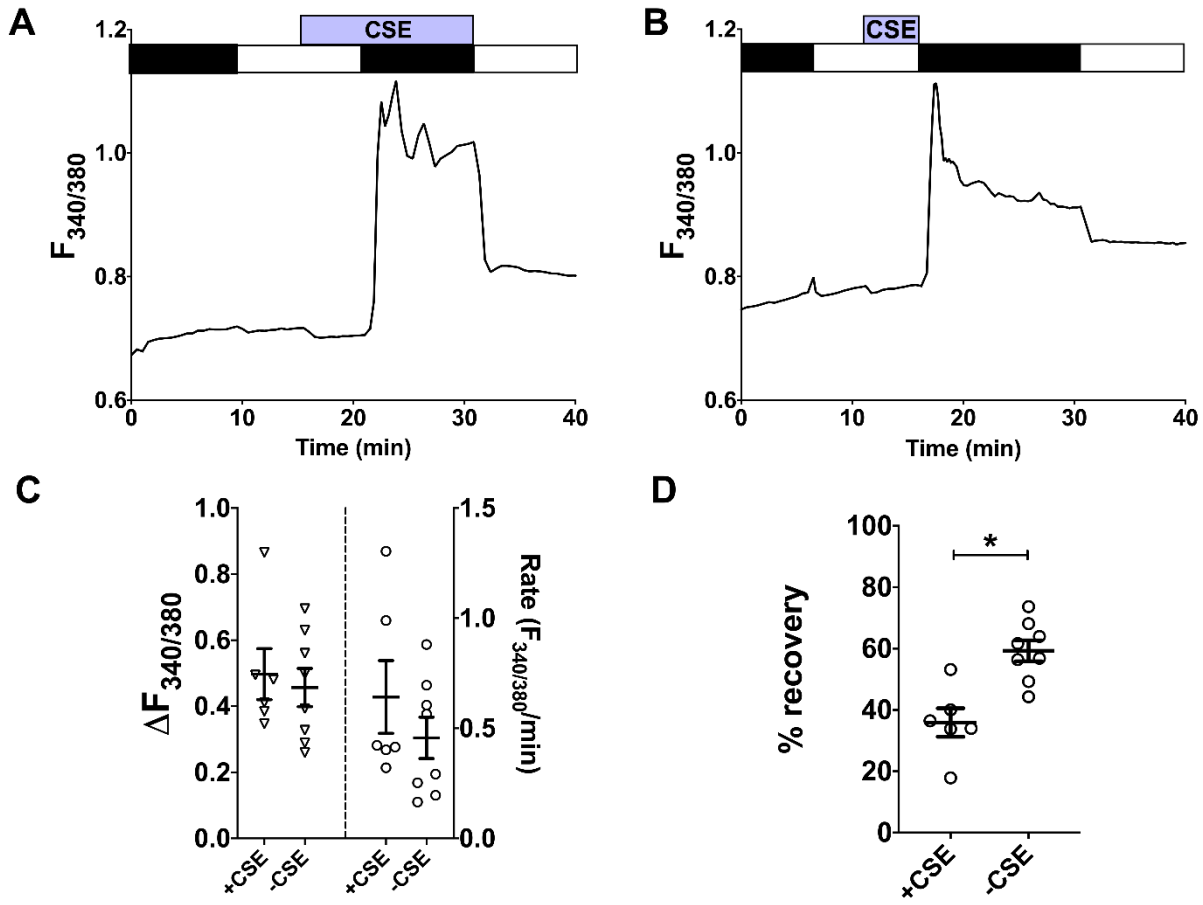

Figure 4.5: CSE-activated Ca^{2+} influx does not require the continuous presence of CSE. (A, B) Representative traces tracking changes in $[Ca^{2+}]_i$ following calcium addback, with (A) or without (B) the presence of 10% CSE, after 5-min perfusion with 10% CSE in the 0 Ca^{2+} solution. (C) Summary of amplitude and rate of $[Ca^{2+}]_i$ changes of the calcium addback responses. (D) Summary of percentage recovery from peak of the calcium addback responses ((peak – plateau)/amplitude * 100%). Data presented as mean ± SEM. Unpaired t-test was performed between the two groups (n=6-8, from 1 donor). * = $p<0.05$.

4.3.4 A reproducible Ca^{2+} influx can be achieved after removal of CSE

Another aspect of CSE-activated Ca^{2+} influx of interest was its reversibility, which was investigated using a repeated addback protocol following a prolonged duration of CSE removal (Figure 4.6A). Following an extended washout period (at least 25 mins after removing CSE),

both the amplitude (0.33±0.06 vs. 0.22±0.04) and rate (0.40±0.08 vs. 0.17±0.03) of the Ca^{2+} addback response were attenuated (Figure 4.6B; $p<0.05$, influx 1 vs. 2), but not abolished, suggesting that activation of the Ca^{2+} influx pathway by CSE was likely to be ultimately reversible.

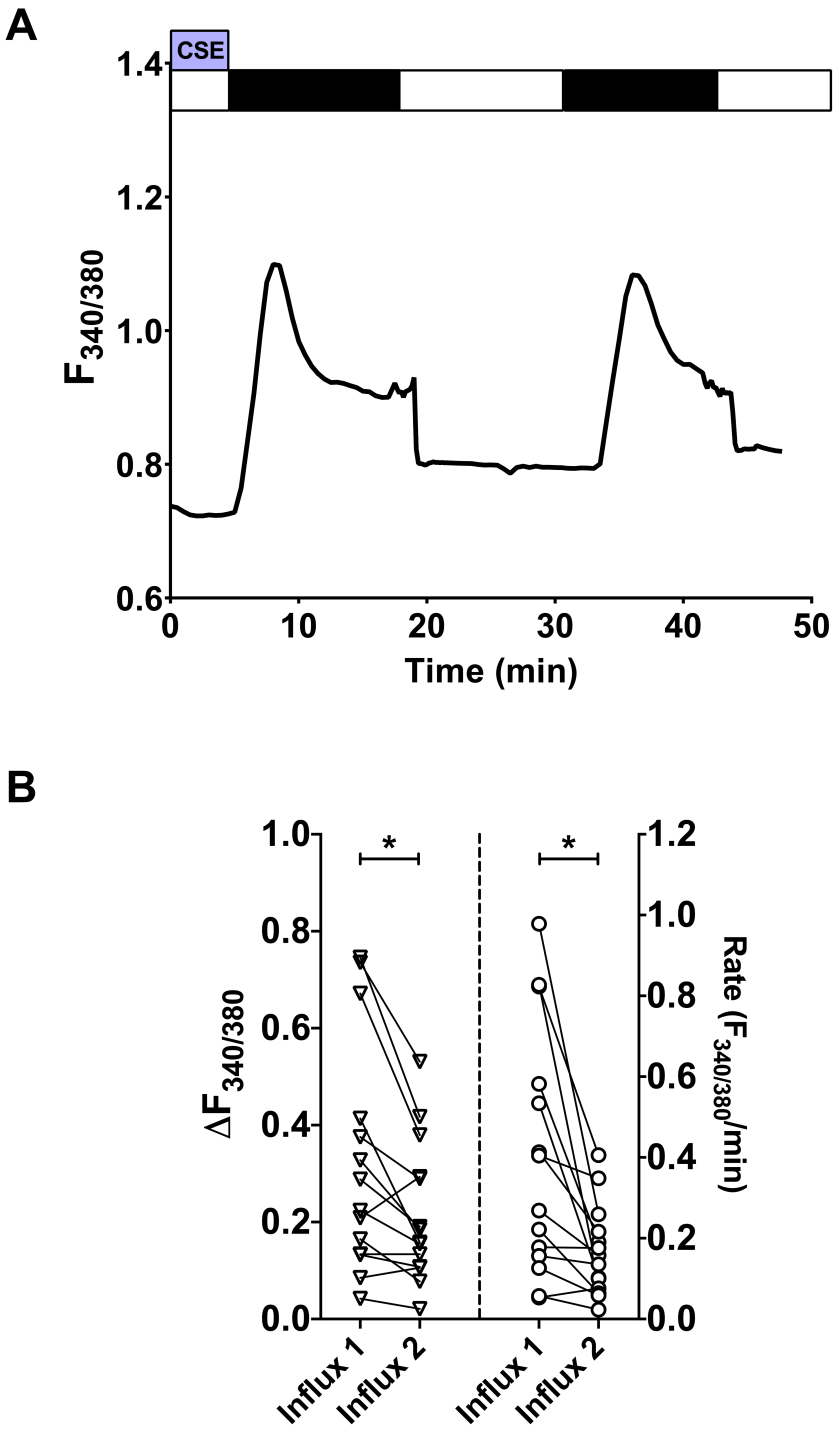

Figure 4.6: CSE-activated Ca^{2+} influx is attenuated following removal of CSE. (A) Representative trace tracking changes in $[Ca^{2+}]_i$ following multiple calcium addbacks, after 5-min perfusion with 10% CSE. Influx 2 was after a 15-min washout period in $0Ca^{2+}$. (B) Amplitude and rate of Ca^{2+} influx following two calcium addbacks. Wilcoxon matched-pairs signed rank test was performed between the two paired influx in the same experiment (3 independent donors; n=14). * = $p<0.05$.

4.3.5 Donor and passage variability of CSE-induced Ca^{2+} response in hASMC

Data presented in this chapter were collected from experiments on hASMC isolated from 4 independent donors, used for calcium imaging studies between passage 2-8. The variability of Ca^{2+} responses amongst donors was examined for three different protocols as shown in Figure 4.7. There was no significant donor-donor variability in the amplitude and rate of the Ca^{2+} response elicited by 10% or 50% CSE in the presence of 1mM extracellular Ca^{2+} (Figure 4.7A, B; $p>0.05$ for all multiple comparisons tests). However, a certain degree of variability was observed in experiments using the addback protocol (Figure 4.7C; $p<0.05$ for multiple comparisons). Specifically, cells from donor 2 exhibited significantly higher amplitude and rate of CSE-activated Ca^{2+} response, whilst cells from donor 4 had the lowest responses. However, it is worth noting that cells from donor 4 were included only in one subset of experiments shown in this chapter (specifically, in Figure 4.13).

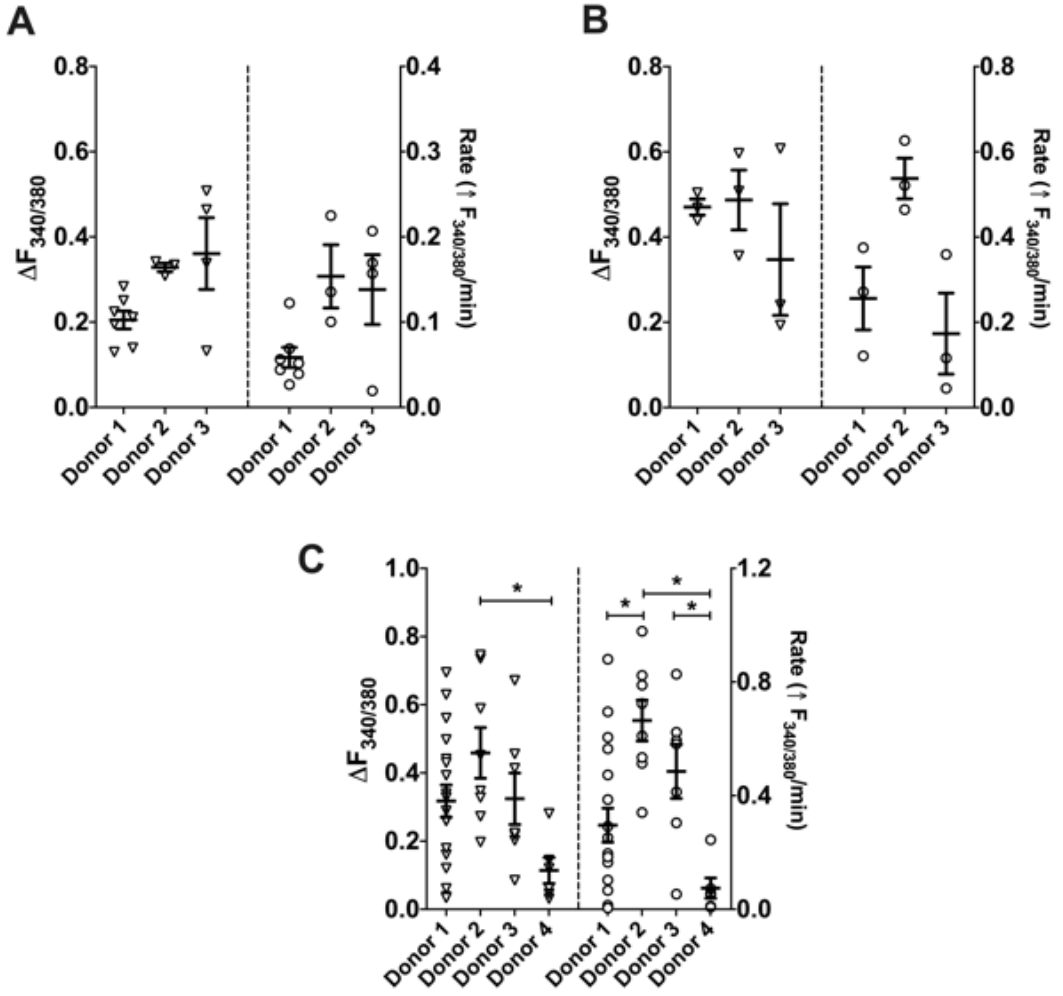

Figure 4.7: Donor-donor variability of CSE-induced Ca^{2+} responses. Summary of amplitude and rate of CSE-induced Ca^{2+} responses in hASMC isolated and cultured from different donors, using three different protocols: (A) 10% CSE in 1mM extracellular Ca^{2+}; (B) 50% CSE in 1mM extracellular Ca^{2+}; (C) Ca^{2+} addback after 5-min perfusion of 10% CSE in $0Ca^{2+}$ solution. Data presented as mean ± SEM. Kruskal Wallis test with Dunn's multiple comparisons was conducted between each individual donor; n=3-18. * = $p<0.05$.

On the other hand, the CSE-activated Ca^{2+} responses in cells from different passages were examined. A regression analysis revealed no significant trends or differences in the responses in cells from passages 2-8 (Figure 4.8).

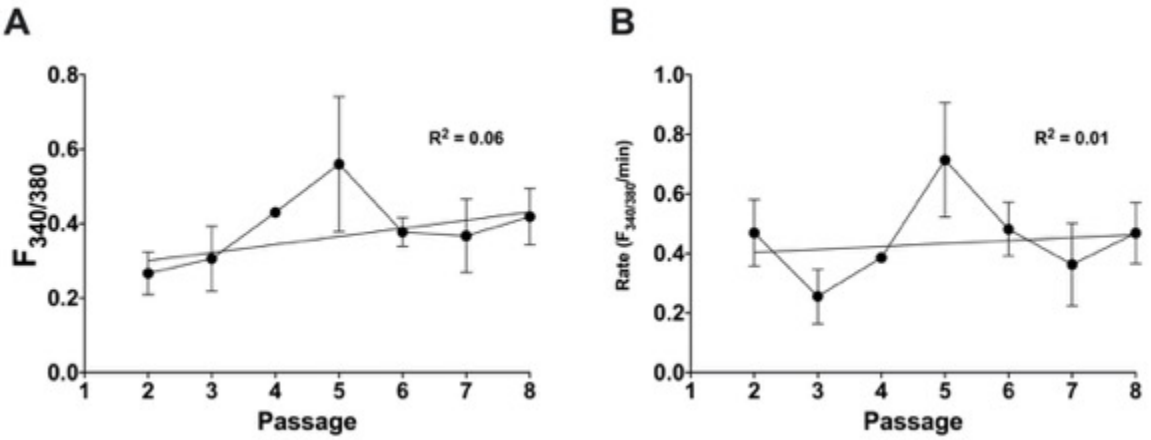

Figure 4.8: Passage-passage variability of CSE-induced Ca^{2+} responses. Summary of amplitude (A) and rate (B) of CSE-induced Ca^{2+} responses in cultured primary hASMC at different passages, using the Ca^{2+} addback protocol. Data presented as mean ± SEM. Linear regression was performed on each curve to examine potential linear correlations. n=1-7.

4.3.6 CSE does not activate Ca^{2+} influx in Calu-3 cells

To examine if CSE-activated Ca^{2+} influx was cell-type specific, the effect of CSE exposure was investigated in Calu-3 cells. Previous works from other groups have shown that exposure to gaseous CS elevates $[Ca^{2+}]_i$ in epithelial cells, including Calu-3 cells (Rasmussen *et al.*, 2014; Sassano *et al.*, 2017), but the effects of diluted CSE on epithelial Ca^{2+} signalling have not been characterised.

Using the same protocol as in Figure 4.5, following 10% CSE exposure, adding back 1mM Ca^{2+} did not trigger an observable, rapid Ca^{2+} influx (Figure 4.9B). The lack of a prominent influx after Ca^{2+} addback was similar to that seen in Calu-3 cells without the CSE challenge (Figure 4.9A), indicating that diluted CSE does not activate the opening of a Ca^{2+} influx pathway in Calu-3 cells.

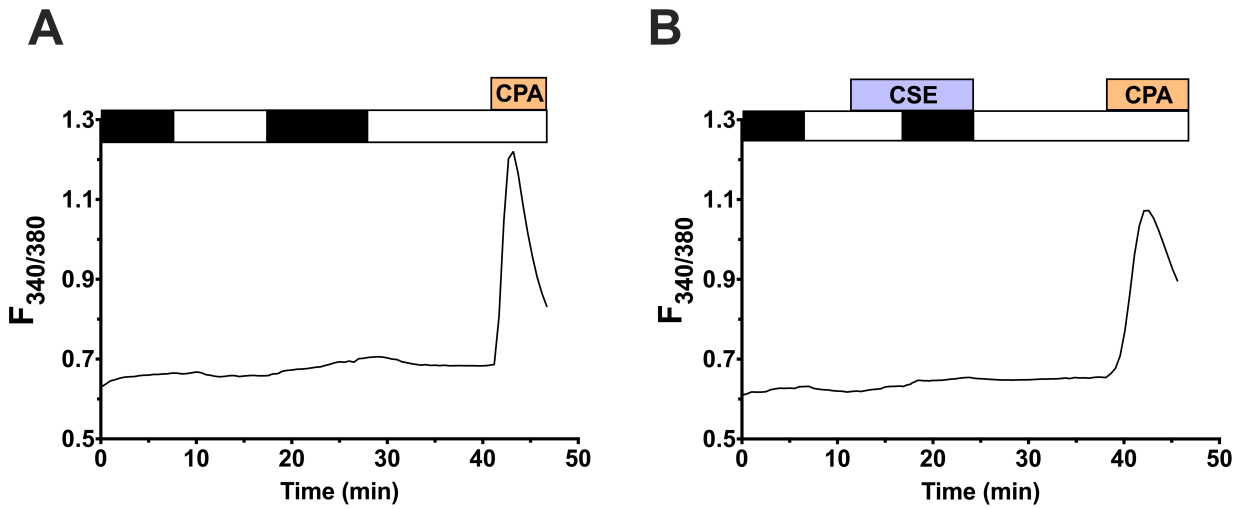

Figure 4.9: CSE does not activate a Ca^{2+} influx pathway in Calu-3 cells. Representative traces tracking changes in $[Ca^{2+}]_i$ following calcium addback without CSE challenge (A), or after 5-min perfusion with 10% CSE (B). 10µm CPA was added at the end of the experiment as a positive control.

4.3.7 CSE-induced Ca^{2+} influx is significantly inhibited by gadolinium

To ascertain if the CSE-activated Ca^{2+} influx pathway in hASMC involved a plasma membrane (PM) Ca^{2+} permeable channel, the effect of gadolinium (Gd^{3+}), a lanthanide ion that non-specifically blocks Ca^{2+}-permeable channels, was tested. Using the addback protocol, hASMC were pre-treated with 100µM Gd^{3+} for 10 mins, then perfused with 10% CSE in $0Ca^{2+}$ for 5 mins (15 min total Gd^{3+} pre-treatment before addback), before calcium was added back (Figure 4.10A). Gd^{3+} was present throughout the experiments. As Gd^{3+} was dissolved in distilled water, a vehicle control was not needed, and so the negative control experiments were simply standard addback experiments without Gd^{3+}. Pre-treatment and continuous presence of Gd^{3+} significantly attenuated both the amplitude (0.44±0.05 vs. 0.11±0.02; 74.8% inhibition) and rate (0.49±0.06 vs. 0.12±0.03; 76.0% inhibition) of CSE-activated Ca^{2+} influx in hASMC (Figure 4.10B; $p<0.05$ control vs. Gd^{3+}-treated), suggesting that Ca^{2+} influx through PM-bound channels was the likely pathway facilitating this response.

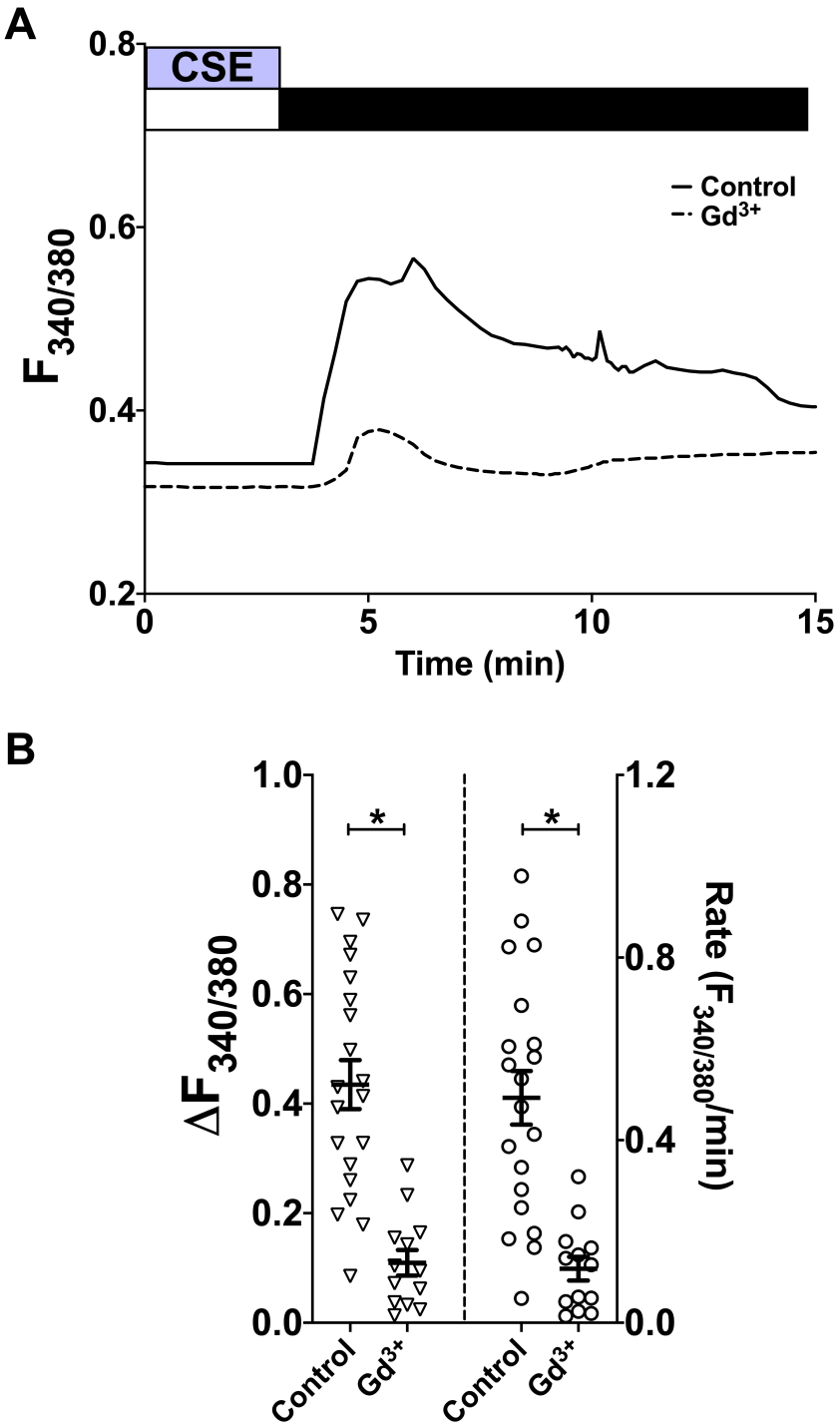

Figure 4.10: CSE-induced Ca^{2+} influx was blocked by Gd^{3+}. (A) Representative traces tracking changes in $[Ca^{2+}]_i$ following calcium addback (1mM Ca^{2+}; black bar) after 5-min perfusion with 10% CSE in a nominally Ca^{2+}-free solution (0 Ca^{2+}; white bar), with or without 10-min pre-treatment with 100μM Gd^{3+}, which was also present throughout the experiment. (B) Summary of amplitude and rate of $[Ca^{2+}]_i$ changes corresponding to experiments in (A). Data presented as mean ± SEM. Unpaired t-test was performed between the control group and the Gd^{3+}-treated group (3 independent donors; n=13-20). * = $p<0.05$.

4.3.8 Validation of LTCC blockers

To further explore plasmalemmal molecular candidates underlying the CSE-activated Ca^{2+} influx in hASMC, the potential contributions of voltage-gated L-type Ca^{2+} channels (LTCC) and store-operated Ca^{2+} channels (SOCC) were investigated, since both of these channels play an important role in refilling SR Ca^{2+} stores in ASMC (Flores-Soto *et al.*, 2013).

Using a similar protocol to the experiments with Gd^{3+} (Figure 4.10), hASMC were pre-treated with the LTCC blocker nifedipine (Gould *et al.*, 1983; Sorkin *et al.*, 1985), before CSE-activated Ca^{2+} influx was triggered by calcium addback (Figure 4.11A). The negative control experiments included both vehicle control, and some CSE-activated addback experiments without any solvents, performed on cells from the same donor. Surprisingly, both the amplitude (1.06±0.05 vs. 0.46±0.06) and rate (1.71±0.58 vs. 0.46±0.09) were markedly higher after pre-treatment with nifedipine (Figure 4.11B; $p<0.05$ control vs. nifedipine). This enhancement of CSE-induced Ca^{2+} influx may be due to an off-target effect of nifedipine. Therefore, whether nifedipine on its own was able to produce a Ca^{2+} response in hASMC was then investigated. Indeed, 10μM nifedipine, in the presence of 1mM extracellular Ca^{2+}, led to a rapid increase in $[Ca^{2+}]_i$ (Figure 4.11C). Even when the concentration was lowered to 1μM, the elevation in $[Ca^{2+}]_i$ was smaller and slower but still rather prominent (Figure 4.11C, D). Two different batches of nifedipine, from Sigma and Tocris respectively, were tested, and each gave similar results. This off-target effect prevented further use of nifedipine in this study.

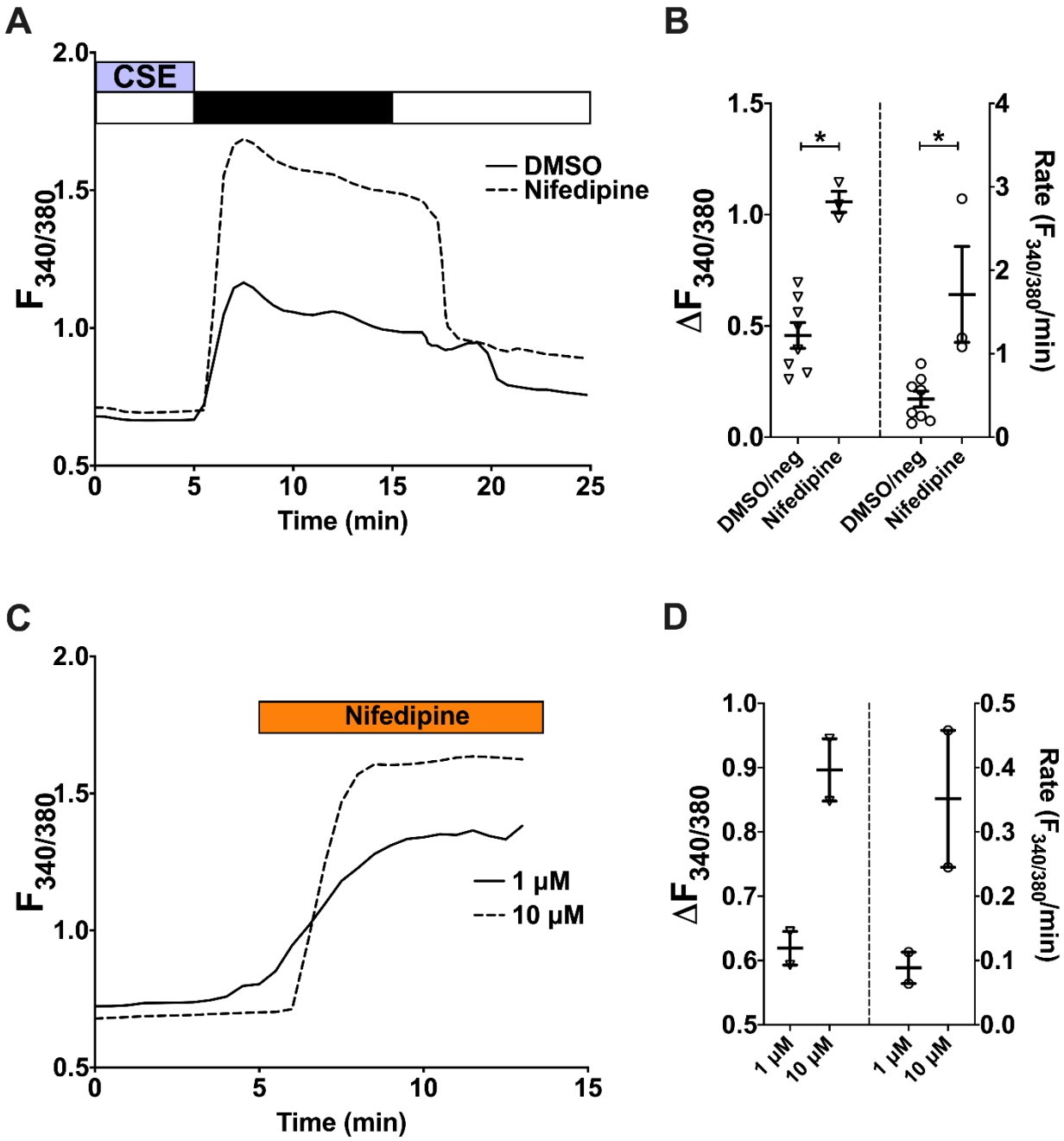

Figure 4.11: The LTCC blocker nifedipine induced an elevation in $[Ca^{2+}]_i$. (A) Representative traces tracking changes in $[Ca^{2+}]_i$ following calcium addback after 5-min perfusion with 10% CSE in a $0Ca^{2+}$ solution, with or without 10-min pre-treatment with 10μM nifedipine, which was also present throughout the experiment. Control experiments were either with equal volume of DMSO, or simply CSE-activated addback without solvents. (B) Summary of amplitude and rate of $[Ca^{2+}]_i$ changes corresponding to experiments in (A). Unpaired t-test was performed between the nifedipine-treated group and the vehicle control group (n=3-8, from 1 donor). (C) Ca^{2+} imaging traces following perfusion with 1 or 10μM nifedipine on its own, in the presence of 1mM extracellular Ca^{2+}. (D) Summary of amplitude and rate of nifedipine responses in (C); n=2, from 1 donor. Data presented as mean ± SEM. * = $p<0.05$.

Since nifedipine was unsuitable, another dihydropyridine, felodipine, which specifically blocks LTCC in favour of other VOCC, was tested (Furukawa *et al.*, 1999). To pre-empt the same problem as nifedipine, it was first tested whether felodipine increased $[Ca^{2+}]_i$ on its own, and whether it was able to sufficiently block LTCC. The activity of LTCC was determined by measuring the Ca^{2+} influx in response to depolarisation, induced by perfusing the cells with a high-K^+ (80mM) solution. For these experiments, cells were pre-treated with 1μM BayK-8644 before depolarisation. BayK-8644 binds to the LTCC in the resting state, and prolongs single-channel open times (Bechem and Hoffmann, 1993), thereby amplifying the calcium signal (Figure 4.12A). The inhibition of BayK-8644-primed, depolarisation-induced Ca^{2+} influx in hASMC by 1μM felodipine was not statistically significant (Figure 4.12B; p=0.06 for both amplitude and rate, DMSO- vs. felodipine-treated). However, in every occasion, felodipine-treated depolarisation-induced Ca^{2+} influx had lower amplitude (86.7% on average) and rate (94.3% on average). Such effective and consistent inhibition gave sufficient confidence to use felodipine to investigate the involvement of LTCC in CSE-induced Ca^{2+} influx.

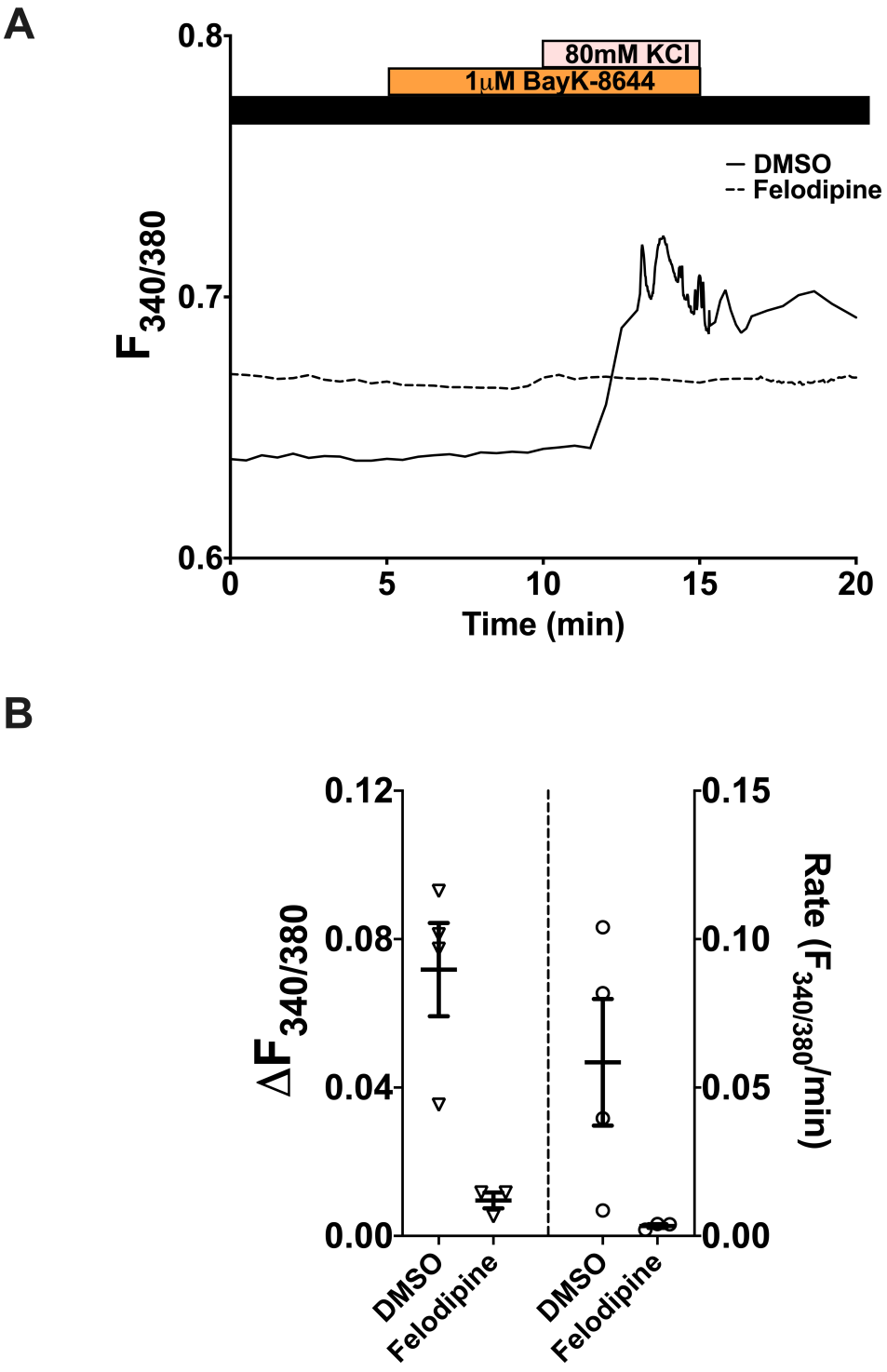

Figure 4.12: 1μM felodipine is sufficient to block LTCC in hASMC. (A) Representative traces tracking changes in $[Ca^{2+}]_i$ following BayK-8644-activated, KCl-induced Ca^{2+} influx, with or without 10-min pre-treatment with 1μM felodipine, which was also present throughout the experiment. Equal volumes of DMSO was used for vehicle control. (B) Summary of amplitude and rate of $[Ca^{2+}]_i$ changes corresponding to experiments in (A). Data presented as mean ± SEM. Mann-Whitney test was performed between the felodipine-treated group and the vehicle control group (n=3-4, from 1 donor).

4.3.9 Inhibiting LTCC does not attenuate CSE-induced Ca^{2+} influx

After validating the efficacy of felodipine, the potential role of LTCC was examined using a similar protocol to that was used in Figure 4.10, by pre-treating the cells with 1μM felodipine for 10 mins before CSE-activated Ca^{2+} addback. The response profiles of the felodipine-treated cells were similar to those of vehicle control experiments (Figure 4.13A). Indeed, neither the amplitude (0.19±0.03 vs. 0.19±0.04) nor the rate (0.24±0.06 vs. 0.25±0.06) of CSE-activated Ca^{2+} influx were significantly attenuated by felodipine (Figure 4.13B; n.s. for both amplitude and rate, DMSO- vs. felodipine-treated), suggesting that LTCC does not mediate CSE-induced Ca^{2+} influx.

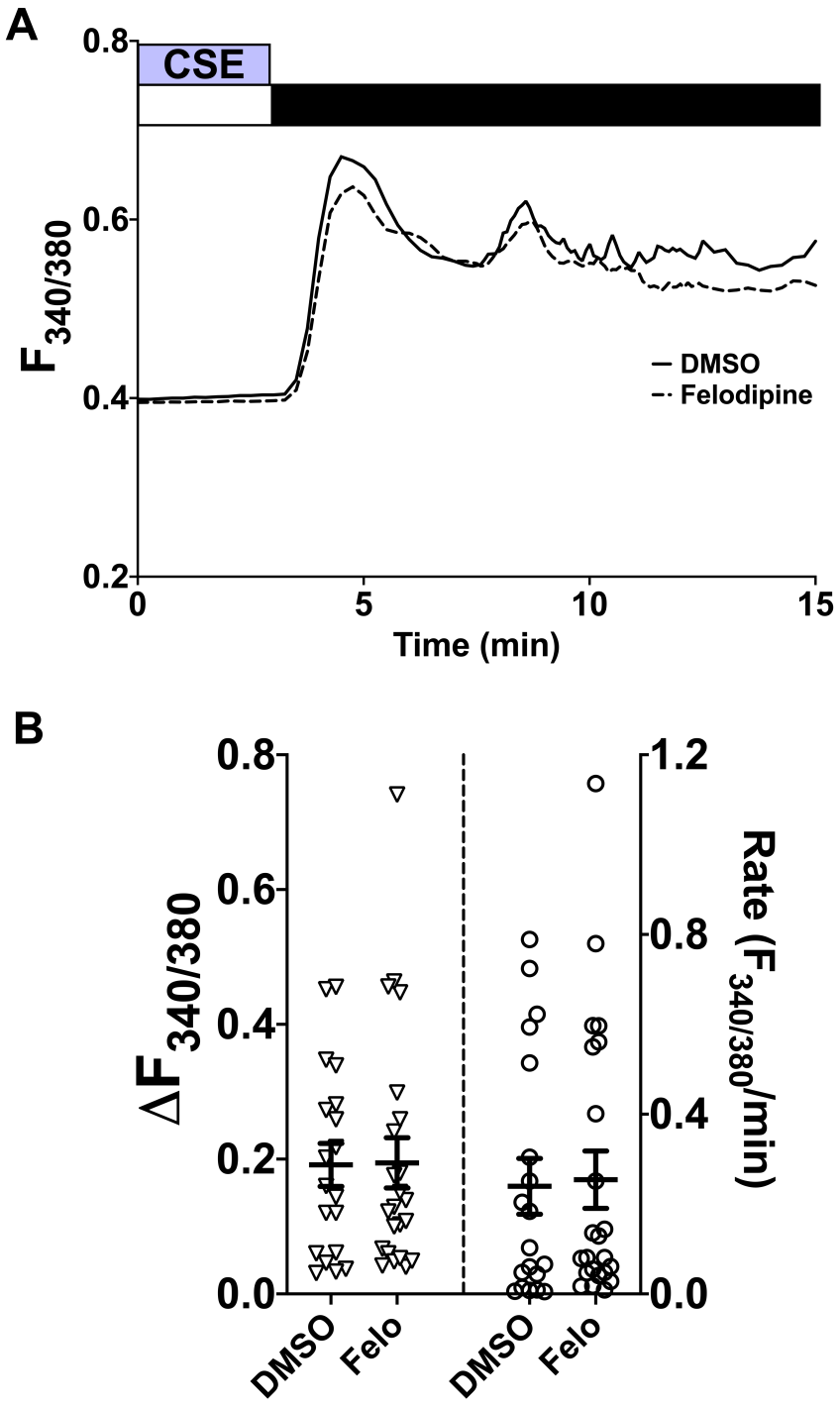

Figure 4.13: Inhibiting LTCC does not attenuate CSE-induced Ca^{2+} influx. (A) Representative traces tracking changes in $[Ca^{2+}]_i$ following calcium addback after 5-min perfusion with 10% CSE in a $0Ca^{2+}$ solution, with or without 10-min pre-treatment with 1μM felodipine, which was also present throughout the experiment. Equal volumes of DMSO was used for vehicle control. (B) Summary of amplitude and rate of $[Ca^{2+}]_i$ changes corresponding to experiments in (A). Data presented as mean ± SEM. Unpaired t-test was performed between the felodipine-treated group and the vehicle control group (4 independent donors; n=19-23).

4.3.10 Validation of SOCC blockers

To investigate the potential contribution of SOCC to the CSE-induced Ca^{2+} influx, two reported specific SOCC inhibitors were studied. The first one was the pyrazole derivative BTP2, also known as YM-58483 (Ishikawa *et al.*, 2003; Zitt *et al.*, 2004). Preliminary experiments showed that a 10-min pre-treatment with 10μM BTP2 did not attenuate the response (Figure 4.14A, B). To ascertain that BTP2 was effective in blocking SOCE in these cells, a repeated CPA-activated SOCE protocol was employed, similar to that described in the previous chapter, with (Figure 4.14C) or without (Figure 4.14D) acute (10-min) pre-treatment with BTP2 before the second influx. This manoeuvre did not significantly inhibit SOCE (Figure 4.14F; multiple comparisons n.s., 0.48±0.11 vs. 0.49±0.05, acute BTP2 vs. vehicle control). Since several studies that have used BTP2 employed a longer pre-treatment period, ranging from 30 mins to 24 hours before experiments (Ishikawa *et al.*, 2003; Zitt *et al.*, 2004), a longer exposure to BTP2 was also tested. BTP2 was added to the cells during fura-2AM loading, ~1h before the start of experiment (~80 mins before SOCE was triggered). This longer exposure to BTP2 did cause an attenuated amplitude of SOCE in 4/6 experiments, but 2/6 of the responses appeared to be in the normal range (Figure 4.14E; both traces were after 1h pre-treatment with BTP2). Overall, the difference between the BTP2-treated set (0.33±0.08) and the vehicle control set (0.49±0.05) was not consistent or statistically significant (Figure 4.14F; multiple comparisons n.s.). Of note, the vehicle control in Figure 4.14 was pooled from experiments with repeated SOCE (e.g. Figure 4.14D; the second SOCE) as well as experiments with only one SOCE (i.e. vehicle control for Figure 4.14E, with 1h pre-treatment of DMSO). Due to this inconsistency, other pharmacological options were explored.

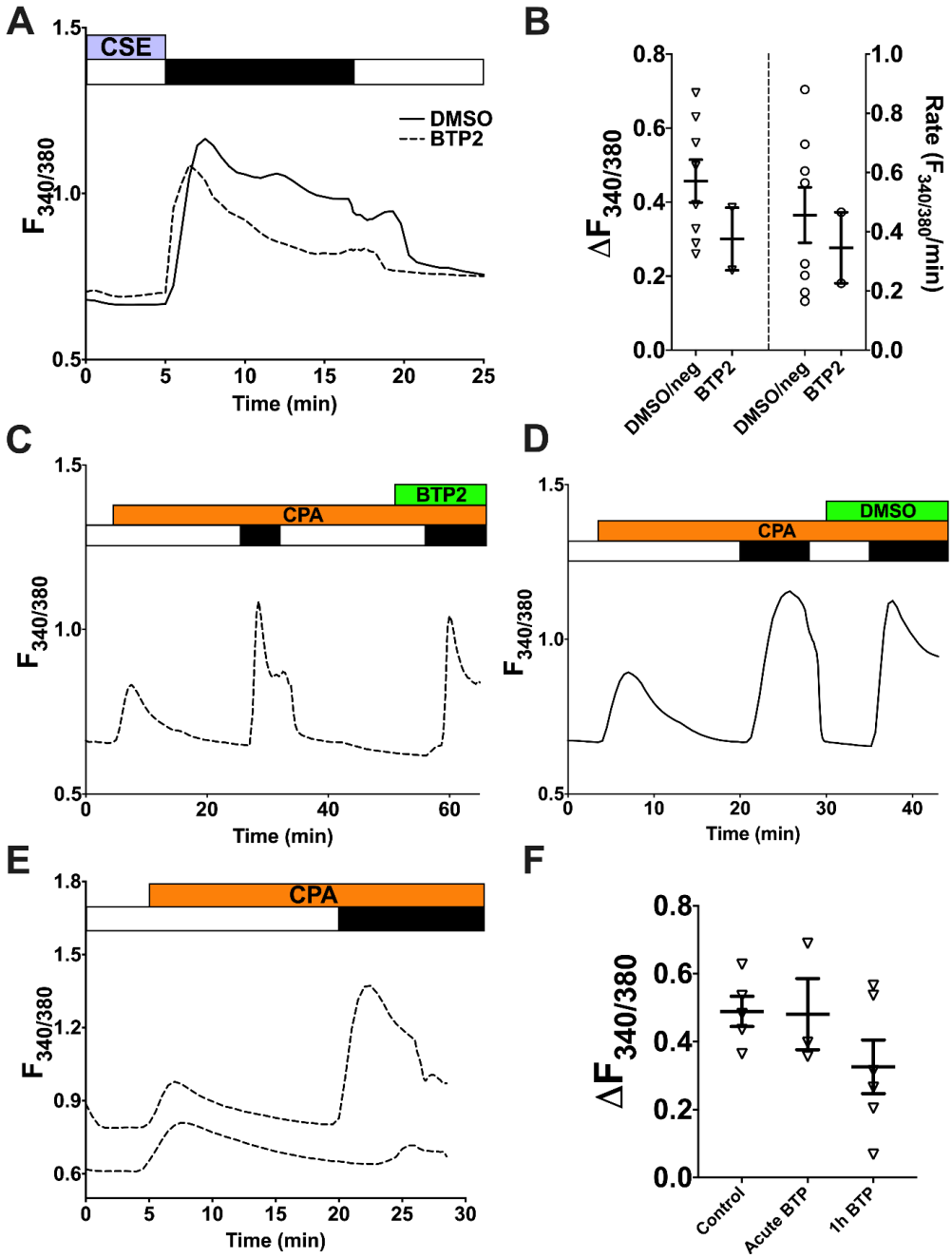

Figure 4.14: BTP2 was ineffective in blocking SOCE in hASMC. (A) Representative trace tracking changes in $[Ca^{2+}]_i$ following calcium addback after 5-min perfusion with 10% CSE in a $0Ca^{2+}$ solution, with or without 10-min pre-treatment with 10μM BTP2, which was also present throughout the experiment. Control experiments were either with equal volume of DMSO, or simply CSE-activated addback without solvents. (B) Summary of amplitude and rate of $[Ca^{2+}]_i$ changes corresponding to experiments in (A); n=2-8, from 1 donor. (C, D) Representative Ca^{2+} imaging traces following repeated CPA-activated SOCE, the second of which was after acute perfusion with 10μM BTP2 (C) or equal volumes of DMSO (D). (E) Representative Ca^{2+} imaging traces following CPA-activated SOCE after 1-hour pre-treatment with BTP2, which was also present throughout the experiment. (F) Summary of amplitude of $[Ca^{2+}]_i$ changes corresponding to experiments in (C-E). Kruskal-Wallis with Dunn's multiple comparisons was performed amongst the three groups in (F); n=3-6, from 1 donor. Data presented as mean ± SEM.

Synta-66 is a relatively highly specific SOCC inhibitor, with a reported IC_{50} of 26nM in human VSMC (Li *et al.*, 2011). Using the same protocol as in Figure 4.14C and D, it was, however, discovered that Synta-66 in a $0Ca^{2+}$ solution increased fura-2 fluorescence ratio (Figure 4.15A). Upon closer inspection, Synta-66 appeared to be autofluorescent at the wavelengths used for exciting fura-2, as fluorescence intensity for both 340nm and 380nm went up, and the ratio changed when Synta-66 was perfused onto a coverslip without any cells or fura-2 present (Figure 4.15B). Filtering solutions containing Synta-66 through a 0.22μm sterile filter abolished the autofluorescence (Figure 4.15C). However, a 10-min pre-treatment with 10μM Synta-66 did not inhibit SOCE (Figure 4.15D; n.s., influx 1 vs. influx 2). The data from both filtered and unfiltered Synta-66 were pooled for analysis. Due to time constraints it was decided not to explore other pharmacological inhibitors.

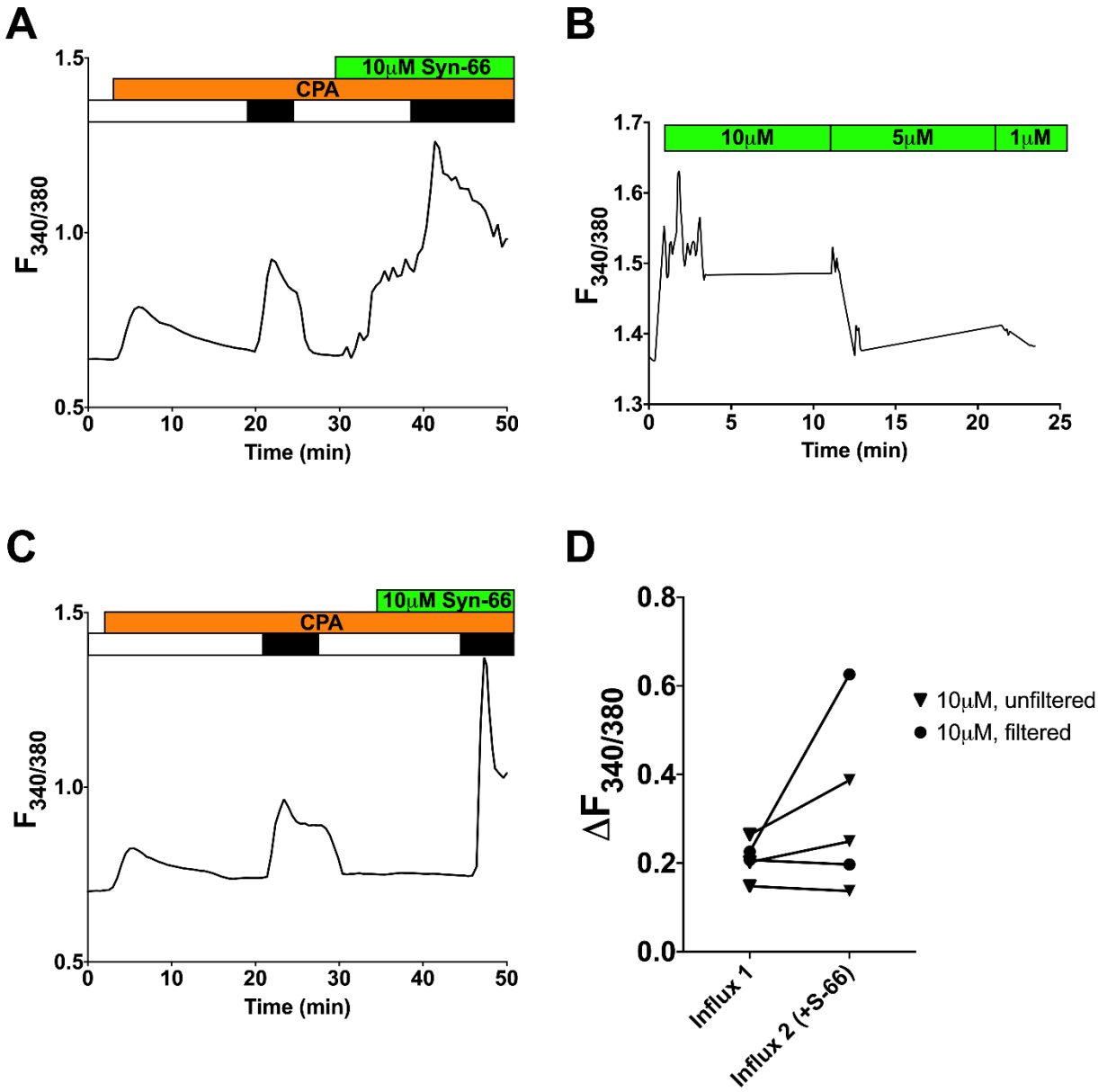

Figure 4.15: Synta-66 was ineffective in blocking SOCE in hASMC. (A) Representative trace tracking changes in $[Ca^{2+}]_i$ following repeated CPA-activated SOCE, the second of which was after acute perfusion with 10μM Synta-66. (B) Autofluorescence of Synta-66 at various concentrations, perfused onto a coverslip without cells or fura-2 present. (C) Representative trace tracking changes in $[Ca^{2+}]_i$ following the same protocol as (A), but with Synta-66 solutions filtered through a 0.22μm sterile filter. (D) Summary of amplitude of $[Ca^{2+}]_i$ changes corresponding to experiments in (A) and (C). Paired t-test was performed between the SOCE without Synta-66 (influx 1) and the SOCE after 10-min perfusion with Synta-66 (influx 2); n=2-3, from 1 donor.

4.3.11 CSE-induced Ca^{2+} influx utilises a different pathway from SOCE

Since use of a suitable inhibitor of SOCC with high enough efficacy was not established, the potential involvement of SOCC was investigated by observing whether CSE could still elicit a similar change in $[Ca^{2+}]_i$ after SOCC activation. For these experiments, SR calcium stores were depleted to activate SOCC by treating the cells with 10μM CPA. After store depletion and the subsequent SOC influx had reached a plateau, cells were then perfused with 10% CSE; if CSE-induced Ca^{2+} influx relied solely on SOCC, exposure to CSE after SOCC activation would be predicted to lead to a smaller response compared to the vehicle control experiment, where SOCC were minimally active. Figure 4.16A shows that the amplitude of the CSE response after SOCC activation was similar to the vehicle control (0.23±0.04 vs. 0.16±0.02), but the rate was significantly attenuated after SOCC activation (Figure 4.16B; $p<0.05$ for rate, 0.14±0.01 vs. 0.06±0.02, DMSO- vs. CPA-treated). The lower rate may be due to a potential role of SOCC in facilitating CSE-induced Ca^{2+} influx, or an artefact produced by the relatively smaller inward concentration gradient for Ca^{2+} influx after SOCE had elevated $[Ca^{2+}]_i$. Either way, SOCC is unlikely to be a major contributor to this response, as the extent of CSE-induced Ca^{2+} influx (amplitude) was similar between the two datasets. Altogether, these data suggest that SOCC and LTCC, two prominent Ca^{2+} channels regulating SMC store refilling, do not make major contributions to the CSE-induced Ca^{2+} influx.

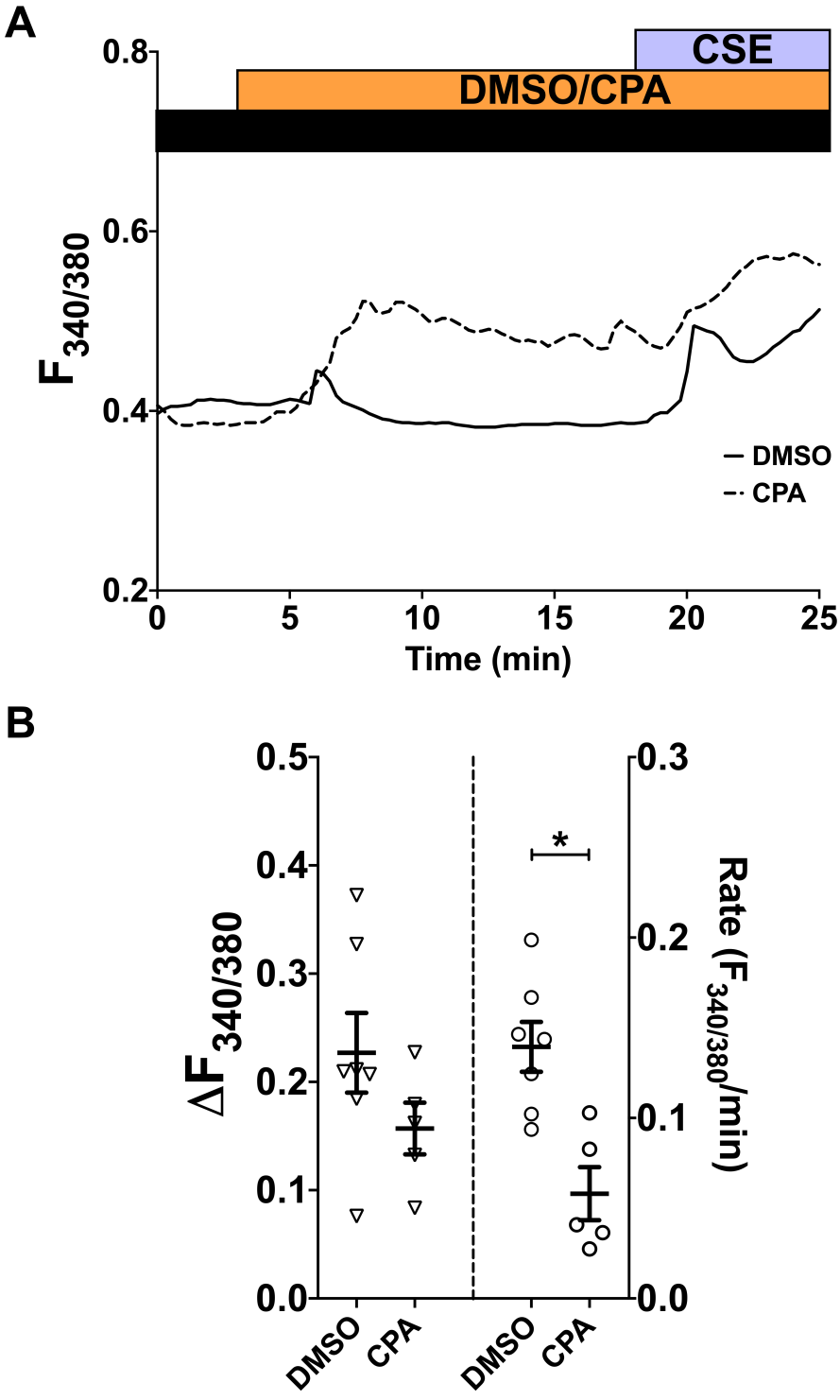

Figure 4.16: CSE-induced Ca^{2+} influx utilises a different pathway from SOCE. (A) Representative traces tracking changes in $[Ca^{2+}]_i$ following perfusion with 10% CSE after 15-min treatment with 10μM CPA. Equal volumes of DMSO was used for vehicle control. (B) Summary of amplitude and rate of CSE-induced $[Ca^{2+}]_i$ changes corresponding to experiments in (A). Unpaired t-test was performed between the CPA-treated group and the vehicle control group (2 independent donors; n=5-7). * = $p<0.05$.

4.3.12 CSE-induced Ca^{2+} influx is inhibited by a specific pharmacological blocker of TRPA1, HC-030031

After establishing that SOCC and LTCC were unlikely targets activated by CS/CSE, a possible alternative candidate was TRPA1, a Ca^{2+}-permeable cation channel that is primarily associated with noxious cold and mechanical sensation as well as inflammatory pain. TRPA1 has been shown to mediate CSE-induced $[Ca^{2+}]_i$ elevation in a number of other cell types, including various neuronal cells and lung epithelial cells (Andre *et al.*, 2008; Nassini *et al.*, 2012; Lin *et al.*, 2015; Nie *et al.*, 2016). To study the involvement of TRPA1, the potent and selective inhibitor HC-030031 was used (McNamara *et al.*, 2007). In the present study on hASMC, the effective concentration of HC-030031 that inhibited Ca^{2+} influx elicited by gaseous CS was determined to be 30-50µM (see Fig. x; explored in Chapter 5). However, one important channel that was not tested in the initial screening studies listed above was SOCC, and so whether HC-030031 had any off-target effects on SOCC was first investigated. At 50µM, a 10-min exposure to HC-030031 did not significantly inhibit SOCE (Figure 4.17A, B; n.s., DMSO- vs. HC-030031-treated), lending more confidence in using this compound to study TRPA1.

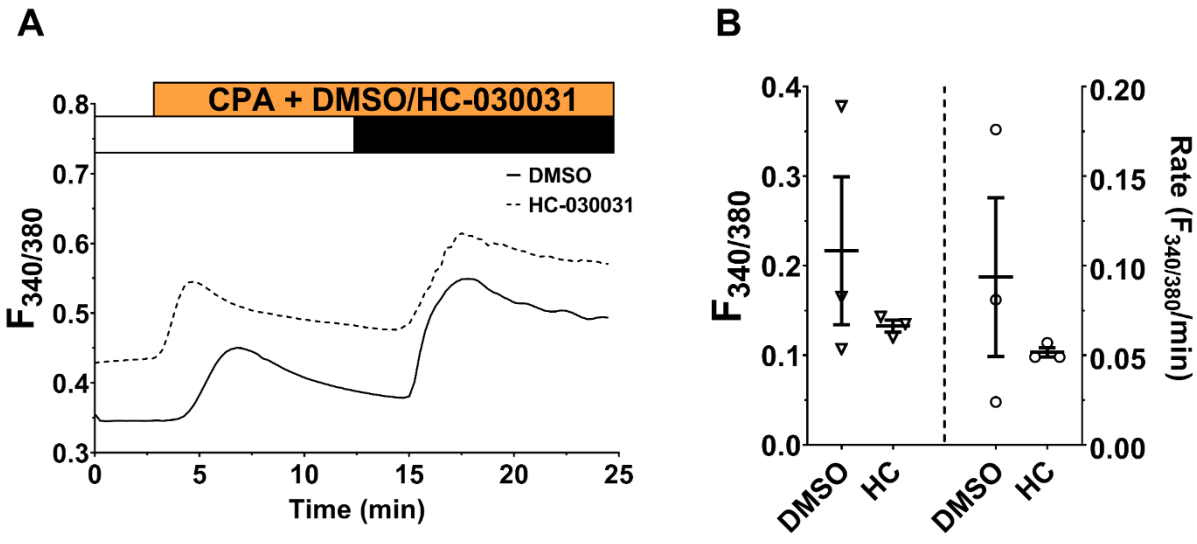

Figure 4.17: HC-030031 does not inhibit SOCE in hASMC. (A) Representative traces tracking changes in $[Ca^{2+}]_i$ following CPA-activated SOCE with or without 10-min pre-treatment with 50µM HC-030031, which was also present throughout the experiment. Equal volumes of DMSO was used for vehicle control. (B) Summary of amplitude and rate of $[Ca^{2+}]_i$ changes corresponding to experiments in (A). Data presented as mean ± SEM. Mann-Whitney test was performed between the HC-treated group and the vehicle control group; n=3, from 1 donor.

Following again a similar protocol, a 10-min pre-treatment with 50μM HC-030031 almost completely abolished the CSE-activated Ca^{2+} influx response (Figure 4.18A). Both amplitude (0.33±0.03 vs. 0.06±0.01; 83.3% inhibition) and rate (0.53±0.06 vs. 0.01±0.00; 97.6% inhibition) of CSE-induced Ca^{2+} influx in hASMC were significantly reduced by HC-030031 (Figure 4.18B; $p<0.05$, DMSO- vs. HC-030031-treated). Such significant inhibition by a potent TRPA1 inhibitor indicated strongly that TRPA1 was the major facilitator of CSE-activated Ca^{2+} influx.

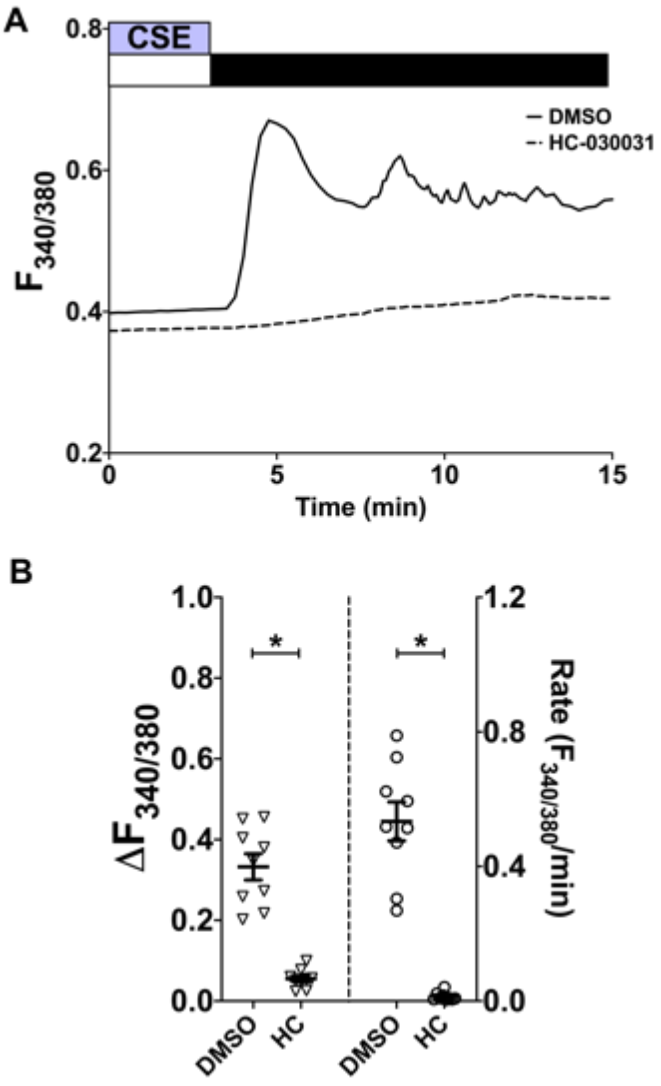

Figure 4.18: The TRPA1 channel blocker HC-030031 inhibited CSE-induced Ca^{2+} influx. (A) Representative traces tracking changes in $[Ca^{2+}]_i$ following calcium addback after 5-min perfusion with 10% CSE in a $0Ca^{2+}$ solution, with or without 10-min pre-treatment with 50μM HC-030031, which was also present throughout the experiment. Equal volumes of DMSO was used for vehicle control. (B) Summary of amplitude and rate of $[Ca^{2+}]_i$ changes corresponding to experiments in (A). Data presented as mean ± SEM. Unpaired t-test was performed between the HC-treated group and the vehicle control group (3 independent donors; n=9). * = $p<0.05$.

4.3.13 TRPA1 mRNA expression correlates with amplitude and rate of CSE-induced Ca^{2+} influx

Despite rather effective inhibition, there was residual Ca^{2+} influx that was not completely blocked by HC-030031 (~6.0-31.0%). Moreover, the concentration used in this study (50μM) was higher than the 10μM that was screened for off-target effect in the initial studies (McNamara *et al.*, 2007; Eid *et al.*, 2008). Hence, an additional approach was taken to investigate the putative role of TRPA1 in mediating CSE-induced Ca^{2+} influx. TRPA1 was knocked down using transient transfection of shRNA targeted towards the gene, as described in section 2.7 of Chapter 2. Out of the three shRNA constructs provided, the one that gave the highest knockdown efficiency (construct "B2") was selected (Figure 4.19). Several transfection conditions, specifically ratio of plasmid DNA to Lipofectamine 3000, were tested to optimise for maximal knockdown efficiency (Figure 4.19). Cells transfected with the vector containing shRNA construct targeted (TV) against TRPA1, grown on coverslips, were subjected to Ca^{2+} imaging studies following a simple CSE-activated calcium addback protocol previously established. Cells transfected with a shRNA sequence containing an empty vector (EV) construct, under the same growth and transfection conditions and used on the same days for Ca^{2+} imaging experiments, were used as a control for the transfection process, controlling for any changes associated with the transfection process itself that may have altered CSE-induced Ca^{2+} responses. After Ca^{2+} imaging experiments, cells were lysed, and mRNA were collected for qPCR analysis to ascertain knockdown of TRPA1. Briefly, relative expression of TRPA1 in shRNA-transfected samples was normalised to two different housekeeping genes (ΔCT), and then normalised to the average TRPA1 ΔCT of samples transfected with the empty vector in the same plate, day/donor-matched.

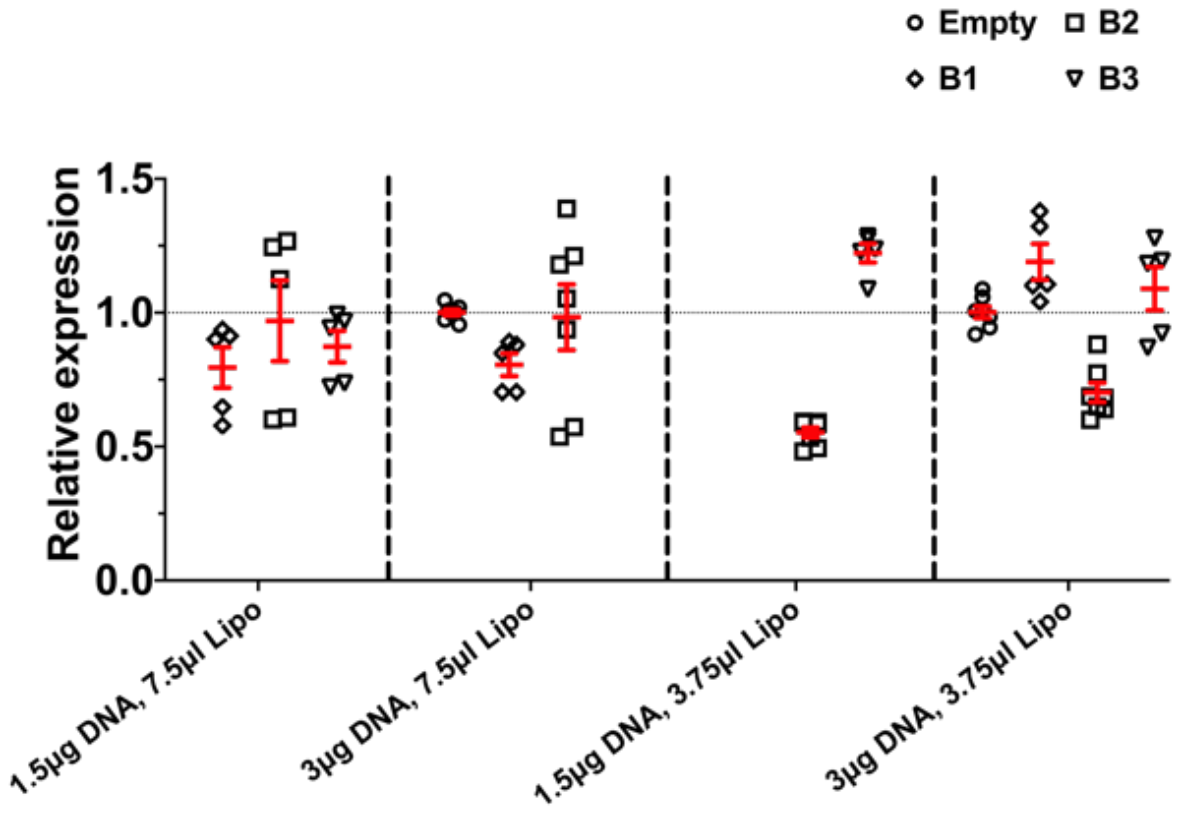

Figure 4.19: Optimisation of transient TRPA1-targeted-shRNA transfection in primary hASMC. Transfection was performed using the empty vector plasmid, or three different plasmids (B1, B2, B3) containing shRNA targeted towards TRPA1, using different amounts of plasmid DNA and Lipofectamine 3000 reagent. Relative expression of TRPA1 in transfected hASMC is presented as $2^{-\Delta\Delta CT}$, normalised to a housekeeping gene (either TBP or GAPDH), then normalised to the day/donor-matched empty vector control (1.0; indicated by the dotted horizontal line). Data presented as mean ± SEM. n=5-7, from 2 independent donors.

The Ca^{2+} imaging results were quite inconsistent even when the same transfection conditions were applied. In 12/15 experiments, the TRPA1-shRNA-transfected cells exhibited attenuated CSE-induced Ca^{2+} influx compared to the average day/donor-matched EV-transfected cells (e.g. Figure 4.20A), but in 3/15 of the experiments the cells transfected with the TV shared a similar response profile with the EV control (e.g. Figure 4.20B). Cells transfected with the TV had a lower amplitude (0.39±0.04 vs. 0.49±0.02, T vs. E; $p<0.05$) of response, but the influx rate (0.71±0.09 vs. 0.86±0.06, T vs. E; n.s.) was not significantly attenuated (Figure 4.20C). The degree of inhibition of the calcium response from TRPA1 knockdown was less (20.6%/17.7% for amplitude and rate, respectively) than the inhibition by HC-030031 (83.3%/97.6%). Inspecting the relative expression of TRPA1 after shRNA-driven knockdown revealed that the knockdown was, on average, only 8.8% efficient when normalised to GAPDH, and 40.3% when normalised to 18S (Figure 4.20D; $p<0.05$ for T vs. E, normalised to 18S). Moreover, some TRPA1-shRNA-trasfected samples were not knocked-down ($2^{-\Delta\Delta CT}$ close to or greater than 1.0). In addition, it was interesting to note that the $2^{-\Delta\Delta CT}$ values for GAPDH and 18S for the knocked-down samples appeared different (0.91 vs. 0.60, GAPDH vs. 18S); i.e. when normalising to 18S, the knockdown was significantly greater than when normalising to GAPDH. This may be due to the TRPA1-targeted shRNA also targeting GAPDH. To rule out such potential confounding factor, the raw CT values of GAPDH and 18S between the cells transfected with the T and E vectors were compared. The CT values for both housekeeping genes were not significantly different between the different transfected vectors, and therefore GAPDH may still be a valid housekeeping gene for normalisation of TRPA1 knockdown efficiency (Figure 4.20E; n.s. T vs. E for both genes).

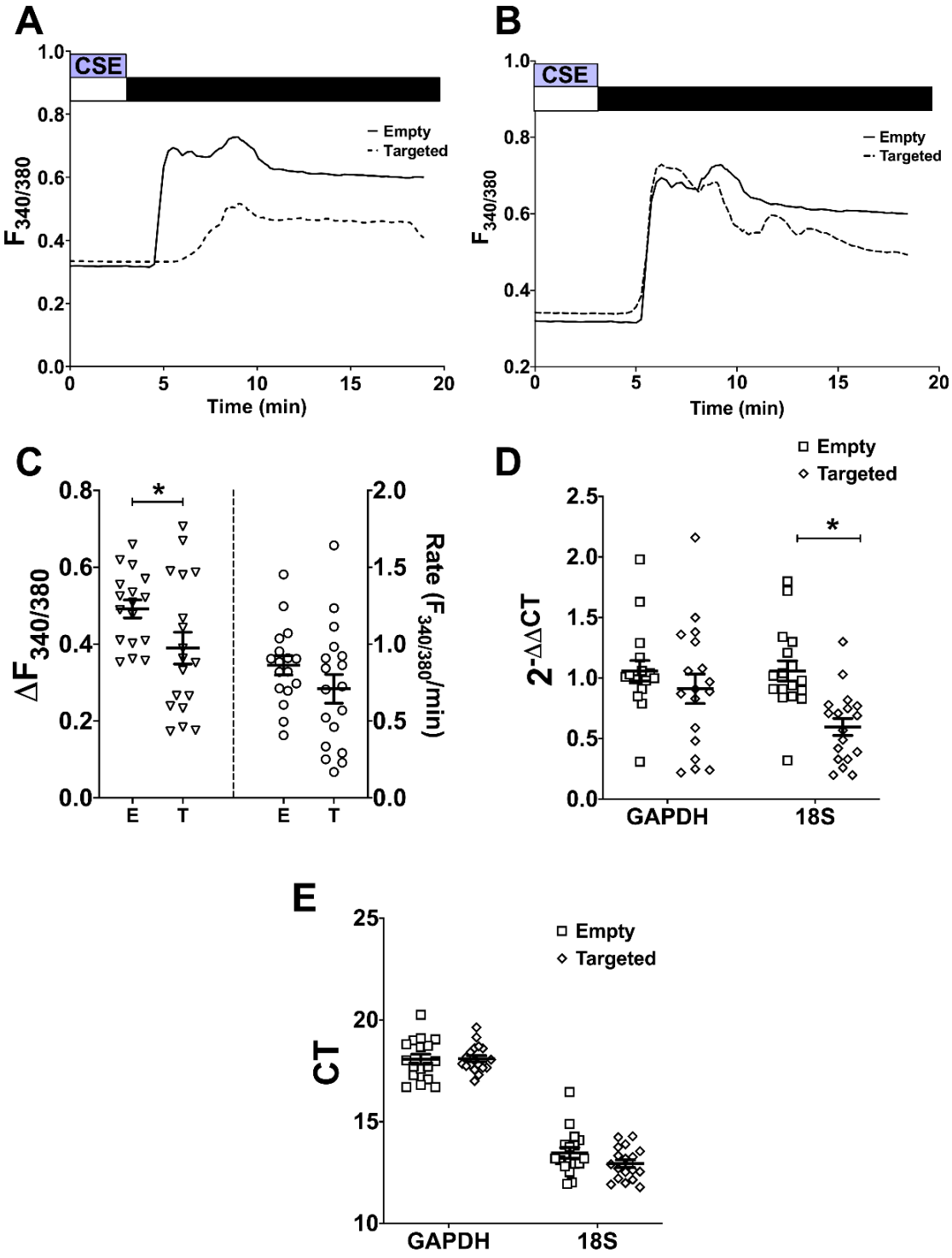

Figure 4.20: The effect of TRPA1 knockdown on CSE-induced Ca^{2+} influx is inconsistent. hASMC were transfected with shRNA containing either the empty (E) vector, or the vector targeted (T) towards TRPA1. (A, B) Representative traces tracking changes in $[Ca^{2+}]_i$ following calcium addback after 5-min perfusion with 10% CSE in transfected hASMC. Pairs of E and T are day/donor matched. (C) Summary of amplitude and rate of CSE-activated Ca^{2+} influx in transfected hASMC. (D) Knockdown efficiency of TRPA1 in transfected hASMC, reported as $2^{-\Delta\Delta CT}$. (E) Raw CT values of housekeeping genes GAPDH and 18S for shRNA-transfected hASMC. Data presented as mean ± SEM, containing of cells from 3 independent donors (n=17-18). Unpaired t-test was performed between the groups transfected with empty vector and those transfected with the TRPA1 targeted vector (C, D, E). * = $p<0.05$.

As samples without significant knockdown obviously affected the ability to determine the role of TRPA1 in the CSE-induced Ca^{2+} response, the removal of these data was carefully explored. Before removing data, whether TRPA1 expression actually correlated with both the amplitude and rate of CSE-induced Ca^{2+} influx, regardless of knockdown, was validated. Plotting normalised CT values of TRPA1 against the amplitude and rate of CSE-induced Ca^{2+} influx revealed an inverse correlation (Figure 4.21). The Pearson's *r* values (-0.25 to -0.50) indicated a moderate negative correlation. That is, higher ΔΔCT, i.e. lower mRNA expression, significantly correlated to lower Ca^{2+} responses, in 3 out of the 4 comparisons (Figure 4.21; $p<0.05$ for all but rate vs. ΔΔCT to GAPDH). Additionally, data points from hASMC transfected with the empty vector (black symbols) and with the targeted vector (red symbols) appeared to cluster differentially – black symbols generally located to the top-left (high amplitude/rate and low CT/high TRPA1 expression) and red symbols bottom-right (vice versa). Such correlations suggested that the knockdown had generally worked and that TRPA1 expression plays a role in CSE-induced calcium influx, providing a rationale for excluding the data where TRPA1 knockdown was minimal.

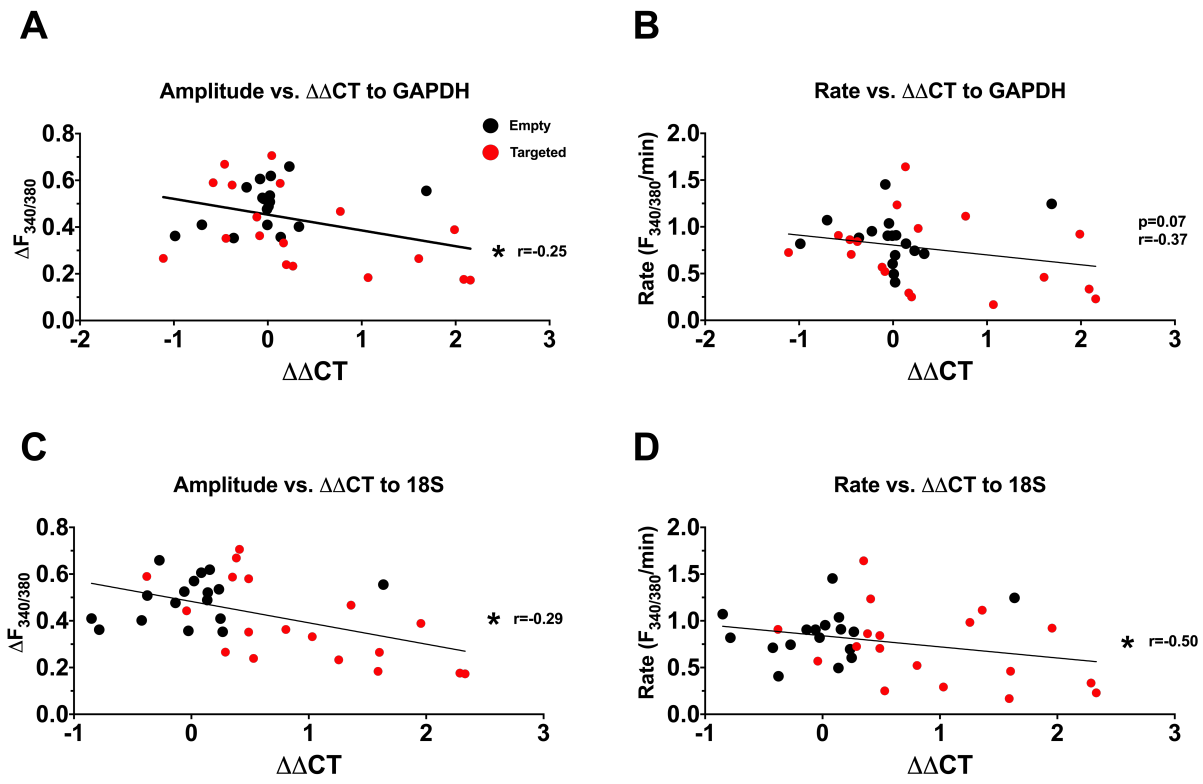

Figure 4.21: CSE-induced Ca^{2+} influx is correlated to TRPA1 mRNA expression. Amplitude (left panels) and rate (right panels) of CSE-induced Ca^{2+} influx were correlated vs. TRPA1 ΔΔCT values (raw TRPA1 CT was normalised to CT of GAPDH (A, B) or 18S (C, D), then normalised to ΔCT of the average empty vector-transfected cells, day/donor-matched). Pearson's correlation analysis was performed between each pair of the parameters indicated (3 independent donors; n=17-18). * = $p<0.05$.

Considering the relatively low average knockdown efficiency, especially the low knockdown efficiency when normalised to GAPDH, it would be logical to exclude experiments where $2^{-\Delta\Delta CT}$ normalised to both genes are high, in order to preserve usable data. The threshold for excluding TRPA1-shRNA-transfected samples with minimal knockdown was set to be of 0.75 to both housekeeping genes, i.e. < 25% knockdown in mRNA expression. Based on this criterion, 6 out of 18 experiments were removed from the subsequent analysis (Figure 4.22A; labelled as "Targeted, excluded"). The excluded experiments, on average, had similar $2^{-\Delta\Delta CT}$ values to samples transfected with the empty vector (1.33±0.19 vs. 1.06±0.09 normalised to GAPDH and 0.91 ±0.09 vs. 1.06±0.08 normalised to 18S; n.s.), but had significantly higher $2^{-\Delta\Delta CT}$ than the remaining TRPA1-targeted samples (0.69±0.12 normalised to GAPDH and 0.44±0.06 normalised to 18S; $p<0.05$). The knockdown efficiency after removing these data points was 30.6%/56.1% (normalised to GAPDH/18S). Following a similar trend, the excluded experiments exhibited significantly higher amplitude (0.54±0.07 vs. 0.31±0.04; 42.5% inhibition) and rate (0.99 ±0.16 vs. 0.57±0.10; 42.5% inhibition) of CSE-induced Ca^{2+} influx when compared to the remaining samples transfected with the targeted shRNA (Figure 4.22B; $p<0.05$, T excluded vs. T). The observation that the Ca^{2+} imaging results from the T excluded group were similar to the E control group, and both were significantly different from the T group where relatively efficient TRPA1 knockdown was achieved, validated the decision to remove these data from subsequent analyses. Removing the confounding factor of the inefficient transfection process would aid in studying the role of TRPA1 with more clarity.

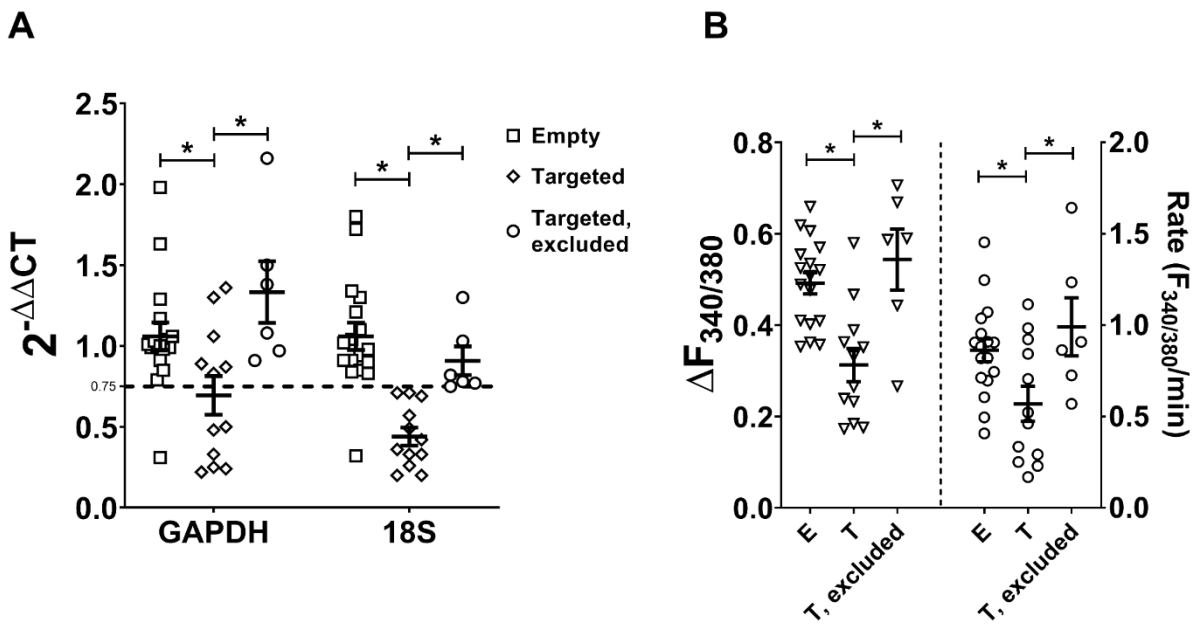

Figure 4.22: Validating removal of experiments with minimal TRPA1 knockdown. (A) Knockdown efficiency of TRPA1 in transfected hASMC, reported as $2^{-\Delta\Delta CT}$. hASMC transfected with the TRPA1-targeted shRNA (T) that had $2^{-\Delta\Delta CT}$ values >0.75 normalised to both housekeeping genes, indicated by the dashed horizontal line, were excluded for subsequent analyses (T, excluded). (B) Summary of amplitude and rate of CSE-activated Ca^{2+} influx in transfected hASMC. Data presented as mean ± SEM, containing of cells from 3 independent donors (n=17-18). One-way ANOVA with Holm-Sidak's multiple comparisons tests were performed amongst the three groups (E, T, and T, excluded). * = $p<0.05$.

4.3.14 shRNA-driven knockdown of TRPA1 attenuates CSE-induced Ca^{2+} influx

After removal of data with minimal TRPA1 knockdown, the relative expression of TRPA1 mRNA, normalised to two housekeeping genes, was significantly lower in cells transfected with the shRNA targeted to TRPA1 than those transfected with the empty vector (Figure 4.23A; $p<0.05$, T vs. E for both housekeeping genes). In cells where TRPA1 was significantly knocked-down, both the amplitude (0.31±0.04 vs. 0.49±0.02; 36.4% inhibition) and rate (0.57±0.10 vs. 0.86±0.06; 34.0% inhibition) of CSE-induced Ca^{2+} influx were significantly attenuated (Figure 4.23B; $p<0.05$, T vs. E). Collectively, these data add to the results from HC-030031 experiments and suggest that TRPA1 is the major contributor to this calcium influx.

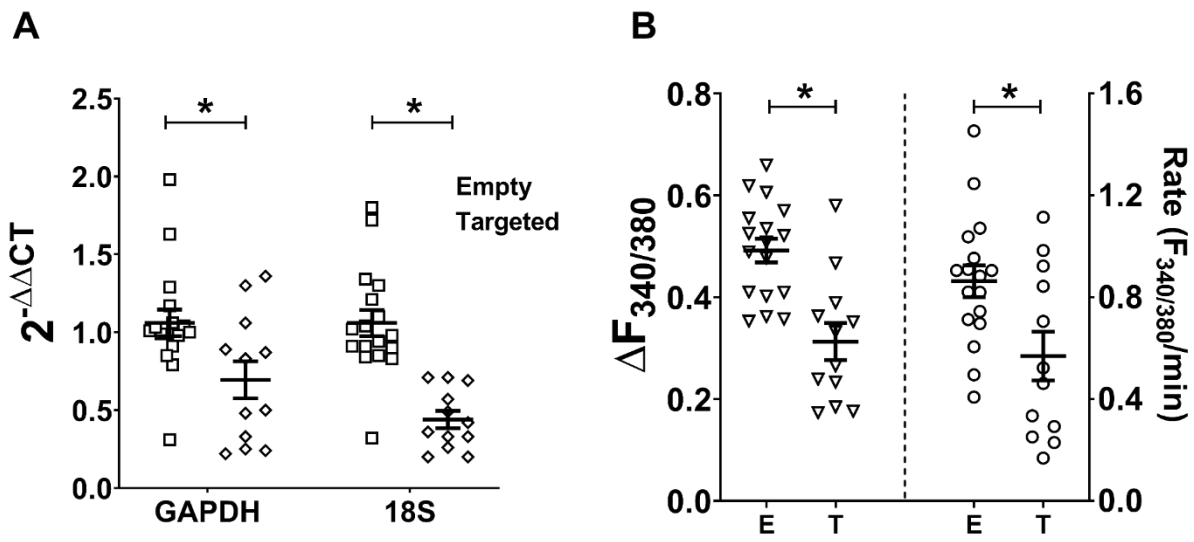

Figure 4.23: TRPA1 knockdown significantly attenuated CSE-induced Ca^{2+} influx. (A) Knockdown efficiency of TRPA1 in transfected hASMC, reported as $2^{-\Delta\Delta CT}$. (B) Summary of amplitude and rate of CSE-activated Ca^{2+} influx in transfected hASMC. Experiments with minimal knockdown were excluded for analysis. Data presented as mean ± SEM, containing of cells from 3 independent donors (n=17-18). Unpaired t-tests were performed between the samples transfected with the empty vector (E) and those transfected with the TRPA1-targeted vector (T). * = $p<0.05$.

4.3.15 TRPA1-mediated, CSE-induced Ca^{2+} influx activates MLC phosphorylation in hASMC

A persistently elevated level of $[Ca^{2+}]_i$ could bring about deleterious downstream effects to the function of ASMC, including the contractile mechanisms of these muscle cells, which is tightly regulated by $[Ca^{2+}]_i$. An important downstream event subsequent to elevated $[Ca^{2+}]_i$ is the phosphorylation of MLC (explored in section 1.3.3). To investigate whether CSE-induced Ca^{2+} influx is sufficient to activate MLC phosphorylation, a Western blot-based MLC phosphorylation assay was performed as described in section 2.9, utilising a phospho-specific antibody that detects p-MLC.

To initially study the effects of CSE on MLC phosphorylation, a time-course protocol was applied to determine the optimal exposure time that elicited the strongest WB signal. After testing several different CSE and protein concentrations, a protocol was established that consistently detected p-MLC in the hASMC lysates (Figure 4.24A; 18 kDa band). However, whether or not CSE treatment led to an increased phosphorylation was not clear, as the HEPES-only (negative control) showed similar signals, especially at 2 and 10 mins, to 50% CSE-treated and postive control sets (Figure 4.24A). This may be attributed to the rapid change of solution (culture media to HEPES-buffered solution) over the relatively short treatment period. To ensure that cells had time to equilibrate after being placed in the HEPES-buffered bathing

solution, they were left in this solution for an hour before various treatments, or collecting the negative control lysate. After these modifications, the p-MLC lanes for the negative control lanes usually had minimal detectable bands, with signals below those of the positive control or CSE-treated samples under the same exposure time, although most comparison sets were not statistically significant, probably due to a low sample size (Figure 4.24B, C). In addition, treatment with 50% CSE was able to elicit MLC phosphorylation to a similar level to that of the positive control at all time points (Figure 4.24C; all comparisons 50% CSE vs. +ve n.s.), providing evidence that CSE-induced Ca^{2+} influx initiated MLC phosphorylation and, therefore, downstream activation of the contractile machinery in hASMC. In terms of the time-course, a 2- or 10-min exposure to 50% CSE generally led to higher levels of p-MLC expression than a 30-s exposure, whilst there was little difference between 2- and 10-min (Figure 4.24C). From these preliminary data, a 2-min treatment with 50% CSE was used to capture near-maximal levels of MLC phosphorylation in subsequent experiments.

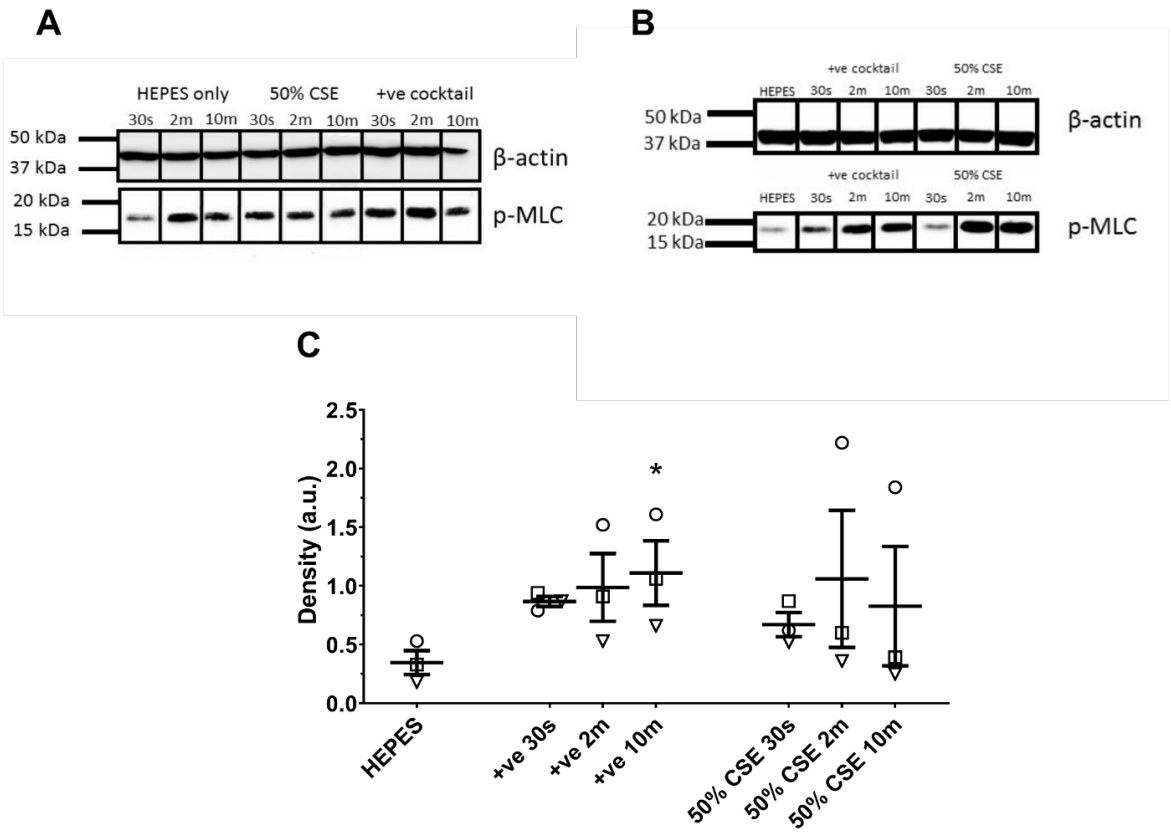

Figure 4.24: Assay optimisation and time-course of MLC phosphorylation in hASMC. (A) Initial western blot image for the MLC phosphorylation assay without equilibrating cells in fresh buffer solution before experiments. (B) Representative western blot image for MLC phosphorylation assay following equilibration of cells in HEPES-buffered solution for an hour prior to assay. (C) Semi-quantitative analysis of MLC phosphorylation following different exposure durations to the positive control cocktail or 50% CSE. Density was normalised to β-actin (density for p-MLC/density for β-actin). Data presented as mean ± SEM. Data points with the same symbol represent day/donor matching. Friedman's test with Dunn's multiple comparisons was applied to HEPES vs. all other groups (2 independent donors; n=3). * = $p<0.05$.

To ascertain the involvement of the CSE-induced activation of TRPA1-dependent Ca^{2+} influx in facilitating MLC phosphorylation, cells were pre-treated with 50µM HC-030031 (or 0.1% DMSO for vehicle control) for 15 minutes before lysis (for the negative control untreated with CSE; UT), or exposed to 50% CSE, with or without HC-030031, for 2 minutes before lysis (Figure 4.25A). As an internal control for the abundance of MLC protein, total levels of MLC protein was used to normalise the band density of p-MLC (same sample, run on the same gel, and probed with two different MLC antibodies). In the negative control, HC-030031 did not significantly affect the band density of p-MLC (Figure 4.25B; 0.54±0.24 vs. 0.57±0.17, UT -HC vs. UT +HC). In contrast, pre-treatment with HC-030031 significantly reduced the band density of p-MLC in CSE-treated samples (Figure 4.25B; $p<0.05$, 1.24±0.13 vs. 0.70±0.10, 50% CSE -HC vs. 50% CSE +HC), suggesting that CSE-induced Ca^{2+} influx activates downstream phosphorylation of MLC, which is primarily mediated by TRPA1.

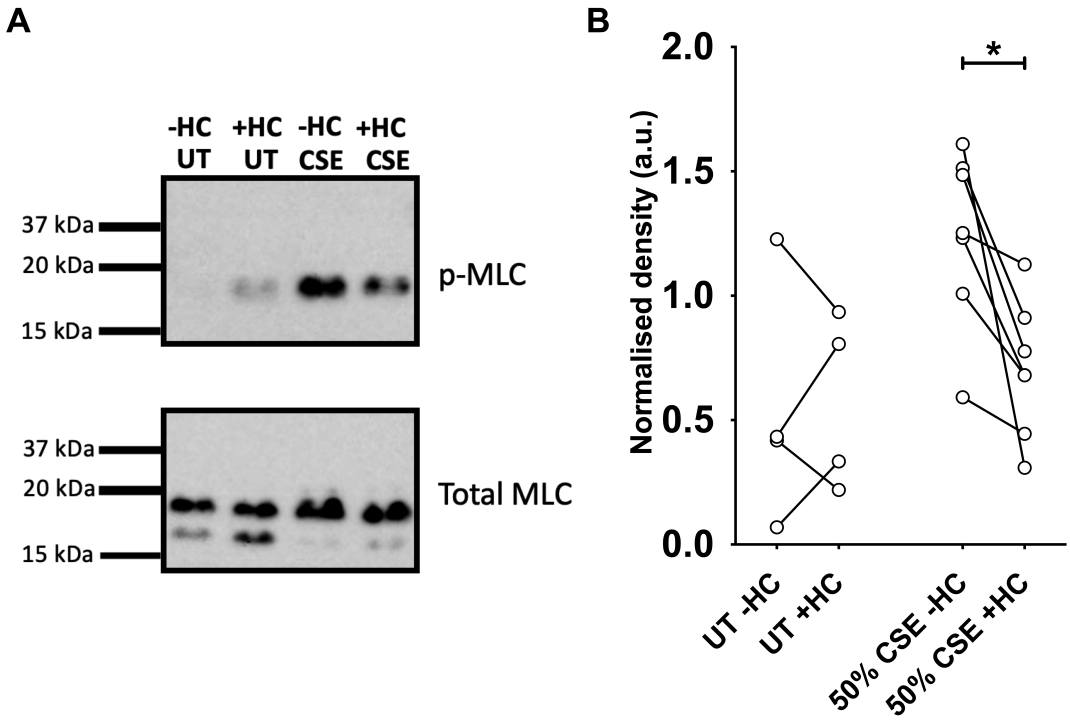

Figure 4.25: CSE induces MLC phosphorylation in hASMC, downstream of TRPA1-mediated Ca^{2+} influx. Cells were equilibrated with HEPES-buffered solution for 1 hour, and lysed after treatment for protein extraction. For the negative control samples without CSE exposure (UT; untreated), cells were treated with 0.1% DMSO (-HC) or 50µM HC-030031 (+HC) for 15 minutes before lysis. For the CSE experiments, cells were pre-treated with 0.1% DMSO (-HC) or 50µM HC-030031 (+HC) for 15 minutes, and then exposed to 50% CSE, with or without HC-030031, for 2 minutes before lysis. 15µg of protein was loaded into each well for gel electrophoresis and western blot analysis. (A) Representative western blot image for MLC phosphorylation assay described above. All 8 lanes shown were part of the same blot, cut vertically to perform staining with two different antibodies. The 4 lanes in the top panel (p-MLC) match the 4 lanes in the bottom panel (total MLC), i.e. the same protein sample run on the same gel, processed under identical blotting and exposure conditions. (B) Semi-quantitative paired comparison of CSE-induced phospho-MLC protein levels with or without pre-treatment with HC-030031. Band density of p-MLC was normalised to the density of total MLC of the same protein sample (3 independent donors; n=4-7). * = $p<0.05$, Wilcoxon matched-pairs signed rank test.

Altogether, the results provide a mechanistic understanding of CSE-induced disruption of Ca^{2+} homeostasis in primary hASMC, chiefly through TRPA1, which led to downstream MLC activation and likely to ASMC contractile mechanisms and hence, potentially, altering the reactivity and tone of ASMC.

4.4 Discussion

The results in this chapter showed that acute exposure to diluted CSE stimulates Ca^{2+} influx in primary hASMC through activation of TRPA1 channels, which induced downstream phosphorylation of myosin light-chain, presenting TRPA1 as an important link between smoking and airway hyperresponsiveness. This activation of a Ca^{2+} influx pathway appeared to be cell-type specific, as the same CSE-activated Ca^{2+} addback protocol did not change $[Ca^{2+}]_i$ in Calu-3 cells (Figure 4.9). TRPA1 is a non-selective cation channel that is primarily associated with noxious cold and mechanical sensation as well as inflammatory pain. Several groups have previously reported that CSE mobilises calcium in neuronal cells, lung epithelia and fibroblasts via TRPA1 (Andre *et al.*, 2008; Nassini *et al.*, 2012; Lin *et al.*, 2015; Nie *et al.*, 2016). However, the results presented in this study are the first to show that CSE activates Ca^{2+} influx via TRPA1 using both pharmacological and genetic tools, in primary hASMC isolated from multiple human donors. Furthermore, due to the significant donor-donor variability (Figure 4.7), the usage of cells from multiple donors for the majority of the datasets presented in this chapter is advantageous compared to studies where cells from a single donor was used.

The data strongly demonstrated that the primary source of CSE-induced Ca^{2+} response was Ca^{2+} influx from extracellular space. However, results from Figure 4.3 indicated that acute exposure to 50% CSE reduced the amplitude of SR Ca^{2+} store release compared to 10% CSE. This suggests that although SR Ca^{2+} release may not be the dominant source of CSE-induced Ca^{2+} response, high concentrations of CSE may partially deplete SR Ca^{2+} stores, either directly or through Ca^{2+}-induced Ca^{2+} release mechanisms activated by elevated $[Ca^{2+}]_i$ from CSE-induced Ca^{2+} influx.

The calcium influx activated by CSE did not require the continual presence of CSE, but the recovery profile and extent was affected by the presence of CSE at the peak of the influx (Figure 4.5). The potential role of CSE in modulating recovery suggests that CSE not only activates Ca^{2+} influx, but may also maintain the open state of such pathways for continual influx. Another possible explanation for this observation was that CSE may inhibit the SERCA, PMCA, or NCX, and so removing CSE would allow these Ca^{2+} removal/reuptake mechanisms to balance out CSE-induced Ca^{2+} influx.

One complication encountered during the search for an effective LTCC blocker was the off-target effect of nifedipine in activating a Ca^{2+} response (Figure 4.11). It has previously been reported that nifedipine at 100μM inhibited Ca^{2+}-sensitive K^+ channels (Kaji, 1990). More likely, however, nifedipine in these experiments did not block LTCC sufficiently, but could potentially activate other Ca^{2+} influx pathways. A report in 2001 (Raicu and Florea, 2001) indicated that nifedipine induced significant SOCE in cultured human aortic SMC, which is consistent with the off-target effect observed here in hASMC.

During the optimisation process for the MLC phosphorylation assay, a high p-MLC signal in negative control experiments was first observed (Figure 4.24). This was then minimised by equilibrating the cells in the HEPES-buffered solution, by which CSE and pharmacological agents were delivered, for 60 min. This suggested the p-MLC signal in the negative control could be physiological, as cells could be responding to physical addition of the HEPES-buffered solution during transfer of the cells from culture media. Indeed, a few studies have shown previously that shear stress causes direct changes in intracellular Ca^{2+} signalling in SMC (Sharma *et al.*, 2002; Song *et al.*, 2014).

TRPA1 is known to be activated by several water-soluble CS components, namely acrolein, crotonaldehyde, extracellular ROS, and nicotine, and is required to mediate neurogenic inflammation and pain following CS exposure (Bautista *et al.*, 2006; Andre *et al.*, 2008; Talavera *et al.*, 2009; Centers for Disease Control and Prevention, 2010; Lin *et al.*, 2015; Prandini *et al.*, 2016). These constituents, individually or together, are likely responsible for CSE-induced acute activation of TRPA1 in hASMC; further exploration studying the role of each individual constituent on hASMC Ca^{2+} influx, as well as modulation of physiological Ca^{2+} responses, is therefore warranted. In particular, acrolein has long been implicated in inducing ASMC hyper-contractility in human and rat airway tracheal/bronchial rings, which was attributed partly to augmented Ca^{2+} signalling, in response to cholinergic agonists (Ben-Jebria *et al.*, 1993; Ben-Jebria *et al.*, 1994; Roux *et al.*, 1998).

At a cellular level, these CSE constituents may regulate TRPA1 channel open probability or inhibit channel de-activation mechanisms. For instance, acrolein was found to covalently modify cysteine and lysine residues on TRPA1 that led to sustained membrane current being activated (Bautista *et al.*, 2006; Hinman *et al.*, 2006; Macpherson *et al.*, 2007). Electrophysiologically, Talavera *et al.* (2009) showed that nicotine stabilised the open state and destabilised the closed state of stably expressed mouse and human TRPA1. However, TRPA1 electrophysiology has not been explored in smooth muscle cells. Accordingly, patch-clamping hASMC to study the kinetics, channel activation/deactivation profiles, and Ca^{2+} permeability

of endogenous TRPA1 would help elucidate the molecular mechanisms of CSE-induced TRPA1 activation.

In addition to showing that the highly selective TRPA1 inhibitor HC-030031 blocked most of the downstream effects of CSE, a genetic approach to investigate the contribution of TRPA1 to CSE-activated Ca^{2+} response was also employed. The shRNA-driven knockdown of TRPA1 was not fully efficient (mean $2^{-\Delta\Delta CT}$ for TRPA1-shRNA transfected cells was 0.44-0.69), and experiments where the knockdown efficiency was <25% when normalised to both housekeeping genes were excluded. Although a ~40% attenuation of CSE-induced Ca^{2+} influx was detected with this knockdown model, a complete knockout animal or cell model would provide more definitive evidence of this interaction. CSE and its components were reported to activate TRPA1-mediated Ca^{2+} influx in sensory neurons of WT, but not TRPA1-deficient, mice (Bautista *et al.*, 2006; Andre *et al.*, 2008); it is therefore reasonable to hypothesise that ASMC from TRPA1-deficient rodents would not respond to CS/CSE challenge.

In this study, only the water-soluble gaseous phase of CS was bubbled into the CSE, as the particulate tar phase was filtered out. However, certain constituents of the particulate phase are cytotoxic or carcinogenic, and can deposit in the respiratory tract and the lungs (Centers for Disease Control and Prevention, 2010); it is therefore possible that acute exposure to the particulate phase could also impact ASMC Ca^{2+} homeostasis. To investigate this possibility in the future, the CS condensate (CSC) should be utilised; the CSC was not studied in the present study due to the technical issue of the particulate matter being autofluorescent at wavelength exciting fura-2 (Figure 2.9, Chapter 2), but this can be circumvented in future studies by using other calcium indicators excited by wavelengths at different regions of the spectrum at which CSC is not autofluorescent.

In summary, this chapter explored the direct effects of acute CSE exposure on primary hASMC Ca^{2+} homeostasis, particularly the mechanism of action of CSE-induced elevation in $[Ca^{2+}]_i$, concluding that this response requires extracellular calcium, and is not facilitated primarily by LTCC or SOCC. TRPA1 was identified to underly the CSE-induced Ca^{2+} response in primary hASMC, which led to downstream MLC phosphorylation. This elevation of $[Ca^{2+}]_i$ could potentially lead to ASMC contraction, and hence exacerbated pulmonary obstruction during smoking, especially under inflamed conditions such as those seen in COPD. The results obtained from these experiments then informed the experimental design of the next chapter, which focuses on the effects of gaseous CS, and how the two models differed.

Chapter 5: Effect of acute gaseous cigarette smoke (CS) exposure on calcium homeostasis in hASMC

5.1 Introduction

In Chapter 4, the effects of CSE on hASMC Ca^{2+} homeostasis and subsequent downstream signalling on the hASMC contractile mechanisms were explored. However, although CSE is a valid model for simulating the aqueous components of CS dissolved in the bloodstream of a smoker, it does not capture the volatile constituents that may be potentially lost through the vigorous bubbling process in producing CSE. Therefore, another delivery model that aims to capture these volatiles is required. In the CS model, gaseous CS is delivered to cells placed in a closed chamber. The frequency and volume of puffing one whole cigarette follows a standardised protocol agreed by the ISO (International Organization for Standardization, 2012), and is designed to simulate the frequency and volume of a smoking session of a typical smoker.

The CS model has been commonly used for acute or chronic animal smoking studies, as well as *in vitro* experiments. However, to date, there are no published studies that have investigated the effect of direct gaseous CS exposure on isolated ASMC, unlike the existent, albeit limited, literature on acute effects of CSE on ASMC function. Therefore, characterising the effect of CS on Ca^{2+} homeostasis would help elucidate the potential role of volatile CS constituents not captured by the CSE model, and whether CS causes similar and/or additional effects on Ca^{2+} homeostasis, other than stimulating Ca^{2+} influx.

5.2 Aims and Objectives

The main aim of this chapter was to explore the direct, acute, effects of gaseous CS on hASMC Ca^{2+} homeostasis. The objectives were:

- To ascertain whether acute CS exposure elevates $[Ca^{2+}]_i$ in hASMC.
- To characterise the cellular mechanisms of any CS-induced changes in Ca^{2+} homeostasis.
- To compare and contrast any effects of CS with that of CSE on hASMC intracellular Ca^{2+} signalling.

5.3 Results

5.3.1 Acute CS exposure elevates $[Ca^{2+}]_i$ in hASMC, and requires extracellular Ca^{2+}

To investigate whether gaseous CS could elevate $[Ca^{2+}]_i$ in isolated primary hASMC, similar to the effects induced by diluted CSE, the cells were exposed to CS from one Kentucky 3R4F reference cigarette as described in the Methods section. Briefly, one 3R4F reference cigarette was combusted and delivered, through an automated smoke machine with a pre-programmed protocol, onto hASMC situated in a closed chamber. Room air puffed with the same volume/frequency was used as a control to account for the physical changes in airflow/pressure in the chamber. Any changes in cytosolic Ca^{2+} were estimated using a calcium imaging setup with the ratiometric calcium indicator fura-2, similar to that used in Chapter 4.

In the presence of 1mM extracellular Ca^{2+}, exposure to the gaseous phase of one whole cigarette led to a rise in hASMC $[Ca^{2+}]_i$ (Figure 5.1). Interestingly, in the Ca^{2+} imaging traces averaged from 10-20 single cells in the same experiment, two different recovery profiles were observed following the initial peak (Figure 5.1A). In 12/25 of the experiments, the averaged $[Ca^{2+}]_i$ of the sampled cells did not rapidly recover following the initial peak, whilst in 13/25 of the experiments, a rapid recovery of $[Ca^{2+}]_i$ occurred to a raised plateau higher than the initial baseline. Figure 5.1B and C illustrate the responses in individual cells that averaged into the sustained plateau profile (B) or the rapid recovery profile (C), respectively. Although the single-cell response profiles were diverse in Figure 5.1B, with $[Ca^{2+}]_i$ in some cells recovering after the initial peak while others were sustained, the mean trace (red dashed line) did not average into a rapid recovery profile. In contrast, the $[Ca^{2+}]_i$ in the majority of cells sampled in Figure 5.1C rapidly recovered, which was unified and rapid enough to be reflected in the averaged trace.

The CS-induced increase in $[Ca^{2+}]_i$ typically began after 8-10 puffs (on average 4.4±0.1 mins), and reached an initial peak 4.5-8 mins (on average 6.4±0.1 mins) after the first puff. On average, the initial peak amplitude (0.42±0.04 vs. 0.07±0.01) and rate (0.30±0.04 vs. 0.00±0.00) of the $[Ca^{2+}]_i$ elevation was significantly greater than the change in $[Ca^{2+}]_i$ elicited by puffing room air, wherein no visible response was observed (Figure 5.1D, E; $p<0.05$ for both amplitude and rate, CS vs. air in 1mM Ca^{2+}). More importantly, the CS-induced $[Ca^{2+}]_i$ increase required extracellular Ca^{2+}, as the response was abolished when CS was administered in a nominally Ca^{2+}-free solution (Figure 5.1D, E; $p<0.05$ for both amplitude (0.42±0.04 vs. 0.13±0.03) and rate (0.30±0.04 vs. 0.01±0.00), CS in 1mM Ca^{2+} vs. 0Ca^{2+}). These results suggest that similar to CSE exposure, acute CS exposure activates a Ca^{2+} influx pathway to facilitate entry from the extracellular space, and that intracellular Ca^{2+} stores do not contribute to this response.

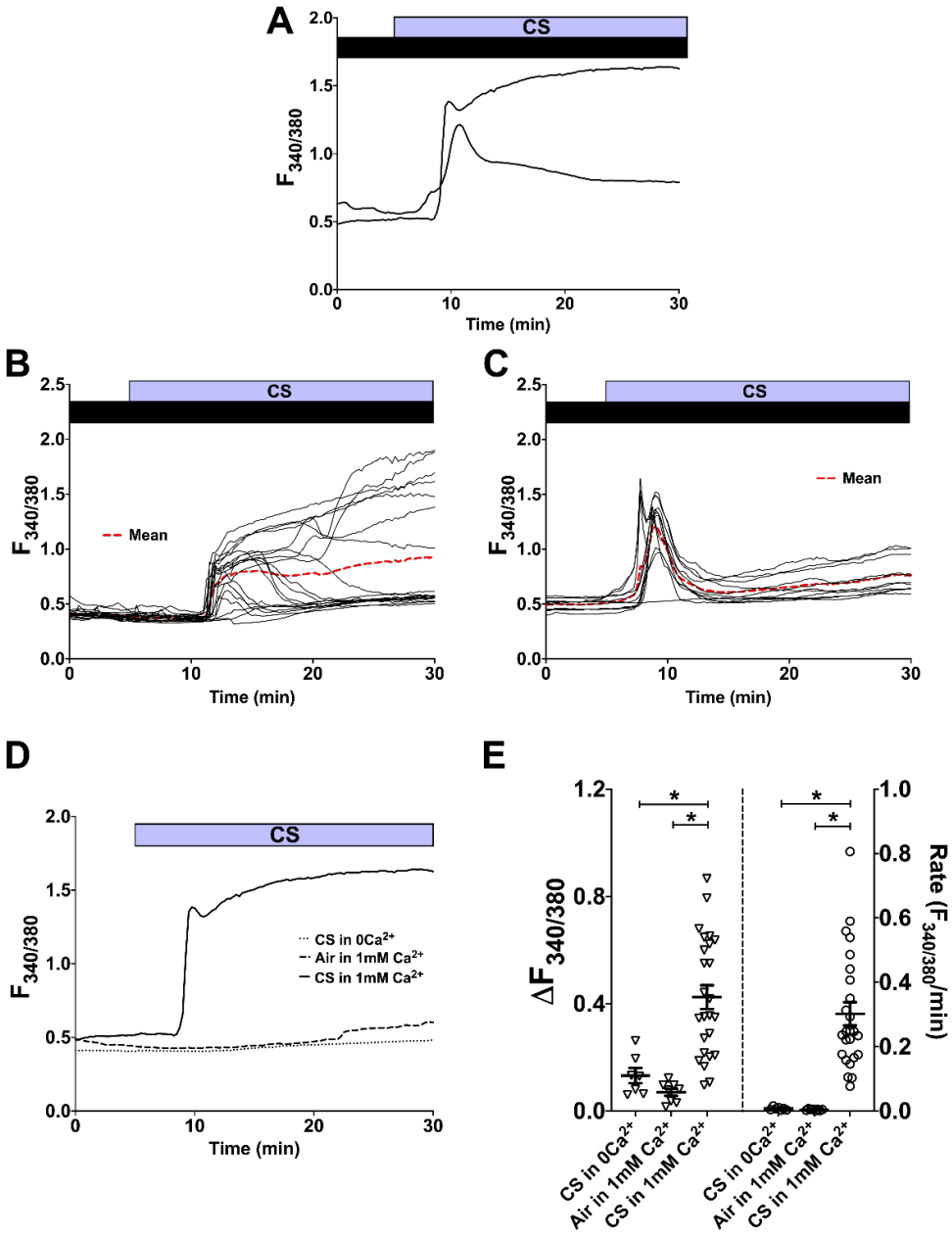

Figure 5.1: Acute CS exposure elevates intracellular Ca^{2+} in hASMC, and requires extracellular Ca^{2+}. (A) Representative mean traces from two independent experiments tracking changes in $[Ca^{2+}]_i$ following puffing one whole cigarette, in the presence of 1mM extracellular Ca^{2+} (black bar), showing different response profiles using the same protocol. (B, C) Representative single-cell traces of the two distinct response profiles shown in (A). The red dashed line is the mean trace of all the single-cell traces (n=19 and 11 for (B) and (C), respectively). (D) Representative Ca^{2+} imaging traces following puffing one whole cigarette, or room air, with or without 1mM extracellular Ca^{2+}. (E) Summary of amplitude and rate of CS- or room air-induced $[Ca^{2+}]_i$ changes. One-way ANOVA with Holm-Sidak's multiple comparisons test was performed amongst the 3 groups (4 independent donors; n=7-25). Data presented as mean ± SEM. * = $p<0.05$.

5.3.2 Donor and passage variability of CS-induced Ca^{2+} response

For the majority of results presented in this chapter, experiments were performed with hASMC isolated from at least 3 independent donors, used for experiments between passages 2-7. Donor- and passage-variability of the amplitude and rate of the CS-induced Ca^{2+} response was examined. Similar to that observed for the CSE-induced Ca^{2+} responses, there was a certain degree of donor-donor variability in both the amplitude and rate of CS-induced Ca^{2+} responses (Figure 5.2A). However, the results from donor 3 were only included in a subset of experiments in this chapter (Figure 5.1 (n=4) and the shRNA experiments (n=5)). On the other hand, in terms of passage variability, there was a trend that the CS-activated Ca^{2+} response was highest in passages 3 and 4, compared to the earlier passage 2 and the higher passages (Figure 5.2B, C).

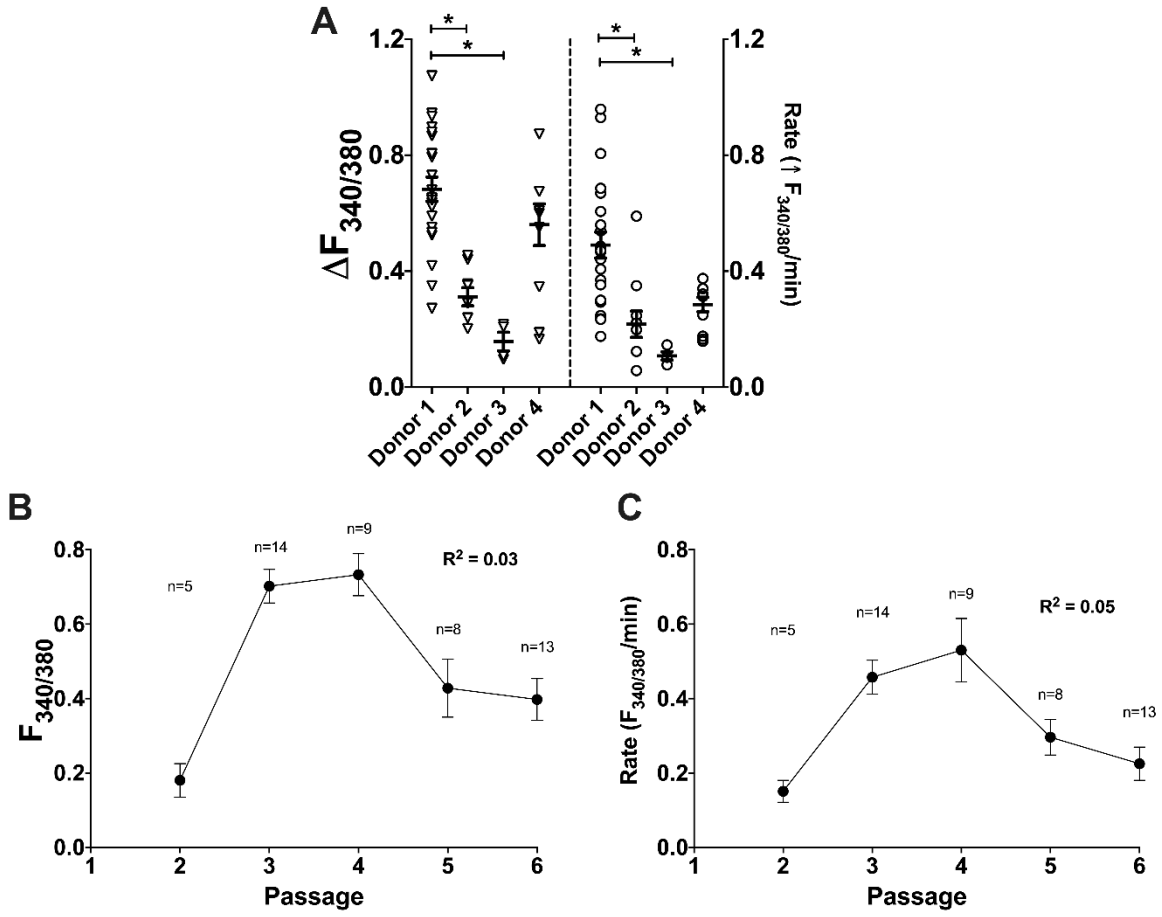

Figure 5.2: Donor and passage variability of CS-induced Ca^{2+} responses. (A) Summary of amplitude and rate of CS-induced Ca^{2+} responses in the presence of 1mM extracellular Ca^{2+}, in hASMC isolated and cultured from different donors. Kruskal Wallis test with Dunn's multiple comparisons was conducted between each individual donor; n = 4-23. * = $p<0.05$. (B, C) Summary of amplitude (B) and rate (C) of CS-induced Ca^{2+} responses in cultured primary hASMC at different passages (at least 2 independent donors for each passage). Linear regression was performed on each curve to examine potential linear correlations. n=5-14. Data presented as mean ± SEM.

5.3.3 CS-induced Ca^{2+} influx is blocked by gadolinium

To further investigate the underlying mechanism of the CS-induced increase in cytosolic Ca^{2+}, the effect of Gd^{3+} was tested by pre-treating the cells with Gd^{3+} for 10 mins prior to a CS challenge. Unlike the CSE-induced Ca^{2+} response, however, pre-treatment with 100µM Gd^{3+} did not inhibit the amplitude (0.72±0.05 vs. 0.65±0.05) or the rate (0.56±0.10 vs. 0.42±0.07) of the CS-induced $[Ca^{2+}]_i$ elevation (Figure 5.3B; $p>0.05$ for both amplitude and rate, Gd^{3+}-treated vs. control).

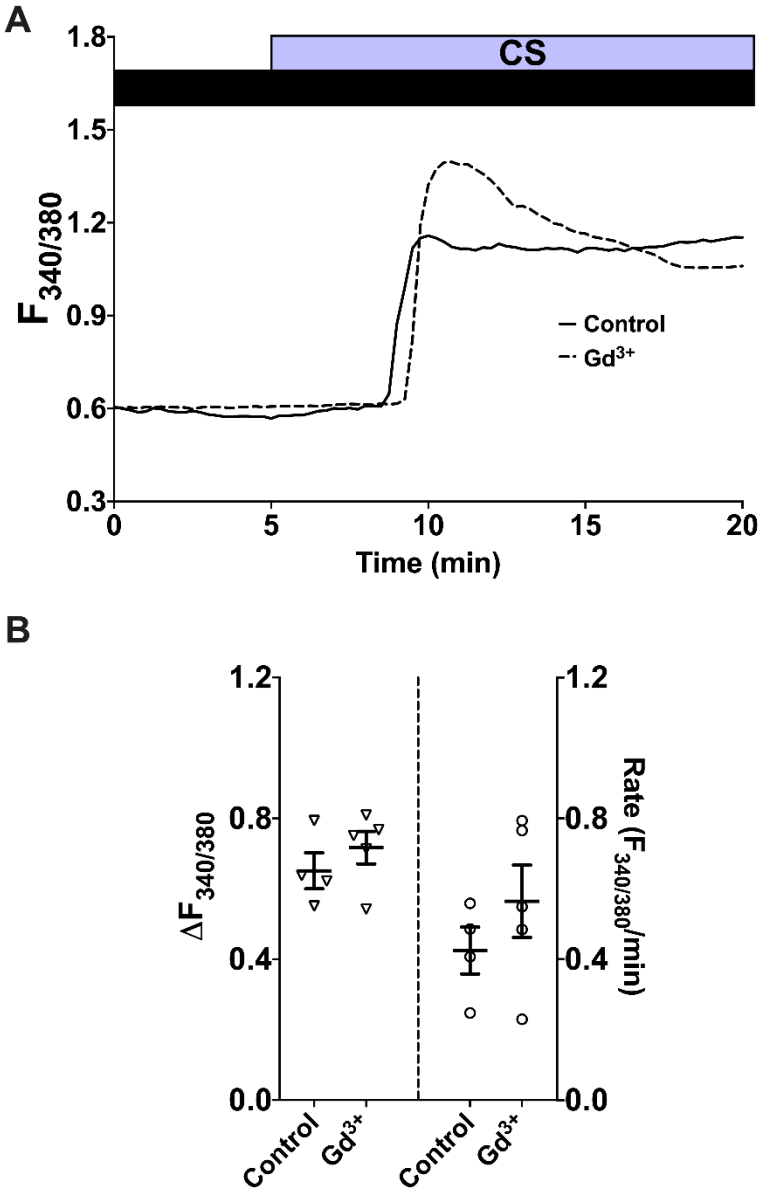

Figure 5.3: 100µM Gd^{3+} did not inhibit CS-induced Ca^{2+} influx. (A) Representative traces tracking changes in $[Ca^{2+}]_i$ following puffing one whole cigarette, in the presence of 1mM extracellular Ca^{2+} (black bar), with or without 10-min pre-treatment with 100µM Gd^{3+}, which was also present throughout the experiment. (B) Summary of amplitude and rate of $[Ca^{2+}]_i$ changes corresponding to experiments in (A). Data presented as mean ± SEM. Mann-Whitney test was performed between the control group and the Gd^{3+}-treated group (n=4-5, from 1 donor).

However, when the concentration of Gd^{3+} was increased to 500µM, it now significantly reduced the amplitude (0.20±0.02 vs. 0.42±0.05; 52.6% inhibition) and rate (0.13±0.03 vs. 0.23±0.02; 43.8% inhibition) of the CS-induced Ca^{2+} response in hASMC (Figure 5.4A, B; $p<0.05$ for both amplitude and rate, Gd^{3+}-treated vs. control). In addition to blocking the rapid influx of Ca^{2+}, 500µM Gd^{3+} also delayed the onset of the response (from an average of 4.7±1.0 minutes in untreated cells to 6.8±1.0 minutes in Gd^{3+}-treated cells; $p<0.05$, Mann-Whitney test). This Gd^{3+}-sensitivity suggests that the CS-induced Ca^{2+} response consists primarily of Ca^{2+} influx through PM-bound channels.

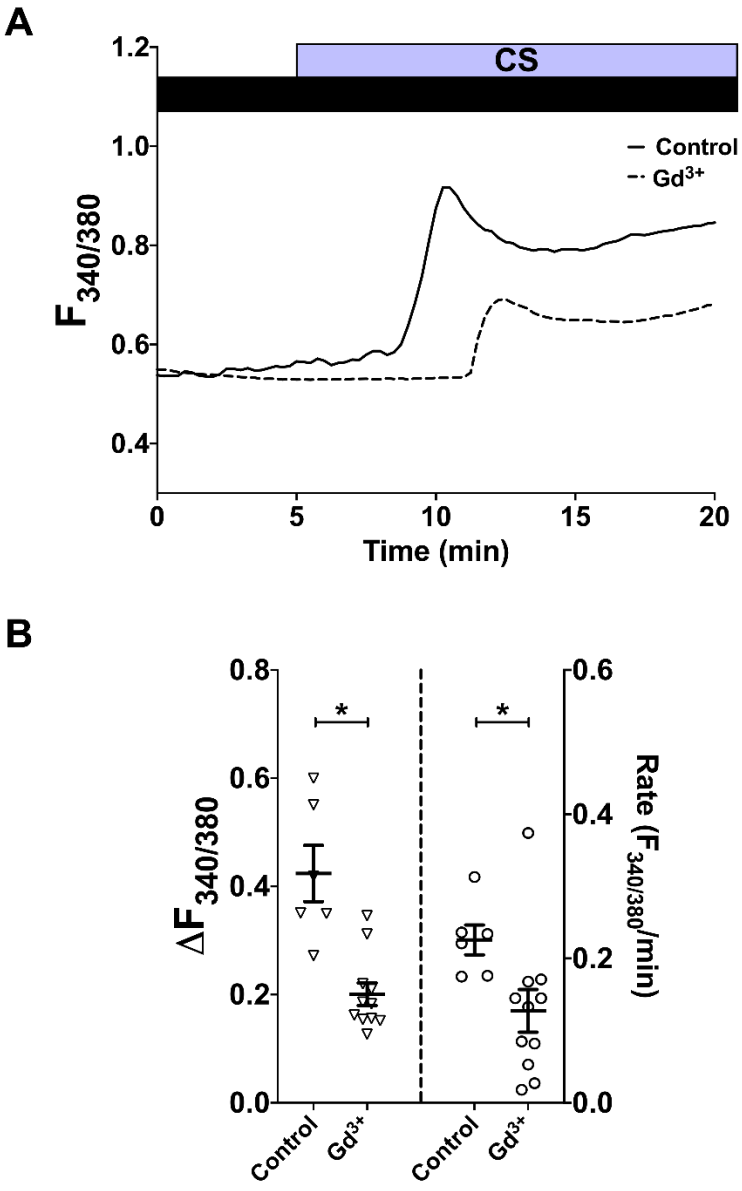

Figure 5.4: CS-induced Ca^{2+} influx was inhibited by Gd^{3+}. (A) Representative traces tracking changes in $[Ca^{2+}]_i$ following puffing one whole cigarette, in the presence of 1mM extracellular Ca^{2+} (black bar), with or without a 10-min pre-treatment with 500µM Gd^{3+}, which was also present throughout the experiment. (B) Summary of amplitude and rate of $[Ca^{2+}]_i$ changes corresponding to experiments in (A). Data presented as mean ± SEM. Unpaired t-test was performed between the control group and the Gd^{3+}-treated group (3 independent donors; n=6-11). * = $p<0.05$.

5.3.4 Inhibiting LTCC does not attenuate CS-induced Ca^{2+} influx

Following a similar approach described for CSE, the involvement of LTCC and SOCC were also investigated to help identify the protein responsible for the CS-induced Ca^{2+} influx. LTCC were inhibited by pre-treating hASMC with 1μM felodipine. A 10-min pre-treatment (and continual presence) of felodipine did not significantly affect the CS-induced Ca^{2+} influx (Figure 5.5A, B; $p>0.05$ for both amplitude (0.48±0.10 vs. 0.57±0.09) and rate (0.35±0.11 vs. 0.29±0.06), felodipine- vs. DMSO-treated, providing evidence that LTCC do not facilitate CS-induced Ca^{2+} influx.

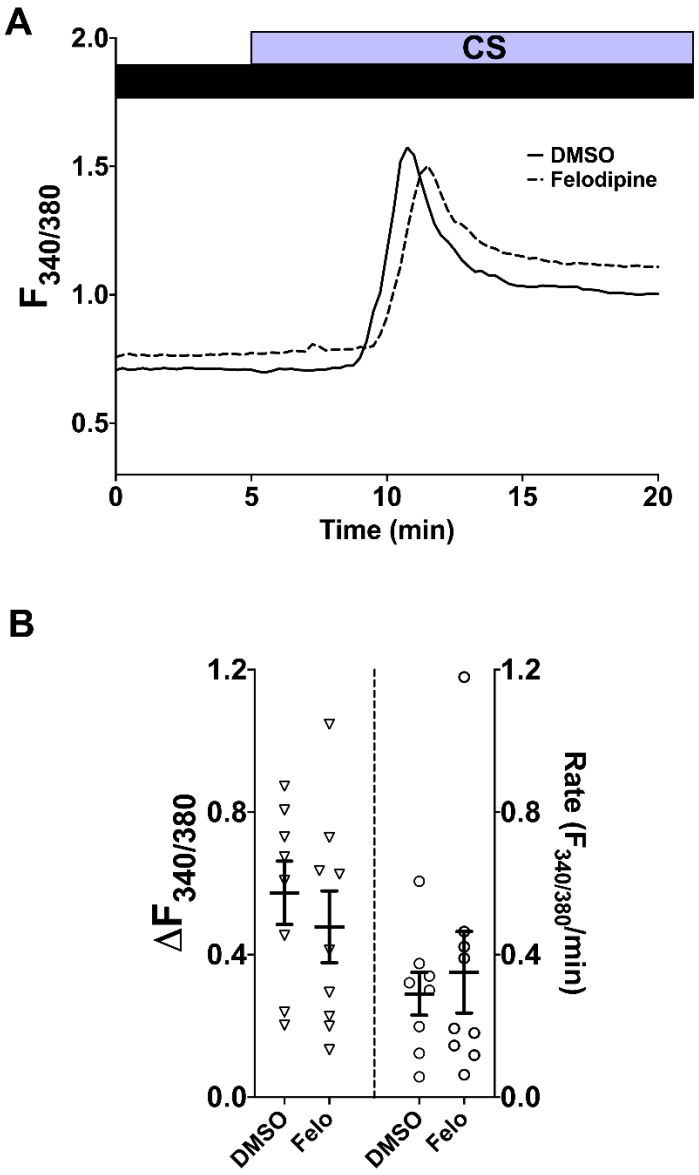

Figure 5.5: Inhibiting LTCC does not attenuate CS-induced Ca^{2+} influx. (A) Representative traces tracking changes in $[Ca^{2+}]_i$ following puffing one whole cigarette with or without 10-min pre-treatment with 1μM felodipine, which was also present throughout the experiment. An equal volume of DMSO was used for vehicle control. (B) Summary of amplitude and rate of $[Ca^{2+}]_i$ changes corresponding to experiments in (A). Data presented as mean ± SEM. Unpaired t-test was performed between the felodipine-treated group and the vehicle control group (3 independent donors; n=8-9).

5.3.5 CS-induced Ca^{2+} influx utilises a different pathway from SOCE

The potential involvement of SOCC in mediating the CS-induced Ca^{2+} influx was studied using the same approach described in the previous chapter. Here, SOCE was first activated with CPA, and the subsequent effect of CS exposure then examined; Figure 5.6A shows that CS was able to instigate an additional elevation in $[Ca^{2+}]_i$ when SOCC were already active, similar to the vehicle control, where SOCC were not activated. Indeed, there was no significant difference in either amplitude (0.35±0.07 vs. 0.33±0.03) or rate (0.24±0.05 vs. 0.17±0.01) between the CPA-treated cells and the vehicle control (Figure 5.6B; $p>0.05$ for both amplitude and rate). Together with results from Figure 5.5, these data suggest that LTCC and SOCC do not contribute to CS-activated Ca^{2+} influx.

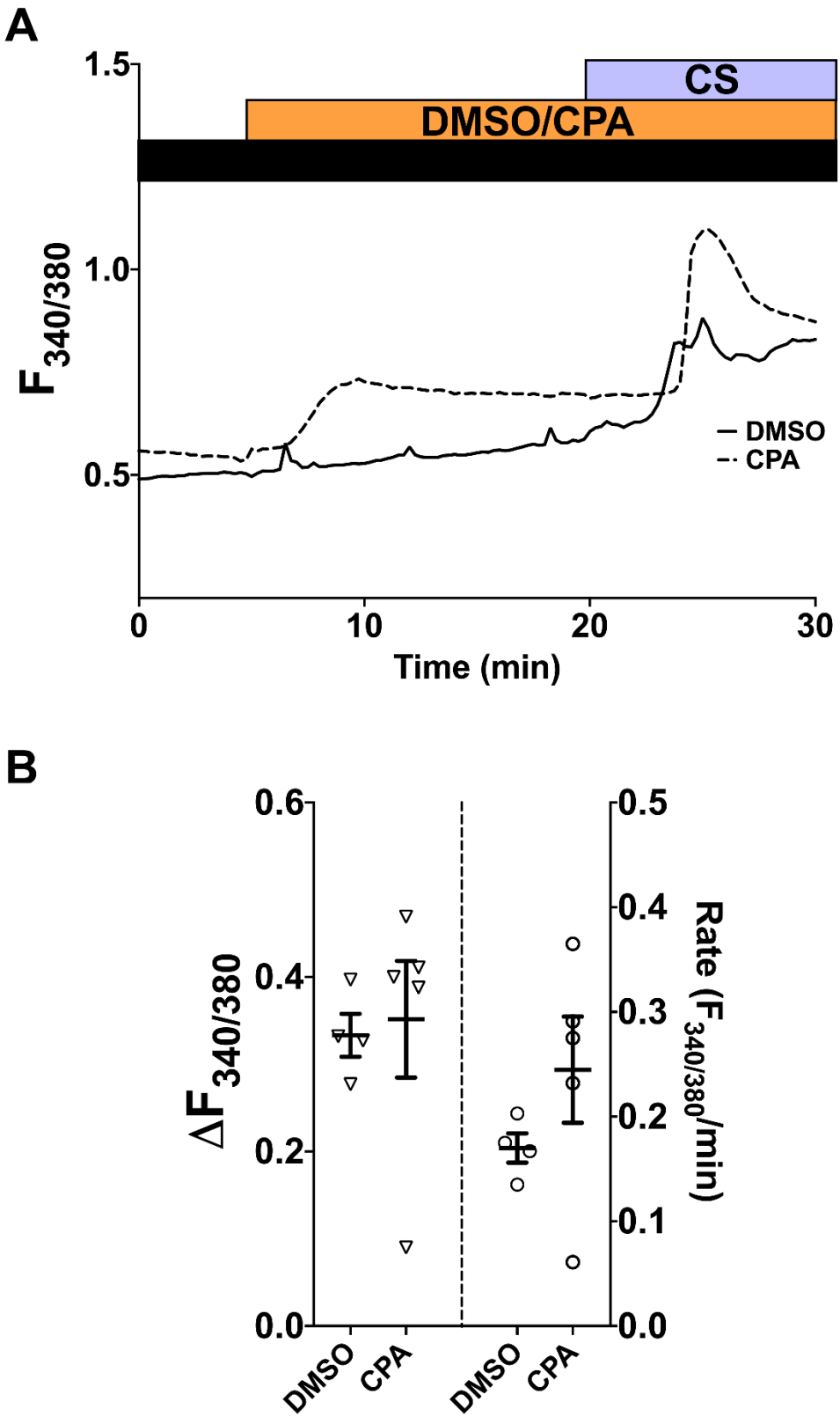

Figure 5.6: CS-induced Ca^{2+} influx utilises a different pathway from SOCE. (A) Representative traces tracking changes in $[Ca^{2+}]_i$ following puffing one whole cigarette after 15-min treatment with 10μM CPA. An equal volume of DMSO was used for the vehicle control. (B) Summary of amplitude and rate of the CS-induced $[Ca^{2+}]_i$ changes corresponding to experiments in (A). Unpaired t-test was performed between the CPA-treated group and the vehicle control group (2 independent donors; n=4-5).

5.3.6 CS-induced Ca^{2+} influx was inhibited by the TRPA1 inhibitor HC-030031

After excluding LTCC and SOCC, the potential role of TRPA1 in mediating the CS-induced Ca^{2+} influx was investigated. Similar to the CSE experiments described in Chapter 4, hASMC were first pre-treated with HC-030031 for 10 minutes before CS was puffed onto the cells. Figure 5.7A shows a typical dose-response to increasing concentrations of HC-030031, ranging from 1-50μM; a full summary of the dose-response data obtained from 1 donor is presented in Figure 5.7B. Inhibition of the CS-induced Ca^{2+} influx amplitude was observed with 1μM HC-030031 (10.5% inhibition), but the rate of influx was not attenuated (Figure 5.7A, B). On the other hand, 10μM (29.5/22.2% inhibition in amplitude/rate) and 30μM (75.6/83.1% inhibition in amplitude/rate) HC-030031 formed the linear phase of the dose-response curve (Figure 5.7B). The calculated IC_{50} for blocking CS-induced Ca^{2+} influx was 16.6±3.9μM for amplitude and 16.3±4.1μM for rate (Figure 5.7B). At 50μM, HC-030031 almost completely attenuated CS-induced Ca^{2+} influx (79.5/94.5% inhibition of amplitude/rate, respectively), and therefore this concentration was used to investigate further the role of TRPA1 in mediating the CS-induced increase in $[Ca^{2+}]_i$.

After repeating the experiment with hASMC from 3 additional donors, the average inhibition of the CS-induced Ca^{2+} influx by 50μM HC-030031 was 71.2% (0.19±0.02 vs. 0.67±0.06) for the amplitude and 94.7% (0.02±0.01 vs. 0.46±0.06) for the rate (Figure 5.7C; $p<0.05$, HC-030031- vs. DMSO-treated). This substantial inhibition by a highly selective TRPA1 blocker indicates that TRPA1 plays a major role in mediating this CS-induced Ca^{2+} influx.

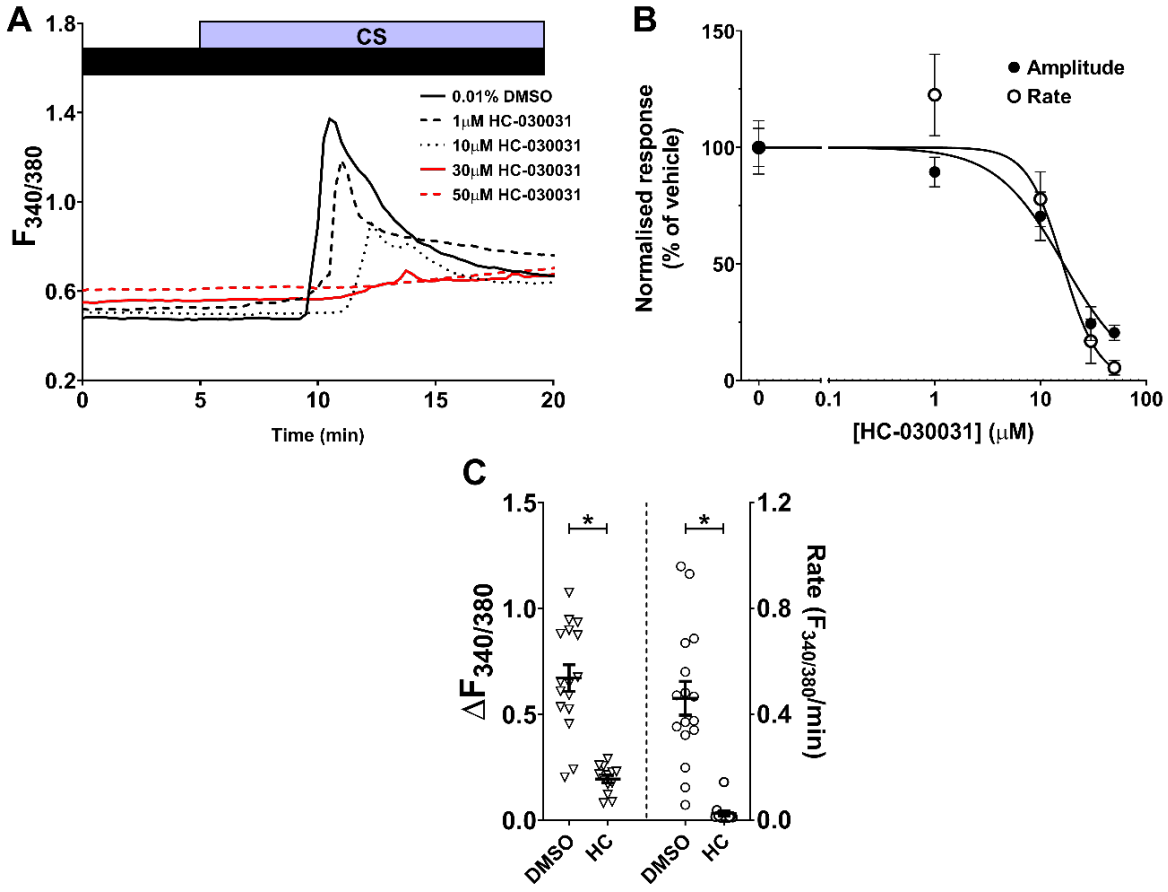

Figure 5.7: CS-induced Ca^{2+} influx was inhibited by HC-030031 in a concentration-dependent manner. (A) Representative traces tracking changes in $[Ca^{2+}]_i$ following puffing one whole cigarette with or without 10-min pre-treatment with various concentrations of HC-030031, which was also present throughout the experiment. An equal volume of DMSO was used for the vehicle control. (B) Dose response curves for the normalised amplitude and rate of the CS-induced Ca^{2+} influx (normalised to % of the mean amplitude/rate of DMSO control) at different concentrations of HC-030031, presented as mean ± SEM (n=3-10, from 1 donor). (C) Summary of the amplitude and rate of the CS-induced $[Ca^{2+}]_i$ changes following pre-treatment with 50μM HC-030031, or DMSO. Data presented as mean ± SEM. Unpaired t-test was performed between the HC-treated group and the vehicle control group (3 independent donors; n=13-16). * = $p<0.05$.

5.3.7 TRPA1 mRNA expression correlates with the amplitude and rate of CS-induced Ca^{2+} influx

Similar to the results with CSE, HC-030031 did not completely abolish the CS-induced Ca^{2+} influx. Therefore, genetic knockdown of TRPA1 was applied to further investigate the role of TRPA1 in mediating this influx, using the same shRNA-driven transient transfection approach as described in Chapter 4. After transfection, hASMC were exposed to CS for Ca^{2+} imaging experiments, and then cells were lysed to extract mRNA for qPCR analysis. Knockdown efficiency was calculated using the $2^{-\Delta\Delta CT}$ method as previously described.

Knockdown of TRPA1 did not consistently attenuate the CS-activated Ca^{2+} influx. 25/32 of the targeted vector (TV)-transfected hASMC exhibited a smaller CS-induced Ca^{2+} response

compared to the average of the day/donor-matched empty vector (EV)-transfected cells (e.g. the pair shown in Figure 5.8A), while 7/32 had similar or higher responses than the average of the EV controls (e.g. the pair shown in Figure 5.8B). Even with such inconsistency, the hASMC transfected with the TV, on average, had a lower amplitude (0.38±0.04 vs. 0.53±0.04, T vs. E) and rate (0.11±0.01 vs. 0.18±0.03, T vs. E) of CS-induced Ca^{2+} response compared to the EV control (Figure 5.8C; $p<0.05$ for both amplitude and rate), despite the large spread in values. However, the average inhibition was relatively low (27.0/39.8% inhibition for amplitude/rate, respectively) compared to that exerted by 50μM HC-030031 (71.2/94.7% for amplitude/rate, respectively). qPCR analysis revealed that the relative expression of TRPA1 was only significantly knocked down when normalised to GAPDH (25.9% efficient, 0.74±0.03 vs. 1.00±0.05, T vs. E; $p<0.05$), but not 18S (5.6% efficient, 0.94±0.10 vs. 1.00±0.07, T vs. E; $p>0.05$) (Figure 5.8D). Moreover, cells from 9/32 coverslips transfected with the TV had a $2^{-\Delta\Delta CT}$ value higher than 1.0, indicating no knockdown of TRPA1 (Figure 5.8D). However, the raw CT values for both housekeeping genes were not significantly different between the cells transfected with the TV and the EV (Figure 5.8E; $p>0.05$ for both GAPDH and 18S, T vs. E), indicating that 18S was not significantly altered by the transfection process, and thus remained a valid housekeeping gene for normalisation of relative TRPA1 expression.

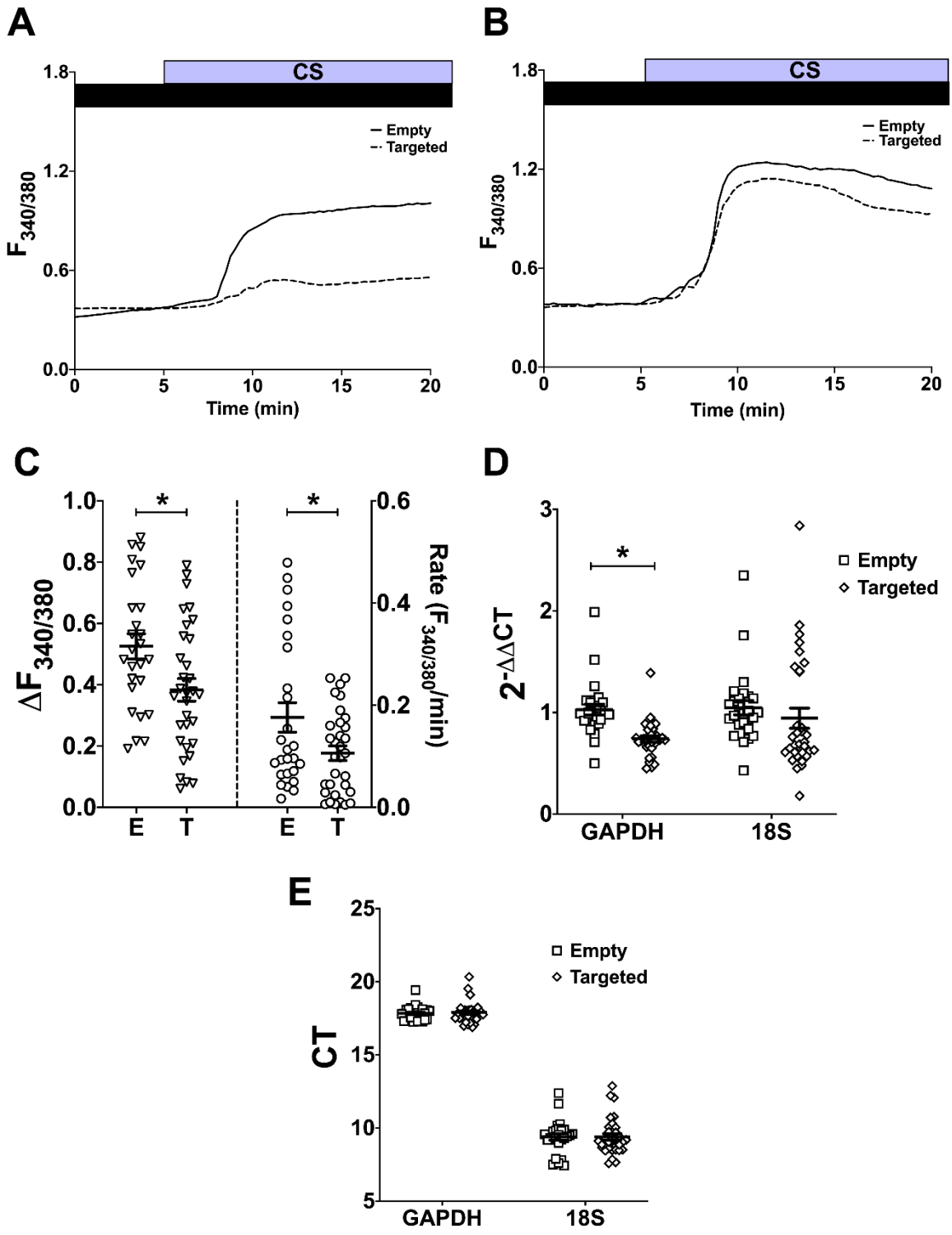

Figure 5.8: The effect of TRPA1 knockdown on CS-induced Ca^{2+} influx was also inconsistent. hASMC were transfected with shRNA containing either the empty (E) vector, or the vector targeted (T) towards TRPA1. (A, B) Representative traces tracking changes in $[Ca^{2+}]_i$ following puffing one whole cigarette onto transfected hASMC. Pairs of E and T are day/donor matched. (C) Summary of amplitude and rate of CS-activated Ca^{2+} influx in transfected hASMC. (D) Knockdown efficiency of TRPA1 in transfected hASMC, reported as $2^{-\Delta\Delta CT}$. (E) Raw CT values of housekeeping genes GAPDH and 18S for shRNA-transfected hASMC. Data presented as mean ± SEM, from 4 independent donors (n=26-32). Unpaired t-test was performed between the groups transfected with empty vector and those transfected with the TRPA1 targeted vector (C, D, E). * = $p<0.05$.

As the average TRPA1 knockdown efficiency was low, especially when normalised to 18S, and a number of experiments had $2^{-\Delta\Delta CT}$>1.0 (Figure 5.8D), removal of experiments where the knockdown was not apparent, may more accurately represent the dataset, and thus could better characterise the role of TRPA1 in mediating CS-induced Ca^{2+} influx. Before data removal, initial analysis was performed to ascertain that TRPA1 expression actually correlated with the CS-induced Ca^{2+} response, regardless of knockdown efficiency. Similar to the results shown in Chapter 4, inverse correlations were observed by plotting TRPA1 ΔΔCT, normalised to GAPDH or 18S, against the amplitude and rate of CS-induced Ca^{2+} influx (Figure 5.9). The Pearson's *r* values were between -0.27-0.34, indicating moderate negative correlations, that is, higher relative expression of TRPA1 correlated to lower CS-induced Ca^{2+} influx. More importantly, the correlations for all four comparisons were statistically significant (Figure 5.9A-D; $p<0.05$). There was also differential clustering observed for E (black) vs. T (red), especially in Figure 5.9A and B, whereby black points clustered towards the top left quadrant (relatively higher Ca^{2+} responses and higher TRPA1 expression), whereas red points clustered towards the bottom right (lower Ca^{2+} responses and lower TRPA1 expression). This significant correlation between TRPA1 relative expression and the amplitude and rate of CS-induced Ca^{2+} influx indicated that TRPA1 expression likely plays a role in this response, thus strengthening the argument for excluding data where TRPA1 knockdown was inefficient.

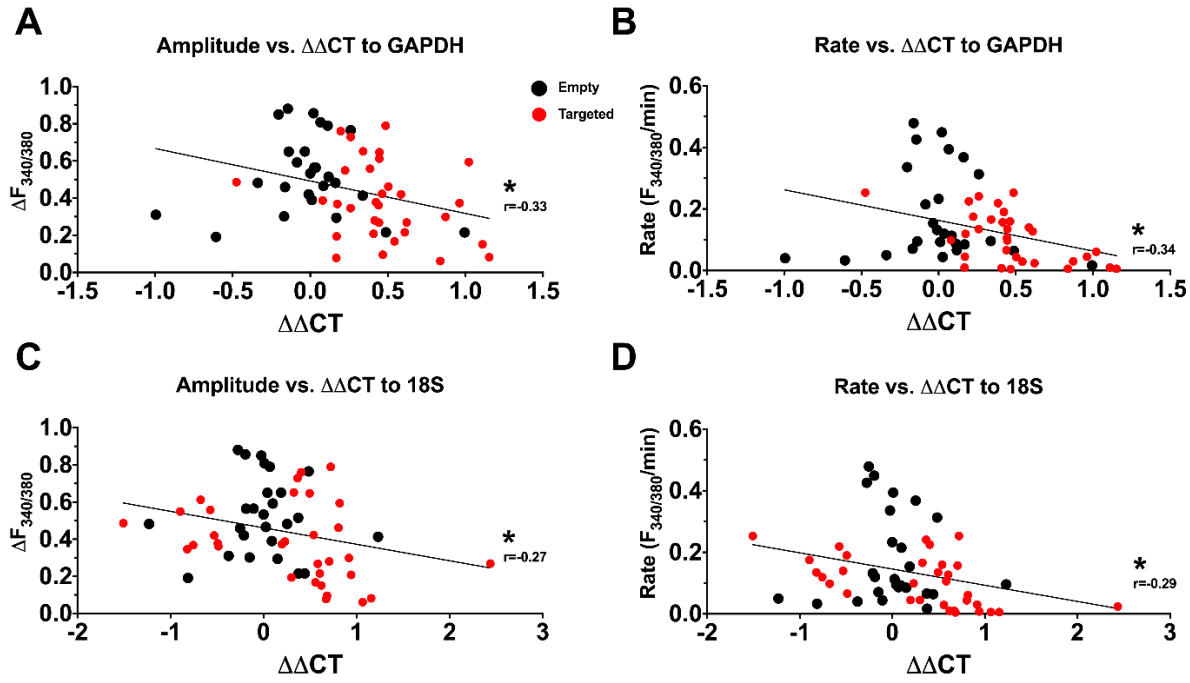

Figure 5.9: CS-induced Ca^{2+} influx is correlated to TRPA1 mRNA expression. Amplitude (left panels) and rate (right panels) of CS-induced Ca^{2+} influx were correlated vs. TRPA1 ΔΔCT values (raw TRPA1 CT was normalised to CT of GAPDH (A, B) or 18S (C, D), then normalised to ΔCT of the average empty vector-transfected cells, day/donor-matched). Pearson's correlation analysis was performed between each pair of the parameters indicated (4 independent donors; n=26-32). * = $p<0.05$.

5.3.8 shRNA-driven TRPA1 knockdown attenuated CS-induced Ca^{2+} influx

Data removal from samples transfected with the TV where TRPA1 knockdown was minimal followed the same criteria as described in Chapter 4, that is, $2^{-\Delta\Delta CT} > 0.75$ when normalised to both housekeeping genes (>25% knockdown on TRPA1 relative expression). After applying this selection criteria, 10 out of 32 experiments were excluded from subsequent analysis ("T, excluded" in Figure 5.10). The average $2^{-\Delta\Delta CT}$ values for this excluded group (0.91±0.06 normalised to GAPDH; 1.37±0.22 normalised to 18S) were similar to those for the EV-transfected samples (1.03±0.05 normalised to GAPDH; 1.05±0.07 normalised to 18S) (Figure 5.10A; $p>0.05$, T excluded vs. E). In contrast, the $2^{-\Delta\Delta CT}$ values for the excluded group were significantly higher than those for the remaining samples transfected with the TRPA1-targeted shRNA vector (0.67±0.02 normalised to GAPDH; 0.75±0.08 normalised to 18S), validating the data removal manoeuvre as samples with minimal knockdown efficiency were separated as a statistically different group (Figure 5.10A; $p<0.05$, T excluded vs. T). On the other hand, the amplitude (0.50±0.06 vs. 0.53±0.04) and rate (0.17±0.02 vs. 0.18±0.03) of Ca^{2+} influx following CS exposure were also similar between the T excluded group and the E group (Figure 5.10B; $p>0.05$, T excluded vs. E), further supporting that hASMC with minimal TRPA1 knockdown responded to CS challenge in a similar manner to the negative control, and hence supporting the removal of this group of results from those with significant TRPA1 knockdown. Removing this confounding factor of inefficient knockdown enabled clearer investigation into TRPA1's contribution to the CS-induced Ca^{2+} influx.

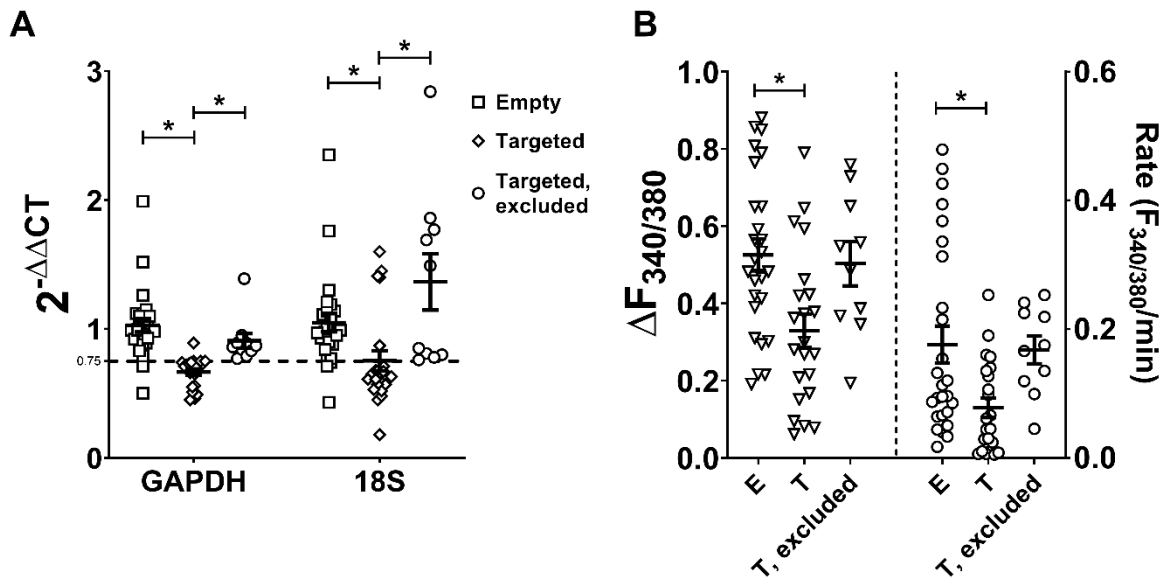

Figure 5.10: Validating removal of experiments with minimal TRPA1 knockdown. (A) Knockdown efficiency of TRPA1 in transfected hASMC, reported as $2^{-\Delta\Delta CT}$. hASMC transfected with the TRPA1-targeted shRNA (T) that had $2^{-\Delta\Delta CT}$ values >0.75 normalised to both housekeeping genes, indicated by the dashed horizontal line, were excluded for subsequent analyses (T, excluded). (B) Summary of amplitude and rate of CS-activated Ca^{2+} influx in transfected hASMC. Data presented as mean ± SEM, consisting of cells from 4 independent donors (n=10-26). One-way ANOVA with Holm-Sidak's multiple comparisons tests were performed amongst the three groups (E, T, and T, excluded). * = $p<0.05$.

After the data removal in Figure 5.10, the TRPA1 knockdown was significant in hASMC transfected with the TV ($2^{-\Delta\Delta CT}$ 0.67±0.02 normalised to GAPDH; 0.75±0.08 normalised to 18S) compared to cells transfected with the EV ($2^{-\Delta\Delta CT}$ 1.03±0.05 normalised to GAPDH; 1.05±0.07 normalised to 18S) (Figure 5.11A; $p<0.05$, T vs. E for both housekeeping genes). These cells where TRPA1 was significantly knocked down exhibited an attenuated amplitude (0.33±0.04 vs. 0.53±0.04; 37.4% inhibition) and rate (0.08±0.02 vs. 0.18±0.03; 55.8% inhibition) of Ca^{2+} influx in response to CS exposure, compared to the negative control (Figure 5.11B; $p<0.05$ for both amplitude and rate, T vs. E), demonstrating the likely role of TRPA1 in mediating Ca^{2+} influx in response to CS.

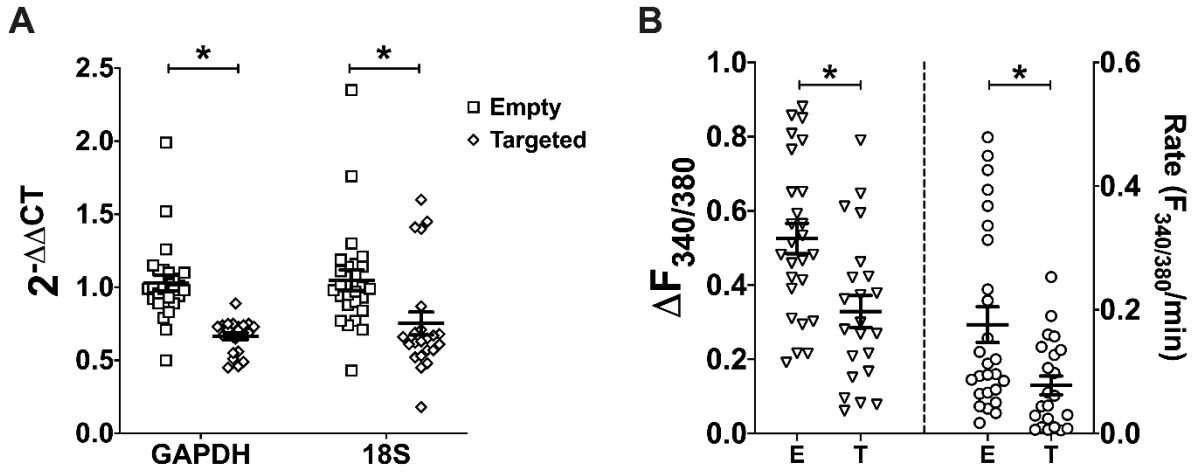

Figure 5.11: TRPA1 knockdown significantly attenuated CS-induced Ca^{2+} influx. (A) Knockdown efficiency of TRPA1 in transfected hASMC, reported as $2^{-\Delta\Delta CT}$. (B) Summary of amplitude and rate of CS-activated Ca^{2+} influx in transfected hASMC. Experiments with minimal knockdown were excluded for analysis. Data presented as mean ± SEM, consisting of cells from 4 independent donors (n=22-26). Unpaired t-tests were performed between the samples transfected with the empty vector (E) and those transfected with the TRPA1-targeted vector (T). * = $p<0.05$.

5.3.9 Comparison between Ca^{2+} responses elicited by CS and CSE

To examine any potential differences between the two tobacco delivery models, a direct comparison of the amplitude and rate of CS-induced Ca^{2+} influx to that activated by 10% or 50% CSE was performed. The peak amplitude of the three groups did not significantly differ (Figure 5.12A; $p>0.05$ for all multiple comparisons pairs), but the rate of the CS- (0.30±0.04) and 50% CSE-induced (0.32±0.07) Ca^{2+} response were both significantly greater than that elicited by 10% CSE (0.10±0.02) (Figure 5.12A; $p<0.05$ for both multiple comparisons pairs).

In Chapter 4, it was observed that the Ca^{2+} influx activated by CSE was concentration-dependent and did not saturate at 10% CSE, as 50% CSE was able to induce a further elevation in $[Ca^{2+}]_i$ (Figure 4.1, Chapter 4). Moreover, both the amplitude (0.42±0.04 vs. 0.43±0.05) and rate (0.30±0.04 vs. 0.32±0.07) of CS-induced Ca^{2+} influx were similar to that induced by 50% CSE (Figure 5.12A; $p>0.05$ for both amplitude and rate). To investigate if CS was able to elevate $[Ca^{2+}]_i$ after a 10% CSE exposure, one whole cigarette was puffed onto hASMC after a 30-min exposure to 10% CSE (Figure 5.12B). As expected, an additional Ca^{2+} response was observed following the CS exposure. However, although not statistically significant, on every occasion the amplitude of this subsequent CS response was lower than the initial response elicited by 10% CSE (Figure 5.12C; $p>0.05$ for the paired responses).

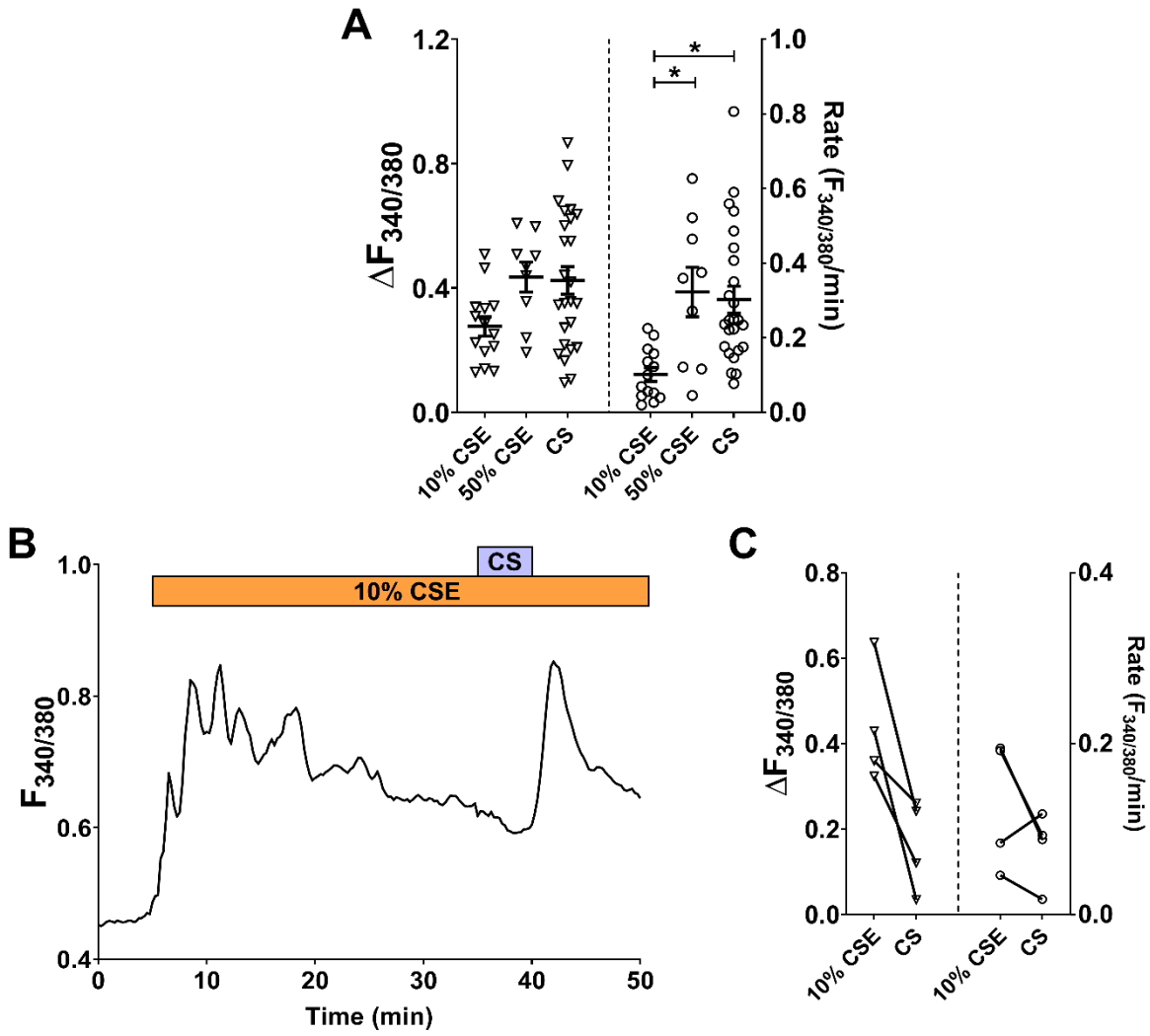

Figure 5.12: Comparison between CS- and CSE-induced Ca^{2+} influx. (A) Summary of amplitude and rate of CS- or CSE-induced $[Ca^{2+}]_i$ changes in the presence of 1mM extracellular Ca^{2+}. (B) Representative trace tracking changes in $[Ca^{2+}]_i$ following exposure to 10% CSE, then puffing one whole cigarette onto hASMC. (C) Paired summary of amplitude and rate of CSE and CS responses from experiments in (B). Wilcoxon matched-pairs signed rank test was performed between the two groups (n=4, from 1 donor).

5.4 Discussion

In this chapter, the cellular mechanisms underlying the CS-induced changes in hASMC intracellular Ca^{2+} signalling was investigated. Using a combination of pharmacological and genetic approaches, the results provide the first known evidence that acute exposure of gaseous CS directly onto hASMC activated Ca^{2+} influx in hASMC primarily through the TRPA1 channel, in the populations of hASMC sampled. At the single-cell level, however, the response profiles varied (e.g. Figure 5.1B, C); the Ca^{2+} imaging traces presented were cumulated means from 10-20 single cells in each independent experiment. Nonetheless, despite such variability in single-cell response profiles, the mean amplitude and rate of the $[Ca^{2+}]_i$ changes in cell

populations provided consistent overall trends that were sufficient to distinguish statistical significance in various datasets.

As shown in Figure 5.1A-C, two distinct response profiles were observed by direct CS stimulation. The obvious mechanisms that underlie the rapid recovery profile are changes in TRPA1 gating, or changes in the calcium extrusion/reuptake pathways (e.g. SERCA, PMCA, NCX). However, the former is unlikely as the TRPA1 channels likely remain open after the initial activation, for at least 15 minutes, and facilitates efflux of cytosolic calcium (Figure 4.6, Chapter 4). On the other hand, active calcium extrusion/reuptake pathways could lead to the rapid recovery profile, and these may be modulated by CS or its constituents. For instance, a delayed recovery was observed in CS- or crotonaldehyde-treated mouse skeletal muscle and cardiomyocytes (Pei *et al.*, 2014; Nogueira *et al.*, 2018), and ROS, contained in CS, was shown to inhibit SERCA and PMCA function (Xu *et al.*, 1997; Zaidi and Michaelis, 1999; Gutierrez-Martin *et al.*, 2004; Kumosani *et al.*, 2008; Pande and Grover, 2014; Gorlach *et al.*, 2015). However, in the present study, SERCA activity was unlikely to underly the transient CS response profile, as the rapid recovery was still observed consistently (5/5 experiments) after SERCA was blocked with CPA (Figure 4.16). Therefore, ruling out the involvement of SERCA and the changes in the intrinsic regulation of TRPA1, the mechanism that underly the rapid recovery following CS stimulation is likely to be PMCA or NCX. A simple method to ascertain this speculation would be pharmacological inhibition of PMCA or NCX; if one of these pathways was indeed responsible for the rapid recovery, inhibition of the pathway would convert the transient response profile to a sustained profile.

The results from both Chapter 4 and 5 indicated that TRPA1 was the main pathway activated by both CS and CSE to facilitate Ca^{2+} influx. However, the CS model used in this chapter is likely to have delivered considerably higher concentrations of active constituents to hASMC, compared to the CSE model, since one cigarette was puffed into a total buffer volume of 1ml (i.e. the final volume of buffer added to the cells before experiment), whereas the stock CSE solution was made using one cigarette per 25 ml. Assuming no loss of gaseous CS from the closed chamber, efficient diffusion and site access, this was equivalent to 2500% CSE. However, it is worth noting that controlling the amount and dissipation rate of gaseous CS, even with a smoke machine and fixed volume in a closed chamber, is relatively challenging, and so this theoretical concentration may not be accurate. Despite the CS model potentially delivering up to 50 times higher concentration of active constituents, direct exposure to gaseous CS and 50% CSE produced comparable Ca^{2+} responses in hASMC (Figure 5.12A), possibly due to saturation of these active constituents. This was supported by the observation that CS

was still able to elicit a further elevation of $[Ca^{2+}]_i$ after the initial response induced by 10% CSE (Figure 5.12B), a similar effect as 50% CSE (Figure 4.1, Chapter 4), the putative saturating concentration. In these experiments (Figure 4.1, Chapter 4 and Figure 5.12 here), it is possible that a proportion of channels have shut after the initial activation by 10% CSE, and a second, higher, dose of 50% CSE or CS re-activated these channels, as well as potentially additional channels that were not activated initially by 10% CSE. Another possible explanation for the similar response amplitude/rate for 50% CSE and CS is that the overwhelming concentration discrepancy may have been counterbalanced by the low bath volume in the CS model, as Bourgeois *et al.* (2016) showed that higher volumes of CSE, at the same nominal concentration, were more cytotoxic. However, despite a similar peak amplitude and rate of the Ca^{2+} response, the greater concentration in the CS model compared to the CSE model may underlie the inability of 100µM Gd^{3+} to inhibit CS-induced Ca^{2+} influx (Figure 5.3). In contrast, the same concentration of Gd^{3+} significantly inhibited the CSE-induced Ca^{2+} response (Figure 4.10, Chapter 4). Moreover, even at a higher Gd^{3+} concentration (500µM vs. 100µM), a lower percentage inhibition by Gd^{3+} (52.6/43.8% vs. 74.8/76.0%; by amplitude/rate) was observed in the CS model.

On the other hand, despite a higher nominal concentration, the average CS-activated Ca^{2+} response had a longer time lag before the initial rise, as well as a longer time to peak, in cytosolic Ca^{2+}. After exposure to 10% or 50% CSE, $[Ca^{2+}]_i$ started to rise within a minute; whereas in the CS model, there was a noticeable time lag of 4.4±0.1 mins before $[Ca^{2+}]_i$ began to elevate. Indeed, on average, it took longer for the CS-induced Ca^{2+} response to reach a peak than the 50% CSE-induced response (6.4±0.1 mins vs. 3.4±1.2 mins), but not the 10% CSE-induced response (6.2±1.3 mins). The difference in time lag between the two delivery systems could be attributed to the CS model relying on passive diffusion of water-soluble components into the bathing solution, as opposed to the vigorous bubbling in the CSE model, and therefore it may take longer for the active compounds to equilibrate and reach a threshold concentration for TRPA1 activation.

Out of the CS constituents speculated to exert effects on TRPA1 (see Discussion of Chapter 4), acrolein and crotonaldehyde are aldehydes, and classed as volatile organic compounds (VOCs), that readily evaporate (Centers for Disease Control and Prevention, 2010). Therefore, a portion of the VOCs are likely lost from vigorous bubbling in the process of CSE production. Thus, in the CS model where these volatiles are contained within a closed chamber, the concentrations of acrolein and crotonaldehyde are likely to be higher, even under the same nominal CSE

concentration, which may account for the differences in Ca^{2+} responses observed using the two delivery models.

The TRPA1 inhibitor used in this study, HC-030031, has been reported to be highly selective. At 10μM, the compound did not inhibit other Ca^{2+} channels and protein targets, including LTCC, NTCC, TRPV1, TRPV3, TRPV4, TRPM8, P_2X receptors, $GABA_A$ and $GABA_B$ receptors (McNamara *et al.*, 2007; Eid *et al.*, 2008). The calculated IC_{50} for inhibition of CS-induced Ca^{2+} influx by HC-030031 in this study was ~16μM, for both amplitude and rate (Figure 4.18B), which is ~2-3 times higher than reported in the initial screening studies (4.9-7.5 μM), albeit in different cell types and against different agonists (McNamara *et al.*, 2007; Eid *et al.*, 2008). Therefore, it is possible that the 50μM concentration used in this study may potentially block non-TRPA1 targets, and hence why a genetic approach was taken to validate the findings with HC-030031. Due to the relatively low knockdown efficiency obtained using the shRNA-driven approach in this study, other potentially more efficient genetic manipulation techniques, such as the siRNA silencing approach or CRISPR-Cas9 gene editing, could be employed to ascertain the effect of TRPA1 knockdown, or knockout, on CS-induced Ca^{2+} influx.

Despite clear evidence that TRPA1 was the primary mediator of the CS-induced Ca^{2+} influx, neither HC-030031 nor TRPA1 knockdown completely abolished this response. Therefore, potential contribution from other Ca^{2+} channels must be considered. An interesting candidate to investigate is TRPV1, since a recent paper provided evidence that TRPV1 was expressed, and mediated CSE-induced Ca^{2+} influx in airway epithelial cells along with TRPA1 (Wang *et al.*, 2019b). However, this was contradicted by two other studies that reported TRPV1 was not involved in CSE-induced Ca^{2+} influx in rat sensory neurons, and its expression in human and mouse airway tissue was absent (Andre *et al.*, 2008; Nassini *et al.*, 2012). Investigating the involvement of TRPV1 in hASMC would better elucidate the potential additive effect of TRPV1 and TRPA1 in facilitating CS-induced Ca^{2+} influx. Other potential targets that were not investigated in the present study include other TRPV channels such as TRPV4 (Jia *et al.*, 2004), various members of the TRPC family (Chow *et al.*, 2011; Jiang *et al.*, 2019), and the reverse-mode NCX (Algara-Suarez *et al.*, 2007), all of which are functionally expressed in hASMC. As CS-induced Ca^{2+} influx was blocked by Gd^{3+}, the TRP channels that were shown to be insensitive or poorly sensitive to Gd^{3+} may be ruled out (e.g. TRPM2, TRPM7, TRPV1, TRPV6, TRPC5), whilst Gd^{3+}-sensitive channels (TRPC1, TRPC6, TRPC7, TRPM3, TRPM4, TRPM8, TRPV2, TRPV3, TRPV4, TRPV5, TRPML1) could be further explored (reviewed in Bouron *et al.* (2015)). Indeed, both TRPV1 and TRPV4 were shown to be activated by CSE to promote ATP release (Baxter *et al.*, 2014), and TRPM8 was activated by CSE directly to facilitate Ca^{2+}

influx and cytokine release in human epithelial cells (Wang *et al.*, 2019a); these therefore are prime candidates to study in hASMC. It is worth nothing, however, that there is no evidence of TRPM8 expression in human airway smooth muscle tissue (Maher *et al.*, 2015). In addition, the Ca^{2+} entry mode of NCX was shown to be activated by 4-(methylnitrosamino)-1-(3-pyridyl)-1-butanone (NNK), a potent carcinogen derived from tobacco smoke, in human esophageal squamous cell carcinoma cells (Wen *et al.*, 2016). The thorough examination of the role of these channels in CS-induced Ca^{2+} influx could be performed using similar pharmacological and genetic methodologies presented in this chapter, applying inhibitors that exhibit high specificity and potency, as well as shRNA-driven or other genetic knockdown/knockout approaches.

In summary, the results in this chapter have characterised the effects and cellular mechanisms of CS-induced disruption in Ca^{2+} homeostasis, complementing data from Chapter 4. In addition, although there were differences in Ca^{2+} responses between the two tobacco delivery models, which could be attributed to differences in the concentration of active constituents, acute exposure to CS and CSE both activated TRPA1 to facilitate rapid Ca^{2+} influx in hASMC, thus showing that they shared a similar response profile.

Chapter 6: Concluding Discussion

6.1 Summary of key findings and strengths/weaknesses of the work

COPD and CF are obstructive airway diseases that share multiple similarities in disease manifestation, including AHR, airway dehydration, prominent inflammation, and recurrent infections. The largest risk factor for the pathogenesis of COPD is chronic cigarette smoking, which is extensively linked to a number of processes including inflammation, remodelling, mucus plugging, infection, and AHR. On the other hand, the pathophysiology of CF is associated with loss-of-function mutations in the CFTR gene, which codes for an epithelial Cl^- channel that regulates Cl^- and fluid secretion. An important link between CF and COPD is that CS exposure induces downregulation of CFTR function in airway epithelia, leading to airway dehydration, reminiscent of CF airway, in COPD smokers, through elevation of $[Ca^{2+}]_i$ (Clunes *et al.*, 2012; Sloane *et al.*, 2012; Raju *et al.*, 2013). Furthermore, CFTR itself also functionally regulates intracellular Ca^{2+} homeostasis in both airway epithelial and various muscle cells, including ASMC (see section 1.6).

The ASMC is the effector of airway hyperresponsiveness, or enhanced sensitivity, to contractile stimuli; changes in ASMC Ca^{2+} homeostasis, which affects the activity of downstream contractile signalling mechanisms, regulates the calibre of the airway. CFTR was reported to be functionally expressed in rat and human ASMC (Robert *et al.*, 2004; Vandebrouck *et al.*, 2006; Michoud *et al.*, 2009; Norez *et al.*, 2014; Cook *et al.*, 2016), but its role in modulating various aspects of ASMC Ca^{2+} homeostasis was poorly understood. Additionally, chronic CS exposure is associated with long-term changes in multiple components of ASMC Ca^{2+} signalling (Sathish *et al.*, 2015; Wylam *et al.*, 2015), but the direct effects of acute exposure to CS, or CSE, on ASMC Ca^{2+} signalling and contractility have not been fully characterised. This project therefore aimed to investigate the role of CFTR in regulating, as well as the mechanisms of acute CS/CSE exposure in disrupting, ASMC Ca^{2+} homeostasis.

6.1.1 CFTR plays a minor role in modulating GPCR-coupled Ca^{2+} release and SOCE in ASMC (Chapter 3)

Investigation into the role of CFTR in regulating ASMC Ca^{2+} signalling began with characterising the effects of various pharmacological modulators of CFTR on epithelial Ca^{2+} homeostasis, in order to establish a robust protocol for subsequent application of these agents in ASMC experiments, and compare and contrast these effects in the two different cell types in which CFTR is differentially localised. Surprisingly, an off-target inhibition of SOCE by $CFTR_{inh}$-172 and GlyH-101, two of the most commonly-used and considered to be relatively

selective CFTR inhibitors in current use, was observed. This was validated in HEK293 cells which do not express CFTR. There appeared to be a time-dependency to this off-target action and, therefore, to circumvent this, a short exposure protocol to $CFTR_{inh}$-172 was established in order to isolate CFTR-specific effects.

In rat ASMC, treatment with $CFTR_{inh}$-172 was found to inhibit the rate, but not maximal amplitude, of SOCE. Furthermore, activation and inhibition of CFTR did not affect the amplitude, rate, or recovery rate of ATP-coupled Ca^{2+} release in rASMC, but had minor effects on the post-response $[Ca^{2+}]_i$ steady-state level following recovery. The lack of substantial effects could be attributed to low CFTR expression in rASMC, in which it was difficult to detect CFTR protein by both Western blot and immunofluorescence. Despite these technical difficulties, the immunofluorescence results corroborated multiple reports showing that CFTR is expressed primarily intracellularly in both rat and human ASMC, likely localising to the SR (Vandebrouck *et al.*, 2006; Michoud *et al.*, 2009; Norez *et al.*, 2014).

The main novelty from results presented in Chapter 3 was the surprising off-target effects of two commonly used pharmacological inhibitors in CFTR-related research, which may have major implications for past and future studies in the field (discussed in section 6.2 below). Additionally, this was the first study to investigate the effects of CFTR modulation on rASMC Ca^{2+} store release and SOCE, contributing to the presently poorly characterised model of how CFTR activity regulates ASMC Ca^{2+} signalling.

The main weakness of the work shown in this chapter was the various technical difficulties, such as the lack of specific pharmacological inhibitors and low CFTR expression, that discouraged substantial effort into further investigating the regulatory contribution of CFTR in various pathways involved in maintaining Ca^{2+} homeostasis. Therefore, it cannot be concluded, from these results alone, that CFTR does not play a major role in regulating calcium homeostasis in ASMC. A number of future experiments that could shine more light into this subject matter was outlined in the Discussion of Chapter 3, most notably utilising genetic tools to validate the results presented, and to visualise localisation of endogenous CFTR mRNA and protein in ASMC. More importantly, studies that could show direct evidence of SR membrane, CFTR-mediated, Cl^- flux could further consolidate CFTR as a counterion channel that modulates Ca^{2+} transport across the SR membrane. Another limitation of this work was that the investigation of CFTR modulation on rASMC Ca^{2+} signalling was performed on one preparation of isolated rASMC, and so biological variation in the effects observed was not explored.

6.1.2 Direct, acute exposure to gaseous CS, or diluted CSE, evoked TRPA1-mediated Ca^{2+} influx and activation of hASMC contractile signalling (Chapter 4 and 5)

On the other hand, acutely exposing cultured primary hASMC, isolated from multiple non-smoking human donors, to gaseous CS generated from one research cigarette, or diluted CSE, led to rapid Gd^{3+}-sensitive Ca^{2+} influx that was dependent on extracellular Ca^{2+}. This is the first study that has described the acute effects of gaseous CS directly on hASMC Ca^{2+} signalling. Using a repeated Ca^{2+} addback protocol, it was shown that CSE-activated Ca^{2+} influx in hASMC was poorly reversible in the short-term. Additionally, experiments utilising a number of pharmacological agents suggested that LTCC and SOCC did not contribute significantly to CS/CSE-induced Ca^{2+} influx. Using the potent TRPA1 pharmacological inhibitor HC-030031, as well as transient shRNA-driven knockdown, it was discovered that the Ca^{2+} influx activated by exposure to CS/CSE was likely to be mediated primarily through TRPA1, a cation channel that has mostly been associated with pain and nociception, in response to environmental irritants, in sensory neurons. Since ASMC contraction is tightly regulated by $[Ca^{2+}]_i$, it was postulated that CS/CSE-induced Ca^{2+} influx would activate the intrinsic contractile machinery of hASMC. Indeed, the results presented in this thesis showed that CSE treatment significantly increased the levels of p-MLC, which was reduced by HC-030031, providing an important mechanistic link between the TRPA1-dependent rise in cytosolic Ca^{2+} by CS/CSE and rapid downstream activation of contractile signalling mechanisms in hASMC.

The most notable strength of this study was the novelty of demonstrating a direct molecular and cellular link between TRPA1 activation by CS and ASMC contractile signalling mechanisms, presenting TRPA1 as an important molecular target for CS constituents, and hence an important contributor to the pathogenesis of CS-related airway diseases. Moreover, multiple analogous experiments were performed using both gaseous CS and aqueous CSE, allowing for direct comparison between different CS delivery models.

Another strength of the results presented in Chapters 4 and 5 was that the majority of the main experiments were performed using cultured hASMC isolated from at least 2-3 human donors, capturing biological variation (Table 2.4). As expected for most complex biological model systems, donor variability in the intracellular Ca^{2+} elevation in response to CS/CSE exposure was observed (Figure 4.7 and Figure 5.2). Despite the donor variability, clear biological effects were consistently identified across experiments with multiple donors, thus strengthening the evidence presented. On the other hand, passage variability observed for magnitude and rate of CS/CSE-induced Ca^{2+} influx pointed to a potential limitation of this study, as multiple passaging of isolated cells was required to obtain materials for sufficient technical replication.

However, the statistically significant results detected reflect apparent biological effects, despite the passage variability, which may have under-estimated the impacts observed.

Although MLC phoshorylation is an essential process in initiating ASMC contraction, a notable weakness of this study was that the direct coupling between intracellular Ca^{2+} elevation and physical contraction of hASMC, in response to acute CSE challenge, has not been demonstrated. Simple tissue myography experiments using *ex vivo* human tracheal/bronchial rings challenged with CS/CSE could provide a simple proof of concept, but signalling from other cell types in the intact airway may be involved, and therefore direct effects on ASMC contraction *per se* would be difficult to isolate. Several techniques that could be used to investigate this include the cell contraction assay to measure shortening of ASMC suspended in a collegen gel lattice (Wu *et al.*, 2017), or atomic force microscopy to study the contractile stiffness and rheology of SMC (Smith *et al.*, 2005; Hemmer *et al.*, 2008).

Another weakness of the work was that all CS/CSE used for experiments shown in Chapters 4 and 5 were generated using the 3R4F reference cigarette. However, the exact compositions of commercially available cigarettes are far from standardised (Centers for Disease Control and Prevention, 2010; Eldridge *et al.*, 2015), and therefore whether the reference cigarette was an accurate model for commercially available cigarettes was not established. To address this limitation, the effect of CSE from three popular brands (Mayfair, Benson and Hedges (B&H), and Malboro) on $[Ca^{2+}]_i$ in hASMC was tested (Figure 6.1A). Perfusion with 50% extract from commercial cigarettes was able to elicit a similar rise in $[Ca^{2+}]_i$ as CSE from the 3R4F reference cigarette (Figure 6.1B; Holm-Sidak multiple comparisons n.s. for all three brands), suggesting that active constituents responsible for CSE-induced Ca^{2+} influx are present in these commercially available cigarettes.

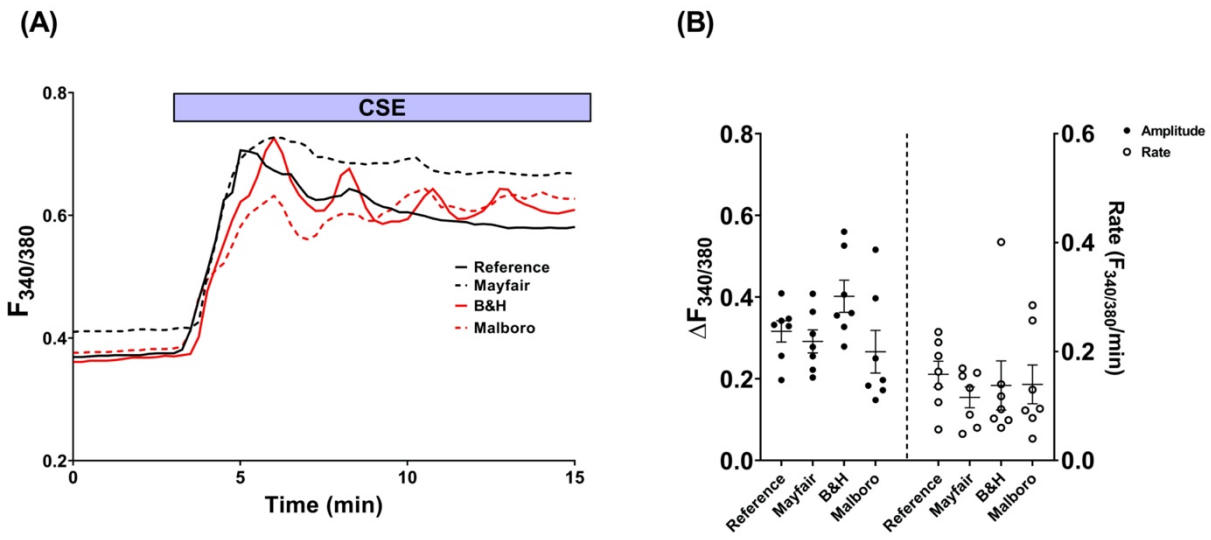

Figure 6.1: Extract from common commercial cigarettes also activate Ca^{2+} influx in hASMC. (A) Representative Ca^{2+} imaging traces tracking changes in $[Ca^{2+}]_i$ following perfusion with 50% CSE, made from the Kentucky 3R4F reference cigarette or 3 different commercial brands of cigarettes, in the presence of 1mM extracellular Ca^{2+}. (B) Summary of amplitude and rate of $[Ca^{2+}]_i$ changes corresponding to experiments in (A). One-way ANOVA with Holm-Sidak's multiple comparisons test was ran between Reference and each of the brands (2 independent donors; n=7 for each brand). 16/28 of these experiments were performed by undergraduate students Helena Gowing and Sophie Davies.

6.2 Implications of off-target effects of various CFTR inhibitors for the field of CF research

In characterising the effects of CFTR modulators on Ca^{2+} signalling in epithelial cells, it was surprisingly discovered that $CFTR_{inh}$-172 and GlyH-101 exerted a previously unknown off-target effect and inhibited SOCE, which was independent of CFTR expression. The specificity of both of these inhibitors for CFTR has been previously challenged, with evidence of VSCC, CaCC, and SLC26A9 (GlyH-101 only) inhibition (Bertrand *et al.*, 2009; Melis *et al.*, 2014), as well as induction of ROS production and mitochondrial dysfunction (Kelly *et al.*, 2010) in epithelial cells. This lack of specificity for CFTR of these inhibitors was already alarming for distinguishing CFTR-mediated anion conductances from those facilitated through other plasmalemmal channels, especially for research into epithelial ion transport in relation to CF. Moreover, the ability of these inhibitors to induce oxidative stress makes it difficult to isolate any effects of long-term $CFTR_{inh}$-172/GlyH-101 treatment solely to alteration in CFTR function. Adding to these complications, the off-target inhibition of SOCE reported here raises additional caution in interpreting experimental results obtained using these inhibitors, since blocking SOCE and disrupting Ca^{2+} homeostasis could affect a myriad of downstream processes. In the context of studying CFTR-mediated ion transport, a number of Ca^{2+}-dependent ion transport pathways, such as CaCC or Ca^{2+}-activated K^+ channels, could

potentially be inhibited by $CFTR_{inh}$-172/GlyH-101, adding confounding variables in interpreting electrophysiological results. Therefore, studies that utilised these inhibitors, as sole evidence for the involvement of CFTR to address biological questions, may need to be revisited using complementary tools, such as comparison with CF models or genetic knockout.

6.3 Clinical relevance of findings for CS-related airway diseases

6.3.1 CS-induced effects on Ca^{2+} homeostasis are cell-type dependent

The results in Chapters 4 and 5 demonstrate that acute exposure of isolated hASMC to diluted CSE, or gaseous CS, activated rapid Ca^{2+} influx. In stark contrast, there was no change in $[Ca^{2+}]_i$ when Calu-3 cells, a human lung carcinoma epithelial cell line, were exposed to the same concentrations of CSE.

The lack of effect of CSE in Calu-3 was surprising because previously, Rasmussen *et al.* (2014) showed contradicting results that exposing human primary airway epithelial cells and various epithelial cell lines to gaseous CS, using the same protocol as presented in Chapter 5, produced a relatively slow and sustained increase in $[Ca^{2+}]_i$, reaching a peak after ~15 mins of the initial CS puff (Rasmussen *et al.*, 2014). Moreover, they showed that extracellular Ca^{2+} chelation did not diminish the CS response, and that CS exposure did not activate ER and mitochondrial Ca^{2+} release. Instead, the main source of the cytosolic Ca^{2+} elevation in lung epithelia was thought to be lysosomal, as the CS-induced Ca^{2+} response was attenuated by bafilomycin A1, which indirectly blocks lysosomal Ca^{2+} acculumation (Rasmussen *et al.*, 2014). The results in Chapter 5 do not support an intracellular origin of the CS-induced Ca^{2+} increase in hASMC, based on the lack of response in the absence of extracellular Ca^{2+}.

The slow, sustained response profile observed by Rasmussen *et al.* (2014) in CS-exposed epithelial cells, including Calu-3 cells, was clearly very different to the rapid influx observed in CS-exposed hASMC, and the complete lack of response in CSE-exposed Calu-3 cells observed here. The distinct response profile and Ca^{2+} source in hASMC suggests that activation of TRPA1 by CS is cell-type dependent, which is supported by the observation that TRPA1 is functionally expressed in a number of human lung epithelial cell types (Nassini *et al.*, 2012; Buch *et al.*, 2013; Lin *et al.*, 2015; Nie *et al.*, 2016), despite CS not stimulating a rapid influx (Rasmussen *et al.*, 2014), and CSE not activating any Ca^{2+} changes in Calu-3 cells. It is possible that TRPA1 in human airway epithelial cells is differentially regulated than in hASMC, but this requires further investigation. On the other hand, the lack of response to CSE in Calu-3 cells can be attributed to the difference in delivery method, as volatile constituents of CS may have been lost during vigorous bubbling when producing CSE. Additionally, there are no known reports of functional TRPA1 expression in Calu-3 cells.

6.3.2 Cigarette smoking sessions may induce acute airway constriction

The experimental models for CS and CSE exposure used in this study were based on the assumption that water-soluble, lipophilic constituents of mainstream CS could reach, and exert effect on, the ASMC following a typical smoking session. This could occur through diffusion of constituents into the circulation during gas exchange at the alveoli, which are then diffused to the ASMC from the circulation. Additionally, these constituents could directly diffuse through the lung submucosa and reach the smooth muscle layer, akin to the delivery of inhaled bronchodilators targeting ASMC (Borghardt *et al.*, 2018). Physiologically, a number of water-soluble CS constituents can pass through the epithelial barrier in the lungs and diffuse into the circulation, and can be detected in the pancreatic juice of smokers (Prokopczyk *et al.*, 2002; Yamaguchi *et al.*, 2007). Indeed, it has been reported that CS constituents such as acrolein, sodium peroxynitrite, as well as various nitrosamines and oxidants, can permeate alveolar walls and remain stable in the circulation (Prokopczyk *et al.*, 2002; Yamaguchi *et al.*, 2007; Raju *et al.*, 2013). In particular, acrolein can form adducts with proteins and DNA, and can accumulate in the body; indeed, elevated levels of acrolein and acrolein-protein adducts were found in serum, and deposited in the lungs, of both healthy and COPD smokers (Kitaguchi *et al.*, 2012; Raju *et al.*, 2013), potentially altering TRPA1-regulated ASMC Ca^{2+} homeostasis both acutely and chronically. The concentration of these putative TRPA1 activators in CSE could be estimated using biochemical methods such as High-Performance Liquid Chromatography (HPLC). Comparing the concentration of these active constituents in CSE and in the circulation of acute or chronic smokers could potentially reveal the pathophysiological relevance of these findings, and conversely, future experiments could investigate whether hASMC TRPA1 would be directly activated by physiological concentrations of these constituents.

Following exposure to gaseous CS, hASMC exhibited varied temporal profiles of global $[Ca^{2+}]_i$ elevation, with either a transient $[Ca^{2+}]_i$ peak followed by rapid recovery, or a sustained peak without significant recovery (Figure 5.1). This would be expected to produce an airway constrictive response. In a study that simultaneously measured vessel diameter and $[Ca^{2+}]_i$ of rat mesenteric arteries, the vessels remained maximally constricted for at least 1 min after recovery of a transient endothelin-1-induced Ca^{2+} response (Shaw *et al.*, 2004). More importantly, two studies by the same group showed that during Ca^{2+} agonist stimulation that led to a transient global Ca^{2+} signal, the contractile force of human mesenteric arteries (Dai *et al.*, 2010) and, more relevantly, human bronchial strips (Dai *et al.*, 2007), began to develop after the peak of the Ca^{2+} transient, and sustained, maximal contraction was observed after recovery of the Ca^{2+} transient. These simultaneous measurements of smooth muscle tissue

contraction and $[Ca^{2+}]_i$ demonstrate that there is a time lag between recovery of $[Ca^{2+}]_i$ and decoupling of the actin-myosin cross-bridges in smooth muscle cells following transient Ca^{2+} agonist stimulations, most likely due to RhoA-mediated Ca^{2+} sensitisation. Thus, despite the transient nature of the CS-induced global $[Ca^{2+}]_i$ elevation, CS exposure could potentially evoke sustained tonal contraction of hASMC, especially considering the narrowing of the airway lumen depends on the spatial summation of all individual ASMC, and some of the cells studied exhibited a sustained CS-activated Ca^{2+} elevation. This was supported by the elevation of p-MLC levels detected in hASMC treated with CSE for 2 mins (Figure 4.25).

However, a cautionary note is that these high experimental concentrations of CS/CSE that may not be wholly reflective of the physiological conditions of smoking. Assuming a blood volume of 5 L, efficient diffusion across the epithelial barriers, and that constituents are stable in the bloodstream, typical consumption of one cigarette would result in a maximum potential concentration of 0.5% CSE in blood; this is 20 times lower than 10% CSE used for most experiments presented in Chapter 4. It was observed that acute exposure to 0.1% CSE did not produce a rapid, detectable Ca^{2+} response, while 1% CSE led to a slow and small elevation in $[Ca^{2+}]_i$ (Figure 4.1). Thus, it is unlikely that smokers would experience detrimental spontaneous asthma-like airway constriction upon smoking one cigarette; indeed, early studies have shown that acute cigarette smoking led to minor, but detectable, changes in airway resistance and airflow in both smokers and non-smokers (Zamel *et al.*, 1963; McDermott and Collins, 1965; Sterling, 1967; Higenbottam *et al.*, 1980). However, stable circulating active constituents could accumulate in the blood, especially for heavy smokers, for whom it is common to smoke a pack a day. Therefore, smoking multiple cigarettes in quick succession may introduce and deposit active CS constituents above the activation threshold for TRPA1-mediated Ca^{2+} influx, leading to airway narrowing events. Furthermore, the data presented in Figure 4.6 suggests that CSE-induced Ca^{2+} influx was poorly reversible after 25 min of washout, indicating that activation of TRPA1 is likely sustained in the short-term. Smoking in quick succession could therefore lead to sustained elevation of ASMC Ca^{2+} levels and hence long-term airway constriction, independent of the inflammatory status and signalling from other cell types of the airway.

However, physiologically, ASMC does not function in isolation, and so the complex crosstalk with neighbouring cell types must be considered, especially as chronic exposure to CS/CSE has been extensively linked to adverse effects in various airway cell types (Tamimi *et al.*, 2012; Caramori *et al.*, 2015; Crotty Alexander *et al.*, 2015). Previously, two groups have reported conflicting results about airway smooth muscle contraction/relaxation in response to acute CSE exposure (Andre *et al.*, 2008; Streck *et al.*, 2010). However, it is important to note that both

studies used the *ex vivo* intact airway, complete with surrounding extracellular matrix, epithelial cells, immune cells, and neurons, which could all modulate ASMC contractility, and so the intrinsic contractility of ASMC was not focused on. Indeed, Andre *et al.* (2008) previously concluded that the rapid contraction they observed was due to a TRPA1-mediated neurogenic inflammatory response. Moreover, the intricate crosstalk network between different airway cell types may underlie why conflicting results have been published regarding airway smooth muscle contractility following chronic CSE treatment in organ and cell cultures (Pera *et al.*, 2010; Xu *et al.*, 2010; Yoon *et al.*, 2011; Xu *et al.*, 2012). The fact that both studies using rat airways reported hyper-contractility (Xu *et al.*, 2010; Xu *et al.*, 2012), while the studies using bovine airway strips and hASMC reported hypo-contractility, may indicate species-difference of CSE-induced AHR (Pera *et al.*, 2010; Yoon *et al.*, 2011). Hyper-contractility may be the result of upregulation of proteins involved in Ca^{2+} signalling, the contractile machinery, and inflammation, while hypo-contractility may be due to excess ASMC cell death and the shift to a proliferative phenotype. The transition between SMC proliferative and contractile phenotypes is another convoluted signalling network, and may be dependent on a number of factors in these cultured ASMC and *ex vivo* airway, including culture conditions as well as CSE preparation protocol, concentration, and incubation time. Another possibility for the discrepancy of hyper- vs. hypo-contractility in response to chronic CSE exposure is the vasodilatory effects of TRPA1 activation, as it was reported that activating TRPA1 in sensory nerves or the endothelium led to vasodilation of rodent mesenteric and cerebral arteries (Bautista *et al.*, 2005; Earley *et al.*, 2009; Pozsgai *et al.*, 2010). More pertinently, TRPA1 agonism has been shown to induce PGE_2 production from both airway epithelial and non-epithelial cells, leading to acute airway relaxation and protection against bronchoconstriction (Cheah *et al.*, 2014; Marsh *et al.*, 2020). Such TRPA1-mediated smooth muscle relaxation, albeit through signalling from other cell types, may provide a counter-balancing force for TRPA1-mediated ASMC contraction in response to cigarette smoking.

6.3.3 Potential chronic effects of disrupted Ca^{2+} homeostasis in COPD pathogenesis

The hASMC used for experiments in this thesis were isolated from donors who were not currently smoking, and were not diagnosed with COPD. Nonetheless, exposure to CS or CSE was able to elicit significant hASMC Ca^{2+} influx and MLC phosphorylation. However, the COPD airway is typically already obstructed due to structural remodelling and mucus plugging; therefore, even a small stimulation leading to airway constriction could significantly impact lung function and gas exchange. Moreover, the COPD lung is hyperinflammatory, and treatment with inflammatory cytokines such as TNF-α, IL-1β, IL-13, interferon-γ was found to

disrupt multiple aspects of ASMC Ca^{2+} homeostasis, including augmentation of GPCR-coupled Ca^{2+} release, upregulation of CD38 (Deshpande *et al.*, 2003; Tliba *et al.*, 2003), enhanced IP_3 production (Hotta *et al.*, 1999), increased density of bradykinin receptors (Schmidlin *et al.*, 1998), upregulation of TRPC3-mediated Ca^{2+} influx (White *et al.*, 2006), upregulation of LTCC (Ding *et al.*, 2019), downregulation of SERCA (Sathish *et al.*, 2009), and reduced sensitivity of β_2-adrenoceptors that facilitate ASMC relaxation (Shore and Moore, 2003). Inflammation is also associated with increased Ca^{2+} sensitivity, for instance, upregulation of contractile proteins and augmented actin polymerisation, that leads to AHR (Sieck *et al.*, 2019). Therefore, under inflamed conditions with upregulated Ca^{2+} signalling and sensitivity, acute CS exposure could potentially bring about greater Ca^{2+} influx and/or activation of contractile mechanisms in hASMC of COPD patients, aggravating airway constriction during smoking. An interesting direction for future experiments would be to examine the responses to CS/CSE in COPD hASMC, and investigate whether CS/CSE would acutely activate additional Ca^{2+} influx or release pathways in addition to TRPA1-mediated influx.

In addition to the acute effects on Ca^{2+} signalling and ASMC contractility, chronic CS exposure was reported to upregulate the expression of TRPA1 in guinea pig tracheal epithelia and in human epithelial cells (Zhong *et al.*, 2015; Nie *et al.*, 2016). It would be interesting to investigate whether TRPA1 expression is upregulated in CS-exposed ASMC, or in chronic smokers with COPD. If TRPA1 is chronically upregulated in smokers, the augmentation in TRPA1-mediated Ca^{2+} influx by CS may not only lead to aggravated ASMC contraction in the short term, but also sustained sensitivity, due to increased channel availability, to Ca^{2+} influx in response to further challege of CS or other TRPA1-sensitive irritants, forming a positive feedback loop. On top of this enhanced TRPA1-mediated Ca^{2+} influx, chronic CS/CSE exposure could also upregulate other aspects of Ca^{2+} homeostasis, such as the augmentation of SOCE and ROCE, as well as expression of STIM1, Orai1, TRPC3, and CD38 (Sathish *et al.*, 2015; Wylam *et al.*, 2015). Combining the upregulation of Ca^{2+} signalling by CS, and the augmentation of Ca^{2+} signalling by airway inflammation, smoking can exert adverse effects on hASMC Ca^{2+} homeostasis, and enhanced sensitivity and tone, in the long term.

Aside from disrupting the intrinsic Ca^{2+} sensitisation and contractility of ASM, chronic smoking is intimately linked to long-term cellular changes that ultimately establish the hyperinflammatory, remodelled and obstructed airway phenotype in COPD. For instance, chronic CS/CSE exposure was reported to enhance ROS generation (Wylam *et al.*, 2015), chemokine secretion (Oltmanns *et al.*, 2005; Chen *et al.*, 2014; Wylam *et al.*, 2015), collagen deposition (Chen *et al.*, 2014), proliferation (Pera *et al.*, 2010; Xu *et al.*, 2010; Xu *et al.*, 2012;

Wylam *et al.*, 2015; Guan *et al.*, 2017; Hong *et al.*, 2017; Jiang *et al.*, 2019), migration (Yoon *et al.*, 2011; Yoshiyama *et al.*, 2011), and inhibition of wound-healing (Chen *et al.*, 2014). Importantly, many of these processes are dependent on Ca^{2+} signalling (Ribeiro *et al.*, 2005b; Gerthoffer, 2008; Mahn *et al.*, 2010; Zou *et al.*, 2011). In fact, nicotine-activated augmentation of ASMC proliferation was dependent on elevation of $[Ca^{2+}]_i$, mediated through TRPC3 (Jiang *et al.*, 2019) and TRPC6 (Hong *et al.*, 2017). Combining the upregulation of Ca^{2+} signalling and the shift towards a pro-inflammatory and remodelling profile in hASMC, it is clear how chronic smoking can lead to AHR and airway obstruction from many different facets. The range of both acute and chronic adverse effects of CS exposure on ASMC function that contributes to the pathogenesis of COPD is illustrated in **Figure 6.2**.

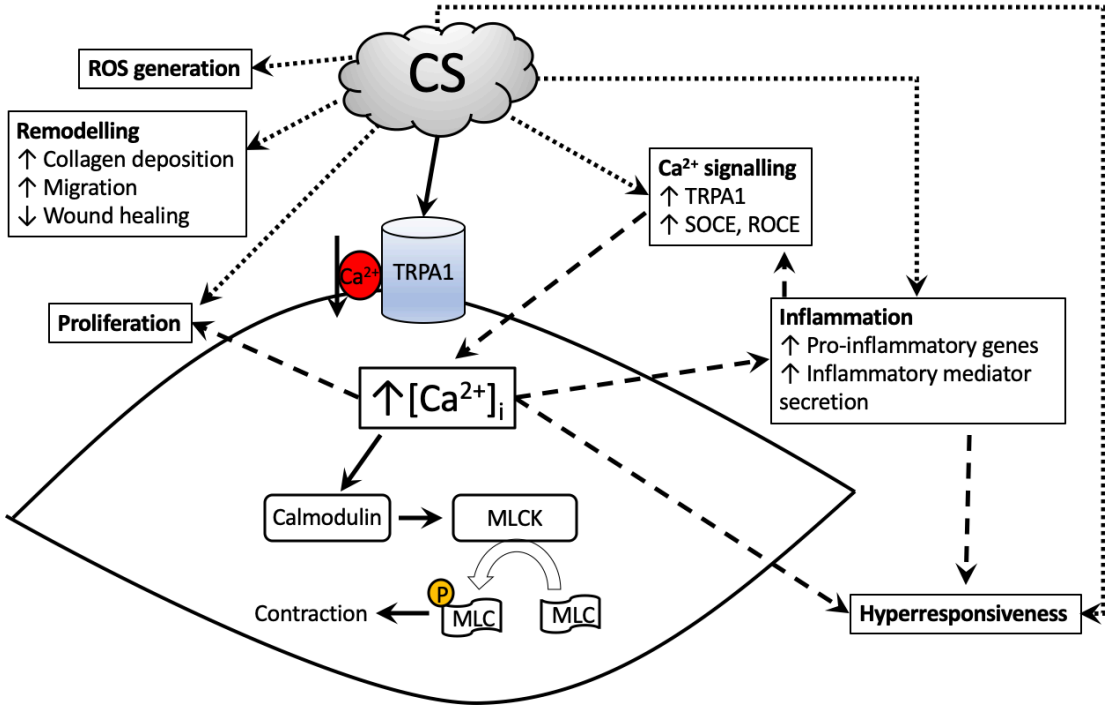

Figure 6.2: Acute and chronic adverse effects of CS exposure on ASMC function. Acute effects are denoted by solid arrowheads; long-term changes that are directly associated with chronic CS exposure are denoted by dotted arrowheads; chronic changes associated with elevation of $[Ca^{2+}]_i$, or inflammation, are denoted by dashed arrowheads. CS contains constituents, such as acrolein, crotonaldehyde, and nicotine, that could directly activate TRPA1 to induce Ca^{2+} influx. Transient elevation of $[Ca^{2+}]_i$ activates the contractile signalling mechanism, by Ca^{2+} binding to calmodulin, which activates MLCK, which then phosphorylates MLC; p-MLC forms cross-bridges with actin filaments, and the cycling of actin-myosin cross-bridges generates contractile force, that may lead to airway constriction. Chronic CS exposure induces changes in ASMC that contribute to COPD pathogenesis, such as increased ROS generation, proliferation, various aspects of airway remodelling, upregulation of Ca^{2+} signalling, inflammation, and airway hyperresponsiveness. Additionally, expression of pro-inflammatory genes, cytokine secretion, proliferation, and ASMC hyperresponsiveness are all regulated by intracellular Ca^{2+} signalling. Inflammation is also linked to AHR, as well as disruption of Ca^{2+} homeostasis.

6.4 Implications for COPD therapeutics

6.4.1 Current treatments for COPD

COPD is characterised by a wide range of disease manifestation and severity, and may involve sudden exacerbation of symptoms. Currently, complete cure of COPD is not possible, due to a number of irreversible structural changes and tissue injury in the airway. However, for CS-associated COPD, smoking cessation may be able to partially restore lung function, delay disease progression, and reduce mortality in the long-term (Anthonisen *et al.*, 1994; Anthonisen *et al.*, 2005; Willemse *et al.*, 2005). On the other hand, pharmacological treatment options can help to manage COPD symptoms and reduce exacerbations. The current most common therapy for managing stable COPD, according to the guidelines of most European countries, is bronchodilators such as long-acting β_2-agonist (LABA; e.g. salmeterol (Rossi *et al.*, 2008)) and long-acting muscarinic antagonist (LAMA; e.g. tiotropium (Tashkin *et al.*, 2008)), or the combination of the two (Rosenberg and Kalhan, 2017; GOLD, 2020). LABA directly activates cAMP-mediated bronchodilation, whereas LAMA blocks endogenous cholinergic bronchoconstriction. The combination treatment demonstrated higher efficacy to reduce COPD symptoms, frequency and severity of exacerbations, and to improve FEV_1, than either LABA or LAMA alone (reviewed in Calzetta *et al.* (2013); Rosenberg and Kalhan (2017); GOLD (2020)). Other classes of drugs that were found to bring relatively smaller improvements in lung function and mortality, such as inhaled corticosteroids, antibiotics, methylxanthines and mucolytic agents, are reviewed in Drummond *et al.* (2008); Miravitlles *et al.* (2016); GOLD (2020). In light of results from the present study, it would be interesting to investigate the potential protective effects of these agents, especially LABA and LAMA, against CS/CSE-induced acute airway constriction, e.g. in *ex vivo* tissue myography.

Moreover, recent research on the role of CS-induced CFTR defects, the emerging role of CFTR in regulating ASMC contractility, as well as the present findings of CS-activated TRPA1-mediated Ca^{2+} influx, advocate that potential novel therapeutic options targeting these processes should be considered.

6.4.2 CFTR activators promote airway hydration and bronchorelaxation

CS-induced CFTR deficiency leads to airway dehydration and disrupted mucociliary clearance in COPD smokers, and restoring ASL hydration has been recently explored as a potential treatment for COPD with chronic bronchitis (Bennett *et al.*, 2016; Solomon *et al.*, 2017). The clinical benefits of rehydrating the ASL were apparent in a few studies (Clunes *et al.*, 2012; Anderson *et al.*, 2015), where inhaled hypertonic saline, to drive fluid secretion, improved mucus transport and clearance in COPD patients with chronic bronchitis. On the other hand,

due to acquired CFTR defects in COPD smokers, restoring CFTR function using the potentiator ivacaftor reversed CS-induced reduction in CFTR currents, ASL hydration, ciliary beat frequency, and mucus transport in primary human airway epithelial cultures (Sloane *et al.*, 2012; Raju *et al.*, 2017a). However, in a pilot clinical study, detectable, but non-significant, improvements in sweat chloride and nasal PD by ivacaftor were observed in COPD patients with chronic bronchitis, raising questions about the effectiveness of CFTR potentiation in restoring CS-induced defects in Cl^- secretion in a clinical setting (Solomon *et al.*, 2016); larger scale clinical trials are now underway to validate these findings.

On the other hand, several selective cyclic nucleotide phosphodiesterase 3 and/or 4 (PDE3/4) inhibitors, which elevate intracellular cAMP levels by reducing cAMP metabolism, and hence activate CFTR, are clinically approved as add-on therapy for severe exacerbations in COPD with chronic bronchitis (Rabe, 2010; Page and Spina, 2012; Abbott-Banner and Page, 2014; Cazzola *et al.*, 2016). In particular, long-term treatment with roflumilast, a PDE4 inhibitor, significantly improved lung function and reduced exacerbations in severe COPD patients (Calverley *et al.*, 2009; Fabbri *et al.*, 2009). Roflumilast was found to restore CFTR-dependent anion transport, fluid secretion, and ciliary beat frequency in CS-exposed human bronchial epithelial cells, as well as in a chronic smoking mouse model (Lambert *et al.*, 2014; Schmid *et al.*, 2015; Raju *et al.*, 2017b). Nonetheless, the development of airway hydration strategies as treatment for COPD is still at its infancy, and several factors, such as the severity and phenotype of COPD, smoking history, and CFTR function of the patient, need to be considered before deploying the treatment.

Other than airway rehydration, which is regulated predominantly by the airway epithelia, pharmacological activators of CFTR have also shown bronchodilating properties. Agents that activate CFTR through elevation of intracellular cAMP levels, such as β_2-adrenergic agonists, theophylline and forskolin (Norez *et al.*, 2014), are obvious bronchodilators since cAMP regulates several downstream pathways that facilitates ASMC relaxation (see section 1.3.3). However, CFTR activity might be directly involved in bronchodilation. Norez *et al.* (2014) reported that MPB-104, which activates CFTR independent of cAMP (Becq *et al.*, 1999), relaxed pre-constricted human bronchial rings denuded of the epithelium; this bronchorelaxation was inhibited by $CFTR_{inh}$-172. Furthermore, the specific CFTR potentiator ivacaftor has also been shown to inhibit cholinergic-induced narrowing of WT porcine lung slices (Cook *et al.*, 2016). Extending beyond *ex vivo* and animal models, it was discovered that in CF patients with the G551D-CFTR mutation, which leads to a gating defect, acute administration of ivacaftor rapidly increased the distensibility of smaller airways and relaxed

vascular tone (Adam *et al.*, 2016). However, it was not clear whether the functional expression of CFTR could directly alter the intrinsic Ca^{2+} signalling and contractility of ASMC, since these papers did not study isolated ASMC. It is possible that the bronchodilating effect of CFTR activation involves signalling through other neighbouring cell types. In this thesis, it was shown that CFTR activation did not affect ATP-induced Ca^{2+} store release, whereas inhibition of CFTR slowed down the rate of SOCE; both of these findings, in addition to the low expression of CFTR protein, do not support a major role of CFTR in lowering ASMC $[Ca^{2+}]_i$ and therefore airway smooth muscle tone. Nonetheless, these studies provide a promising justification for re-purposing CFTR activators as COPD treatment, although further fundamental understanding of CFTR's role in regulating ASMC Ca^{2+} signalling, or CFTR-dependent signalling through other cell types to facilitate bronchodilation, is required.

6.4.3 TRPA1 as a potential therapeutic target for COPD

Since Ca^{2+} influx from the extracellular space represents an important mechanism of regulating $[Ca^{2+}]_i$, plasmalemma-bound Ca^{2+} channels have also been considered as drug targets for modulating airway smooth muscle tone. For instance, the potential for various TRP channels expressed in ASMC, many of which are permeant to Ca^{2+} and regulate various aspects of ASMC function, as drug targets for treating airway diseases have been considered (Gosling *et al.*, 2005; Grace *et al.*, 2014; Belvisi and Birrell, 2017). However, the findings in the present study may enthuse interest in targeting TRPA1 in ASMC as its role in modulating ASMC Ca^{2+} signalling becomes evident.

Due to the prevalent expression of TRPA1 in sensory neurons, the potential and challenges of TRPA1 modulators in pain therapy has long been suggested and discussed (Viana and Ferrer-Montiel, 2009; Andrade *et al.*, 2012; Chen and Hackos, 2015; Belvisi and Birrell, 2017). However, despite promising pre-clinical data, very few of these modulators have proceeded to clinical trials (notably GRC-17536, ODM-108, CB-625), and none have advanced beyond phase 2 (reviewed in Koivisto *et al.* (2018); Heber and Fischer (2019)). More recently, in light of emerging evidence for the role of TRPA1 in modulating the function of a range of airway cell types, both acutely and chronically, the potential for TRPA1 to be a therapeutic target for respiratory disorders should be considered (reviewed in Jha *et al.* (2015); Mukhopadhyay *et al.* (2016); Belvisi and Birrell (2017)). Notably, TRPA1 in sensory neurons was reported to facilitate neurogenic inflammation (Andre *et al.*, 2008; Hox *et al.*, 2013), cough reflex (Birrell *et al.*, 2009; Mukhopadhyay *et al.*, 2014), and bronchoconstriction reflex (Andre *et al.*, 2008; Raemdonck *et al.*, 2012; Hox *et al.*, 2013) in the airway. On the other hand, in non-neuronal airway cells, TRPA1 activation led to increased secretion of IL-8 from airway epithelial cells,

ASMC, and fibroblasts (Nassini *et al.*, 2012), and was associated with upregulation of inflammatory genes, generation of intracellular ROS and cell injury in human airway epithelial cells (Lin *et al.*, 2015; Prandini *et al.*, 2016; Wang *et al.*, 2019b).

Considering the key finding in the present study that acute CS exposure directly activated TRPA1-mediated Ca^{2+} influx, which may directly evoke airway constriction, the potential for a long-acting TRPA1 antagonist as a supplementary bronchodilator for managing the symptoms of CS-related COPD should be considered, in addition to its potential anti-inflammatory effects. This potential is supported by results from asthma rodent model studies, whereby TRPA1 KO mice, as well as HC-030031-treated WT mice and rats, exhibited reduced inflammation and bronchoconstriction in response to ovalbumin challenge (Caceres *et al.*, 2009; Raemdonck *et al.*, 2012). A recent 2020 study provided more insights into the role of TRPA1 in COPD pathogenesis, as Hajna *et al.* (2020) demonstrated that TRPA1 KO mice were protected against CSE-induced emphysema and decline in lung function. It is, therefore, possible that inhibiting TRPA1 in the long-term would protect against CS-induced airway narrowing by directly blocking ASMC Ca^{2+} influx, as well as slowing emphysema progression and reducing inflammation of the airway. However, there are also evidence against TRPA1 antagonism as an effective target for treating hyperresponsive airway diseases; for instance, putative TRPA1 agonism led to acute relaxation of the *ex vivo* airway (Cheah *et al.*, 2014; Marsh *et al.*, 2020), and TRPA1 KO mice were more susceptible to lipopolysaccharide-evoked pneumonitis and AHR (Hajna *et al.*, 2020). These complex, and at times contradicting, results, as well as halted clinical trials for TRPA1 antagonists in the field of pain therapy, suggest that further understanding of TRPA1 pharmacology, electrophysiology, drug delivery, and most importantly its composite role in the cascade of airway cell types, is required before exploring this potential.

6.5 Concluding remarks

The present study investigated smoking-induced changes to ASMC Ca^{2+} homeostasis and contractility, and whether CFTR, which is inhibited by CS in airway epithelia, also plays a part in regulating ASMC function. The results in Chapter 3 show that CFTR played a minor role in modulating GPCR-coupled Ca^{2+} release and SOCE, but evidence is accumulating to point to a possible role of Cl^- channels in SR ion homeostasis during periods of Ca^{2+} flux, and therefore in overall regulation of Ca^{2+} dynamics and ASMC contraction. The exact mechanisms, however, remain to be resolved and offer many opportunities for future experimentation.

More importantly, the results in Chapter 4 and 5 demonstrate that the nociceptive pain receptor channel, TRPA1, was the major Ca^{2+} channel that contributed to CS/CSE-induced Ca^{2+}

response in primary hASMC from multiple non-smoking donors. This acute, rapid elevation of $[Ca^{2+}]_i$ led to downstream phosphorylation of MLC, providing a mechanistic link between CS/CSE exposure, disruption of hASMC Ca^{2+} homeostasis, and hASMC contractility. It is therefore speculated that acute airway narrowing events could occur in response to cigarette smoking, and this could be aggravated under inflamed conditions in chronic smokers with COPD. The acute, TRPA1-mediated changes in cytosolic Ca^{2+} observed in this study may also serve as an initiating factor for further, more chronic pathological effects. For instance, the elevated $[Ca^{2+}]_i$ induced by accumulated CS constituents could increase the expression of Ca^{2+} homeostatic regulators in ASMC, in addition to augmenting adverse responses, such as secretion of inflammatory mediators, ROS generation, proliferation, migration, and ECM deposition, each of which may contribute to chronic airway hyperresponsiveness and remodelling seen in COPD (summarised in Figure 6.2). These results from the present study therefore suggest that TRPA1 has the potential to be a therapeutic target for treating CS-associated airway diseases, such as COPD.

References

Abbott-Banner, K.H. and Page, C.P. (2014) 'Dual PDE3/4 and PDE4 inhibitors: novel treatments for COPD and other inflammatory airway diseases', *Basic Clin Pharmacol Toxicol*, 114(5), pp. 365-76.

Adam, R.J., Hisert, K.B., Dodd, J.D., Grogan, B., Launspach, J.L., Barnes, J.K., Gallagher, C.G., Sieren, J.P., Gross, T.J., Fischer, A.J., Cavanaugh, J.E., Hoffman, E.A., Singh, P.K., Welsh, M.J., McKone, E.F. and Stoltz, D.A. (2016) 'Acute administration of ivacaftor to people with cystic fibrosis and a G551D-CFTR mutation reveals smooth muscle abnormalities', *JCI Insight*, 1(4), p. e86183.

Adcock, I.M., Brown, C.R., Kwon, O. and Barnes, P.J. (1994) 'Oxidative stress induces NF kappa B DNA binding and inducible NOS mRNA in human epithelial cells', *Biochem Biophys Res Commun*, 199(3), pp. 1518-24.

Algara-Suarez, P., Romero-Mendez, C., Chrones, T., Sanchez-Armass, S., Meza, U., Sims, S.M. and Espinosa-Tanguma, R. (2007) 'Functional coupling between the Na+/Ca2+ exchanger and nonselective cation channels during histamine stimulation in guinea pig tracheal smooth muscle', *Am J Physiol Lung Cell Mol Physiol*, 293(1), pp. L191-8.

Alton, E.W., Manning, S.D., Schlatter, P.J., Geddes, D.M. and Williams, A.J. (1991) 'Characterization of a Ca(2+)-dependent anion channel from sheep tracheal epithelium incorporated into planar bilayers', *J Physiol*, 443, pp. 137-59.

Anderson, W.H., Coakley, R.D., Button, B., Henderson, A.G., Zeman, K.L., Alexis, N.E., Peden, D.B., Lazarowski, E.R., Davis, C.W., Bailey, S., Fuller, F., Almond, M., Qaqish, B., Bordonali, E., Rubinstein, M., Bennett, W.D., Kesimer, M. and Boucher, R.C. (2015) 'The Relationship of Mucus Concentration (Hydration) to Mucus Osmotic Pressure and Transport in Chronic Bronchitis', *Am J Respir Crit Care Med*, 192(2), pp. 182-90.

Andrade, E.L., Meotti, F.C. and Calixto, J.B. (2012) 'TRPA1 antagonists as potential analgesic drugs', *Pharmacol Ther*, 133(2), pp. 189-204.

Andre, E., Campi, B., Materazzi, S., Trevisani, M., Amadesi, S., Massi, D., Creminon, C., Vaksman, N., Nassini, R., Civelli, M., Baraldi, P.G., Poole, D.P., Bunnett, N.W., Geppetti, P. and Patacchini, R. (2008) 'Cigarette smoke-induced neurogenic inflammation is mediated by alpha,beta-unsaturated aldehydes and the TRPA1 receptor in rodents', *J Clin Invest*, 118(7), pp. 2574-82.

Anthonisen, N.R., Connett, J.E., Kiley, J.P., Altose, M.D., Bailey, W.C., Buist, A.S., Conway, W.A., Jr., Enright, P.L., Kanner, R.E., O'Hara, P. and et al. (1994) 'Effects of smoking intervention and the use of an inhaled anticholinergic bronchodilator on the rate of decline of FEV1. The Lung Health Study', *JAMA*, 272(19), pp. 1497-505.

Anthonisen, N.R., Skeans, M.A., Wise, R.A., Manfreda, J., Kanner, R.E., Connett, J.E. and Lung Health Study Research, G. (2005) 'The effects of a smoking cessation intervention on 14.5-year mortality: a randomized clinical trial', *Ann Intern Med*, 142(4), pp. 233-9.

Antigny, F., Girardin, N., Raveau, D., Frieden, M., Becq, F. and Vandebrouck, C. (2009) 'Dysfunction of mitochondria Ca2+ uptake in cystic fibrosis airway epithelial cells', *Mitochondrion*, 9(4), pp. 232-41.

Antigny, F., Norez, C., Becq, F. and Vandebrouck, C. (2008a) 'Calcium homeostasis is abnormal in cystic fibrosis airway epithelial cells but is normalized after rescue of F508del-CFTR', *Cell Calcium*, 43(2), pp. 175-83.

Antigny, F., Norez, C., Becq, F. and Vandebrouck, C. (2011a) 'CFTR and Ca Signaling in Cystic Fibrosis', *Front Pharmacol*, 2, p. 67.

Antigny, F., Norez, C., Cantereau, A., Becq, F. and Vandebrouck, C. (2008b) 'Abnormal spatial diffusion of Ca2+ in F508del-CFTR airway epithelial cells', *Respir Res*, 9, p. 70.

Antigny, F., Norez, C., Dannhoffer, L., Bertrand, J., Raveau, D., Corbi, P., Jayle, C., Becq, F. and Vandebrouck, C. (2011b) 'Transient receptor potential canonical channel 6 links Ca2+ mishandling to cystic fibrosis transmembrane conductance regulator channel dysfunction in cystic fibrosis', *Am J Respir Cell Mol Biol*, 44(1), pp. 83-90.

Ay, B., Iyanoye, A., Sieck, G.C., Prakash, Y.S. and Pabelick, C.M. (2006) 'Cyclic nucleotide regulation of store-operated Ca2+ influx in airway smooth muscle', *Am J Physiol Lung Cell Mol Physiol*, 290(2), pp. L278-83.

Babcock, D.F., Herrington, J., Goodwin, P.C., Park, Y.B. and Hille, B. (1997) 'Mitochondrial participation in the intracellular Ca2+ network', *J Cell Biol*, 136(4), pp. 833-44.

Bai, Y. and Sanderson, M.J. (2006) 'Airway smooth muscle relaxation results from a reduction in the frequency of Ca2+ oscillations induced by a cAMP-mediated inhibition of the IP3 receptor', *Respir Res*, 7, p. 34.

Balghi, H., Robert, R., Rappaz, B., Zhang, X., Wohlhuter-Haddad, A., Evagelidis, A., Luo, Y., Goepp, J., Ferraro, P., Romeo, P., Trebak, M., Wiseman, P.W., Thomas, D.Y. and Hanrahan, J.W. (2011) 'Enhanced Ca2+ entry due to Orai1 plasma membrane insertion increases IL-8 secretion by cystic fibrosis airways', *FASEB J*, 25(12), pp. 4274-91.

Barnes, P.J. (2004) 'Alveolar macrophages in chronic obstructive pulmonary disease (COPD)', *Cell Mol Biol (Noisy-le-grand)*, 50 Online Pub, pp. OL627-37.

Barnes, P.J. (2014) 'Cellular and molecular mechanisms of chronic obstructive pulmonary disease', *Clin Chest Med*, 35(1), pp. 71-86.

Barnes, P.J., Shapiro, S.D. and Pauwels, R.A. (2003) 'Chronic obstructive pulmonary disease: molecular and cellular mechanisms', *Eur Respir J*, 22(4), pp. 672-88.

Barrett, K.E., Barman, S.M., Boitano, S. and Brooks, H. (2015) *Ganong's Review of Medical Physiology 25th Edition*. McGraw-Hill Education.

Barro-Soria, R., Aldehni, F., Almaca, J., Witzgall, R., Schreiber, R. and Kunzelmann, K. (2010) 'ER-localized bestrophin 1 activates Ca2+-dependent ion channels TMEM16A and SK4 possibly by acting as a counterion channel', *Pflugers Arch*, 459(3), pp. 485-97.

Basbaum, C., Lemjabbar, H., Longphre, M., Li, D., Gensch, E. and McNamara, N. (1999) 'Control of mucin transcription by diverse injury-induced signaling pathways', *Am J Respir Crit Care Med*, 160(5 Pt 2), pp. S44-8.

Bautista, D.M., Jordt, S.E., Nikai, T., Tsuruda, P.R., Read, A.J., Poblete, J., Yamoah, E.N., Basbaum, A.I. and Julius, D. (2006) 'TRPA1 mediates the inflammatory actions of environmental irritants and proalgesic agents', *Cell*, 124(6), pp. 1269-82.

Bautista, D.M., Movahed, P., Hinman, A., Axelsson, H.E., Sterner, O., Hogestatt, E.D., Julius, D., Jordt, S.E. and Zygmunt, P.M. (2005) 'Pungent products from garlic activate the sensory ion channel TRPA1', *Proc Natl Acad Sci U S A*, 102(34), pp. 12248-52.

Baxter, M., Eltom, S., Dekkak, B., Yew-Booth, L., Dubuis, E.D., Maher, S.A., Belvisi, M.G. and Birrell, M.A. (2014) 'Role of transient receptor potential and pannexin channels in cigarette smoke-triggered ATP release in the lung', *Thorax*, 69(12), pp. 1080-9.

Bebok, Z., Varga, K., Hicks, J.K., Venglarik, C.J., Kovacs, T., Chen, L., Hardiman, K.M., Collawn, J.F., Sorscher, E.J. and Matalon, S. (2002) 'Reactive oxygen nitrogen species decrease cystic fibrosis transmembrane conductance regulator expression and cAMP-mediated Cl- secretion in airway epithelia', *J Biol Chem*, 277(45), pp. 43041-9.

Bechem, M. and Hoffmann, H. (1993) 'The molecular mode of action of the Ca agonist (-) BAY K 8644 on the cardiac Ca channel', *Pflugers Arch*, 424(3-4), pp. 343-53.

Becq, F., Mettey, Y., Gray, M.A., Galietta, L.J., Dormer, R.L., Merten, M., Metaye, T., Chappe, V., Marvingt-Mounir, C., Zegarra-Moran, O., Tarran, R., Bulteau, L., Derand, R., Pereira, M.M., McPherson, M.A., Rogier, C., Joffre, M., Argent, B.E., Sarrouilhe, D., Kammouni, W., Figarella, C., Verrier, B., Gola, M. and Vierfond, J.M. (1999) 'Development of substituted Benzo[c]quinolizinium compounds as novel activators of the cystic fibrosis chloride channel', *J Biol Chem*, 274(39), pp. 27415-25.

Belvisi, M.G. and Birrell, M.A. (2017) 'The emerging role of transient receptor potential channels in chronic lung disease', *Eur Respir J*, 50(2).

Ben-Jebria, A., Marthan, R., Rossetti, M., Savineau, J.P. and Ultman, J.S. (1993) 'Effect of in vitro exposure to acrolein on carbachol responses in rat trachealis muscle', *Respir Physiol*, 93(1), pp. 111-23.

Ben-Jebria, A., Marthan, R., Rossetti, M., Savineau, J.P. and Ultman, J.S. (1994) 'Human bronchial smooth muscle responsiveness after in vitro exposure to acrolein', *Am J Respir Crit Care Med*, 149(2 Pt 1), pp. 382-6.

Bennett, W.D., Henderson, A.G. and Donaldson, S.H. (2016) 'Hydrator Therapies for Chronic Bronchitis. Lessons from Cystic Fibrosis', *Ann Am Thorac Soc*, 13 Suppl 2, pp. S186-90.

Benowitz, N.L. (2010) 'Nicotine addiction', *N Engl J Med*, 362(24), pp. 2295-303.

Bergner, A., Kellner, J., Silva, A.K., Gamarra, F. and Huber, R.M. (2006) 'Ca2+-signaling in airway smooth muscle cells is altered in T-bet knock-out mice', *Respir Res*, 7, p. 33.

Bernstein, K., Vink, J.Y., Fu, X.W., Wakita, H., Danielsson, J., Wapner, R. and Gallos, G. (2014) 'Calcium-activated chloride channels anoctamin 1 and 2 promote murine uterine smooth muscle contractility', *Am J Obstet Gynecol*, 211(6), pp. 688 e1-10.

Berridge, M.J. (2006) 'Calcium microdomains: organization and function', *Cell Calcium*, 40(5-6), pp. 405-12.

Berridge, M.J., Bootman, M.D. and Roderick, H.L. (2003) 'Calcium signalling: dynamics, homeostasis and remodelling', *Nat Rev Mol Cell Biol*, 4(7), pp. 517-29.

Bers, D.M. (2002) 'Cardiac excitation-contraction coupling', *Nature*, 415(6868), pp. 198-205.

Bertrand, C.A., Zhang, R., Pilewski, J.M. and Frizzell, R.A. (2009) 'SLC26A9 is a constitutively active, CFTR-regulated anion conductance in human bronchial epithelia', *J Gen Physiol*, 133(4), pp. 421-38.

Billet, A. and Hanrahan, J.W. (2013) 'The secret life of CFTR as a calcium-activated chloride channel', *J Physiol*, 591(21), pp. 5273-8.

Billet, A., Luo, Y., Balghi, H. and Hanrahan, J.W. (2013) 'Role of tyrosine phosphorylation in the muscarinic activation of the cystic fibrosis transmembrane conductance regulator (CFTR)', *J Biol Chem*, 288(30), pp. 21815-23.

Birrell, M.A., Belvisi, M.G., Grace, M., Sadofsky, L., Faruqi, S., Hele, D.J., Maher, S.A., Freund-Michel, V. and Morice, A.H. (2009) 'TRPA1 agonists evoke coughing in guinea pig and human volunteers', *Am J Respir Crit Care Med*, 180(11), pp. 1042-7.

Bogeski, I., Kummerow, C., Al-Ansary, D., Schwarz, E.C., Koehler, R., Kozai, D., Takahashi, N., Peinelt, C., Griesemer, D., Bozem, M., Mori, Y., Hoth, M. and Niemeyer, B.A. (2010) 'Differential redox regulation of ORAI ion channels: a mechanism to tune cellular calcium signaling', *Sci Signal*, 3(115), p. ra24.

Bonvin, E., Le Rouzic, P., Bernaudin, J.F., Cottart, C.H., Vandebrouck, C., Crie, A., Leal, T., Clement, A. and Bonora, M. (2008) 'Congenital tracheal malformation in cystic fibrosis transmembrane conductance regulator-deficient mice', *J Physiol*, 586(13), pp. 3231-43.

Borghardt, J.M., Kloft, C. and Sharma, A. (2018) 'Inhaled Therapy in Respiratory Disease: The Complex Interplay of Pulmonary Kinetic Processes', *Can Respir J*, 2018, p. 2732017.

Bose, S.J., Krainer, G., Ng, D.R.S., Schenkel, M., Shishido, H., Yoon, J.S., Haggie, P.M., Schlierf, M., Sheppard, D.N. and Skach, W.R. (2020) 'Towards next generation therapies for cystic fibrosis: Folding, function and pharmacology of CFTR', *J Cyst Fibros*, 19 Suppl 1, pp. S25-S32.

Bosken, C.H., Wiggs, B.R., Pare, P.D. and Hogg, J.C. (1990) 'Small airway dimensions in smokers with obstruction to airflow', *Am Rev Respir Dis*, 142(3), pp. 563-70.

Bourgeois, J.S., Jacob, J., Garewal, A., Ndahayo, R. and Paxson, J. (2016) 'The Bioavailability of Soluble Cigarette Smoke Extract Is Reduced through Interactions with Cells and Affects the Cellular Response to CSE Exposure', *PLoS One*, 11(9), p. e0163182.

Bouron, A., Kiselyov, K. and Oberwinkler, J. (2015) 'Permeation, regulation and control of expression of TRP channels by trace metal ions', *Pflugers Arch*, 467(6), pp. 1143-64.

Buch, T.R., Schafer, E.A., Demmel, M.T., Boekhoff, I., Thiermann, H., Gudermann, T., Steinritz, D. and Schmidt, A. (2013) 'Functional expression of the transient receptor potential channel TRPA1, a sensor for toxic lung inhalants, in pulmonary epithelial cells', *Chem Biol Interact*, 206(3), pp. 462-71.

Burnett, D., Chamba, A., Hill, S.L. and Stockley, R.A. (1987) 'Neutrophils from subjects with chronic obstructive lung disease show enhanced chemotaxis and extracellular proteolysis', *Lancet*, 2(8567), pp. 1043-6.

Burns, D.M. (1991) 'Cigarettes and cigarette smoking', *Clin Chest Med*, 12(4), pp. 631-42.

Burns, M. and Valdivia, H. (2008) 'Modelling the limit of detection in real-time quantitative PCR', *European Food Research and Technology*, 226(6), pp. 1513-1524.

Caceres, A.I., Brackmann, M., Elia, M.D., Bessac, B.F., del Camino, D., D'Amours, M., Witek, J.S., Fanger, C.M., Chong, J.A., Hayward, N.J., Homer, R.J., Cohn, L., Huang, X., Moran, M.M. and Jordt, S.E. (2009) 'A sensory neuronal ion channel essential for airway inflammation and hyperreactivity in asthma', *Proc Natl Acad Sci U S A*, 106(22), pp. 9099-104.

Calverley, P.M., Rabe, K.F., Goehring, U.M., Kristiansen, S., Fabbri, L.M., Martinez, F.J., M and groups, M.s. (2009) 'Roflumilast in symptomatic chronic obstructive pulmonary disease: two randomised clinical trials', *Lancet*, 374(9691), pp. 685-94.

Calzetta, L., Page, C.P., Spina, D., Cazzola, M., Rogliani, P., Facciolo, F. and Matera, M.G. (2013) 'Effect of the mixed phosphodiesterase 3/4 inhibitor RPL554 on human isolated bronchial smooth muscle tone', *J Pharmacol Exp Ther*, 346(3), pp. 414-23.

Cantin, A.M., Bilodeau, G., Ouellet, C., Liao, J. and Hanrahan, J.W. (2006a) 'Oxidant stress suppresses CFTR expression', *Am J Physiol Cell Physiol*, 290(1), pp. C262-70.

Cantin, A.M., Hanrahan, J.W., Bilodeau, G., Ellis, L., Dupuis, A., Liao, J., Zielenski, J. and Durie, P. (2006b) 'Cystic fibrosis transmembrane conductance regulator function is suppressed in cigarette smokers', *Am J Respir Crit Care Med*, 173(10), pp. 1139-44.

Capiod, T. (2013) 'The need for calcium channels in cell proliferation', *Recent Pat Anticancer Drug Discov*, 8(1), pp. 4-17.

Caramori, G., Kirkham, P., Barczyk, A., Di Stefano, A. and Adcock, I. (2015) 'Molecular pathogenesis of cigarette smoking-induced stable COPD', *Ann N Y Acad Sci*, 1340, pp. 55-64.

Carnevali, S., Nakamura, Y., Mio, T., Liu, X., Takigawa, K., Romberger, D.J., Spurzem, J.R. and Rennard, S.I. (1998) 'Cigarette smoke extract inhibits fibroblast-mediated collagen gel contraction', *Am J Physiol*, 274(4), pp. L591-8.

Carnevali, S., Petruzzelli, S., Longoni, B., Vanacore, R., Barale, R., Cipollini, M., Scatena, F., Paggiaro, P., Celi, A. and Giuntini, C. (2003) 'Cigarette smoke extract induces oxidative stress and apoptosis in human lung fibroblasts', *Am J Physiol Lung Cell Mol Physiol*, 284(6), pp. L955-63.

Cazzola, M., Calzetta, L., Rogliani, P. and Matera, M.G. (2016) 'The discovery of roflumilast for the treatment of chronic obstructive pulmonary disease', *Expert Opin Drug Discov*, 11(7), pp. 733-44.

Centers for Disease Control and Prevention (2010) *How tobacco smoke causes disease: The biology and behavioral basis for smoking-attributable disease: A report of the surgeon general*.

Cheah, E.Y., Burcham, P.C., Mann, T.S. and Henry, P.J. (2014) 'Acrolein relaxes mouse isolated tracheal smooth muscle via a TRPA1-dependent mechanism', *Biochem Pharmacol*, 89(1), pp. 148-56.

Chen, H., Liao, K., Cui-Zhao, L., Qiang-Wen, F., Feng-Zeng, X., Ping-Wu, F., Liang-Guo, S. and Juan-Chen, Y. (2015) 'Cigarette smoke extract induces apoptosis of rat alveolar Type II cells via the PLTP/TGF-beta1/Smad2 pathway', *Int Immunopharmacol*, 28(1), pp. 707-14.

Chen, J. and Hackos, D.H. (2015) 'TRPA1 as a drug target--promise and challenges', *Naunyn Schmiedebergs Arch Pharmacol*, 388(4), pp. 451-63.

Chen, J. and Sanderson, M.J. (2017) 'Store-operated calcium entry is required for sustained contraction and Ca2+ oscillations of airway smooth muscle', *J Physiol*, 595(10), pp. 3203-3218.

Chen, L., Ge, Q., Tjin, G., Alkhouri, H., Deng, L., Brandsma, C.A., Adcock, I., Timens, W., Postma, D., Burgess, J.K., Black, J.L. and Oliver, B.G. (2014) 'Effects of cigarette smoke extract on human airway smooth muscle cells in COPD', *Eur Respir J*, 44(3), pp. 634-46.

Chen, T.X., Xu, X.Y., Zhao, Z., Zhao, F.Y., Gao, Y.M., Yan, X.H. and Wan, Y. (2017) 'Hydrogen peroxide is a critical regulator of the hypoxia-induced alterations of store-operated Ca(2+) entry into rat pulmonary arterial smooth muscle cells', *Am J Physiol Lung Cell Mol Physiol*, 312(4), pp. L477-L487.

Cheng, S.H., Gregory, R.J., Marshall, J., Paul, S., Souza, D.W., White, G.A., O'Riordan, C.R. and Smith, A.E. (1990) 'Defective intracellular transport and processing of CFTR is the molecular basis of most cystic fibrosis', *Cell*, 63(4), pp. 827-34.

Chiba, Y., Murata, M., Ushikubo, H., Yoshikawa, Y., Saitoh, A., Sakai, H., Kamei, J. and Misawa, M. (2005) 'Effect of cigarette smoke exposure in vivo on bronchial smooth muscle contractility in vitro in rats', *Am J Respir Cell Mol Biol*, 33(6), pp. 574-81.

Chow, J.Y., Estrema, C., Orneles, T., Dong, X., Barrett, K.E. and Dong, H. (2011) 'Calcium-sensing receptor modulates extracellular Ca(2+) entry via TRPC-encoded receptor-operated channels in human aortic smooth muscle cells', *Am J Physiol Cell Physiol*, 301(2), pp. C461-8.

Christensen, K.A., Myers, J.T. and Swanson, J.A. (2002) 'pH-dependent regulation of lysosomal calcium in macrophages', *J Cell Sci*, 115(Pt 3), pp. 599-607.

Clunes, L.A., Davies, C.M., Coakley, R.D., Aleksandrov, A.A., Henderson, A.G., Zeman, K.L., Worthington, E.N., Gentzsch, M., Kreda, S.M., Cholon, D., Bennett, W.D., Riordan, J.R., Boucher, R.C. and Tarran, R. (2012) 'Cigarette smoke exposure induces CFTR internalization and insolubility, leading to airway surface liquid dehydration', *FASEB J*, 26(2), pp. 533-45.

Collawn, J.F., Lazrak, A., Bebok, Z. and Matalon, S. (2012) 'The CFTR and ENaC debate: how important is ENaC in CF lung disease?', *Am J Physiol Lung Cell Mol Physiol*, 302(11), pp. L1141-6.

Conti, M.A. and Adelstein, R.S. (1981) 'The relationship between calmodulin binding and phosphorylation of smooth muscle myosin kinase by the catalytic subunit of 3':5' cAMP-dependent protein kinase', *J Biol Chem*, 256(7), pp. 3178-81.

Cook, D.P., Rector, M.V., Bouzek, D.C., Michalski, A.S., Gansemer, N.D., Reznikov, L.R., Li, X., Stroik, M.R., Ostedgaard, L.S., Abou Alaiwa, M.H., Thompson, M.A., Prakash, Y.S., Krishnan, R., Meyerholz, D.K., Seow, C.Y. and Stoltz, D.A. (2016) 'Cystic Fibrosis Transmembrane Conductance Regulator in Sarcoplasmic Reticulum of Airway Smooth Muscle. Implications for Airway Contractility', *Am J Respir Crit Care Med*, 193(4), pp. 417-26.

Courville, C.A., Tidwell, S., Liu, B., Accurso, F.J., Dransfield, M.T. and Rowe, S.M. (2014) 'Acquired defects in CFTR-dependent beta-adrenergic sweat secretion in chronic obstructive pulmonary disease', *Respir Res*, 15, p. 25.

Criddle, D.N., de Moura, R.S., Greenwood, I.A. and Large, W.A. (1996) 'Effect of niflumic acid on noradrenaline-induced contractions of the rat aorta', *Br J Pharmacol*, 118(4), pp. 1065-71.

Crotty Alexander, L.E., Shin, S. and Hwang, J.H. (2015) 'Inflammatory Diseases of the Lung Induced by Conventional Cigarette Smoke: A Review', *Chest*, 148(5), pp. 1307-1322.

Crystal, R.G., Randell, S.H., Engelhardt, J.F., Voynow, J. and Sunday, M.E. (2008) 'Airway epithelial cells: current concepts and challenges', *Proc Am Thorac Soc*, 5(7), pp. 772-7.

Dai, J.M., Kuo, K.H., Leo, J.M., Pare, P.D., van Breemen, C. and Lee, C.H. (2007) 'Acetylcholine-induced asynchronous calcium waves in intact human bronchial muscle bundle', *Am J Respir Cell Mol Biol*, 36(5), pp. 600-8.

Dai, J.M., Syyong, H., Navarro-Dorado, J., Redondo, S., Alonso, M., van Breemen, C. and Tejerina, T. (2010) 'A comparative study of alpha-adrenergic receptor mediated Ca(2+) signals and contraction in intact human and mouse vascular smooth muscle', *Eur J Pharmacol*, 629(1-3), pp. 82-8.

Dalemans, W., Barbry, P., Champigny, G., Jallat, S., Dott, K., Dreyer, D., Crystal, R.G., Pavirani, A., Lecocq, J.P. and Lazdunski, M. (1991) 'Altered chloride ion channel kinetics associated with the delta F508 cystic fibrosis mutation', *Nature*, 354(6354), pp. 526-8.

Dam, V.S., Boedtkjer, D.M., Nyvad, J., Aalkjaer, C. and Matchkov, V. (2014) 'TMEM16A knockdown abrogates two different Ca(2+)-activated Cl (-) currents and contractility of smooth muscle in rat mesenteric small arteries', *Pflugers Arch*, 466(7), pp. 1391-409.

Danielsson, J., Kuforiji, A.S., Yocum, G.T., Zhang, Y., Xu, D., Gallos, G. and Emala, C.W., Sr. (2020) 'Agonism of the TMEM16A calcium-activated chloride channel modulates airway smooth muscle tone', *Am J Physiol Lung Cell Mol Physiol*, 318(2), pp. L287-L295.

Danielsson, J., Perez-Zoghbi, J., Bernstein, K., Barajas, M.B., Zhang, Y., Kumar, S., Sharma, P.K., Gallos, G. and Emala, C.W. (2015) 'Antagonists of the TMEM16A calcium-activated chloride channel modulate airway smooth muscle tone and intracellular calcium', *Anesthesiology*, 123(3), pp. 569-81.

Danielsson, J., Yim, P., Rinderspacher, A., Fu, X.W., Zhang, Y., Landry, D.W. and Emala, C.W. (2014) 'Chloride channel blockade relaxes airway smooth muscle and potentiates relaxation by beta-agonists', *Am J Physiol Lung Cell Mol Physiol*, 307(3), pp. L273-82.

Davis, A.J., Forrest, A.S., Jepps, T.A., Valencik, M.L., Wiwchar, M., Singer, C.A., Sones, W.R., Greenwood, I.A. and Leblanc, N. (2010) 'Expression profile and protein translation of TMEM16A in murine smooth muscle', *Am J Physiol Cell Physiol*, 299(5), pp. C948-59.

de Boer, W.I., Alagappan, V.K. and Sharma, H.S. (2007) 'Molecular mechanisms in chronic obstructive pulmonary disease: potential targets for therapy', *Cell Biochem Biophys*, 47(1), pp. 131-48.

de Boer, W.I., Sont, J.K., van Schadewijk, A., Stolk, J., van Krieken, J.H. and Hiemstra, P.S. (2000) 'Monocyte chemoattractant protein 1, interleukin 8, and chronic airways inflammation in COPD', *J Pathol*, 190(5), pp. 619-26.

de Boer, W.I., van Schadewijk, A., Sont, J.K., Sharma, H.S., Stolk, J., Hiemstra, P.S. and van Krieken, J.H. (1998) 'Transforming growth factor beta1 and recruitment of macrophages and mast cells in airways in chronic obstructive pulmonary disease', *Am J Respir Crit Care Med*, 158(6), pp. 1951-7.

Dekhuijzen, P.N., Aben, K.K., Dekker, I., Aarts, L.P., Wielders, P.L., van Herwaarden, C.L. and Bast, A. (1996) 'Increased exhalation of hydrogen peroxide in patients with stable and

unstable chronic obstructive pulmonary disease', *Am J Respir Crit Care Med*, 154(3 Pt 1), pp. 813-6.

Demedts, I.K., Demoor, T., Bracke, K.R., Joos, G.F. and Brusselle, G.G. (2006a) 'Role of apoptosis in the pathogenesis of COPD and pulmonary emphysema', *Respir Res*, 7, p. 53.

Demedts, I.K., Morel-Montero, A., Lebecque, S., Pacheco, Y., Cataldo, D., Joos, G.F., Pauwels, R.A. and Brusselle, G.G. (2006b) 'Elevated MMP-12 protein levels in induced sputum from patients with COPD', *Thorax*, 61(3), pp. 196-201.

Deshpande, D.A., Dogan, S., Walseth, T.F., Miller, S.M., Amrani, Y., Panettieri, R.A. and Kannan, M.S. (2004) 'Modulation of calcium signaling by interleukin-13 in human airway smooth muscle: role of CD38/cyclic adenosine diphosphate ribose pathway', *Am J Respir Cell Mol Biol*, 31(1), pp. 36-42.

Deshpande, D.A., Walseth, T.F., Panettieri, R.A. and Kannan, M.S. (2003) 'CD38/cyclic ADP-ribose-mediated Ca2+ signaling contributes to airway smooth muscle hyper-responsiveness', *FASEB J*, 17(3), pp. 452-4.

Devor, D.C., Singh, A.K., Lambert, L.C., DeLuca, A., Frizzell, R.A. and Bridges, R.J. (1999) 'Bicarbonate and chloride secretion in Calu-3 human airway epithelial cells', *J Gen Physiol*, 113(5), pp. 743-60.

Di Stefano, A., Capelli, A., Lusuardi, M., Balbo, P., Vecchio, C., Maestrelli, P., Mapp, C.E., Fabbri, L.M., Donner, C.F. and Saetta, M. (1998) 'Severity of airflow limitation is associated with severity of airway inflammation in smokers', *Am J Respir Crit Care Med*, 158(4), pp. 1277-85.

Di Stefano, A., Turato, G., Maestrelli, P., Mapp, C.E., Ruggieri, M.P., Roggeri, A., Boschetto, P., Fabbri, L.M. and Saetta, M. (1996) 'Airflow limitation in chronic bronchitis is associated with T-lymphocyte and macrophage infiltration of the bronchial mucosa', *Am J Respir Crit Care Med*, 153(2), pp. 629-32.

Ding, K.H., Husain, S., Akhtar, R.A., Isales, C.M. and Abdel-Latif, A.A. (1997) 'Inhibition of muscarinic-stimulated polyphosphoinositide hydrolysis and Ca2+ mobilization in cat iris sphincter smooth muscle cells by cAMP-elevating agents', *Cell Signal*, 9(6), pp. 411-21.

Ding, S., Zhang, J., Yin, S., Lu, J., Hu, M., Du, J., Huang, J. and Shen, B. (2019) 'Inflammatory cytokines tumour necrosis factor-alpha and interleukin-8 enhance airway smooth muscle contraction by increasing L-type Ca(2+) channel expression', *Clin Exp Pharmacol Physiol*, 46(1), pp. 56-64.

Divangahi, M., Balghi, H., Danialou, G., Comtois, A.S., Demoule, A., Ernest, S., Haston, C., Robert, R., Hanrahan, J.W., Radzioch, D. and Petrof, B.J. (2009) 'Lack of CFTR in skeletal muscle predisposes to muscle wasting and diaphragm muscle pump failure in cystic fibrosis mice', *PLoS Genet*, 5(7), p. e1000586.

Domingue, J.C., Ao, M., Sarathy, J., George, A., Alrefai, W.A., Nelson, D.J. and Rao, M.C. (2014) 'HEK-293 cells expressing the cystic fibrosis transmembrane conductance regulator (CFTR): a model for studying regulation of Cl- transport', *Physiol Rep*, 2(9).

Dransfield, M.T., Wilhelm, A.M., Flanagan, B., Courville, C., Tidwell, S.L., Raju, S.V., Gaggar, A., Steele, C., Tang, L.P., Liu, B. and Rowe, S.M. (2013) 'Acquired cystic fibrosis transmembrane conductance regulator dysfunction in the lower airways in COPD', *Chest*, 144(2), pp. 498-506.

Drummond, M.B., Dasenbrook, E.C., Pitz, M.W., Murphy, D.J. and Fan, E. (2008) 'Inhaled corticosteroids in patients with stable chronic obstructive pulmonary disease: a systematic review and meta-analysis', *JAMA*, 300(20), pp. 2407-16.

Duan, D. (2009) 'Phenomics of cardiac chloride channels: the systematic study of chloride channel function in the heart', *J Physiol*, 587(Pt 10), pp. 2163-77.

Earley, S., Gonzales, A.L. and Crnich, R. (2009) 'Endothelium-dependent cerebral artery dilation mediated by TRPA1 and Ca2+-Activated K+ channels', *Circ Res*, 104(8), pp. 987-94.

Ebina, M., Yaegashi, H., Chiba, R., Takahashi, T., Motomiya, M. and Tanemura, M. (1990) 'Hyperreactive site in the airway tree of asthmatic patients revealed by thickening of bronchial muscles. A morphometric study', *Am Rev Respir Dis*, 141(5 Pt 1), pp. 1327-32.

Eid, S.R., Crown, E.D., Moore, E.L., Liang, H.A., Choong, K.C., Dima, S., Henze, D.A., Kane, S.A. and Urban, M.O. (2008) 'HC-030031, a TRPA1 selective antagonist, attenuates inflammatory- and neuropathy-induced mechanical hypersensitivity', *Mol Pain*, 4, p. 48.

Eisner, M.D., Anthonisen, N., Coultas, D., Kuenzli, N., Perez-Padilla, R., Postma, D., Romieu, I., Silverman, E.K., Balmes, J.R., Committee on Nonsmoking Copd, E. and Occupational Health, A. (2010) 'An official American Thoracic Society public policy statement: Novel risk factors and the global burden of chronic obstructive pulmonary disease', *Am J Respir Crit Care Med*, 182(5), pp. 693-718.

Eldridge, A., Betson, T.R., Gama, M.V. and McAdam, K. (2015) 'Variation in tobacco and mainstream smoke toxicant yields from selected commercial cigarette products', *Regul Toxicol Pharmacol*, 71(3), pp. 409-27.

Erle, D.J. and Sheppard, D. (2014) 'The cell biology of asthma', *J Cell Biol*, 205(5), pp. 621-31.

Evans, J.H. and Sanderson, M.J. (1999) 'Intracellular calcium oscillations regulate ciliary beat frequency of airway epithelial cells', *Cell Calcium*, 26(3-4), pp. 103-10.

Fabbri, L.M., Calverley, P.M., Izquierdo-Alonso, J.L., Bundschuh, D.S., Brose, M., Martinez, F.J., Rabe, K.F., M and groups, M.s. (2009) 'Roflumilast in moderate-to-severe chronic obstructive pulmonary disease treated with longacting bronchodilators: two randomised clinical trials', *Lancet*, 374(9691), pp. 695-703.

Facchinetti, F., Amadei, F., Geppetti, P., Tarantini, F., Di Serio, C., Dragotto, A., Gigli, P.M., Catinella, S., Civelli, M. and Patacchini, R. (2007) 'Alpha,beta-unsaturated aldehydes in cigarette smoke release inflammatory mediators from human macrophages', *Am J Respir Cell Mol Biol*, 37(5), pp. 617-23.

Finlay, G.A., O'Driscoll, L.R., Russell, K.J., D'Arcy, E.M., Masterson, J.B., FitzGerald, M.X. and O'Connor, C.M. (1997) 'Matrix metalloproteinase expression and production by alveolar macrophages in emphysema', *Am J Respir Crit Care Med*, 156(1), pp. 240-7.

Flores-Soto, E., Reyes-Garcia, J., Sommer, B. and Montano, L.M. (2013) 'Sarcoplasmic reticulum Ca(2+) refilling is determined by L-type Ca(2+) and store operated Ca(2+) channels in guinea pig airway smooth muscle', *Eur J Pharmacol*, 721(1-3), pp. 21-8.

Frisch, S.M. and Screaton, R.A. (2001) 'Anoikis mechanisms', *Curr Opin Cell Biol*, 13(5), pp. 555-62.

Fullerton, D.G., Bruce, N. and Gordon, S.B. (2008) 'Indoor air pollution from biomass fuel smoke is a major health concern in the developing world', *Trans R Soc Trop Med Hyg*, 102(9), pp. 843-51.

Furukawa, T., Yamakawa, T., Midera, T., Sagawa, T., Mori, Y. and Nukada, T. (1999) 'Selectivities of dihydropyridine derivatives in blocking Ca(2+) channel subtypes expressed in Xenopus oocytes', *J Pharmacol Exp Ther*, 291(2), pp. 464-73.

Gadsby, D.C., Nagel, G. and Hwang, T.C. (1995) 'The CFTR chloride channel of mammalian heart', *Annu Rev Physiol*, 57, pp. 387-416.

Gallos, G., Remy, K.E., Danielsson, J., Funayama, H., Fu, X.W., Chang, H.Y., Yim, P., Xu, D. and Emala, C.W., Sr. (2013) 'Functional expression of the TMEM16 family of calcium-activated chloride channels in airway smooth muscle', *Am J Physiol Lung Cell Mol Physiol*, 305(9), pp. L625-34.

Ganesan, S., Comstock, A.T. and Sajjan, U.S. (2013) 'Barrier function of airway tract epithelium', *Tissue Barriers*, 1(4), p. e24997.

Gensch, E., Gallup, M., Sucher, A., Li, D., Gebremichael, A., Lemjabbar, H., Mengistab, A., Dasari, V., Hotchkiss, J., Harkema, J. and Basbaum, C. (2004) 'Tobacco smoke control of mucin production in lung cells requires oxygen radicals AP-1 and JNK', *J Biol Chem*, 279(37), pp. 39085-93.

Gerthoffer, W.T. (2008) 'Migration of airway smooth muscle cells', *Proc Am Thorac Soc*, 5(1), pp. 97-105.

Gessner, C., Scheibe, R., Wotzel, M., Hammerschmidt, S., Kuhn, H., Engelmann, L., Hoheisel, G., Gillissen, A., Sack, U. and Wirtz, H. (2005) 'Exhaled breath condensate cytokine patterns in chronic obstructive pulmonary disease', *Respir Med*, 99(10), pp. 1229-40.

Ghorani, V., Boskabady, M.H., Khazdair, M.R. and Kianmeher, M. (2017) 'Experimental animal models for COPD: a methodological review', *Tob Induc Dis*, 15, p. 25.

GOLD (2020) *Global Strategy for the Diagnosis, Management, and Prevention of Chronic Obstructive Lung Disease, Global Initiative for Chronic Obstructive Lung Disease*. [Online]. Available at: http://www.goldcopd.org/.

Gordon, S.B., Bruce, N.G., Grigg, J., Hibberd, P.L., Kurmi, O.P., Lam, K.B., Mortimer, K., Asante, K.P., Balakrishnan, K., Balmes, J., Bar-Zeev, N., Bates, M.N., Breysse, P.N., Buist, S., Chen, Z., Havens, D., Jack, D., Jindal, S., Kan, H., Mehta, S., Moschovis, P., Naeher, L., Patel, A., Perez-Padilla, R., Pope, D., Rylance, J., Semple, S. and Martin, W.J., 2nd (2014) 'Respiratory risks from household air pollution in low and middle income countries', *Lancet Respir Med*, 2(10), pp. 823-60.

Gorlach, A., Bertram, K., Hudecova, S. and Krizanova, O. (2015) 'Calcium and ROS: A mutual interplay', *Redox Biol*, 6, pp. 260-271.

Gosling, M., Poll, C. and Li, S. (2005) 'TRP channels in airway smooth muscle as therapeutic targets', *Naunyn Schmiedebergs Arch Pharmacol*, 371(4), pp. 277-84.

Gould, B., Hornung, R., Mann, S., Subramanian, V.B. and Raftery, E. (1983) 'Nifedipine or verapamil as sole treatment of hypertension. An intraarterial study', *Hypertension*, 5(4_pt_2), p. II91.

Govindaraju, V., Michoud, M.C., Ferraro, P., Arkinson, J., Safka, K., Valderrama-Carvajal, H. and Martin, J.G. (2008) 'The effects of interleukin-8 on airway smooth muscle contraction in cystic fibrosis', *Respir Res*, 9, p. 76.

Grace, M.S., Baxter, M., Dubuis, E., Birrell, M.A. and Belvisi, M.G. (2014) 'Transient receptor potential (TRP) channels in the airway: role in airway disease', *Br J Pharmacol*, 171(10), pp. 2593-607.

Grynkiewicz, G., Poenie, M. and Tsien, R.Y. (1985) 'A new generation of Ca2+ indicators with greatly improved fluorescence properties', *J Biol Chem*, 260(6), pp. 3440-50.

Guan, P., Cai, W., Yu, H., Wu, Z., Li, W., Wu, J., Chen, J. and Feng, G. (2017) 'Cigarette smoke extract promotes proliferation of airway smooth muscle cells through suppressing C/EBP-alpha expression', *Exp Ther Med*, 13(4), pp. 1408-1414.

Gunter, T.E. and Pfeiffer, D.R. (1990) 'Mechanisms by which mitochondria transport calcium', *Am J Physiol*, 258(5 Pt 1), pp. C755-86.

Guo, J.J., Stoltz, D.A., Zhu, V., Volk, K.A., Segar, J.L., McCray, P.B., Jr. and Roghair, R.D. (2014) 'Genotype-specific alterations in vascular smooth muscle cell function in cystic fibrosis piglets', *J Cyst Fibros*, 13(3), pp. 251-9.

Gupta, V., Khan, A., Higham, A., Lemon, J., Sriskantharajah, S., Amour, A., Hessel, E.M., Southworth, T. and Singh, D. (2016) 'The effect of phosphatidylinositol-3 kinase inhibition on matrix metalloproteinase-9 and reactive oxygen species release from chronic obstructive pulmonary disease neutrophils', *Int Immunopharmacol*, 35, pp. 155-162.

Gutierrez-Martin, Y., Martin-Romero, F.J., Inesta-Vaquera, F.A., Gutierrez-Merino, C. and Henao, F. (2004) 'Modulation of sarcoplasmic reticulum Ca(2+)-ATPase by chronic and acute exposure to peroxynitrite', *Eur J Biochem*, 271(13), pp. 2647-57.

Hajna, Z., Cseko, K., Kemeny, A., Kereskai, L., Kiss, T., Perkecz, A., Szitter, I., Kocsis, B., Pinter, E. and Helyes, Z. (2020) 'Complex Regulatory Role of the TRPA1 Receptor in Acute and Chronic Airway Inflammation Mouse Models', *Int J Mol Sci*, 21(11).

Halls, M.L. and Cooper, D.M. (2011) 'Regulation by Ca2+-signaling pathways of adenylyl cyclases', *Cold Spring Harb Perspect Biol*, 3(1), p. a004143.

Haq, I.J., Gray, M.A., Garnett, J.P., Ward, C. and Brodlie, M. (2016) 'Airway surface liquid homeostasis in cystic fibrosis: pathophysiology and therapeutic targets', *Thorax*, 71(3), pp. 284-7.

Hardaker, E.L., Bacon, A.M., Carlson, K., Roshak, A.K., Foley, J.J., Schmidt, D.B., Buckley, P.T., Comegys, M., Panettieri, R.A., Jr., Sarau, H.M. and Belmonte, K.E. (2004) 'Regulation of TNF-alpha- and IFN-gamma-induced CXCL10 expression: participation of the airway smooth muscle in the pulmonary inflammatory response in chronic obstructive pulmonary disease', *FASEB J*, 18(1), pp. 191-3.

Hatipoglu, U. and Stoller, J.K. (2016) 'alpha1-Antitrypsin Deficiency', *Clin Chest Med*, 37(3), pp. 487-504.

Hawkins, B.J., Irrinki, K.M., Mallilankaraman, K., Lien, Y.C., Wang, Y., Bhanumathy, C.D., Subbiah, R., Ritchie, M.F., Soboloff, J., Baba, Y., Kurosaki, T., Joseph, S.K., Gill, D.L. and Madesh, M. (2010) 'S-glutathionylation activates STIM1 and alters mitochondrial homeostasis', *J Cell Biol*, 190(3), pp. 391-405.

Heber, S. and Fischer, M.J.M. (2019) 'Non-Analgesic Symptomatic or Disease-Modifying Potential of TRPA1', *Med Sci (Basel)*, 7(10).

Heijink, I.H., Brandenburg, S.M., Postma, D.S. and van Oosterhout, A.J. (2012) 'Cigarette smoke impairs airway epithelial barrier function and cell-cell contact recovery', *Eur Respir J*, 39(2), pp. 419-28.

Hemmer, J.D., Dean, D., Vertegel, A., Langan, E., 3rd and LaBerge, M. (2008) 'Effects of serum deprivation on the mechanical properties of adherent vascular smooth muscle cells', *Proc Inst Mech Eng H*, 222(5), pp. 761-72.

Henke, N., Albrecht, P., Bouchachia, I., Ryazantseva, M., Knoll, K., Lewerenz, J., Kaznacheyeva, E., Maher, P. and Methner, A. (2013) 'The plasma membrane channel ORAI1 mediates detrimental calcium influx caused by endogenous oxidative stress', *Cell Death Dis*, 4, p. e470.

Herman, M. and Tarran, R. (2020) 'E-cigarettes, nicotine, the lung and the brain: multi-level cascading pathophysiology', *J Physiol*.

Hiemstra, P.S. and Bals, R. (2016) 'Basic science of electronic cigarettes: assessment in cell culture and in vivo models', *Respir Res*, 17(1), p. 127.

Higenbottam, T., Feyeraband, C. and Clark, T.J. (1980) 'Cigarette smoke inhalation and the acute airway response', *Thorax*, 35(4), pp. 246-54.

Hinman, A., Chuang, H.H., Bautista, D.M. and Julius, D. (2006) 'TRP channel activation by reversible covalent modification', *Proc Natl Acad Sci U S A*, 103(51), pp. 19564-8.

Hirota, S., Helli, P. and Janssen, L.J. (2007a) 'Ionic mechanisms and Ca2+ handling in airway smooth muscle', *Eur Respir J*, 30(1), pp. 114-33.

Hirota, S., Pertens, E. and Janssen, L.J. (2007b) 'The reverse mode of the Na(+)/Ca(2+) exchanger provides a source of Ca(2+) for store refilling following agonist-induced Ca(2+) mobilization', *Am J Physiol Lung Cell Mol Physiol*, 292(2), pp. L438-47.

Hirota, S., Trimble, N., Pertens, E. and Janssen, L.J. (2006) 'Intracellular Cl- fluxes play a novel role in Ca2+ handling in airway smooth muscle', *Am J Physiol Lung Cell Mol Physiol*, 290(6), pp. L1146-53.

Hogg, J.C., Chu, F., Utokaparch, S., Woods, R., Elliott, W.M., Buzatu, L., Cherniack, R.M., Rogers, R.M., Sciurba, F.C., Coxson, H.O. and Pare, P.D. (2004) 'The nature of small-airway obstruction in chronic obstructive pulmonary disease', *N Engl J Med*, 350(26), pp. 2645-53.

Holzmann, C., Kilch, T., Kappel, S., Dorr, K., Jung, V., Stockle, M., Bogeski, I. and Peinelt, C. (2015) 'Differential Redox Regulation of Ca(2)(+) Signaling and Viability in Normal and Malignant Prostate Cells', *Biophys J*, 109(7), pp. 1410-9.

Hong, W., Peng, G., Hao, B., Liao, B., Zhao, Z., Zhou, Y., Peng, F., Ye, X., Huang, L., Zheng, M., Pu, J., Liang, C., Yi, E., Peng, H., Li, B. and Ran, P. (2017) 'Nicotine-Induced Airway Smooth Muscle Cell Proliferation Involves TRPC6-Dependent Calcium Influx Via alpha7 nAChR', *Cell Physiol Biochem*, 43(3), pp. 986-1002.

Hooper, R., Burney, P., Vollmer, W.M., McBurnie, M.A., Gislason, T., Tan, W.C., Jithoo, A., Kocabas, A., Welte, T. and Buist, A.S. (2012) 'Risk factors for COPD spirometrically defined from the lower limit of normal in the BOLD project', *Eur Respir J*, 39(6), pp. 1343-53.

Hoshino, Y., Mio, T., Nagai, S., Miki, H., Ito, I. and Izumi, T. (2001) 'Cytotoxic effects of cigarette smoke extract on an alveolar type II cell-derived cell line', *Am J Physiol Lung Cell Mol Physiol*, 281(2), pp. L509-16.

Hotta, K., Emala, C.W. and Hirshman, C.A. (1999) 'TNF-alpha upregulates Gialpha and Gqalpha protein expression and function in human airway smooth muscle cells', *Am J Physiol*, 276(3), pp. L405-11.

Hox, V., Vanoirbeek, J.A., Alpizar, Y.A., Voedisch, S., Callebaut, I., Bobic, S., Sharify, A., De Vooght, V., Van Gerven, L., Devos, F., Liston, A., Voets, T., Vennekens, R., Bullens, D.M., De Vries, A., Hoet, P., Braun, A., Ceuppens, J.L., Talavera, K., Nemery, B. and Hellings, P.W. (2013) 'Crucial role of transient receptor potential ankyrin 1 and mast cells in

induction of nonallergic airway hyperreactivity in mice', *Am J Respir Crit Care Med*, 187(5), pp. 486-93.

Huang, F., Zhang, H., Wu, M., Yang, H., Kudo, M., Peters, C.J., Woodruff, P.G., Solberg, O.D., Donne, M.L., Huang, X., Sheppard, D., Fahy, J.V., Wolters, P.J., Hogan, B.L., Finkbeiner, W.E., Li, M., Jan, Y.N., Jan, L.Y. and Rock, J.R. (2012) 'Calcium-activated chloride channel TMEM16A modulates mucin secretion and airway smooth muscle contraction', *Proc Natl Acad Sci U S A*, 109(40), pp. 16354-9.

Hussey, J., Gormley, J., Leen, G. and Greally, P. (2002) 'Peripheral muscle strength in young males with cystic fibrosis', *J Cyst Fibros*, 1(3), pp. 116-21.

Hwang, T.C. and Sheppard, D.N. (2009) 'Gating of the CFTR Cl- channel by ATP-driven nucleotide-binding domain dimerisation', *J Physiol*, 587(Pt 10), pp. 2151-61.

Hybiske, K., Fu, Z., Schwarzer, C., Tseng, J., Do, J., Huang, N. and Machen, T.E. (2007) 'Effects of cystic fibrosis transmembrane conductance regulator and DeltaF508CFTR on inflammatory response, ER stress, and Ca2+ of airway epithelia', *Am J Physiol Lung Cell Mol Physiol*, 293(5), pp. L1250-60.

Ihn, H. (2002) 'Pathogenesis of fibrosis: role of TGF-beta and CTGF', *Curr Opin Rheumatol*, 14(6), pp. 681-5.

Imai, K., Dalal, S.S., Chen, E.S., Downey, R., Schulman, L.L., Ginsburg, M. and D'Armiento, J. (2001) 'Human collagenase (matrix metalloproteinase-1) expression in the lungs of patients with emphysema', *Am J Respir Crit Care Med*, 163(3 Pt 1), pp. 786-91.

International Organization for Standardization (2012) *ISO 3308:2012 Routine analytical cigarette-smoking machine — Definitions and standard conditions*. Switzerland.

Ishikawa, J., Ohga, K., Yoshino, T., Takezawa, R., Ichikawa, A., Kubota, H. and Yamada, T. (2003) 'A pyrazole derivative, YM-58483, potently inhibits store-operated sustained Ca2+ influx and IL-2 production in T lymphocytes', *J Immunol*, 170(9), pp. 4441-9.

Jacquot, J., Maizieres, M., Spilmont, C., Millot, J.M., Sebille, S., Merten, M., Kammouni, W. and Manfait, M. (1996) 'Intracellular free Ca2+ dynamic changes to histamine are reduced in cystic fibrosis human tracheal gland cells', *FEBS Lett*, 386(2-3), pp. 123-7.

James, A.F., Sabirov, R.Z. and Okada, Y. (2010) 'Clustering of protein kinase A-dependent CFTR chloride channels in the sarcolemma of guinea-pig ventricular myocytes', *Biochem Biophys Res Commun*, 391(1), pp. 841-5.

Jansen, H.M., Sachs, A.P. and van Alphen, L. (1995) 'Predisposing conditions to bacterial infections in chronic obstructive pulmonary disease', *Am J Respir Crit Care Med*, 151(6), pp. 2073-80.

Janssen, L.J. (2002) 'Ionic mechanisms and Ca(2+) regulation in airway smooth muscle contraction: do the data contradict dogma?', *Am J Physiol Lung Cell Mol Physiol*, 282(6), pp. L1161-78.

Janssen, L.J. (2012) 'Airway smooth muscle electrophysiology in a state of flux?', *Am J Physiol Lung Cell Mol Physiol*, 302(8), pp. L730-2.

Janssen, L.J., Tazzeo, T. and Zuo, J. (2004) 'Enhanced myosin phosphatase and Ca(2+)-uptake mediate adrenergic relaxation of airway smooth muscle', *Am J Respir Cell Mol Biol*, 30(4), pp. 548-54.

Jha, A., Sharma, P., Anaparti, V., Ryu, M.H. and Halayko, A.J. (2015) 'A role for transient receptor potential ankyrin 1 cation channel (TRPA1) in airway hyper-responsiveness?', *Can J Physiol Pharmacol*, 93(3), pp. 171-6.

Jia, Y., Wang, X., Varty, L., Rizzo, C.A., Yang, R., Correll, C.C., Phelps, P.T., Egan, R.W. and Hey, J.A. (2004) 'Functional TRPV4 channels are expressed in human airway smooth muscle cells', *Am J Physiol Lung Cell Mol Physiol*, 287(2), pp. L272-8.

Jiang, K., Jiao, S., Vitko, M., Darrah, R., Flask, C.A., Hodges, C.A. and Yu, X. (2016) 'The impact of Cystic Fibrosis Transmembrane Regulator Disruption on cardiac function and stress response', *J Cyst Fibros*, 15(1), pp. 34-42.

Jiang, Y., Zhou, Y., Peng, G., Tian, H., Pan, D., Liu, L., Yang, X., Li, C., Li, W., Chen, L., Ran, P. and Dai, A. (2019) 'TRPC channels mediated calcium entry is required for proliferation of human airway smooth muscle cells induced by nicotine-nAChR', *Biochimie*, 158, pp. 139-148.

Jin, X., Shah, S., Du, X., Zhang, H. and Gamper, N. (2016) 'Activation of Ca(2+) -activated Cl(-) channel ANO1 by localized Ca(2+) signals', *J Physiol*, 594(1), pp. 19-30.

Jones, R.L., Noble, P.B., Elliot, J.G. and James, A.L. (2016) 'Airway remodelling in COPD: It's not asthma!', *Respirology*, 21(8), pp. 1347-1356.

Jung, M., Davis, W.P., Taatjes, D.J., Churg, A. and Mossman, B.T. (2000) 'Asbestos and cigarette smoke cause increased DNA strand breaks and necrosis in bronchiolar epithelial cells in vivo', *Free Radic Biol Med*, 28(8), pp. 1295-9.

Kaji, D.M. (1990) 'Nifedipine Inhibits Calcium-Activated K-Transport in Human Erythrocytes', *American Journal of Physiology*, 259(2), pp. C332-C339.

Kanazawa, H. and Yoshikawa, J. (2005) 'Elevated oxidative stress and reciprocal reduction of vascular endothelial growth factor levels with severity of COPD', *Chest*, 128(5), pp. 3191-7.

Kang, M.J., Oh, Y.M., Lee, J.C., Kim, D.G., Park, M.J., Lee, M.G., Hyun, I.G., Han, S.K., Shim, Y.S. and Jung, K.S. (2003) 'Lung matrix metalloproteinase-9 correlates with cigarette smoking and obstruction of airflow', *J Korean Med Sci*, 18(6), pp. 821-7.

Keatings, V.M., Collins, P.D., Scott, D.M. and Barnes, P.J. (1996) 'Differences in interleukin-8 and tumor necrosis factor-alpha in induced sputum from patients with chronic obstructive pulmonary disease or asthma', *Am J Respir Crit Care Med*, 153(2), pp. 530-4.

Kelly, M., Trudel, S., Brouillard, F., Bouillaud, F., Colas, J., Nguyen-Khoa, T., Ollero, M., Edelman, A. and Fritsch, J. (2010) 'Cystic fibrosis transmembrane regulator inhibitors CFTR(inh)-172 and GlyH-101 target mitochondrial functions, independently of chloride channel inhibition', *J Pharmacol Exp Ther*, 333(1), pp. 60-9.

Kerem, B., Rommens, J.M., Buchanan, J.A., Markiewicz, D., Cox, T.K., Chakravarti, A., Buchwald, M. and Tsui, L.C. (1989) 'Identification of the cystic fibrosis gene: genetic analysis', *Science*, 245(4922), pp. 1073-80.

Kim, H., Liu, X., Kobayashi, T., Conner, H., Kohyama, T., Wen, F.Q., Fang, Q., Abe, S., Bitterman, P. and Rennard, S.I. (2004) 'Reversible cigarette smoke extract-induced DNA damage in human lung fibroblasts', *Am J Respir Cell Mol Biol*, 31(5), pp. 483-90.

Kitaguchi, Y., Taraseviciene-Stewart, L., Hanaoka, M., Natarajan, R., Kraskauskas, D. and Voelkel, N.F. (2012) 'Acrolein induces endoplasmic reticulum stress and causes airspace enlargement', *PLoS One*, 7(5), p. e38038.

Kitamura, K. and Yamazaki, J. (2001) 'Chloride channels and their functional roles in smooth muscle tone in the vasculature', *Jpn J Pharmacol*, 85(4), pp. 351-7.

Koivisto, A., Jalava, N., Bratty, R. and Pertovaara, A. (2018) 'TRPA1 Antagonists for Pain Relief', *Pharmaceuticals (Basel)*, 11(4).

Koller, A., Schlossmann, J., Ashman, K., Uttenweiler-Joseph, S., Ruth, P. and Hofmann, F. (2003) 'Association of phospholamban with a cGMP kinase signaling complex', *Biochem Biophys Res Commun*, 300(1), pp. 155-60.

Kranenburg, A.R., Willems-Widyastuti, A., Moori, W.J., Sterk, P.J., Alagappan, V.K., de Boer, W.I. and Sharma, H.S. (2006) 'Enhanced bronchial expression of extracellular matrix proteins in chronic obstructive pulmonary disease', *Am J Clin Pathol*, 126(5), pp. 725-35.

Kreindler, J.L., Jackson, A.D., Kemp, P.A., Bridges, R.J. and Danahay, H. (2005) 'Inhibition of chloride secretion in human bronchial epithelial cells by cigarette smoke extract', *Am J Physiol Lung Cell Mol Physiol*, 288(5), pp. L894-902.

Kubo, M. and Okada, Y. (1992) 'Volume-regulatory Cl- channel currents in cultured human epithelial cells', *J Physiol*, 456, pp. 351-71.

Kubo, S., Kobayashi, M., Masunaga, Y., Ishii, H., Hirano, Y., Takahashi, K. and Shimizu, Y. (2005) 'Cytokine and chemokine expression in cigarette smoke-induced lung injury in guinea pigs', *Eur Respir J*, 26(6), pp. 993-1001.

Kumosani, T.A., Elshal, M.F., Al-Jonaid, A.A. and Abduljabar, H.S. (2008) 'The influence of smoking on semen quality, seminal microelements and Ca2+-ATPase activity among infertile and fertile men', *Clin Biochem*, 41(14-15), pp. 1199-203.

Kuwano, K., Bosken, C.H., Pare, P.D., Bai, T.R., Wiggs, B.R. and Hogg, J.C. (1993) 'Small airways dimensions in asthma and in chronic obstructive pulmonary disease', *Am Rev Respir Dis*, 148(5), pp. 1220-5.

Kuzumoto, M., Takeuchi, A., Nakai, H., Oka, C., Noma, A. and Matsuoka, S. (2008) 'Simulation analysis of intracellular Na+ and Cl- homeostasis during beta 1-adrenergic stimulation of cardiac myocyte', *Prog Biophys Mol Biol*, 96(1-3), pp. 171-86.

Lader, A.S., Wang, Y., Jackson, G.R., Jr., Borkan, S.C. and Cantiello, H.F. (2000) 'cAMP-activated anion conductance is associated with expression of CFTR in neonatal mouse cardiac myocytes', *Am J Physiol Cell Physiol*, 278(2), pp. C436-50.

Lamb, F.S. and Barna, T.J. (1998) 'Chloride ion currents contribute functionally to norepinephrine-induced vascular contraction', *Am J Physiol*, 275(1), pp. H151-60.

Lambert, J.A., Raju, S.V., Tang, L.P., McNicholas, C.M., Li, Y., Courville, C.A., Farris, R.F., Coricor, G.E., Smoot, L.H., Mazur, M.M., Dransfield, M.T., Bolger, G.B. and Rowe, S.M. (2014) 'Cystic fibrosis transmembrane conductance regulator activation by roflumilast contributes to therapeutic benefit in chronic bronchitis', *Am J Respir Cell Mol Biol*, 50(3), pp. 549-58.

Lamhonwah, A.M., Bear, C.E., Huan, L.J., Kim Chiaw, P., Ackerley, C.A. and Tein, I. (2010) 'Cystic fibrosis transmembrane conductance regulator in human muscle: Dysfunction causes abnormal metabolic recovery in exercise', *Ann Neurol*, 67(6), pp. 802-8.

Leblanc, N., Ledoux, J., Saleh, S., Sanguinetti, A., Angermann, J., O'Driscoll, K., Britton, F., Perrino, B.A. and Greenwood, I.A. (2005) 'Regulation of calcium-activated chloride channels in smooth muscle cells: a complex picture is emerging', *Can J Physiol Pharmacol*, 83(7), pp. 541-56.

Lee, H., Park, J.R., Kim, E.J., Kim, W.J., Hong, S.H., Park, S.M. and Yang, S.R. (2016) 'Cigarette smoke-mediated oxidative stress induces apoptosis via the MAPKs/STAT1 pathway in mouse lung fibroblasts', *Toxicol Lett*, 240(1), pp. 140-8.

Lee, R.J. and Foskett, J.K. (2010) 'cAMP-activated Ca2+ signaling is required for CFTR-mediated serous cell fluid secretion in porcine and human airways', *J Clin Invest*, 120(9), pp. 3137-48.

Lewis, R.S. (2020) 'Store-Operated Calcium Channels: From Function to Structure and Back Again', *Cold Spring Harb Perspect Biol*, 12(5).

Li, J., McKeown, L., Ojelabi, O., Stacey, M., Foster, R., O'Regan, D., Porter, K.E. and Beech, D.J. (2011) 'Nanomolar potency and selectivity of a Ca(2)(+) release-activated Ca(2)(+) channel inhibitor against store-operated Ca(2)(+) entry and migration of vascular smooth muscle cells', *Br J Pharmacol*, 164(2), pp. 382-93.

Liesker, J.J., Ten Hacken, N.H., Zeinstra-Smith, M., Rutgers, S.R., Postma, D.S. and Timens, W. (2009) 'Reticular basement membrane in asthma and COPD: similar thickness, yet different composition', *Int J Chron Obstruct Pulmon Dis*, 4, pp. 127-35.

Lin, A.H., Liu, M.H., Ko, H.K., Perng, D.W., Lee, T.S. and Kou, Y.R. (2015) 'Lung Epithelial TRPA1 Transduces the Extracellular ROS into Transcriptional Regulation of Lung

Inflammation Induced by Cigarette Smoke: The Role of Influxed Ca(2)(+)', *Mediators Inflamm*, 2015, p. 148367.

Lin, X., Yang, C., Huang, L., Chen, M., Shi, J., Ouyang, L., Tang, T., Zhang, W., Li, Y., Liang, R. and Jiang, S. (2016) 'Upregulation of TRPM7 augments cell proliferation and interleukin-8 release in airway smooth muscle cells of rats exposed to cigarette smoke', *Mol Med Rep*, 13(6), pp. 4995-5004.

Liu, A.N., Mohammed, A.Z., Rice, W.R., Fiedeldey, D.T., Liebermann, J.S., Whitsett, J.A., Braciale, T.J. and Enelow, R.I. (1999) 'Perforin-independent CD8(+) T-cell-mediated cytotoxicity of alveolar epithelial cells is preferentially mediated by tumor necrosis factor-alpha: relative insensitivity to Fas ligand', *Am J Respir Cell Mol Biol*, 20(5), pp. 849-58.

Livak, K.J. and Schmittgen, T.D. (2001) 'Analysis of relative gene expression data using real-time quantitative PCR and the 2(-Delta Delta C(T)) Method', *Methods*, 25(4), pp. 402-8.

Ma, T., Thiagarajah, J.R., Yang, H., Sonawane, N.D., Folli, C., Galietta, L.J. and Verkman, A.S. (2002) 'Thiazolidinone CFTR inhibitor identified by high-throughput screening blocks cholera toxin-induced intestinal fluid secretion', *J Clin Invest*, 110(11), pp. 1651-8.

Ma, X., Wang, Y. and Stephens, N.L. (1998) 'Serum deprivation induces a unique hypercontractile phenotype of cultured smooth muscle cells', *Am J Physiol*, 274(5 Pt 1), pp. C1206-14.

MacDonald, K.D., McKenzie, K.R. and Zeitlin, P.L. (2007) 'Cystic fibrosis transmembrane regulator protein mutations: 'class' opportunity for novel drug innovation', *Paediatr Drugs*, 9(1), pp. 1-10.

MacLennan, D.H. and Kranias, E.G. (2003) 'Phospholamban: a crucial regulator of cardiac contractility', *Nat Rev Mol Cell Biol*, 4(7), pp. 566-77.

Macpherson, L.J., Dubin, A.E., Evans, M.J., Marr, F., Schultz, P.G., Cravatt, B.F. and Patapoutian, A. (2007) 'Noxious compounds activate TRPA1 ion channels through covalent modification of cysteines', *Nature*, 445(7127), pp. 541-5.

Maher, S., Birrell, M., Bonvini, S., Wortley, M., Dubuis, E., Shala, F., Jones, V., Flajolet, P., Negreskul, Y. and Britton, Z. (2015) 'Beneficial effects of menthol are mediated via a TRPM8-independent mechanism'. Eur Respiratory Soc.

Mahn, K., Ojo, O.O., Chadwick, G., Aaronson, P.I., Ward, J.P. and Lee, T.H. (2010) 'Ca(2+) homeostasis and structural and functional remodelling of airway smooth muscle in asthma', *Thorax*, 65(6), pp. 547-52.

Mall, M., Kreda, S.M., Mengos, A., Jensen, T.J., Hirtz, S., Seydewitz, H.H., Yankaskas, J., Kunzelmann, K., Riordan, J.R. and Boucher, R.C. (2004) 'The DeltaF508 mutation results in loss of CFTR function and mature protein in native human colon', *Gastroenterology*, 126(1), pp. 32-41.

Marklew, A.J., Patel, W., Moore, P.J., Tan, C.D., Smith, A.J., Sassano, M.F., Gray, M.A. and Tarran, R. (2019) 'Cigarette Smoke Exposure Induces Retrograde Trafficking of CFTR to the Endoplasmic Reticulum', *Sci Rep*, 9(1), p. 13655.

Marsh, B.J., Fryer, A.D., Jacoby, D.B. and Drake, M.G. (2020) 'Transient receptor potential ankyrin-1 causes rapid bronchodilation via nonepithelial PGE2', *Am J Physiol Lung Cell Mol Physiol*, 318(5), pp. L943-L952.

Martins, J.R., Kongsuphol, P., Sammels, E., Dahimene, S., Aldehni, F., Clarke, L.A., Schreiber, R., de Smedt, H., Amaral, M.D. and Kunzelmann, K. (2011) 'F508del-CFTR increases intracellular Ca(2+) signaling that causes enhanced calcium-dependent Cl(-) conductance in cystic fibrosis', *Biochim Biophys Acta*, 1812(11), pp. 1385-92.

Mayer, A.S. and Newman, L.S. (2001) 'Genetic and environmental modulation of chronic obstructive pulmonary disease', *Respir Physiol*, 128(1), pp. 3-11.

McDermott, M. and Collins, M.M. (1965) 'Acute effects of smoking on lung airways resistance in normal and bronchitic subjects', *Thorax*, 20(6), pp. 562-9.

McGraw, D.W., Fogel, K.M., Kong, S., Litonjua, A.A., Kranias, E.G., Aronow, B.J. and Liggett, S.B. (2006) 'Transcriptional response to persistent beta2-adrenergic receptor signaling reveals regulation of phospholamban, which alters airway contractility', *Physiol Genomics*, 27(2), pp. 171-7.

McGuinness, A.J. and Sapey, E. (2017) 'Oxidative Stress in COPD: Sources, Markers, and Potential Mechanisms', *J Clin Med*, 6(2).

McNamara, C.R., Mandel-Brehm, J., Bautista, D.M., Siemens, J., Deranian, K.L., Zhao, M., Hayward, N.J., Chong, J.A., Julius, D., Moran, M.M. and Fanger, C.M. (2007) 'TRPA1 mediates formalin-induced pain', *Proc Natl Acad Sci U S A*, 104(33), pp. 13525-30.

Melis, N., Tauc, M., Cougnon, M., Bendahhou, S., Giuliano, S., Rubera, I. and Duranton, C. (2014) 'Revisiting CFTR inhibition: a comparative study of CFTRinh -172 and GlyH-101 inhibitors', *Br J Pharmacol*, 171(15), pp. 3716-27.

Michaeloudes, C., Kuo, C.H., Haji, G., Finch, D.K., Halayko, A.J., Kirkham, P., Chung, K.F., Adcock, I.M. and Copdmap (2017) 'Metabolic re-patterning in COPD airway smooth muscle cells', *Eur Respir J*, 50(5).

Michoud, M.C., Robert, R., Hassan, M., Moynihan, B., Haston, C., Govindaraju, V., Ferraro, P., Hanrahan, J.W. and Martin, J.G. (2009) 'Role of the cystic fibrosis transmembrane conductance channel in human airway smooth muscle', *Am J Respir Cell Mol Biol*, 40(2), pp. 217-22.

Middleton, P.G., Mall, M.A., Drevinek, P., Lands, L.C., McKone, E.F., Polineni, D., Ramsey, B.W., Taylor-Cousar, J.L., Tullis, E., Vermeulen, F., Marigowda, G., McKee, C.M., Moskowitz, S.M., Nair, N., Savage, J., Simard, C., Tian, S., Waltz, D., Xuan, F., Rowe, S.M., Jain, R. and Group, V.X.S. (2019) 'Elexacaftor-Tezacaftor-Ivacaftor for Cystic Fibrosis with a Single Phe508del Allele', *N Engl J Med*, 381(19), pp. 1809-1819.

Miglino, N., Roth, M., Lardinois, D., Sadowski, C., Tamm, M. and Borger, P. (2012) 'Cigarette smoke inhibits lung fibroblast proliferation by translational mechanisms', *Eur Respir J*, 39(3), pp. 705-11.

Miner, K., Labitzke, K., Liu, B., Wang, P., Henckels, K., Gaida, K., Elliott, R., Chen, J.J., Liu, L., Leith, A., Trueblood, E., Hensley, K., Xia, X.Z., Homann, O., Bennett, B., Fiorino, M., Whoriskey, J., Yu, G., Escobar, S., Wong, M., Born, T.L., Budelsky, A., Comeau, M., Smith, D., Phillips, J., Johnston, J.A., McGivern, J.G., Weikl, K., Powers, D., Kunzelmann, K., Mohn, D., Hochheimer, A. and Sullivan, J.K. (2019) 'Drug Repurposing: The Anthelmintics Niclosamide and Nitazoxanide Are Potent TMEM16A Antagonists That Fully Bronchodilate Airways', *Front Pharmacol*, 10, p. 51.

Mio, T., Romberger, D.J., Thompson, A.B., Robbins, R.A., Heires, A. and Rennard, S.I. (1997) 'Cigarette smoke induces interleukin-8 release from human bronchial epithelial cells', *Am J Respir Crit Care Med*, 155(5), pp. 1770-6.

Miravitlles, M., Vogelmeier, C., Roche, N., Halpin, D., Cardoso, J., Chuchalin, A.G., Kankaanranta, H., Sandstrom, T., Sliwinski, P., Zatloukal, J. and Blasi, F. (2016) 'A review of national guidelines for management of COPD in Europe', *Eur Respir J*, 47(2), pp. 625-37.

Mitchell, I., Corey, M., Woenne, R., Krastins, I.R. and Levison, H. (1978) 'Bronchial hyperreactivity in cystic fibrosis and asthma', *J Pediatr*, 93(5), pp. 744-8.

Miyashita, L. and Foley, G. (2020) 'E-cigarettes and respiratory health: the latest evidence', *J Physiol*.

Molet, S., Belleguic, C., Lena, H., Germain, N., Bertrand, C.P., Shapiro, S.D., Planquois, J.M., Delaval, P. and Lagente, V. (2005) 'Increase in macrophage elastase (MMP-12) in lungs from patients with chronic obstructive pulmonary disease', *Inflamm Res*, 54(1), pp. 31-6.

Montoro, D.T., Haber, A.L., Biton, M., Vinarsky, V., Lin, B., Birket, S.E., Yuan, F., Chen, S., Leung, H.M., Villoria, J., Rogel, N., Burgin, G., Tsankov, A.M., Waghray, A., Slyper, M., Waldman, J., Nguyen, L., Dionne, D., Rozenblatt-Rosen, O., Tata, P.R., Mou, H., Shivaraju, M., Bihler, H., Mense, M., Tearney, G.J., Rowe, S.M., Engelhardt, J.F., Regev, A. and Rajagopal, J. (2018) 'A revised airway epithelial hierarchy includes CFTR-expressing ionocytes', *Nature*, 560(7718), pp. 319-324.

Muanprasat, C., Sonawane, N.D., Salinas, D., Taddei, A., Galietta, L.J. and Verkman, A.S. (2004) 'Discovery of glycine hydrazide pore-occluding CFTR inhibitors: mechanism, structure-activity analysis, and in vivo efficacy', *J Gen Physiol*, 124(2), pp. 125-37.

Mukhopadhyay, I., Kulkarni, A., Aranake, S., Karnik, P., Shetty, M., Thorat, S., Ghosh, I., Wale, D., Bhosale, V. and Khairatkar-Joshi, N. (2014) 'Transient receptor potential ankyrin 1 receptor activation in vitro and in vivo by pro-tussive agents: GRC 17536 as a promising anti-tussive therapeutic', *PLoS One*, 9(5), p. e97005.

Mukhopadhyay, I., Kulkarni, A. and Khairatkar-Joshi, N. (2016) 'Blocking TRPA1 in Respiratory Disorders: Does It Hold a Promise?', *Pharmaceuticals (Basel)*, 9(4).

Nagel, G., Hwang, T.C., Nastiuk, K.L., Nairn, A.C. and Gadsby, D.C. (1992) 'The protein kinase A-regulated cardiac Cl- channel resembles the cystic fibrosis transmembrane conductance regulator', *Nature*, 360(6399), pp. 81-4.

Nakamura, Y., Romberger, D.J., Tate, L., Ertl, R.F., Kawamoto, M., Adachi, Y., Mio, T., Sisson, J.H., Spurzem, J.R. and Rennard, S.I. (1995) 'Cigarette smoke inhibits lung fibroblast proliferation and chemotaxis', *Am J Respir Crit Care Med*, 151(5), pp. 1497-503.

Namkung, W., Thiagarajah, J.R., Phuan, P.W. and Verkman, A.S. (2010) 'Inhibition of Ca2+-activated Cl- channels by gallotannins as a possible molecular basis for health benefits of red wine and green tea', *FASEB J*, 24(11), pp. 4178-86.

Nassini, R., Pedretti, P., Moretto, N., Fusi, C., Carnini, C., Facchinetti, F., Viscomi, A.R., Pisano, A.R., Stokesberry, S., Brunmark, C., Svitacheva, N., McGarvey, L., Patacchini, R., Damholt, A.B., Geppetti, P. and Materazzi, S. (2012) 'Transient receptor potential ankyrin 1 channel localized to non-neuronal airway cells promotes non-neurogenic inflammation', *PLoS One*, 7(8), p. e42454.

Nelson, M.T., Conway, M.A., Knot, H.J. and Brayden, J.E. (1997) 'Chloride channel blockers inhibit myogenic tone in rat cerebral arteries', *J Physiol*, 502 (Pt 2), pp. 259-64.

Nie, Y., Huang, C., Zhong, S., Wortley, M.A., Luo, Y., Luo, W., Xie, Y., Lai, K. and Zhong, N. (2016) 'Cigarette smoke extract (CSE) induces transient receptor potential ankyrin 1(TRPA1) expression via activation of HIF1alphain A549 cells', *Free Radic Biol Med*, 99, pp. 498-507.

Ning, W., Dong, Y., Sun, J., Li, C., Matthay, M.A., Feghali-Bostwick, C.A. and Choi, A.M. (2007) 'Cigarette smoke stimulates matrix metalloproteinase-2 activity via EGR-1 in human lung fibroblasts', *Am J Respir Cell Mol Biol*, 36(4), pp. 480-90.

Nobukuni, S., Watanabe, K., Inoue, J., Wen, F.Q., Tamaru, N. and Yoshida, M. (2002) 'Cigarette smoke inhibits the growth of lung fibroblasts from patients with pulmonary emphysema', *Respirology*, 7(3), pp. 217-23.

Nogueira, L., Trisko, B.M., Lima-Rosa, F.L., Jackson, J., Lund-Palau, H., Yamaguchi, M. and Breen, E.C. (2018) 'Cigarette smoke directly impairs skeletal muscle function through capillary regression and altered myofiber calcium kinetics in mice', *J Physiol*.

Noguera, A., Batle, S., Miralles, C., Iglesias, J., Busquets, X., MacNee, W. and Agusti, A.G. (2001) 'Enhanced neutrophil response in chronic obstructive pulmonary disease', *Thorax*, 56(6), pp. 432-7.

Nolan, T., Hands, R.E. and Bustin, S.A. (2006) 'Quantification of mRNA using real-time RT-PCR', *Nat Protoc*, 1(3), pp. 1559-82.

Norez, C., Antigny, F., Becq, F. and Vandebrouck, C. (2006) 'Maintaining low Ca2+ level in the endoplasmic reticulum restores abnormal endogenous F508del-CFTR trafficking in airway epithelial cells', *Traffic*, 7(5), pp. 562-73.

Norez, C., Jayle, C., Becq, F. and Vandebrouck, C. (2014) 'Bronchorelaxation of the human bronchi by CFTR activators', *Pulm Pharmacol Ther*, 27(1), pp. 38-43.

Oltmanns, U., Chung, K.F., Walters, M., John, M. and Mitchell, J.A. (2005) 'Cigarette smoke induces IL-8, but inhibits eotaxin and RANTES release from airway smooth muscle', *Respir Res*, 6, p. 74.

Owen, C.A. (2005) 'Proteinases and oxidants as targets in the treatment of chronic obstructive pulmonary disease', *Proc Am Thorac Soc*, 2(4), pp. 373-85; discussion 394-5.

Owen, C.A. (2008) 'Roles for proteinases in the pathogenesis of chronic obstructive pulmonary disease', *Int J Chron Obstruct Pulmon Dis*, 3(2), pp. 253-68.

Page, C.P. and Spina, D. (2012) 'Selective PDE inhibitors as novel treatments for respiratory diseases', *Curr Opin Pharmacol*, 12(3), pp. 275-86.

Pande, J. and Grover, A.K. (2014) 'Effects of Reactive Oxygen Species on Sarco-/Endoplasmic Reticulum Ca2+ Pump in Pig Coronary Artery', in Laher, I. (ed.) *Systems Biology of Free Radicals and Antioxidants*. Berlin, Heidelberg: Springer Berlin Heidelberg, pp. 1077-1090.

Panettieri, R.A., Jr. (2001) 'Isolation and culture of human airway smooth muscle cells', *Methods Mol Med*, 56, pp. 155-60.

Paone, G., Conti, V., Vestri, A., Leone, A., Puglisi, G., Benassi, F., Brunetti, G., Schmid, G., Cammarella, I. and Terzano, C. (2011) 'Analysis of sputum markers in the evaluation of lung inflammation and functional impairment in symptomatic smokers and COPD patients', *Dis Markers*, 31(2), pp. 91-100.

Paradiso, A.M., Ribeiro, C.M. and Boucher, R.C. (2001) 'Polarized signaling via purinoceptors in normal and cystic fibrosis airway epithelia', *J Gen Physiol*, 117(1), pp. 53-67.

Parameswaran, K., Willems-Widyastuti, A., Alagappan, V.K., Radford, K., Kranenburg, A.R. and Sharma, H.S. (2006) 'Role of extracellular matrix and its regulators in human airway smooth muscle biology', *Cell Biochem Biophys*, 44(1), pp. 139-46.

Parekh, A.B. (2010) 'Store-operated CRAC channels: function in health and disease', *Nat Rev Drug Discov*, 9(5), pp. 399-410.

Pasyk, E.A. and Foskett, J.K. (1995) 'Mutant (delta F508) cystic fibrosis transmembrane conductance regulator Cl- channel is functional when retained in endoplasmic reticulum of mammalian cells', *J Biol Chem*, 270(21), pp. 12347-50.

Patel, W., Moore, P.J., Sassano, M.F., Lopes-Pacheco, M., Aleksandrov, A.A., Amaral, M.D., Tarran, R. and Gray, M.A. (2019) 'Increases in cytosolic Ca(2+) induce dynamin- and calcineurin-dependent internalisation of CFTR', *Cell Mol Life Sci*, 76(5), pp. 977-994.

Pei, Z., Zhuang, Z., Sang, H., Wu, Z., Meng, R., He, E.Y., Scott, G.I., Maris, J.R., Li, R. and Ren, J. (2014) 'alpha,beta-Unsaturated aldehyde crotonaldehyde triggers cardiomyocyte contractile dysfunction: role of TRPV1 and mitochondrial function', *Pharmacol Res*, 82, pp. 40-50.

Pera, T., Gosens, R., Lesterhuis, A.H., Sami, R., van der Toorn, M., Zaagsma, J. and Meurs, H. (2010) 'Cigarette smoke and lipopolysaccharide induce a proliferative airway smooth muscle phenotype', *Respir Res*, 11, p. 48.

Perez, J.F. and Sanderson, M.J. (2005) 'The frequency of calcium oscillations induced by 5-HT, ACH, and KCl determine the contraction of smooth muscle cells of intrapulmonary bronchioles', *J Gen Physiol*, 125(6), pp. 535-53.

Petersen, O.H., Courjaret, R. and Machaca, K. (2017) 'Ca(2+) tunnelling through the ER lumen as a mechanism for delivering Ca(2+) entering via store-operated Ca(2+) channels to specific target sites', *J Physiol*, 595(10), pp. 2999-3014.

Philippe, R., Antigny, F., Buscaglia, P., Norez, C., Becq, F., Frieden, M. and Mignen, O. (2015) 'SERCA and PMCA pumps contribute to the deregulation of Ca2+ homeostasis in human CF epithelial cells', *Biochim Biophys Acta*, 1853(5), pp. 892-903.

Pillsbury, H.C., Bright, C.C., O'Connor, K.J. and Irish, F.W. (1969) 'Tar and Nicotine in Cigarette Smoke', *Journal of Association of Official Analytical Chemists*, 52(3), pp. 458-462.

Pini, L., Pinelli, V., Modina, D., Bezzi, M., Tiberio, L. and Tantucci, C. (2014) 'Central airways remodeling in COPD patients', *Int J Chron Obstruct Pulmon Dis*, 9, pp. 927-32.

Plasschaert, L.W., Zilionis, R., Choo-Wing, R., Savova, V., Knehr, J., Roma, G., Klein, A.M. and Jaffe, A.B. (2018) 'A single-cell atlas of the airway epithelium reveals the CFTR-rich pulmonary ionocyte', *Nature*, 560(7718), pp. 377-381.

Pollock, N.S., Kargacin, M.E. and Kargacin, G.J. (1998) 'Chloride channel blockers inhibit Ca2+ uptake by the smooth muscle sarcoplasmic reticulum', *Biophys J*, 75(4), pp. 1759-66.

Pozsgai, G., Bodkin, J.V., Graepel, R., Bevan, S., Andersson, D.A. and Brain, S.D. (2010) 'Evidence for the pathophysiological relevance of TRPA1 receptors in the cardiovascular system in vivo', *Cardiovasc Res*, 87(4), pp. 760-8.

Prakash, Y.S. (2016) 'Emerging concepts in smooth muscle contributions to airway structure and function: implications for health and disease', *Am J Physiol Lung Cell Mol Physiol*, 311(6), pp. L1113-L1140.

Prakash, Y.S., van der Heijden, H.F., Kannan, M.S. and Sieck, G.C. (1997) 'Effects of salbutamol on intracellular calcium oscillations in porcine airway smooth muscle', *J Appl Physiol (1985)*, 82(6), pp. 1836-43.

Prakriya, M. and Lewis, R.S. (2015) 'Store-Operated Calcium Channels', *Physiol Rev*, 95(4), pp. 1383-436.

Prandini, P., De Logu, F., Fusi, C., Provezza, L., Nassini, R., Montagner, G., Materazzi, S., Munari, S., Gilioli, E., Bezzerri, V., Finotti, A., Lampronti, I., Tamanini, A., Dechecchi, M.C., Lippi, G., Ribeiro, C.M., Rimessi, A., Pinton, P., Gambari, R., Geppetti, P. and Cabrini, G. (2016) 'Transient Receptor Potential Ankyrin 1 Channels Modulate Inflammatory Response in Respiratory Cells from Patients with Cystic Fibrosis', *Am J Respir Cell Mol Biol*, 55(5), pp. 645-656.

Prokopczyk, B., Hoffmann, D., Bologna, M., Cunningham, A.J., Trushin, N., Akerkar, S., Boyiri, T., Amin, S., Desai, D., Colosimo, S., Pittman, B., Leder, G., Ramadani, M., Henne-Bruns, D., Beger, H.G. and El-Bayoumy, K. (2002) 'Identification of tobacco-derived compounds in human pancreatic juice', *Chem Res Toxicol*, 15(5), pp. 677-85.

Pryor, W.A. (1992) 'Biological effects of cigarette smoke, wood smoke, and the smoke from plastics: the use of electron spin resonance', *Free Radic Biol Med*, 13(6), pp. 659-76.

Rabe, K.F. (2010) 'Roflumilast for the treatment of chronic obstructive pulmonary disease', *Expert Rev Respir Med*, 4(5), pp. 543-55.

Raemdonck, K., de Alba, J., Birrell, M.A., Grace, M., Maher, S.A., Irvin, C.G., Fozard, J.R., O'Byrne, P.M. and Belvisi, M.G. (2012) 'A role for sensory nerves in the late asthmatic response', *Thorax*, 67(1), pp. 19-25.

Ragland, M.F., Benway, C.J., Lutz, S.M., Bowler, R.P., Hecker, J., Hokanson, J.E., Crapo, J.D., Castaldi, P.J., DeMeo, D.L., Hersh, C.P., Hobbs, B.D., Lange, C., Beaty, T.H., Cho, M.H. and Silverman, E.K. (2019) 'Genetic Advances in Chronic Obstructive Pulmonary Disease. Insights from COPDGene', *Am J Respir Crit Care Med*, 200(6), pp. 677-690.

Rahman, I., Morrison, D., Donaldson, K. and MacNee, W. (1996) 'Systemic oxidative stress in asthma, COPD, and smokers', *Am J Respir Crit Care Med*, 154(4 Pt 1), pp. 1055-60.

Raicu, M. and Florea, S. (2001) 'Deleterious effects of nifedipine on smooth muscle cells implies alterations of intracellular calcium signaling', *Fundam Clin Pharmacol*, 15(6), pp. 387-92.

Raju, S.V., Jackson, P.L., Courville, C.A., McNicholas, C.M., Sloane, P.A., Sabbatini, G., Tidwell, S., Tang, L.P., Liu, B., Fortenberry, J.A., Jones, C.W., Boydston, J.A., Clancy, J.P., Bowen, L.E., Accurso, F.J., Blalock, J.E., Dransfield, M.T. and Rowe, S.M. (2013) 'Cigarette smoke induces systemic defects in cystic fibrosis transmembrane conductance regulator function', *Am J Respir Crit Care Med*, 188(11), pp. 1321-30.

Raju, S.V., Lin, V.Y., Liu, L., McNicholas, C.M., Karki, S., Sloane, P.A., Tang, L., Jackson, P.L., Wang, W., Wilson, L., Macon, K.J., Mazur, M., Kappes, J.C., DeLucas, L.J., Barnes, S., Kirk, K., Tearney, G.J. and Rowe, S.M. (2017a) 'The Cystic Fibrosis Transmembrane Conductance Regulator Potentiator Ivacaftor Augments Mucociliary Clearance Abrogating Cystic Fibrosis Transmembrane Conductance Regulator Inhibition by Cigarette Smoke', *Am J Respir Cell Mol Biol*, 56(1), pp. 99-108.

Raju, S.V., Rasmussen, L., Sloane, P.A., Tang, L.P., Libby, E.F. and Rowe, S.M. (2017b) 'Roflumilast reverses CFTR-mediated ion transport dysfunction in cigarette smoke-exposed mice', *Respir Res*, 18(1), p. 173.

Randell, S.H., Fulcher, M.L., O'Neal, W. and Olsen, J.C. (2011) 'Primary epithelial cell models for cystic fibrosis research', *Methods Mol Biol*, 742, pp. 285-310.

Rasmussen, J.E., Sheridan, J.T., Polk, W., Davies, C.M. and Tarran, R. (2014) 'Cigarette smoke-induced Ca2+ release leads to cystic fibrosis transmembrane conductance regulator (CFTR) dysfunction', *J Biol Chem*, 289(11), pp. 7671-81.

Reinlib, L., Jefferson, D.J., Marini, F.C. and Donowitz, M. (1992) 'Abnormal secretagogue-induced intracellular free Ca2+ regulation in cystic fibrosis nasal epithelial cells', *Proc Natl Acad Sci U S A*, 89(7), pp. 2955-9.

Rennard, S.I., Togo, S. and Holz, O. (2006) 'Cigarette smoke inhibits alveolar repair: a mechanism for the development of emphysema', *Proc Am Thorac Soc*, 3(8), pp. 703-8.

Retamales, I., Elliott, W.M., Meshi, B., Coxson, H.O., Pare, P.D., Sciurba, F.C., Rogers, R.M., Hayashi, S. and Hogg, J.C. (2001) 'Amplification of inflammation in emphysema and its association with latent adenoviral infection', *Am J Respir Crit Care Med*, 164(3), pp. 469-73.

Ribeiro, C.M., Paradiso, A.M., Carew, M.A., Shears, S.B. and Boucher, R.C. (2005a) 'Cystic fibrosis airway epithelial Ca2+ i signaling: the mechanism for the larger agonist-mediated Ca2+ i signals in human cystic fibrosis airway epithelia', *J Biol Chem*, 280(11), pp. 10202-9.

Ribeiro, C.M., Paradiso, A.M., Schwab, U., Perez-Vilar, J., Jones, L., O'Neal, W. and Boucher, R.C. (2005b) 'Chronic airway infection/inflammation induces a Ca2+i-dependent hyperinflammatory response in human cystic fibrosis airway epithelia', *J Biol Chem*, 280(18), pp. 17798-806.

Riordan, J.R., Rommens, J.M., Kerem, B., Alon, N., Rozmahel, R., Grzelczak, Z., Zielenski, J., Lok, S., Plavsic, N., Chou, J.L. and et al. (1989) 'Identification of the cystic fibrosis gene: cloning and characterization of complementary DNA', *Science*, 245(4922), pp. 1066-73.

Rizzo, C.A., Yang, R., Greenfeder, S., Egan, R.W., Pauwels, R.A. and Hey, J.A. (2002) 'The IL-5 receptor on human bronchus selectively primes for hyperresponsiveness', *J Allergy Clin Immunol*, 109(3), pp. 404-9.

Robert, R., Norez, C. and Becq, F. (2005) 'Disruption of CFTR chloride channel alters mechanical properties and cAMP-dependent Cl- transport of mouse aortic smooth muscle cells', *J Physiol*, 568(Pt 2), pp. 483-95.

Robert, R., Savineau, J.P., Norez, C., Becq, F. and Guibert, C. (2007) 'Expression and function of cystic fibrosis transmembrane conductance regulator in rat intrapulmonary arteries', *Eur Respir J*, 30(5), pp. 857-64.

Robert, R., Thoreau, V., Norez, C., Cantereau, A., Kitzis, A., Mettey, Y., Rogier, C. and Becq, F. (2004) 'Regulation of the cystic fibrosis transmembrane conductance regulator channel by beta-adrenergic agonists and vasoactive intestinal peptide in rat smooth muscle cells and its role in vasorelaxation', *J Biol Chem*, 279(20), pp. 21160-8.

Robison, P., Sussan, T.E., Chen, H., Biswal, S., Schneider, M.F. and Hernandez-Ochoa, E.O. (2017) 'Impaired calcium signaling in muscle fibers from intercostal and foot skeletal muscle in a cigarette smoke-induced mouse model of COPD', *Muscle Nerve*, 56(2), pp. 282-291.

Rosenberg, S.R. and Kalhan, R. (2017) 'Recent advances in the management of chronic obstructive pulmonary disease', *F1000Res*, 6, p. 863.

Rossi, A., Khirani, S. and Cazzola, M. (2008) 'Long-acting beta2-agonists (LABA) in chronic obstructive pulmonary disease: efficacy and safety', *Int J Chron Obstruct Pulmon Dis*, 3(4), pp. 521-9.

Roux, E., Hyvelin, J.M., Savineau, J.P. and Marthan, R. (1998) 'Calcium signaling in airway smooth muscle cells is altered by in vitro exposure to the aldehyde acrolein', *Am J Respir Cell Mol Biol*, 19(3), pp. 437-44.

Rowell, T.R. and Tarran, R. (2015) 'Will chronic e-cigarette use cause lung disease?', *Am J Physiol Lung Cell Mol Physiol*, 309(12), pp. L1398-409.

Russell, R.E., Culpitt, S.V., DeMatos, C., Donnelly, L., Smith, M., Wiggins, J. and Barnes, P.J. (2002) 'Release and activity of matrix metalloproteinase-9 and tissue inhibitor of metalloproteinase-1 by alveolar macrophages from patients with chronic obstructive pulmonary disease', *Am J Respir Cell Mol Biol*, 26(5), pp. 602-9.

Saetta, M., Ghezzo, H., Kim, W.D., King, M., Angus, G.E., Wang, N.S. and Cosio, M.G. (1985) 'Loss of alveolar attachments in smokers. A morphometric correlate of lung function impairment', *Am Rev Respir Dis*, 132(4), pp. 894-900.

Saetta, M., Turato, G., Baraldo, S., Zanin, A., Braccioni, F., Mapp, C.E., Maestrelli, P., Cavallesco, G., Papi, A. and Fabbri, L.M. (2000) 'Goblet cell hyperplasia and epithelial inflammation in peripheral airways of smokers with both symptoms of chronic bronchitis and chronic airflow limitation', *Am J Respir Crit Care Med*, 161(3 Pt 1), pp. 1016-21.

Saetta, M., Turato, G., Facchini, F.M., Corbino, L., Lucchini, R.E., Casoni, G., Maestrelli, P., Mapp, C.E., Ciaccia, A. and Fabbri, L.M. (1997) 'Inflammatory cells in the bronchial glands of smokers with chronic bronchitis', *Am J Respir Crit Care Med*, 156(5), pp. 1633-9.

Sailland, J., Grosche, A., Baumlin, N., Dennis, J.S., Schmid, A., Krick, S. and Salathe, M. (2017) 'Role of Smad3 and p38 Signalling in Cigarette Smoke-induced CFTR and BK dysfunction in Primary Human Bronchial Airway Epithelial Cells', *Sci Rep*, 7(1), p. 10506.

Saint-Criq, V. and Gray, M.A. (2017) 'Role of CFTR in epithelial physiology', *Cell Mol Life Sci*, 74(1), pp. 93-115.

Sakamoto, H., Kawasaki, M., Uchida, S., Sasaki, S. and Marumo, F. (1996) 'Identification of a new outwardly rectifying Cl- channel that belongs to a subfamily of the ClC Cl- channels', *J Biol Chem*, 271(17), pp. 10210-6.

Samanta, K. and Parekh, A.B. (2017) 'Spatial Ca(2+) profiling: decrypting the universal cytosolic Ca(2+) oscillation', *J Physiol*, 595(10), pp. 3053-3062.

Sassano, M.F., Ghosh, A. and Tarran, R. (2017) 'Tobacco Smoke Constituents Trigger Cytoplasmic Calcium Release', *Appl In Vitro Toxicol*, 3(2), pp. 193-198.

Sathish, V., Freeman, M.R., Long, E., Thompson, M.A., Pabelick, C.M. and Prakash, Y.S. (2015) 'Cigarette Smoke and Estrogen Signaling in Human Airway Smooth Muscle', *Cell Physiol Biochem*, 36(3), pp. 1101-15.

Sathish, V., Thompson, M.A., Bailey, J.P., Pabelick, C.M., Prakash, Y.S. and Sieck, G.C. (2009) 'Effect of proinflammatory cytokines on regulation of sarcoplasmic reticulum Ca2+ reuptake in human airway smooth muscle', *Am J Physiol Lung Cell Mol Physiol*, 297(1), pp. L26-34.

Schmid, A., Baumlin, N., Ivonnet, P., Dennis, J.S., Campos, M., Krick, S. and Salathe, M. (2015) 'Roflumilast partially reverses smoke-induced mucociliary dysfunction', *Respir Res*, 16, p. 135.

Schmidlin, F., Scherrer, D., Daeffler, L., Bertrand, C., Landry, Y. and Gies, J.P. (1998) 'Interleukin-1beta induces bradykinin B2 receptor gene expression through a prostanoid cyclic AMP-dependent pathway in human bronchial smooth muscle cells', *Mol Pharmacol*, 53(6), pp. 1009-15.

Schroeder, B.C., Cheng, T., Jan, Y.N. and Jan, L.Y. (2008) 'Expression cloning of TMEM16A as a calcium-activated chloride channel subunit', *Cell*, 134(6), pp. 1019-29.

Sellers, Z.M., De Arcangelis, V., Xiang, Y. and Best, P.M. (2010) 'Cardiomyocytes with disrupted CFTR function require CaMKII and Ca(2+)-activated Cl(-) channel activity to maintain contraction rate', *J Physiol*, 588(Pt 13), pp. 2417-29.

Sethi, S. (2000) 'Bacterial infection and the pathogenesis of COPD', *Chest*, 117(5 Suppl 1), pp. 286S-91S.

Seys, L.J., Verhamme, F.M., Dupont, L.L., Desauter, E., Duerr, J., Seyhan Agircan, A., Conickx, G., Joos, G.F., Brusselle, G.G., Mall, M.A. and Bracke, K.R. (2015) 'Airway Surface Dehydration Aggravates Cigarette Smoke-Induced Hallmarks of COPD in Mice', *PLoS One*, 10(6), p. e0129897.

Shao, M.X., Nakanaga, T. and Nadel, J.A. (2004) 'Cigarette smoke induces MUC5AC mucin overproduction via tumor necrosis factor-alpha-converting enzyme in human airway epithelial (NCI-H292) cells', *Am J Physiol Lung Cell Mol Physiol*, 287(2), pp. L420-7.

Sharma, R., Yellowley, C.E., Civelek, M., Ainslie, K., Hodgson, L., Tarbell, J.M. and Donahue, H.J. (2002) 'Intracellular calcium changes in rat aortic smooth muscle cells in response to fluid flow', *Ann Biomed Eng*, 30(3), pp. 371-8.

Shaw, L., O'Neill, S., Jones, C.J., Austin, C. and Taggart, M.J. (2004) 'Comparison of U46619-, endothelin-1- or phenylephrine-induced changes in cellular Ca2+ profiles and Ca2+ sensitisation of constriction of pressurised rat resistance arteries', *Br J Pharmacol*, 141(4), pp. 678-88.

Shen, B.Q., Finkbeiner, W.E., Wine, J.J., Mrsny, R.J. and Widdicombe, J.H. (1994) 'Calu-3: a human airway epithelial cell line that shows cAMP-dependent Cl- secretion', *Am J Physiol*, 266(5 Pt 1), pp. L493-501.

Sheppard, D.N. and Welsh, M.J. (1992) 'Effect of ATP-sensitive K+ channel regulators on cystic fibrosis transmembrane conductance regulator chloride currents', *J Gen Physiol*, 100(4), pp. 573-91.

Shim, J.J., Dabbagh, K., Ueki, I.F., Dao-Pick, T., Burgel, P.R., Takeyama, K., Tam, D.C. and Nadel, J.A. (2001) 'IL-13 induces mucin production by stimulating epidermal growth factor receptors and by activating neutrophils', *Am J Physiol Lung Cell Mol Physiol*, 280(1), pp. L134-40.

Shore, S.A. and Moore, P.E. (2003) 'Regulation of beta-adrenergic responses in airway smooth muscle', *Respir Physiol Neurobiol*, 137(2-3), pp. 179-95.

Sieck, G.C., Dogan, M., Young-Soo, H., Osorio Valencia, S. and Delmotte, P. (2019) 'Mechanisms underlying TNFalpha-induced enhancement of force generation in airway smooth muscle', *Physiol Rep*, 7(17), p. e14220.

Sloane, P.A., Shastry, S., Wilhelm, A., Courville, C., Tang, L.P., Backer, K., Levin, E., Raju, S.V., Li, Y., Mazur, M., Byan-Parker, S., Grizzle, W., Sorscher, E.J., Dransfield, M.T. and Rowe, S.M. (2012) 'A pharmacologic approach to acquired cystic fibrosis transmembrane conductance regulator dysfunction in smoking related lung disease', *PLoS One*, 7(6), p. e39809.

Smirnova, M.G., Birchall, J.P. and Pearson, J.P. (2000) 'TNF-alpha in the regulation of MUC5AC secretion: some aspects of cytokine-induced mucin hypersecretion on the in vitro model', *Cytokine*, 12(11), pp. 1732-6.

Smith, B.A., Tolloczko, B., Martin, J.G. and Grutter, P. (2005) 'Probing the viscoelastic behavior of cultured airway smooth muscle cells with atomic force microscopy: stiffening induced by contractile agonist', *Biophys J*, 88(4), pp. 2994-3007.

Solbach, T.F., Paulus, B., Weyand, M., Eschenhagen, T., Zolk, O. and Fromm, M.F. (2008) 'ATP-binding cassette transporters in human heart failure', *Naunyn Schmiedebergs Arch Pharmacol*, 377(3), pp. 231-43.

Solomon, G.M., Fu, L., Rowe, S.M. and Collawn, J.F. (2017) 'The therapeutic potential of CFTR modulators for COPD and other airway diseases', *Curr Opin Pharmacol*, 34, pp. 132-139.

Solomon, G.M., Hathorne, H., Liu, B., Raju, S.V., Reeves, G., Acosta, E.P., Dransfield, M.T. and Rowe, S.M. (2016) 'Pilot evaluation of ivacaftor for chronic bronchitis', *Lancet Respir Med*, 4(6), pp. e32-3.

Song, S., Yamamura, A., Yamamura, H., Ayon, R.J., Smith, K.A., Tang, H., Makino, A. and Yuan, J.X. (2014) 'Flow shear stress enhances intracellular Ca2+ signaling in pulmonary artery smooth muscle cells from patients with pulmonary arterial hypertension', *Am J Physiol Cell Physiol*, 307(4), pp. C373-83.

Sorkin, E.M., Clissold, S.P. and Brogden, R.N. (1985) 'Nifedipine', *Drugs*, 30(3), pp. 182-274.

Sterling, G.M. (1967) 'Mechanism of bronchoconstriction caused by cigarette smoking', *Br Med J*, 3(5560), pp. 275-7.

Streck, E., Jorres, R.A., Huber, R.M. and Bergner, A. (2010) 'Effects of cigarette smoke extract and nicotine on bronchial tone and acetylcholine-induced airway contraction in mouse lung slices', *J Investig Allergol Clin Immunol*, 20(4), pp. 324-30.

Taggart, C., Cervantes-Laurean, D., Kim, G., McElvaney, N.G., Wehr, N., Moss, J. and Levine, R.L. (2000) 'Oxidation of either methionine 351 or methionine 358 in alpha 1-antitrypsin causes loss of anti-neutrophil elastase activity', *J Biol Chem*, 275(35), pp. 27258-65.

Takeyama, K., Agusti, C., Ueki, I., Lausier, J., Cardell, L.O. and Nadel, J.A. (1998) 'Neutrophil-dependent goblet cell degranulation: role of membrane-bound elastase and adhesion molecules', *Am J Physiol*, 275(2), pp. L294-302.

Takeyama, K., Jung, B., Shim, J.J., Burgel, P.R., Dao-Pick, T., Ueki, I.F., Protin, U., Kroschel, P. and Nadel, J.A. (2001) 'Activation of epidermal growth factor receptors is responsible for mucin synthesis induced by cigarette smoke', *Am J Physiol Lung Cell Mol Physiol*, 280(1), pp. L165-72.

Talavera, K., Gees, M., Karashima, Y., Meseguer, V.M., Vanoirbeek, J.A., Damann, N., Everaerts, W., Benoit, M., Janssens, A., Vennekens, R., Viana, F., Nemery, B., Nilius, B. and Voets, T. (2009) 'Nicotine activates the chemosensory cation channel TRPA1', *Nat Neurosci*, 12(10), pp. 1293-9.

Tamashiro, E., Xiong, G., Anselmo-Lima, W.T., Kreindler, J.L., Palmer, J.N. and Cohen, N.A. (2009) 'Cigarette smoke exposure impairs respiratory epithelial ciliogenesis', *Am J Rhinol Allergy*, 23(2), pp. 117-22.

Tamimi, A., Serdarevic, D. and Hanania, N.A. (2012) 'The effects of cigarette smoke on airway inflammation in asthma and COPD: therapeutic implications', *Respir Med*, 106(3), pp. 319-28.

Tanaka, Y., Yamashita, Y., Yamaki, F., Horinouchi, T., Shigenobu, K. and Koike, K. (2003) 'MaxiK channel mediates beta2-adrenoceptor-activated relaxation to isoprenaline through cAMP-dependent and -independent mechanisms in guinea-pig tracheal smooth muscle', *J Smooth Muscle Res*, 39(6), pp. 205-19.

Tang, K., Rossiter, H.B., Wagner, P.D. and Breen, E.C. (2004) 'Lung-targeted VEGF inactivation leads to an emphysema phenotype in mice', *J Appl Physiol (1985)*, 97(4), pp. 1559-66; discussion 1549.

Tashkin, D.P., Altose, M.D., Bleecker, E.R., Connett, J.E., Kanner, R.E., Lee, W.W. and Wise, R. (1992) 'The lung health study: airway responsiveness to inhaled methacholine in smokers with mild to moderate airflow limitation. The Lung Health Study Research Group', *Am Rev Respir Dis*, 145(2 Pt 1), pp. 301-10.

Tashkin, D.P., Altose, M.D., Connett, J.E., Kanner, R.E., Lee, W.W. and Wise, R.A. (1996) 'Methacholine reactivity predicts changes in lung function over time in smokers with early chronic obstructive pulmonary disease. The Lung Health Study Research Group', *Am J Respir Crit Care Med*, 153(6 Pt 1), pp. 1802-11.

Tashkin, D.P., Celli, B., Senn, S., Burkhart, D., Kesten, S., Menjoge, S., Decramer, M. and Investigators, U.S. (2008) 'A 4-year trial of tiotropium in chronic obstructive pulmonary disease', *N Engl J Med*, 359(15), pp. 1543-54.

Tashkin, D.P., Simmons, M.S., Chang, P., Liu, H. and Coulson, A.H. (1993) 'Effects of smoked substance abuse on nonspecific airway hyperresponsiveness', *Am Rev Respir Dis*, 147(1), pp. 97-103.

Tian, Y., Kongsuphol, P., Hug, M., Ousingsawat, J., Witzgall, R., Schreiber, R. and Kunzelmann, K. (2011) 'Calmodulin-dependent activation of the epithelial calcium-dependent chloride channel TMEM16A', *FASEB J*, 25(3), pp. 1058-68.

Tiddens, H.A., Pare, P.D., Hogg, J.C., Hop, W.C., Lambert, R. and de Jongste, J.C. (1995) 'Cartilaginous airway dimensions and airflow obstruction in human lungs', *Am J Respir Crit Care Med*, 152(1), pp. 260-6.

Tliba, O., Deshpande, D., Chen, H., Van Besien, C., Kannan, M., Panettieri, R.A., Jr. and Amrani, Y. (2003) 'IL-13 enhances agonist-evoked calcium signals and contractile responses in airway smooth muscle', *Br J Pharmacol*, 140(7), pp. 1159-62.

Togo, S., Holz, O., Liu, X., Sugiura, H., Kamio, K., Wang, X., Kawasaki, S., Ahn, Y., Fredriksson, K., Skold, C.M., Mueller, K.C., Branscheid, D., Welker, L., Watz, H., Magnussen, H. and Rennard, S.I. (2008) 'Lung fibroblast repair functions in patients with chronic obstructive pulmonary disease are altered by multiple mechanisms', *Am J Respir Crit Care Med*, 178(3), pp. 248-60.

Tsai, M., Byun, M.K., Shin, J. and Crotty Alexander, L.E. (2020) 'Effects of e-cigarettes and vaping devices on cardiac and pulmonary physiology', *J Physiol*.

UK Cystic Fibrosis Registry: Annual Data Report 2019 (2020). Available at: https://www.cysticfibrosis.org.uk/~/media/documents/the-work-we-do/uk-cf-registry/2019-registry-annual-data-report_sep-2020.ashx?la=en.

Vachel, L., Norez, C., Jayle, C., Becq, F. and Vandebrouck, C. (2015) 'The low PLC-delta1 expression in cystic fibrosis bronchial epithelial cells induces upregulation of TRPV6 channel activity', *Cell Calcium*, 57(1), pp. 38-48.

Valavanidis, A., Vlachogianni, T. and Fiotakis, K. (2009) 'Tobacco smoke: involvement of reactive oxygen species and stable free radicals in mechanisms of oxidative damage, carcinogenesis and synergistic effects with other respirable particles', *Int J Environ Res Public Health*, 6(2), pp. 445-62.

Van Asperen, P., Mellis, C.M., South, R.T. and Simpson, S.J. (1981) 'Bronchial reactivity in cystic fibrosis with normal pulmonary function', *Am J Dis Child*, 135(9), pp. 815-9.

Van Goor, F., Hadida, S., Grootenhuis, P.D., Burton, B., Cao, D., Neuberger, T., Turnbull, A., Singh, A., Joubran, J., Hazlewood, A., Zhou, J., McCartney, J., Arumugam, V., Decker, C., Yang, J., Young, C., Olson, E.R., Wine, J.J., Frizzell, R.A., Ashlock, M. and Negulescu, P. (2009) 'Rescue of CF airway epithelial cell function in vitro by a CFTR potentiator, VX-770', *Proc Natl Acad Sci U S A*, 106(44), pp. 18825-30.

van Haren, E.H., Lammers, J.W., Festen, J. and van Herwaarden, C.L. (1992) 'Bronchial vagal tone and responsiveness to histamine, exercise and bronchodilators in adult patients with cystic fibrosis', *Eur Respir J*, 5(9), pp. 1083-8.

Vandebrouck, C., Melin, P., Norez, C., Robert, R., Guibert, C., Mettey, Y. and Becq, F. (2006) 'Evidence that CFTR is expressed in rat tracheal smooth muscle cells and contributes to bronchodilation', *Respir Res*, 7, p. 113.

Vernooy, J.H., Lindeman, J.H., Jacobs, J.A., Hanemaaijer, R. and Wouters, E.F. (2004) 'Increased activity of matrix metalloproteinase-8 and matrix metalloproteinase-9 in induced sputum from patients with COPD', *Chest*, 126(6), pp. 1802-10.

Viana, F. and Ferrer-Montiel, A. (2009) 'TRPA1 modulators in preclinical development', *Expert Opin Ther Pat*, 19(12), pp. 1787-99.

Virgin, F.W., Azbell, C., Schuster, D., Sunde, J., Zhang, S., Sorscher, E.J. and Woodworth, B.A. (2010) 'Exposure to cigarette smoke condensate reduces calcium activated chloride channel transport in primary sinonasal epithelial cultures', *Laryngoscope*, 120(7), pp. 1465-9.

Vizza, C.D., Lynch, J.P., Ochoa, L.L., Richardson, G. and Trulock, E.P. (1998) 'Right and left ventricular dysfunction in patients with severe pulmonary disease', *Chest*, 113(3), pp. 576-83.

Wallace, H.L., Southern, K.W., Connell, M.G., Wray, S. and Burdyga, T. (2013) 'Abnormal tracheal smooth muscle function in the CF mouse', *Physiol Rep*, 1(6), p. e00138.

Wang, J., Yang, G., Li, M. and Zhou, X. (2019a) 'Transient Receptor Potential Melastatin 8 (TRPM8)-Based Mechanisms Underlie Both the Cold Temperature-Induced Inflammatory

Reactions and the Synergistic Effect of Cigarette Smoke in Human Bronchial Epithelial (16HBE) Cells', *Front Physiol*, 10, p. 285.

Wang, M., Zhang, Y., Xu, M., Zhang, H., Chen, Y., Chung, K.F., Adcock, I.M. and Li, F. (2019b) 'Roles of TRPA1 and TRPV1 in cigarette smoke -induced airway epithelial cell injury model', *Free Radic Biol Med*, 134, pp. 229-238.

Wang, Q., Wang, Y.X., Yu, M. and Kotlikoff, M.I. (1997) 'Ca(2+)-activated Cl- currents are activated by metabolic inhibition in rat pulmonary artery smooth muscle cells', *Am J Physiol*, 273(2 Pt 1), pp. C520-30.

Warth, J.D., Collier, M.L., Hart, P., Geary, Y., Gelband, C.H., Chapman, T., Horowitz, B. and Hume, J.R. (1996) 'CFTR chloride channels in human and simian heart', *Cardiovasc Res*, 31(4), pp. 615-24.

Welsh, M.J. (1983) 'Cigarette smoke inhibition of ion transport in canine tracheal epithelium', *J Clin Invest*, 71(6), pp. 1614-23.

Wen, J., Pang, Y., Zhou, T., Qi, X., Zhao, M., Xuan, B., Meng, X., Guo, Y., Liu, Q., Liang, H., Li, Y., Dong, H. and Wang, Y. (2016) 'Essential role of Na+/Ca2+ exchanger 1 in smoking-induced growth and migration of esophageal squamous cell carcinoma', *Oncotarget*, 7(39), pp. 63816-63828.

White, T.A., Xue, A., Chini, E.N., Thompson, M., Sieck, G.C. and Wylam, M.E. (2006) 'Role of transient receptor potential C3 in TNF-alpha-enhanced calcium influx in human airway myocytes', *Am J Respir Cell Mol Biol*, 35(2), pp. 243-51.

Wickenden, J.A., Clarke, M.C., Rossi, A.G., Rahman, I., Faux, S.P., Donaldson, K. and MacNee, W. (2003) 'Cigarette smoke prevents apoptosis through inhibition of caspase activation and induces necrosis', *Am J Respir Cell Mol Biol*, 29(5), pp. 562-70.

Wiegman, C.H., Michaeloudes, C., Haji, G., Narang, P., Clarke, C.J., Russell, K.E., Bao, W., Pavlidis, S., Barnes, P.J., Kanerva, J., Bittner, A., Rao, N., Murphy, M.P., Kirkham, P.A., Chung, K.F., Adcock, I.M. and Copdmap (2015) 'Oxidative stress-induced mitochondrial dysfunction drives inflammation and airway smooth muscle remodeling in patients with chronic obstructive pulmonary disease', *J Allergy Clin Immunol*, 136(3), pp. 769-80.

Willemse, B.W., ten Hacken, N.H., Rutgers, B., Lesman-Leegte, I.G., Postma, D.S. and Timens, W. (2005) 'Effect of 1-year smoking cessation on airway inflammation in COPD and asymptomatic smokers', *Eur Respir J*, 26(5), pp. 835-45.

Wong, F.H., AbuArish, A., Matthes, E., Turner, M.J., Greene, L.E., Cloutier, A., Robert, R., Thomas, D.Y., Cosa, G., Cantin, A.M. and Hanrahan, J.W. (2017) 'Cigarette smoke activates CFTR through ROS-stimulated cAMP signaling in human bronchial epithelial cells', *Am J Physiol Cell Physiol*, p. ajpcell 00099 2017.

Wong, K.R., Trezise, A.E., Crozatier, B. and Vandenberg, J.I. (2000) 'Loss of the normal epicardial to endocardial gradient of cftr mRNA expression in the hypertrophied rabbit left ventricle', *Biochem Biophys Res Commun*, 278(1), pp. 144-9.

Wu, T., Huang, J., Moore, P.J., Little, M.S., Walton, W.G., Fellner, R.C., Alexis, N.E., Peter Di, Y., Redinbo, M.R., Tilley, S.L. and Tarran, R. (2017) 'Identification of BPIFA1/SPLUNC1 as an epithelium-derived smooth muscle relaxing factor', *Nat Commun*, 8, p. 14118.

Wu, Z.X. and Lee, L.Y. (1999) 'Airway hyperresponsiveness induced by chronic exposure to cigarette smoke in guinea pigs: role of tachykinins', *J Appl Physiol (1985)*, 87(5), pp. 1621-8.

Wylam, M.E., Sathish, V., VanOosten, S.K., Freeman, M., Burkholder, D., Thompson, M.A., Pabelick, C.M. and Prakash, Y.S. (2015) 'Mechanisms of Cigarette Smoke Effects on Human Airway Smooth Muscle', *PLoS One*, 10(6), p. e0128778.

Xu, C.B., Lei, Y., Chen, Q., Pehrson, C., Larsson, L. and Edvinsson, L. (2010) 'Cigarette smoke extracts promote vascular smooth muscle cell proliferation and enhances contractile responses in the vasculature and airway', *Basic Clin Pharmacol Toxicol*, 107(6), pp. 940-8.

Xu, G.N., Yang, K., Xu, Z.P., Zhu, L., Hou, L.N., Qi, H., Chen, H.Z. and Cui, Y.Y. (2012) 'Protective effects of anisodamine on cigarette smoke extract-induced airway smooth muscle cell proliferation and tracheal contractility', *Toxicol Appl Pharmacol*, 262(1), pp. 70-9.

Xu, H. and Ren, D. (2015) 'Lysosomal physiology', *Annu Rev Physiol*, 77, pp. 57-80.

Xu, K.Y., Zweier, J.L. and Becker, L.C. (1997) 'Hydroxyl radical inhibits sarcoplasmic reticulum Ca(2+)-ATPase function by direct attack on the ATP binding site', *Circ Res*, 80(1), pp. 76-81.

Xu, L.J., Dandurand, R.J., Lei, M. and Eidelman, D.H. (1993) 'Airway hyperresponsiveness in cigarette smoke-exposed rats', *Lung*, 171(2), pp. 95-107.

Yaghi, A., Zaman, A., Cox, G. and Dolovich, M.B. (2012) 'Ciliary beating is depressed in nasal cilia from chronic obstructive pulmonary disease subjects', *Respir Med*, 106(8), pp. 1139-47.

Yajima, T., Nagashima, H., Tsutsumi-Sakai, R., Hagiwara, N., Hosoda, S., Quertermous, T., Kasanuki, H. and Kawana, M. (1997) 'Functional activity of the CFTR Cl- channel in human myocardium', *Heart Vessels*, 12(6), pp. 255-61.

Yamaguchi, Y., Nasu, F., Harada, A. and Kunitomo, M. (2007) 'Oxidants in the gas phase of cigarette smoke pass through the lung alveolar wall and raise systemic oxidative stress', *J Pharmacol Sci*, 103(3), pp. 275-82.

Yamanaka, J., Nishimura, J., Hirano, K. and Kanaide, H. (2003) 'An important role for the Na+-Ca2+ exchanger in the decrease in cytosolic Ca2+ concentration induced by isoprenaline in the porcine coronary artery', *J Physiol*, 549(Pt 2), pp. 553-62.

Yamazaki, J. and Hume, J.R. (1997) 'Inhibitory effects of glibenclamide on cystic fibrosis transmembrane regulator, swelling-activated, and Ca(2+)-activated Cl- channels in mammalian cardiac myocytes', *Circ Res*, 81(1), pp. 101-9.

Ye, L., Zhu, W., Backx, P.H., Cortez, M.A., Wu, J., Chow, Y.H., McKerlie, C., Wang, A., Tsui, L.C., Gross, G.J. and Hu, J. (2011) 'Arrhythmia and sudden death associated with elevated cardiac chloride channel activity', *J Cell Mol Med*, 15(11), pp. 2307-16.

Yim, P.D., Gallos, G., Perez-Zoghbi, J.F., Trice, J., Zhang, Y., Siviski, M., Sonett, J. and Emala, C.W., Sr. (2013) 'Chloride channel blockers promote relaxation of TEA-induced contraction in airway smooth muscle', *J Smooth Muscle Res*, 49, pp. 112-24.

Yoon, C.H., Park, H.J., Cho, Y.W., Kim, E.J., Lee, J.D., Kang, K.R., Han, J. and Kang, D. (2011) 'Cigarette Smoke Extract-induced Reduction in Migration and Contraction in Normal Human Bronchial Smooth Muscle Cells', *Korean J Physiol Pharmacol*, 15(6), pp. 397-403.

Yoshiyama, S., Horinouchi, T., Miwa, S., Wang, H.H., Kohama, K. and Nakamura, A. (2011) 'Effect of cigarette smoke components on vascular smooth muscle cell migration toward platelet-derived growth factor BB', *J Pharmacol Sci*, 115(4), pp. 532-5.

Yuan, X.J. (1997) 'Role of calcium-activated chloride current in regulating pulmonary vasomotor tone', *Am J Physiol*, 272(5 Pt 1), pp. L959-68.

Zaidi, A. and Michaelis, M.L. (1999) 'Effects of reactive oxygen species on brain synaptic plasma membrane Ca(2+)-ATPase', *Free Radic Biol Med*, 27(7-8), pp. 810-21.

Zamel, N., Youssef, H.H. and Prime, F.J. (1963) 'Airway resistance and peak expiratory flow-rate in smokers and non-smokers', *Lancet*, 1(7293), pp. 1237-8.

Zeng, M., Li, Y., Jiang, Y., Lu, G., Huang, X. and Guan, K. (2013) 'Local and systemic oxidative stress status in chronic obstructive pulmonary disease patients', *Can Respir J*, 20(1), pp. 35-41.

Zhang, C.H., Li, Y., Zhao, W., Lifshitz, L.M., Li, H., Harfe, B.D., Zhu, M.S. and ZhuGe, R. (2013) 'The transmembrane protein 16A Ca(2+)-activated Cl- channel in airway smooth muscle contributes to airway hyperresponsiveness', *Am J Respir Crit Care Med*, 187(4), pp. 374-81.

Zhang, X.Y., Xu, Y.J., Liu, X.S. and Zhang, Z.X. (2010) 'Cigarette smoke extract promotes proliferation of airway smooth muscle cells in asthmatic rats via regulating cyclin D1 expression', *Chin Med J (Engl)*, 123(13), pp. 1709-14.

Zhong, S., Nie, Y.C., Gan, Z.Y., Liu, X.D., Fang, Z.F., Zhong, B.N., Tian, J., Huang, C.Q., Lai, K.F. and Zhong, N.S. (2015) 'Effects of Schisandra chinensis extracts on cough and pulmonary inflammation in a cough hypersensitivity guinea pig model induced by cigarette smoke exposure', *J Ethnopharmacol*, 165, pp. 73-82.

Zitt, C., Strauss, B., Schwarz, E.C., Spaeth, N., Rast, G., Hatzelmann, A. and Hoth, M. (2004) 'Potent inhibition of Ca2+ release-activated Ca2+ channels and T-lymphocyte activation by the pyrazole derivative BTP2', *J Biol Chem*, 279(13), pp. 12427-37.

Zou, J.J., Gao, Y.D., Geng, S. and Yang, J. (2011) 'Role of STIM1/Orai1-mediated store-operated Ca(2)(+) entry in airway smooth muscle cell proliferation', *J Appl Physiol (1985)*, 110(5), pp. 1256-63.